Page

17    Equation (1 - 7) should read:

$$\phi(\Omega) = \frac{27.8 \times 10^{-6}}{\Omega^{1.77}} \; ft^2/rad/ft$$

35    The 5th and 4th lines from the bottom of the page should read:

    the values proposed by Houbolt (ref. 20), i.e. n = 2, and $\overline{C}$ = 6.7 x $10^{-6}$ and 20 x $10^{-6}$ for good and rough runways respectively. - - - - - - -

36    Immediately after equation (1 - 19),

    delete:      which results in a curve with two linear segments on the log-log axes.

    and insert:  which results in a smooth curve on the log-log axes.

80    The 4th line after the title should read:

    The mean-square value  - - - - - - -

80    The 1st line of equation (4 - 2) should read:

$$\phi_{\ddot{x}}(\omega_f) = \omega_f^4 \cdot \phi_x(\omega_f)$$

80    The 2nd line of equation (4 - 2) should read:

$$= \omega_f^4 \cdot H_{\frac{x}{q}}^2(\omega_f) \cdot \phi_q(\omega_f)$$

82    Equation (4 - 4) should read:

$$= (\cos \frac{d}{V} \cdot \omega_f + - - - - - - -$$

Page

82     Equation (4 - 6) should read:

$$\dot{h}_1 = i\,\omega_f(\cos\frac{d.}{V}\,\omega_f + i\sin\frac{d.}{V}\,\omega_f)\,e^{i\,\omega_f t}$$

95     Line 2.

4.5 and 4.6 should read:    4.7 and 4.8

106     The equation immediately after equation (4 - 30) should read:

$$H(i\,\omega)_{\frac{x}{h}} = \ \text{-----} \ = \frac{1}{(K - M\,\omega_f^2) + i(C\,\omega_f)}$$

106     Half way down page:

$$\therefore \ H(i\,\omega)_{\frac{h}{r}} = \sqrt{\phantom{xxxx}} \ \ x\sqrt{\phantom{xxxx}}$$

should read:

$$\therefore \ \left|H(i\,\omega)_{\frac{h}{r}}\right| = \sqrt{\phantom{xxxx}} \ \ x\sqrt{\phantom{xxxx}}$$

107     Equation (4 - 33) should read:

$$\left|H(i\,\omega)_{\frac{x}{r}}\right| = \sqrt{\phantom{xxxx}} \ \ x\sqrt{\phantom{xxxx}}$$

107     Equation (4 - 34) should read:

$$\overline{x^2} = \int_{\omega_1}^{\omega_2} \omega^4 . \left|H(i\,\omega)_{\frac{x}{r}}\right|^2 . \oint_r(\omega)\,d\omega$$

108     The two lines immediately after equation (4 - 38) should read:

The troughs on the curve will occur when

$$\cos\frac{d.}{V}\,\omega_f = -1$$

125     Line 19.

delete:        from table 4.3

and insert:     used to produce the values in table 4.3

Page

126    Lines 12 and 13.

        delete:        Thus, for a given set of parameters, coupling
                          tends to lower the modal damping substantially.

        and insert:    Although the values of $\beta = 0.0448$ and $0.0295$
                          reflect an effective increase in damping due
                          to the neglect of tyre stiffness, causing lower
                          resonant frequencies, there is indication that,
                          for a given set of parameters, coupling tends to
                          lower the modal damping.

133    3rd line from the bottom of the page.

        Figure 4.2.4 should read:   Figure 4.24

198    Line 14.

        Davidson should read:    Davidon

210    The 10th line after the title should read:

        realised, particularly for high stiffness and low damping. - -

248    Equation (A - 13) should read:

$$\bar{\delta}^2 < \int^{\infty} \frac{4\,\bar{c}}{\Omega^2} \, d\Omega$$

$$\Omega = \frac{2\pi}{L}$$

252    Line 6.

        after:        These values are plotted on figure B1.

        insert:       The curves have been approximated by straight
                        lines, although strictly, for an arithmetic mean,
                        each pair of points would be connected by a
                        curved line.

RESPONSE OF A LINEARIZED AIRCRAFT TO RUNWAY DISTURBANCES

by

BARRIE HUTCHINSON, M.Sc.

A Doctoral Thesis

Submitted in partial fulfilment of the requirements for the award of

Doctor of Philosophy of the Loughborough University of Technology.

October 1974

Supervisor:    Professor F.D.Hales, Ph.D.

    Department of Transport Technology.

## ACKNOWLEDGEMENTS

The author would like to express his sincere appreciation to his Supervisor, Professor F.D.Hales, for his guidance in this research and for his enthusiasm for the project.

He would also like to thank his wife, Shirley, for her typing of the manuscript, the interpretation of which must have been more than a little difficult.

## SUMMARY

A statistical analysis has been developed, using power spectral density methods, to examine the response of an aircraft to runway unevenness. The analysis includes rigid body heave and pitch and any number of symmetrical flexural modes of the airframe, linear values of main and nose oleo and tyre stiffness and damping, and wheel masses. The analysis has been used to produce computer programs for response and optimisation studies, to investigate the effects on response of flexural modes, taxiing velocity, oleo stiffness and damping, and undercarriage position.

It is found that for the aircraft used for the investigation (the values are based on the Boeing 707) a good estimate of the response can be obtained by considering rigid body modes only. Of the flexural modes the 1st and 4th are by far the most predominant, but their effects tend to counterbalance each other.

The response acceleration at any position on the fuselage generally increases with increased taxiing velocity, although this is not always a steady increase. Undulations are apparent on the response curves, particularly for the pilot location, where they are caused by the effects of the phased undercarriage inputs on the pitching mode. Those on the mainwheel response curve, due to the heave mode, are less pronounced.

Reducing the oleo stiffness is by far the most effective way of reducing the response, the main oleo having by far the most effect

on the mainwheel location response, which is predominantly due to heave, but both oleos having a large effect on the pilot location response, which has large contributions from both heave and pitch. Increasing the damping also causes a reduction in response, but only to a quite small extent.

As the mainwheels are moved aft from their original position, the response at the pilot location decreases, but that at the mainwheel location increases, the sum of the two responses remaining remarkably unaffected by undercarriage position.

An approximation to the response has been developed, which, when used as an optimisation function, produces good working optima in very short computer times.

The simplified system developed in this thesis is useful for preliminary design, for the study of the effects of parameter variations, and for optimisation.

# CONTENTS

<u>NOTATION</u>

The following is a list of symbols used in this thesis. Any symbols or suffices used which are not included in this list are explained in the text. Where symbols or suffices can represent more than one quantity their use is made clear in the text.

| | |
|---|---|
| $a$ | distance from aircraft cg to main undercarriage |
| $a_o$ , $a_1$ | displacements in rigid body and first flexural modes respectively for equivalent 3 mass system |
| $b$ | distance from aircraft cg to nose undercarriage |
| $C_{Nm}$ , $C_{Nn}$ | non-linear $(V\vert V\vert)$ damping coefficients for main and nose oleos respectively |
| $C_{em}$ , $C_{en}$ | equivalent linear (viscous) damping coefficients for main and nose oleos respectively |
| $C_m$ , $C_1$ | viscous damping coefficient for main oleo |
| $C_n$ , $C_2$ | viscous damping coefficient for nose oleo |
| $C_{t1}$ , $C_{t2}$ | linear tyre damping coefficients for main and nose undercarriages respectively |
| $C_{crit}$ | critical viscous damping coefficient |
| $C$ | equivalent viscous oleo damping coefficient for rigid body heave mode |
| $C_e$ | equivalent viscous oleo damping coefficient for rigid body pitch mode |
| $C_j$ | linear structural damping coefficient for jth mode |
| $\overline{C}$ | runway unevenness constant |
| $\overline{C}_a$ , $\overline{C}_b$ | $\overline{C}$ for lower frequency and higher frequency lines respectively for geometric mean runway |

| | |
|---|---|
| $d$ | longitudinal distance between main and nose undercarriages |
| $e$ | distance from aircraft cg to pilot location |
| $F_{di}$ | oleo damping force for ith oleo |
| $F_{ti}$ | tyre force for ith oleo |
| $F_{si}$ | nett oleo spring force for ith oleo |
| $F_s$ | force transmitted to the airframe from the two oleos |
| $H_{\underline{x}}(\omega)$ $\overline{y}$ | frequency response function relating output x to input y |
| $h$ | runway profile elevation; heave input to undercarriage system |
| $h_1$ , $h_2$ | runway profile elevations at main and nose undercarriages respectively |
| $I,J$ | moment of inertia in pitch of aircraft about cg |
| $K$ | equivalent linear oleo stiffness for rigid body heave mode |
| $K_e$ | equivalentlinear oleo stiffness for rigid body pitch mode |
| $k_1$ , $k_2$ | linear spring stiffnesses for main and nose oleos respectively |
| $k_{t1}$ , $k_{t2}$ | linear tyre stiffnesses for main and nose undercarriages respectively |
| $L$ | runway unevenness wavelength |
| $L_m$ , $L_n$ | distance from aircraft cg to main and nose undercarriages respectively |
| $M_o$ | proportion of the aircraft mass carried by main undercarriage |

| | |
|---|---|
| $M_1$ , $M_2$ | unsprung masses of main and nose undercarriages respectively |
| $M_3$ , $M_4$ | generalized masses for rigid body heave and pitch modes respectively |
| $M_j$ | generalized mass in jth mode |
| N | total number of modes including undercarriage modes $N = N_1 + 4$ |
| $N_1$ | number of flexural modes |
| NM | number of modes including rigid body modes but excluding undercarriage modes $NM = N_1 + 2$ |
| n | minus the slope of the straight-line PSD function |
| $n_a$ , $n_b$ | n for lower frequency and higher frequency lines respectively for geometric mean runway |
| $P_j(t)$ | generalized forcing function in jth mode |
| p | Laplace transform variable |
| $Q_1$ , $Q_2$ | main and nose landing gear forces respectively |
| $\bar{Q}_1$ , $\bar{Q}_2$ | static values of $Q_1$ , $Q_2$ respectively |
| R $(\chi)$ | autocorrelation function |
| $S_i$ | stroke of ith oleo from static equilibrium position |
| $U_i$ | vertical displacement at ith location on airframe |
| V | taxiing velocity of aircraft |
| $W_1$ , $W_2$ | unsprung weights of main and nose undercarriages respectively |
| $X_1$ , $X_2$ | vertical displacements of main and nose wheel masses respectively |
| $X_3$ , $X_4$ | generalized coordinates of rigid body heave and pitch modes respectively |

| | |
|---|---|
| $X_j(t)$ | generalized coordinate of jth mode ( $j = 5$ to $N$ for flexural modes ) |
| $\overline{X}_1$ , $\overline{X}_2$ | static displacements of masses $M_1$ , $M_2$ respectively |
| $x$ | displacement along the runway |
| $\overline{x}^2$ | mean-square-value of x |
| $y(x)$ | vertical displacement at any position x along the runway |
| $Z(x,y,t)$ | vertical displacement of any point on airframe |
| $\beta$ | structural damping coefficient |
| $\Delta_n$ | largest acceleration peak |
| $\Delta_{n_{10}}$ | magnitude of acceleration peak that occurs 10 times during a take-off run |
| $\delta$ | central deviation from a straight edge |
| $\delta(t)$ | unit impulse function |
| $\delta_i$ | modal displacement at the point where the ith oleo joins the airframe |
| $\Theta_o$ | pitch input to undercarriage system |
| $\lambda$ | eigenvalue |
| $\sigma$ | root-mean-square value of disturbance y(x) |
| $\sigma'$ | average peak amplitude of unevenness |
| $\Phi(\Omega)$ | power spectral density ( PSD ) of a quantity at spacial frequency $\Omega$ |
| $\Phi_x(\omega)$ | PSD of response displacement at circular frequency $\omega$ |
| $\Phi_y(\omega)$ | PSD of runway unevenness amplitude |
| $\Phi_{\ddot{x}}(\omega)$ | PSD of response acceleration |
| $\phi_i^j(x,y)$ | jth mode shape at ith location on airframe |
| $\Omega$ | spacial frequency ( $= \frac{2\pi}{L}$ ) |
| $\omega$ | circular frequency |

$\omega_d$     natural damped frequency

$\omega_f$     frequency of input disturbance

$\omega_j$     modal frequency in the jth mode

$\omega_n$     natural undamped frequency

$[C]$     damping matrix of equations of motion of aircraft defined by equation ( 3 - 29 )

$[CA_j]$     damping matrix defined by equation (3 - 23), j = 3 to N

$\{F(t)\}$     forcing function column matrix defined by equation (3 - 31)

$\{G\}$     forcing function column matrix defined by equation (4 - 9)

$[k]$     stiffness matrix of equations of motion of aircraft defined by equation (3 - 30)

$[kA_j]$     stiffness matrix defined by equation (3 - 24), j = 3 to N

$\lceil M \rfloor$     diagonal mass matrix of $M_j$ , j = 1 to N

$\lceil M_j \rfloor$     diagonal matrix of generalized masses, j = 3 to N

$\{P_j\}$     column matrix of generalized forcing functions $P_j(t)$, j = 3 to N

$[U(p)]^{-1}$     matrix of transfer functions for aircraft system defined by equations (4 - 11) and (4 - 12)

$\{X\}$     column matrix of generalized coordinates $X_j$ , j = 1 to N

$\{X_j\}$     column matrix of generalized coordinates $X_j$ , j = 3 to N

$\{X(i\omega_f)\}$     column matrix of generalized coordinates of frequency response functions in the various modes defined by equation (4 - 15)

$[\phi_i^j]$     row matrix of mode shapes at ith location on aircraft, j = 3 to N

$\{\phi_i^j X_j(i\omega_f)\}$     column matrix of frequency response functions in the various modes

$\lceil \omega_j \rfloor$         diagonal matrix of modal frequencies, $j = 3$ to $N$,

$\omega_j = 0$ for $j = 3,4$

$[\ \ ]^{-1}$         inverse of matrix

$[\ \ ]^{T}$         transpose of matrix

$A$         matrix

$\underline{b}$

$\underline{v}$

$\underline{w}$              vectors

$\underline{x}$

# INTRODUCTION

With the advent of larger more flexible aircraft the undercarriage designed purely to withstand landing impact is no longer a completely satisfactory vibration absorber for ground movement, i.e. for taxiing, take-off runs, and landing runs. Many problems are associated with vibration of the aircraft during ground manoeuvring, such as fatigue in the airframe, degradation of a pilot's ability to control the aircraft during the critical rotation phase of take-off, and crew and passenger discomfort.

Several criteria have been proposed as limits for the level of vibration response in the pilot compartment, and as limits to the level of runway unevenness which may be tolerated. Most runway roughness criteria have been presented in the form of power spectral densities of unevenness amplitude of the runway profile. There is a requirement of course for reliable methods of analysis so that the aircraft may be designed so as not to produce excessive response levels.

Analytical methods of estimating the dynamic response of an aircraft to runway unevenness fall into two broad categories: deterministic, and statistical. The deterministic method involves the solution, by digital or analogue means, of the differential equations of the airframe and undercarriage system, using a deterministic input such as discrete values of elevation along a runway profile. These methods in general have the disadvantage of requiring large amounts of computer time, but can produce very

accurate results. The statistical methods use linearized equations of motion of the airframe and undercarriage system, in conjunction with the power spectral density function of a runway, to produce a statistical analysis of the response. These methods generally have the disadvantages that only statistical information about the response is obtained, such as root-mean-square values of acceleration, and that an average response along a runway is produced, so that individual rough areas cannot be detected. However, the method is concise, and generally thought to be of particular use when the response to many runways is required, for example, for fatigue studies. Authors who have presented statistical analyses have only generally considered two modes of vibration, either rigid body heave and pitch (usually uncoupled), or rigid body heave and the first flexural mode.

The aim of this thesis is to develop a statistical analysis, using power spectral density methods, in which any number of modes of the airframe may be used, and to use the analysis in computer programs for response and optimisation studies to investigate the effect of various undercarriage parameters on the rms value of the response acceleration of the aircraft. The analysis will include rigid body heave and pitch and any number of symmetrical flexural modes of the airframe, linear values of main and nose oleo and tyre stiffness and damping, and wheel masses. The effects on response of flexural modes, taxiing velocity, main and nose oleo stiffness and damping, and undercarriage position will be investigated.

SECTION 1

DISCUSSION OF THE PROBLEM WITH REFERENCE TO PREVIOUS WORK

For many years aircraft undercarriages have been designed
primarily to absorb landing impact, and the landing problem has been
extensively investigated. For many practical purposes the air-pressure
force and the seal friction in the oleo unit, and the lower or unsprung
mass, can be completely ignored, and the tyre-force deflection
relationship can be assumed to be linear (ref. 1). The forces and
responses induced on landing are predominantly dependent on the oleo
damping characteristics.

While aircraft were relatively stiff and had low take-off
and landing speeds they were not particularly susceptible to runway
roughness induced vibrations, and the undercarriage designed purely
for the landing case was perfectly satisfactory. In current
subsonic and supersonic transports the change of mass distribution,
coupled with increased structural flexibility and higher speeds on
the ground, results in a dynamic system with several flexible modes
whose frequencies are low enough to be excited by the runway
wavelength variations present in the runway unevenness. Furthermore
the lower frequency modes may have frequencies of the same order as,
and be closely coupled with, the rigid body heave and pitch modes.

The problem of runway induced vibrations has been discussed
in an introduction to a previous work by the author (ref. 2), which
was mainly concerned with experimental investigations into the
feasibility of applying power spectral density (PSD) techniques to the

determination of response to runway unevenness.    Further discussion

of the problem, with a different emphasis, can be useful here, since

the object of this thesis is to use PSD techniques to investigate the

response of a linearized aircraft to runway unevenness, and of course

further literature has become available since reference 2 was produced.

There would be no problems of taxiing vibrations if all

runways and taxiways were perfectly smooth and flat.    This is of

course not a feasible possibility.    The practical difficulties

involved, and the cost incurred, in creating and maintaining such

perfect surfaces would be prohibitive.    There is thus a need to

establish reliable methods of predicting aircraft dynamic response,

during taxiing, take-off and landing, with a view to improving the

vibration isolation characteristics of undercarriage units, so that the

aircraft designer can provide a landing gear and airframe structure

which can operate safely and comfortably from existing runways.

However, an aircraft can only be designed with shock absorbing

capabilities for withstanding a finite and known level of roughness.

Thus there is still a need to produce reliable methods of measuring

and describing runway roughness, criteria for indicating acceptable

levels of runway roughness, and methods of effecting repairs

economically.

## 1.1 Runway profiles and unevenness criteria

Runway longitudinal profiles contain, in a somewhat random manner, waves of different wavelengths with the amplitudes generally becoming larger as the wavelengths increase. There are several methods by which the runway profile can be specified. Figure 1.1 shows one such method. Runway elevations are simply plotted against distance along the runway. The same information can also be presented as a list of ordinates of runway elevation measured at say 2 ft intervals along the runway. A very simple method of giving a numerical value to the runway unevenness is to state the maximum deviation from a straight edge held on the runway surface.

The runway unevenness characteristics may also be presented as shown in figure 1.2. Here the elevation measurements from figure 1.1 have been converted to PSD plots. The ordinate in figure 1.2 is the power spectral density, $\phi$, which is a measure of the power contained (proportional to the square of the amplitudes) in the unevenness corresponding to the wavelengths shown on the abscissa. Hence the higher the curve in figure 1.2, the higher the indicated roughness level. The power spectrum gives a concise picture of unevenness make-up of a given random profile, which clearly indicates the wavelengths that are troublesome, and from which additional information about the profile may be derived. The area under the PSD curve is equal to the mean-square value of the elevation values of the given profile. Furthermore, if it is assumed that the random profile is of a given nature (for example a Gaussian stationary random process), other properties such as the number of peaks above

a given level of elevation may be deduced. However, the PSD variation with wavelength represents an average roughness over the entire runway length for various wavelengths. It does not therefore distinguish between many bumps of small amplitude and a few bumps of large amplitude at a given wavelength, nor does it give any indication of the location of unevenness along the runway.

In the 1950's almost all significant aircraft response occurred in the very narrow frequency range of $1\frac{1}{2}$ to 2 Hz (ref. 3), giving runway profile wavelengths of concern, due to the range of ground speeds then used, of 17 to 150 feet. This range has been extended considerably by modern generations of aircraft. Of particular interest are the trend towards lower resonant frequencies for the larger more flexible aircraft, and the increase in runway speeds. Coleman and Hall (ref. 4) showed that the frequencies of the predominant responses for a large jet transport and a fighter aircraft of the early 1960's were about 1 and 3 Hz respectively. These give ranges of runway wavelengths of concern of about 40 to 270 feet for the transport and 14 to 70 feet for the fighter. The variation of wavelength with taxiing speed for several frequencies is shown in figure 1.3. Shaded areas have been drawn covering wavelengths capable of exciting response in the fighter and the transport. The fighter, with its relatively rigid airframe, would ride over unevenness wavelengths of 200 to 300 feet with little or no response, whereas the same unevenness could be expected to excite considerable response in the jet transport, with its higher runway speeds and modes of lower resonant frequency. Less response is expected to be excited at lower speeds for both aircraft. Hence a runway which is satisfactory for

some aircraft may cause complaints by pilots of other types (see for example refs 5, 6).

An investigation by Morris (ref. 7) in 1965 showed the predominant normal acceleration responses of two transport aircraft to be at about $\frac{3}{4}$ Hz and $1\frac{1}{2}$ to $1\frac{3}{4}$ Hz for the centre of gravity (cg) and about $\frac{3}{4}$ Hz for the pilot compartment. Mitchell (ref. 8) has reported similar response frequencies for a Boeing 707 - 436 passenger transport at a maximum take-off weight of 310000 lbf. Heavy pitching of the aircraft occurred at 0.7 to 0.9 Hz, and heaving at $1\frac{1}{4}$ Hz, with structural vibrations at higher frequencies. In 1970, Morris investigated the response characteristics of 6 aircraft ranging from a small jet trainer to a heavy bomber (ref. 6). Significant acceleration responses of these aircraft extended over a frequency range from $\frac{3}{4}$ to over 13 Hz, with pitching frequencies ranging from 2/3rds to $1\frac{3}{4}$ Hz, the larger aircraft producing the lowest frequency resonances. The responses of the large aircraft were generally associated with runway unevenness with peak-to-trough elevation differences of 0.05 to 0.25 feet with wavelengths of up to 250 feet.

The first generation of supersonic transports has extended the range of wavelengths of concern even further. Calculations and initial taxiing trials have shown (ref. 9) that the symmetric response of Concorde during take-off would be characterized by 3 main modes: pitching at 0.7 Hz, heaving at 1.3 Hz, and elastic vibration at 2.3 to about 8 Hz. The lowest frequency could be excited by wavelengths up to 460 feet. Concorde pitches more than a subsonic transport aircraft, probably because of its long fuselage and short wheelbase.

It was calculated that even on a relatively smooth runway, the nose
undercarriage load would vary between 10000 and 40000 lbf at 0.7 Hz
for about half the take-off run;   on rougher runways the nosewheel
could be bouncing off the runway from about 60 knots upwards.   The
heaving at 1.3 Hz would cause fluctuation of main undercarriage loads,
the maximum load occurring during rotation as a result of the elevator
down load needed to initiate rotation.   The elastic modes would also
be strongly excited, particularly the fundamental at 2.3 Hz, which
would be excited by wavelengths up to 140 feet at 190 knots.

Thus, frequencies in the range of about 0.7 to 13 Hz may
be excited in modern aircraft by runway unevenness wavelengths up to
almost 500 feet.   Clearly vibrations anywhere in this frequency
range can cause fatigue damage in the airframe, and particularly in the
undercarriages and their associated structure, depending on the
amplitude of the vibration.   Also, in some exceptional circumstances,
the amplitudes may be large enough to cause limit loads, thus making
the aircraft taxi-critical.   However, in addition to causing structural
damage problems, the vibration environment affects the crew and
passengers.

Human discomfort or disturbance by vibration will depend to
some extent on individual susceptibility and particular circumstances,
and discomfort, or lack of it, is not necessarily a reliable guide to
whether or not working efficiency is lowered or health impaired (ref.10).
However, the tolerance of the human body to vibration is in general a
function of applied frequency, acceleration amplitude, and duration of
exposure, the performance of tasks involving co-ordination between hand

and eye being most easily degraded by whole body vibration in the
frequency range 4 to 8 Hz (refs 10, 11).    Also visual blurring
can be equally distracting, and thus a threat to efficiency, whether
it is caused by vibration of the eye or of the object being observed.
Whilst it has been shown that lateral vibrations are more critical
than vertical vibrations with respect to a pilot's difficulty in
reading instruments etc, since this thesis is concerned only with
vertical response, the discussion will be limited to this aspect.

Levels of vibration at the pilot location of an aircraft
can be twice those at the cg (refs 6, 7, 8, 12), even more in a
supersonic transport.    Calculated values of pilot compartment/cg rms
acceleration ratio (ref. 13) showed a value of 2.84 for the proposed
American supersonic transport Boeing 733-94, taxiing at 100 ft/s on
the Langley runway, as opposed to 1.92 for a Boeing 707.    Calculations
and initial taxiing trials on Concorde have shown (ref. 9) that the
cockpit/cg vertical acceleration ratio would average about 3 during
take-off, but would be higher when pitching motion was occurring.    The
vertical acceleration in the cockpit on a given runway would be more
than twice that for a subsonic transport.    However, these values had
not been borne out in practice, and it appeared that the calculations in
some cases overestimated the aircraft response considerably.    In a
later report (ref. 14) Mitchell has stated that on Concorde the flying
controls are very precise, and control of the rotation manoeuvre has
proved to be easier than on subsonic transports.    Pitching on the
runway has not been found to introduce any piloting problems.

Although the question of whether a runway is rough or not is partially a subjective one, depending on pilot interpretation and experience, there are many effects from which a roughness criterion can be obtained objectively. For example, particular ranges of amplitude and frequency of vibrations will lead to calculable fatigue damage or to definite physiological effects, regardless of whether or not the crew finds these vibrations unduly uncomfortable.

Criteria for roughness can be presented in two major ways. The criterion may simply be a measure of runway roughness, or it may be a measure of level of vibration at some point on an aircraft taxiing on the runway. In other words the criterion can either be a measure of the environment, or of response to the environment. The two methods are not necessarily compatible for different aircraft on the same runway, due to the differences in dynamic response characteristics between aircraft, and the method used would in general depend upon the problem being faced.

The most widely accepted response criterion, proposed by Morris and Hall (ref. 5), is that the maximum vertical acceleration in the cockpit should not exceed $\pm 0.4g$ for sections of the runway where precise aircraft control is required. Several authors have expressed agreement with this criterion. Notably, in a later paper, after a comprehensive series of tests on 6 different aircraft types (ref. 6), Morris concluded that the figure of $\pm 0.4g$ in the cockpit was approximately the dividing line between satisfactory and unsatisfactory runways from the pilot's viewpoint, but did not represent a sharp

"cut-off". Pilots described peak acclerations greater than 0.6g as objectionable, peaks between 0.4 and 0.5g as slightly severe, and raised no objection to peaks less than 0.4g. Cockpit acceleration peaks in excess of 1g had resulted in pilots' complaints of actual physical discomfort, considerable doubt as to their ability to control the aircraft, and difficulty in reading the airspeed indicator.

Although an acceleration response of $\pm 0.4$g was generally considered objectionable, this does not necessarily mean that this represents a dangerous level. In measurements of cockpit vertical vibration in a Boeing 707-436 during routine flying by a British airline (ref. 8) vertical vibration of up to $\pm 0.4$g with occasional peaks of $\pm 0.7$g did not affect the accuracy of the speed at which the crew initiated rotation for take-off.

Mitchell has found (ref. 9) that a good measure of the severity of a take-off is the magnitude of the acceleration peak that occurs 10 times during the take-off run. This was given the symbol $\Delta n_{10}$. The acceleration peak was defined as the sum of successive peaks of incremental acceleration of opposite signs, the peak of incremental acceleration being defined as the largest peak between successive zero crossings. It was found empirically that for both Concorde and VC 10 accelerations the overall rms value was $0.37 \Delta n_{10}$, and that $\Delta n_{10}$ was a more consistent measure of the intensity of the vibration than the more easily observed single peak acceleration. However, on average, for cockpit accelerations, the lagest peak $\Delta n$ was $1.47 \Delta n_{10}$. Hence, it may easily be deduced that the overall rms was, on average, $0.252 \Delta n$.

Measurements of vertical acceleration in the cockpit of a Boeing 707 (ref. 15) showed that a $\Delta n_{1o}$ of 0.3g was exceeded frequently on take-off, and 0.5g on landing. These levels appeared to be acceptable. However, accelerations of $\Delta n_{1o}= 0.5$g with a typical peak acceleration of 0.7g, measured in the cockpit of a Super VC 10 during take-off at Addis Ababa (ref. 9), produced crew complaints of inability to read instruments, and concern about overloading the airframe and undercarriage. Similarly, peak cockpit accelerations of $\pm 0.4$g, with a $\Delta n_{1o}$ of 0.28g, recorded in a prototype Trident I (ref. 16), were rated by the crew as unacceptable. If this is compared with the Boeing 707 values above, the vibration should have been acceptable. However, whilst the report did not indicate why the vibration was considered too severe to be accepted, it is interesting to note that the predominant vibration mode was at 5.5 Hz, i.e. in the range where the performance of tasks involving the skilled use of hand and eye is most easily degraded. On the other hand, it would be expected that the predominant response of the Boeing 707 would be at a much lower frequency.

Thus runway unevenness can induce vibrations in aircraft of such frequencies, and sufficient amplitude, as to cause not only structural fatigue and crew and passenger discomfort, but also in some severe cases a hazard to safety. There is little the pilot can do to reduce the response other than taxi at a very low speed (ref. 3). However, the speed of the aircraft, particularly on take-off and landing runs of course, is dictated by other operational requirements, as is the control of lift.

Mitchell has produced evidence (ref. 8) to show that when the cockpit acceleration exceeds about 0.3g the control column is moved in sympathy with the acceleration; the pilot is trying, possibly subconsciously, to reduce the acceleration. However, his action may well have the opposite effect. Operational data has shown (ref. 17) that for the case of hard landings pilot attempts to correct the effects of an initial bounce usually resulted in increased structural loads on the second bounce due to the differently phased responses of the aircraft and the control system.

Criteria for runway profile unevenness may be expressed in several ways, the two major methods being (a) deterministic, and (b) power spectral. The deterministic method usually defines the measured profile, the actual profile defined by measurements made at regular intervals. Unevenness criteria may be expressed as deviations from a straight edge placed on the runway surface. The PSD of an actual or measured runway profile will produce a line such as those presented in figure 1.2. Clearly more regular curves than these are desirable for use as unevenness criteria, and most proposals have been in the form of straight lines on the log-log scales. In spite of the disadvantages of the power spectral method of depicting criteria, and the condemnation of the method by several authors (refs 4, 5, 18, 19) as being insufficient to define acceptable levels of runway unevenness, most criteria have been proposed in power spectral terms. Some, however, have been proposed in other terms.

A proposal by Milwitzky (ref. 3) suggests criteria in the form of maximum deviations from straight edges placed on the runway.

Figure 1(i) shows the average peak amplitude $\sigma'$ of the unevenness within any given horizontal distance **L**.
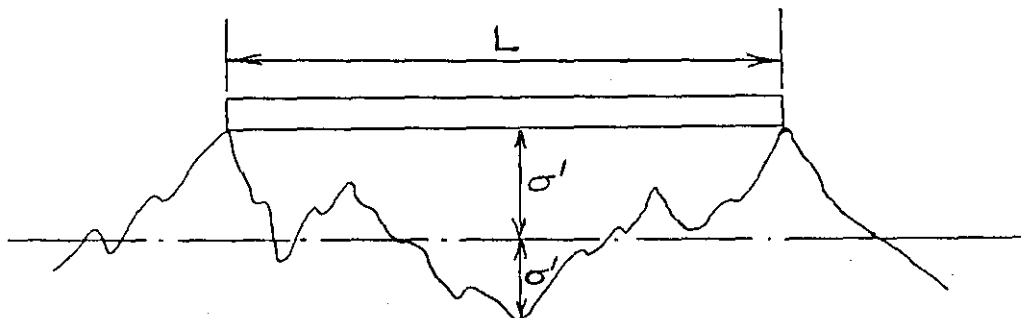


Fig. 1 (i)

Maximum deviations $2\sigma'$, for "new construction" and "needs repair", were based on measurements of a very good commercial runway, and are shown in table 1(i).

| | Straight edge length (feet) | Maximum deviation from straight edge, $2\sigma'$ (inches) | |
| --- | --- | --- | --- |
| | | Milwitzky | Houbolt |
| New construction | 17<br>80<br>150 | .156<br>.281<br>.344 | .144<br>.313<br>.428 |
| Needs repair | 17<br>80<br>150 | .313<br>.562<br>.688 | .250<br>.543<br>.741 |

Table 1(i)

It is worthy of note that Milwitzky's criteria were published in 1959, at which time the runway wavelengths of concern were about 17 to 150 feet. Because the upper limit of wavelengths of concern is now of

the order of 500 feet, criteria expressed in this way should now include maximum deviations over much longer wavelengths.

Milwitzky also produced power spectra corresponding to the above criteria. These are shown in figure 1.4, together with the power spectra of the four runways examined.

In a review of previous runway unevenness studies (ref.20) Houbolt sets out criteria, similar to those shown in figure 1.4. His criterion for new construction is

$$\phi(\Omega) = \frac{6.7 \times 10^{-6}}{\Omega^2} \text{ ft}^2/\text{rad}/\text{ft} \qquad (1-1)$$

and for "needs repair" is

$$\phi(\Omega) = \frac{20 \times 10^{-6}}{\Omega^2} \text{ ft}^2/\text{rad}/\text{ft} \qquad (1-2)$$

The criterion for new construction yields a value for maximum deviation from the mean in a length L ft of $0.00146\sqrt{L}$. This may be derived as shown in Appendix A, and corresponds to Milwitzky's $\sigma'$ in figure 1(i), so that the maximum deviation from a straight edge placed on the runway, for new construction, is given by

$$2\sigma' = 0.00292\sqrt{L} \text{ ft} \qquad (1-3)$$

Similarly, the "needs repair" criterion yields

$$2\sigma' = 0.00505\sqrt{L} \text{ ft} \qquad (1-4)$$

Table 1(i) compares Milwitzky's maximum deviation criteria with those calculated from equations (1 - 3) and (1 - 4). In Houbolt's criteria the deviations for "needs repair" are $\sqrt{3}$ times those for "new construction", whereas the corresponding factor in Milwitzky's criteria is 2.

Houbolt also derives a central deviation $\delta$ between a

straight edge and the runway.    Referring to figure 1(ii), the

central deviation $\delta$ from a straight edge of length L, for the "hew
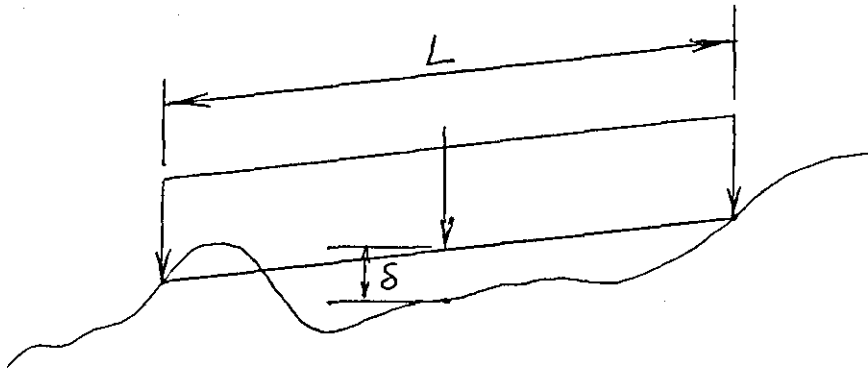


Fig. 1 (ii)

construction" criterion, is derived as

$$\delta = 0.00324 \sqrt{L} \text{ ft} \qquad\qquad (1 - 5)$$

Comparing $\delta$ in figure 1(ii) with $2\sigma'$ in figure 1(i), and noting

that $2\sigma'$ is a maximum deviation, whilst $\delta$ is a central deviation,

and also that whilst Milwitzky's straight edge is an actual straight

edge placed on the runway surface, Houbolt's "straight edge" is in

fact a straight line drawn between any two points on the runway

profile, and can thus "cut off" peaks as shown in the figure, it is

felt that $\delta$ cannot possibly be greater than $2\sigma'$ .    It would

indeed be possible for $\delta$ to be a negative quantity.    A suggested

value of central deviation from a straight edge of length L, to

replace Houbolt's value in equation (1 - 5) is

$$\delta = 0.00206 \sqrt{L} \text{ ft} \qquad\qquad (1 - 6)$$

This is derived in Appendix A, where it is also proved that $\delta$ cannot

indeed exceed $2\sigma'$ , and could be expected to be of the order of $\sqrt{2}\,\sigma'$.

The United States Air Force specification MIL-A-008862A(USAF)

also quotes runway unevenness criteria in terms of "straight-line"

PSD's, the criterion for a paved runway being

$$\phi(\Omega) = \frac{27.8 \times 10^{-6}}{1.77} \text{ ft}^2/\text{rad/ft} \qquad (1-7)$$

The specification also states that acceptable runway roughness shall
be in accordance with the data specified in figure 1.5. This shows
a further means of expressing criteria, the height of discrete
(1 - cosine) undulations being plotted against their wavelengths.

Coleman and Hall have shown (ref. 4) what level of
smoothness could be obtained with the construction criteria which had
been used for many years. The maximum permissible deviation for
most runways constructed since about 1945 had been $\pm\frac{1}{8}$ inch from a
straight edge, 10 to 16 feet long, placed on the runway surface.
This permissible deviation represented a compromise between increased
construction costs and increased roughness. An indication of the
level of smoothness which could be realized under these criteria is
shown in figure 1.6 (reproduced from ref. 4). The power spectrum
of roughness of a new runway at an international commercial airport
is far below that specified by Milwitzky's criterion for new
construction. Experience with a number of runways had indicated that
a runway would be satisfactory for most, if not all, aircraft current
at that time (1963) provided its roughness power spectrum did not
exceed the "new construction" line.

In general then, newly constructed runways have had a
satisfactory level of smoothness. Of major concern has been the
development of roughness as the runway deteriorates with age and usage.

This deterioration may be general, such as would be expected to be caused by settling of the runway base or movement of the surface due to environmental changes, or more localized, such as would be caused by landing impacts or auxiliary runway construction.

It has been indicated (ref. 4) that runway roughness power spectra are not a reliable basis for judging when a runway needs repair. The major reason for this is the inherent limitation of the spectrum for describing the detailed characteristics and location of the roughness, when the roughness is localized. In an investigation of the location and simulated repair of rough areas of a given runway (ref. 19) Hall and Kopelson used analogue techniques of analysis. The aircraft was simulated by a very simple mathematical model incorporating rigid body heave and pitch only, and undercarriages with linear characteristics. The time histories of the simulated responses to 3 runways indicated several distinct runway irregularities as being the primary cause of the various peak responses. The "runway repairs" were made simply by "cutting off" peaks on the runway surface by means of horizontal lines produced by a diode limiting circuit. Considerable reduction in response of the aircraft was obtained in this manner. However, a comparison of time histories of 2 runways showed that one was rougher in most cases than the other, whereas the power spectra indicated about the same roughness. Thus, power spectra based on whole runway averages did not appear to be suitable for this type of problem, where specific areas were of interest.

Most of the published data on runway roughness is also in PSD form. In addition to the limitations of the method already discussed, the applicability of much of this data is limited for the following reasons:

(a) Most of the data was obtained in the late 1950's. Thus it may not be representative of the runways as they exist today, and in general the spectra were calculated to cover only the range of wavelengths of concern at that time, i.e. up to about 150 feet.

(b) Many of the published spectra may be in error (ref. 21). The PSD's at the longer wavelengths have been overestimated due to a contaminating effect of very long wavelengths such as runway grades. It is for this reason that the values of root-mean-square roughness derived from the power spectra have not been considered a reliable measure of runway roughness, since most of the rms value comes from wavelengths in excess of about 60 feet.

(c) Most of the data is single-track, thus providing no information for the determination of roll response to runway unevenness.

With regard to this last limitation, Wignot et al have shown (ref. 22) that analyses which assumed the unevenness to be uniform across the runway overestimated the cg response by factors of about 1.5 to 2.0. However, this result should be viewed with reservation, since the single-track analysis used in the comparisons used a single gear representation of the aircraft, no pitching contribution from the runway being considered. Since the aircraft

pitching motion contributes significantly to the wing bending (ref. 22)
it might well also modify the contribution to the cg response from
the flexible modes, and hence modify the results of the single-
track analysis above. Experience on the Constellation, the L188
and the P-3 aircraft have shown (ref. 23) that anti-symmetric and
symmetric modes were approximately equally excited, whilst on the
C130 and the C-141A rigid rolling occurred, but the anti-symmetric
elastic modes were not excited significantly.

There is evidence then, although not conclusive, that the
use of 3-track profiles might be desirable in analyses. Morris
(ref. 24) has presented 3-track runway elevation profiles for 2
operational runways at United States Government installations, the
profiles being defined along the centre-line of each runway and
along tracks 10 feet on either side of the centre-line, and Wignot
et al (ref. 22) have presented a method of developing properly
correlated tracks, for any wheel tread, from longitudinal profiles
at small lateral intervals across a runway. The task of collecting
the vast amount of data which would be required to produce such
correlated tracks, for many runways, would be almost prohibitive.
Furthermore, it is felt that as long wavelengths in the runway
unevenness are more significant in exciting response of larger more
flexible aircraft, since the anti-symmetric component of runway
unevenness is less significant at longer wavelengths, 3-track
analysis may not be so important for later generations of aircraft.

Finally, although much has been said about runways, it must

be remembered that aircraft spend in the region of 80% of their ground manoeuvring time on taxiways, which are generally rougher than runways and are not surveyed.

## 1.2 Analytical methods of estimating the dynamic response.

Analytical methods of estimating the dynamic response of an aircraft to runway unevenness during taxiing fall into two broad categories:

(a) deterministic, and

(b) statistical.

In order for the exact response of a particular aircraft taxiing along a given runway to be obtained by deterministic means the requirements are simply:

(a) the equations of motion of the airframe,

(b) an accurate mathematical description of the undercarriages, and

(c) an accurately measured runway profile.

The accuracy with which the above requirements are formulated dictates the accuracy of the results.

Requirements (a) and (c) are relatively easily obtained; the elastic modes and frequencies of the airframe can be determined with a high degree of reliability, and runway profiles can be measured to an acceptable degree of reproduction. However, the second requirement is not so easily obtained. The oleo-pneumatic undercarriage unit is extremely non-linear, particularly over large displacements. The stiffness depends on the polytropic compression and expansion of air in a tube, damping is by oil being forced through orifices, and friction is present between the sliding members of the oleo; tyres also have mild non-linearities. Many other factors have an effect on the non-linearities.

However, oleo stroking displacements are relatively small during taxiing. Experimental investigations by the present author (ref. 2) indicated that at very low oleo stroking velocities compression was almost isothermal and orifice damping was negligible, all the useful damping being provided by friction in the seals. Furthermore, this friction did not produce the classical Coulomb friction, $\pm F$, but a damping effect dependent on the nth power of the stroking velocity, where n is less than unity.

Notwithstanding the above complications, very good mathematical models of the undercarriage system can be formulated, and thus the deterministic approach can be made to yield good results.

The power spectral approach is easily applied if the equations are linear. However, since the undercarriage system is non-linear, methods used in general try to arrive at near equivalent linearized systems. Thus the same degree of accuracy may not be expected from a power spectral analysis. Furthermore, detailed information about the response, such as peak values, cannot be obtained, but only statistical information such as root mean square values. However, if the nature of the random process is known, expected peak values may be predicted.

It is now generally considered that there is a place for both categories of analysis in the investigation of runway unevenness induced vibrations; the deterministic method is incomparable for specific studies such as the response of a particular aircraft at say

a runway intersection, whilst the power spectral techniques can provide a concise and extremely useful method for such studies as the effects of parameter variations.

1.2.1 Deterministic Solution

The deterministic method of analysis consists briefly of:

(a) setting up the coupled differential equations of motion of the airframe and undercarriage system which govern the response,

(b) determining the forcing functions, or inputs, to be introduced into these equations, and

(c) solving these equations of motion by digital or analogue means.

In a digital computer study (ref. 13) the dynamic responses of the Boeing 707 aircraft and the proposed Boeing 733-94 supersonic aircraft were computed using deterministic runway input. The analysis considered only symmetrical modes, 2 rigid body and 6 flexural, and the undercarriage models incorporated non-linear oleos with Coulomb friction, and linear (but undamped) tyres. The 10 coupled differential equations of motion were solved by a numerical step-by-step method using an IBM 7090 digital computer. The time required to compute the response of the 707 aircraft for a run of 3000 feet at 100 ft/s was about 32 minutes when 6 elastic modes were included and about 10.5 minutes when only the rigid body modes were included.

The large computer times required is one of the major

disadvantages of the deterministic methods where actual runway

profiles are to be used as input. The conventional methods of

solution of the differential equations of motion involve numerical

step-by-step or forward integration procedures. In computations

on the effects of runway unevenness on a supersonic transport

aircraft (ref. 14) Mitchell used a relatively simple mathematical

model of the aircraft, incorporating rigid body heave and pitch

and symmetrical flexural modes, non-linear undercarriages, and

aerodynamic lift and pitching moment. A fourth-order Runge-Kutta

step-by-step integration routine was used, runs being made with a

number of different step lengths to find a value for which the

integration converged to give results that did not vary with step

length. The final step lengths and computer times were not

stated, but it was stated that the simplifications had been made

to reduce computing time, and thus make practicable the study of

the influence of several undercarriage parameters on the dynamic

loads during taxiing. The quality of agreement of calculations

for Concorde with flight measurements was very good, the measured

vibration being 0.8 of the predicted. However, agreements with

this program had not always been that good; the measured cockpit

acceleration on a VC 10 had been only 0.6 of that calculated,

whilst main undercarriage rms loads for the P-3A were over-

estimated by up to a factor of 3.

In a deterministic method for the optimisation of

undercarriage suspension characteristics (ref. 25) an extremely

ambitious mathematical model was selected. It included both symmetric

and asymmetric modes of vibration, and complicated undercarriage non-linearities. The analysis was not restricted to small motion, and therefore many effects were included which might normally be considered negligible. The equations of motion were to be solved using a Runge-Kutta numerical forward integration procedure, a complicated cost function being optimised by means of a Rosenbrock technique, and were programmed for solution on a large digital computer. However, the number of time increments required for an acceptably accurate solution was large, and for optimisation studies using this program the computer time was prohibitive. Even employing simplifications, feasible use of the program was thought to be limited. Hence, an alternative method was proposed using a much simpler model (symmetric, 2-dimensional) and a hybrid computer.

Another very complicated mathematical model was used by Wignot et al (ref. 22) in a deterministic analysis, the equations of motion being integrated numerically by means of a linear integration subroutine using a fixed integration interval. An integration interval of 0.0002 seconds gave good accuracy in most cases.

It will be seen from the above examples that the computer time required for the large number of runs required in optimisation, or in investigations of the effects of parameter variations, using a deterministic method with a very complicated model is prohibitive. The model must be greatly simplified, and even then the computer time is great, very short time intervals being required along the runway for accuracy.

However, the disturbance under investigation may be quite discrete in nature;    there is a very valuable place in analysis for discrete bumps such as steps or ramps.    Wignot et al.(ref.22) list several bump shapes which have been used in reports concerning unprepared runways.    An obvious advantage of using discrete bumps is that the computer time required to find the response to a short series of discrete bumps is much less than that required to find the response over an entire runway;    this is one reason why discrete bumps analysis has been popular with aircraft manufacturers. A disadvantage is that the mixed wavelengths found in the natural runway are not represented.

Thus, it is important that the mathematical representation of the aircraft be as complete and detailed as is practical, bearing in mind the types of result required and the need to economise as much as possible on computer time.    Wignot et al (ref. 22) suggest programs of varying refinement, the types of model they employed ranging from an idealized linear single-degree-of-freedom system, used in studies relating to parameter variations, to a 3-gear flexible system with non-linear undercarriages, used for correlation with experience.

The deterministic method can be used equally well on hybrid and analogue computers, the selection of the type of computer to use being dependent on the nature of the work to be performed. Hybrid and analogue computers are most efficient where a high yield is required with only minor changes in input.    An example is the

work done by Hall and Kopelson on the location and simulated repair
of rough areas of a runway (ref. 19).    However, set-up and check-
out time on complex programs can be very time consuming, so that
a digital program would be more efficient where a variety of
individual cases are to be processed, the results of one run being
required to determine data for the next run.

### 1.2.2  Statistical analysis by the power spectral density method

The power spectrum of runway elevation fluctuations
provides a description of the frequency content of the runway
height variations.    Since runway unevenness is a space disturbance
rather than a disturbance in time, it is often desirable to define
the power spectral density in terms of the frequency argument $\Omega$
in radians per foot, rather than $\omega$ in radians per second, in which
case the power spectral density function $\phi(\Omega)$ of the disturbance
y(x) is defined as :

$$\phi(\Omega) = \lim_{X \to \infty} \frac{1}{2\pi X} \left| \int_{-X}^{X} y(x) e^{-i\Omega x} dx \right|^2 \quad (1-8)$$

Whilst the PSD function may be evaluated directly from
observed data by use of equation (1-8), it has been found more
convenient and less tedious in practice to make use of the
autocorrelation function $R(\chi)$, defined as:

$$R(\chi) = \lim_{X \to \infty} \frac{1}{2X} \int_{-X}^{X} y(x) \, y(x+\chi) \, dx \quad (1-9)$$

This function has the symmetrical property $R(\chi) = R(-\chi)$, and is
related to the PSD function by a Fourier cosine transform pair,
so that :

$$\phi(\Omega) = \frac{2}{\pi} \int_0^\infty R(x) \cos \Omega x \, dx \quad\quad (1-10)$$

$$R(x) = \int_0^\infty \phi(\Omega) \cos \Omega x \, d\Omega \quad\quad (1-11)$$

From equations (1-9) and (1-11)

$$R(o) = \overline{y^2(x)} = \sigma^2 = \int_0^\infty \phi(\Omega) \, d\Omega \quad (1-12)$$

Ideally, the values of elevation of the runway profile from which the power spectrum is to be calculated should have a zero mean value, and the sampling length should be long enough to give a reliable estimate of the average values calculated. Unfortunately runway profiles generally have a non-zero mean, and long wavelength trends. There may also be distortion of the data points in the form of extraneous "noise" signals, caused by such things as instrument limitations. For these reasons the runway data is usually modified during its processing so that the final spectrum obtained is a true reflection of the roughness which is important to the aircraft response problem. The details of the operations used are not important to this discussion, and have been described many times elsewhere (see for example refs. 26 to 30), together with descriptions of the basic power spectral theory referred to above (see also 20, 31, 32).

The statistical expressions in equations (1-8) to (1-12) may be expressed in terms of the circular frequency $\omega$. The frequencies, wavelengths of unevenness, and associated spectra are related as follows:

$$\Omega = \frac{2\pi}{L} = \frac{\omega}{V} \quad\quad (1-13)$$

$$\bar{\phi}(\Omega) = V \cdot \bar{\phi}(\omega) \qquad\qquad (1 - 14)$$

The use of a lower integration limit of $\Omega = 0$ in expression (1-12) implies that unevenness with infinite wavelength exists in the runway profile. The rms value of unevenness contained within wavelengths below a certain finite length L is normally required, so that a lower limit of $\Omega = \dfrac{2\pi}{L_1}$ is usually used. Similarly, wavelengths below say $L_2$ would not be expected to excite measurable response in a given aircraft, and in any case wavelengths below 4 feet have not been adequately specified by most measured data, so that equation (1-12) usually becomes

$$\overline{y^2}(x) = \sigma^2 = \int_{\Omega_1 = \frac{2\pi}{L_1}}^{\Omega_2 = \frac{2\pi}{L_2}} \bar{\phi}(\Omega)\, d\Omega \qquad (1 - 15)$$

The power spectrum of any desired response quantity is related to the power spectrum of the runway unevenness through the frequency response function for the response quantity under consideration. The frequency response function is defined as the response due to a unit sinusoidal input of varying frequencies, and reflects the dynamic characteristics of the airframe and undercarriage system in the output. The statistical properties of the response time history may thus be deduced without actually evaluating the time history. Thus, the PSD of the response acceleration, $\bar{\phi}_{\ddot{x}}(\omega)$, is given by

$$\bar{\phi}_{\ddot{x}}(\omega) = \omega^4 \, \bar{\phi}_x(\omega)$$
$$= \omega^4 \, H_{\frac{x}{y}}^2(\omega) \cdot \bar{\phi}_y(\omega) \qquad (1 - 16)$$

from which the mean square value of response acceleration is given by

$$\overline{\ddot{x}^2} = \int_{\omega_1}^{\omega_2} \Phi_{\ddot{x}}(\omega)\, d\omega \qquad (1-17)$$

Equation (1-16) relies on the assumption of a time-invariant linear system, giving a unique frequency response function, that the response is due to a single input, and that the input is a stationary random process, some of the statistical results which may be obtained relying on the assumption that the random process is Gaussian in its distribution.

Power spectral techniques of analysis have been developed to a large extent in the analysis of aircraft response to atmospheric gusts. Atmospheric turbulence may be fairly uniform over regions of many miles. Furthermore, an aircraft traversing continuous turbulence will encounter a different environment from a time history viewpoint than an aircraft which traversed the same area the previous day, so that it has been found very realistic to describe atmospheric turbulence as a continuous stationary random process.

Compared to the atmosphere and its properties, the surface unevenness environment provided by runways is deterministic in character. Two aircraft passing along the runway on successive days should encounter identical environments, assuming of course that either the aircraft follow the same track or the runway profile is invariant across the width of the runway. Furthermore, runway roughness is often found to be quite localized, the bump shapes which may be encountered being of a wide variety, but not necessarily

occurring as a continuous random profile. However, for good

quality runways in commercial use, having rms displacements less

than 0.06 feet, the probability density function can be considered

Gaussian (ref. 33). It is worthy of note that approximately half

the surfaces surveyed in reference 26 came into this category of

smoothness. For rougher surfaces Gaussian distribution could

not be assured without further investigation.

It is now generally considered that, particularly where

analysis is being made which concerns response to a large number of

runways, the assumption that the profiles are stationary random

processes, with statistical properties similar to those of known

surveyed runways, is valid.

A more important obstacle to applying a statistical

analysis to the aircraft taxiing problem is that of non-linearities

in the undercarriages. The equations of motion of the airframe

may be considered essentially linear in character, and hence gust

analysis has no such problem in this respect. Similarly, the

airframe equations provide little problem for the ground case. The

undercarriage units, however, as already discussed, are highly non-

linear. Morris (refs 7, 18) found that aircraft transfer functions

computed from the ratio of the response acceleration spectra of

aircraft to the runway input spectra varied significantly between

repeated runs for similar test conditions and did not define a unique

transfer function which was independent of amplitude and aircraft

speed.

Since it is not possible to make a direct application of the theory of random processes to non-linear systems, if the method is to be used resort must be made to linearized systems. The accuracy now then will depend not only on the complexity of the model, but on the ability of the linearization method used to give a true representation of the model.

Two important methods of linearization have been developed by Crandall (ref. 34) and Caughey (ref. 35). These are the Perturbation Technique and the Equivalent Linearization Technique respectively. The application of these methods to the non-linear undercarriage characteristics of a taxiing aircraft has been discussed by Tung, Penzien and Horonjeff (ref. 13). Neither method was directly applicable to the problem, both methods having certain disadvantages for some types of non-linearities. It was suggested that an engineering solution to the problem might be to first use the equivalent linearization method to determine the equivalent linear damping coefficients of the non-linear damping forces and the Coulomb friction forces for both landing gears, considering the aircraft as a single-degree-of-freedom system, and then apply the perturbation method with an equivalent linear damping coefficient and a polynomial representation for the non-linear air spring force, considering the system as a multi-degree-of-freedom system. The reference does not, however, present a program for the implementation of this solution.

Linear models do, however, have an important place in

analysis. Such a model was used by Hall and Kopelson (ref. 19) in the runway repair studies already described. Whilst it was realized that the actual aircraft landing gear could not be easily approximated by linearization, the simulated aircraft was believed to represent a typical jet transport in that the resonant frequencies of the 2 rigid body modes were representative. Thus, although the magnitude of acceleration response to a given input was questionable, it was thought that the relative response to runway roughness would indicate which sections of the runway caused the most severe response, and that these same areas would produce the most severe response in an actual aircraft having the same resonant frequencies in heave and pitch.

Runway unevenness normally constitutes 3 inputs, through the nose wheel and the 2 main wheels. The assumption of multiple inputs can greatly increase the complexity of the analysis, and requires considerably more measured runway data, if indeed measured data is to be used. In a comparison of predicted responses of vehicle components to random road-surface undulations with those actually measured on the vehicle (ref. 36) Robson and Dodds applied standard techniques of random vibration analysis to a series of analytical models of increasing complexity. The models varied from a very simple 2-degree-of-freedom linear system, subjected to a single random displacement input, to a 4-wheel model requiring 4 inputs. For the particular vehicle and road surface used, the 4-input model gave virtually no improvement in accuracy over the 2-input model, and even the single-input model gave remarkably good

results considering its simplicity. However, with systems having

resonances of the order of say 10 Hz a 4-input model should give

better results, since the anti-symmetric component from the surface

would be much more significant at this frequency.

The report concluded that simple random vibration theory

is relevant to vehicle response analysis, though care must be taken

to match the sophistication of the model to the needs of the

particular problem; increased sophistication may not be justified

in terms of increased accuracy, since the spectral description of

roads may still contain important sources of error arising both

from difficulties of analysis and measurement.

In order to simplify runway input data mathematical

expressions have been proposed to approximate the power spectra of

runway profile displacements. The most common have been single

straight lines on the log-log axes of PSD against frequency, with

expressions of the form

$$\phi(\Omega) = \frac{\bar{C}}{\Omega^n} \qquad (1 - 18)$$

Silsby (ref. 12), Kirk (ref. 37) and Kirk and Perry (ref. 38) have

all used expressions of this form in statistical analyses, using

the values proposed by Houbolt (ref. 20), i.e. $n = 2$, and $\bar{C} = 6.7 \times 10^{-6}$

for good and rough runways respectively. One American aircraft

company uses expressions of this form with 2 sets of values:

(a) $\bar{C} = 174 \times 10^{-6}$ and $n = 2$, and (b) $\bar{C} = 5.777 \times 10^{-6}$ and $n = 2.576$

(ref. 22).

As an aid to including PSD representations of various environments in computer programs, Wignot et al (ref. 22) have proposed an expression of the form

$$\phi(\Omega) = \frac{\overline{C_1}}{\Omega^{n_1}} + \frac{\overline{C_2}}{\Omega^{n_2}} \qquad (1 - 19)$$

which results in a curve with two linear segments on the log-log axes.

In a statistical analysis to determine the response of an aircraft with rigid vertical translation and one flexible mode (ref. 39), Kirk used an input PSD function of the form.

$$\phi(\Omega) = \frac{1}{A\Omega^3 + B\Omega^2 + C\Omega} \qquad (1 - 20)$$

The values of A, B and C were found by matching the function at 3 values of $\Omega$ to an actual PSD curve. A different function of the form of equation (1-20) was determined for each taxiing velocity V, the values of $\Omega$ used in the matching being chosen quite close together in the region of the major peak of the frequency response function.

Silsby has applied the power spectral method of analysis to compute the uncoupled heave-pitch response of a rigid aircraft, with linear undercarriages, to random runway unevenness (ref. 12). Kirk (ref. 37) has extended Silsby's analysis to include non-linear oleo damping and Coulomb friction. He used a method developed by Kirk and Perry (ref. 38) to obtain an equivalent linear damping coefficient which dissipated the same average energy during random

vibration as the non-linear damping and Coulomb friction. $\sqrt{}$ Wignot
et al (ref. 22) had shown that if this method is used with the
assumption that the motion is simple harmonic the equivalent linear
viscous damping coefficient obtained underestimates the actual
damping. $\sqrt{}$ It was assumed that the damping was symmetric, and
the oleos never locked. The equivalent linear damping coefficient
was calculated from the root-mean-square value of the oleo stroking
velocity, using an iterative process. In all other respects the
analysis was similar to Silsby's, the heave and pitch being analysed
separately and their complex frequency response functions added to
obtain the final response.

Both Silsby and Kirk investigated the effect of taxiing
velocity on response, Kirk in particular showing interesting
undulations on the curves of cg and pilot location acceleration
against taxiing velocity. These results will be discussed in
sub-section 1.4.

Cook and Milwitzky have suggested (ref. 40) that for
landing impact calculations the effects of rigid body-elastic mode
interaction can be approximately taken into account by considering
the oleo force produced by the interaction of the rigid body heave
mode with the first symmetric elastic mode, the resulting oleo force
being used to obtain the responses in the individual higher modes,
which are assumed to be uncoupled. This neglect of coupling can
only be justified of course if the modal frequencies are well
separated. In a statistical analysis of taxiing induced vibrations
in aircraft (ref. 38) Kirk and Perry used a mathematical model based

on this suggestion, and used the iterative method described above
for computing the equivalent linear damping coefficient. A single
random input was assumed, account being taken of the rigid body
heave mode of the aircraft and the first symmetrical flexural mode
of the airframe. A wheel mass was included, with a tyre having
linear stiffness and no damping, and the oleo was assumed to have
a linear spring, with stiffness equal to the slope of the air
spring compression curve of the oleo at the static equilibrium
position. After findings published in references 13 and 41, the
latter assumption was expected to lead to an overestimate of taxiing
dynamic response.

The mathematical representation of the aircraft consisted
of a 3 mass system whose parameters were derived in a rather
interesting way. The equations of motion of the rigid body heave
and first elastic modes of an airframe were written thus:

for the rigid body mode,

$$M_0 \ddot{a}_0 = -F_s \qquad\qquad (1 - 21)$$

for the first elastic mode,

$$M_1 \ddot{a}_1 + C_1 \dot{a}_1 + M_1 \omega_1^2 a_1 = -F_s \xi_1 \qquad\qquad (1 - 22)$$

The top 2 masses of the 3-mass system, and the linear spring and
damper connecting them, were made dynamically equivalent to
equations (1-21) and (1-22), so that their masses and the stiffness
and damping were expressed in terms of the parameters in these
equations; the representation of the oleo and the wheel and tyre
was independent of the system resting on the oleo.

The response acceleration of a Boeing 707 aircraft was

calculated, and found to be 50% greater than that calculated in
reference 13 by a deterministic method using 6 flexural modes.
It was concluded from this that the spectral method of analysis
overestimates rms response by about 50%, the discrepancy being
attributed to the assumption of stationarity, and that the method
yields an upper bound on response. However, elastic modes above
the first were neglected in this analysis; it will be shown in
sub-section 4.3.1 that considerable care must be taken in the
selection of modes to neglect if accurate estimates of response
are to be obtained.

In a further work on this subject (ref. 39) Kirk used the
same method of analysis as above, but used a runway unevenness PSD
input of the form of equation (1-20). The variation of response
with taxiing velocity was computed, this time the curve showing only
mild undulations compared to the large undulations found in
reference 37. It will be shown in sub-section 4.3.2.1 that these
mild undulations are of the form one would expect if pitching is
neglected.

1. 3  Effect of flexural modes

Although several authors have commented on the effect on
calculated response of neglecting all flexural modes of the
airframe, no investigations appear to have been made on the effects
of individual modes.   Furthermore, agreement on the effect of
neglecting all flexural modes has not been good.   For example,
failure to include the flexural modes led to an overestimate of main
and nose tyre forces and undercarriage loads on a Boeing 707 and
the proposed supersonic Boeing 733-94 (ref. 13), but did not
significantly alter those on the Constellation (ref. 22).   Cook
and Milwitzky found (ref. 40) that on one aircraft neglect of the
flexural modes led to an overestimate of undercarriage loads, and
subsequent overestimate of structural loads, but on another aircraft,
with higher structural frequencies (i.e. a relatively stiff aircraft),
the effects of dynamic magnification when flexural modes were
included more than overcame the reduction in landing gear force due
to rigid body-flexural mode interaction, resulting in increased
structural loads.

It was also observed in reference 13 that the inclusion of
flexural modes in the dynamic analysis reduced the magnitude of the
rigid body translation.   However, it should be noted that it was
the rigid body mode generalized co-ordinate which was reduced, and
not the total cg displacement.   On the other hand, contributions
from the flexural modes increased the rigid body acceleration levels
by approximately 20% for the C-141A (ref. 22), whilst on the

Constellation the rigid body motions of the aircraft were not
significantly altered by the addition of flexural modes, since the
driving gear forces were not significantly altered, although the true
cg acceleration, including the flexural mode contributions, was
significantly increased, as was the pilot compartment acceleration,
the dynamic magnification factors due to flexural modes being
approximately 1.25 to 1.50 for the cg and 1.90 for the pilot location.
Similarly the inclusion of flexural mode response gave considerably
higher accelerations in the pilot compartment at higher frequencies
for the Boeings (ref. 13), but the pilot compartment response
displacement was due primarily to rigid body rotation.

There has been general agreement that to be sure of
accurate results it is necessary to include the flexural modes in
analysis, particularly for response at the pilot location.  However,
the significance of the number of flexural modes selected for
inclusion in an analysis depends on the aircraft response quantity
being investigated.  Wignot et al have shown (ref. 22) that the
internal loads at the extremities, such as the outer wing panels,
will require a greater number of modes to define the loads than will
the wing root, fuselage, and landing gear.  It is perhaps also
clear from the above that if it is desired to neglect flexural
modes in the interest of ease of analysis, or economy of computer
time, an investigation must be made for the individual aircraft in
order to determine the effect.

## 1. 4 Parameter variations

In general, parameters which may affect the aircraft response may be associated with the landing gear, the airframe, or the operations. This discussion will be limited to variation of taxiing velocity, and those parameters associated with the landing gear, since the following computer studies will be concerned with these parameters.

It is now well known that the response of an aircraft increases as the taxiing speed increases. In power spectral terms, if a linear system is assumed, and it is assumed that the runway input spectrum is of the form

$$\overline{\phi}(\omega) = \frac{\overline{cv}}{\omega^2},$$

it can easily be shown that the mean-square value of response is proportional to the taxiing velocity V. Taxi tests on a B-29 aircraft (ref. 42) produced linear results for lower taxiing velocities, but showed a drop-off in the mean-square acceleration at higher velocities, which was attributed to the more frequent overcoming of stiction, and therefore more oleo sliding movement, at the higher velocities, producing more damping.

Milwitzky (ref. 3) and Silsby (ref. 12) have both produced by theoretical analysis, and Morris (ref. 6) by actual measurements on aircraft, curves of response at the cg and pilot

locations against taxiing velocity, which have shown slight undulations.
In a statistical analysis of uncoupled heave-pitch response (ref.37)
Kirk has shown pronounced undulations on the curves of response
against velocity for a Boeing 707, particularly at the pilot
compartment (fig. 1.7). The undulations on the curve for the
pilot compartment were shown to be caused by phasing of the pitch
frequency response with the nosewheel-mainwheel lag frequency
response. It will be seen that, neglecting the undulations, the
general trend of the curves shows the response to be approximately
proportional to the square root of the taxiing velocity, as
indicated in reference 42. There is a drop-off at the high
velocities due to the effect of the last peak.

Mitchell has shown (ref. 8) in actual measurements during
airline operations that the maximum cockpit acceleration in a Boeing
707 during take-off is likely to occur at approximately 80 or 120
knots, which shows a fair agreement with Kirk's curves, whilst
Concorde (ref. 14) reached its maximum response at 120 knots. In
a later statistical analysis (ref. 39), this time neglecting the
rigid body pitch mode but incorporating the first flexural mode,
Kirk showed very mild undulations on the cg response-velocity
curve for a Boeing 707, the maximum response occurring at 124 knots.

The effect of oleo airspring stiffness on response has
not been extensively investigated, but in general a reduction in
oleo airspring stiffness results in a reduction in aircraft response.
Wignot et al (ref. 22) have shown that the significant parameter is
the combined effective stiffness of the tyre and oleo in series.

A large tyre stiffness change only has a small effect on this parameter, and hence causes only a slight change in aircraft response. However, analytical studies made on a Constellation aircraft indicated that softening of the maingear airspring by a factor of 2, which resulted in a reduction of about 30% in equivalent linear stiffness of the oleo and tyre in series, reduced both the passenger and crew station accelerations by 25%. Kirk has compared the effects of two linearized airspring stiffnesses (ref. 39), corresponding to isothermal compression (n = 1.0) and isentropic compression (n = 1.3), and found that the stiffer airspring yielded rms responses at the cg which were 25% greater than those yielded by the softer spring.

It must be remembered that with the non-linear oleo airspring the stiffness depends on the compression, and hence will be affected by anything which affects the compression. The stiffness will be greatest at the aircraft's maximum all-up weight, and Kirk and Perry have shown (ref. 38) that the response of the aircraft increases as its weight increases. Similarly, Vignot et al have shown (ref. 22) that the neglect of lift in a dynamic analysis can lead to an overestimate in response of up to 50% at the final stage of a take-off run. The stiffness of the nose gear will increase with braking or with down elevator, causing an increase in pitching response, and hence response acceleration at the pilot location (refs. 8, 22).

The most important parameters for Concorde are the airspring stiffness, and friction, of the main undercarriage (ref. 14), the response generally decreasing as the stiffness is reduced.

However, to obtain the potential benefit, the softer the spring, the lower the oleo friction must be.

Variation in oleo damping appears to be less effective than variation in oleo stiffness in reducing aircraft response. In an analogue study (ref. 38) Kirk and Perry have shown that a tenfold increase in main oleo damping coefficient would be required for the Boeing 707 to decrease the cg acceleration by 58%, whilst Wignot et al have shown (ref. 22) that varying the hydraulic damping has negligible effect on crew and passenger vertical accelerations. The main problem with the oleo damping, of course, is that since orifice damping gives a force proportional to the square of the stroking velocity, at the very low stroking velocities associated with taxiing the damping forces are very small. Hall has shown (ref. 43) that a linear damper having the same maximum stroke as an orifice damper, would not only be markedly superior in taxiing operations, but would give a 10% reduction in strut force in heavy landings.

Thompson has shown (ref. 44) that the optimum damping value for ride comfort in a road vehicle depends on the statistical properties of the road, the speed of the vehicle, and the dynamic properties of the seat. Calculated values of linear damping rate for minimum response acceleration corresponded to damping ratios varying from 0.075 to 0.29, depending on the roughness spectrum of the road. However, Kirk has shown (ref.45) that the optimum equivalent linear damping ratio is greater than 0.5, whereas typical equivalent damping ratios during taxiing have been shown to be of the order of 0.05.

Positioning of the undercarriages has more repercussions on the airframe design than variation of the other parameters. Wignot et al (ref. 22) considered that location of the main gear was not a parameter that could be used in taxi load optimisation studies, but there was a greater degree of freedom in selecting the location of the nose gear. However, moving the nose gear $\pm 16\%$ of the distance between the nose and main gears, for a supersonic transport design, had negligible effect on the pilot location incremental load factor. Silsby (ref. 12) and Kirk (ref. 37) have investigated the effect of undercarriage location, using statistical analyses. Both found that as the distance between the main gear and the aircraft cg was increased, the distance between main and nose gears being kept constant, the cg response acceleration was reduced, but the acceleration at the pilot location was increased, although Silsby found that the pilot location displacement was decreased.

1. 5  Design criteria

Design criteria and procedures for taxiing aircraft should establish both the design loads and the fatigue spectra.    No manufacturer appears to have optimised the undercarriage characteristics to produce minimum response;    the undercarriages have generally been designed for the landing case and then, if at all, analysed to ensure their integrity, and that of the airframe, during ground operations.    Whilst, in general, ground operations have not provided the limit load case for the airframe, they have done so in some cases;    for example the Constellation, 1049G, was taxi critical because of the external fuel tanks installed on the wingtips.

The design loads or the fatigue spectrum may be calculated either from arbitrary criteria, such as a 2g static load factor for limit loads or application of arbitrary numbers of given incremental load factors for fatigue, or from rational criteria in which the response to a runway with a design level of roughness is obtained by either deterministic or statistical means. A problem which arises with stress analysis by statistical means is that no phasing is available to indicate in what proportions the various design-level loads, such as wingshear and torsion, combine. Two methods which have been developed to overcome this problem are the "matching condition" technique (ref. 46) and a "joint probability" technique (ref. 47);    both methods are believed to offer entirely acceptable approaches for airworthiness requirements.

In a massive and very comprehensive report (ref. 22)
Wignot et al have carried out a survey to establish the dynamic
taxi analytical methods and design criteria used by various airframe
manufacturers.   10 approaches to design methods were obtained from
7 airframe manufacturers.   Findings of particular interest were as
follows:  2 do not specify a design load criterion, the remaining 8
all using some kind of arbitrary criterion or discrete bump;  4 do
not specify a fatigue criterion, whilst 1 of the remaining 6 uses a
random profile traversed at constant velocity for 5 minutes per flight;
only 4 use runway profiles, either directly or by use of PSD's;  9 use
complete non-linear representation of struts and tyres, whilst the
other does not analyse landing gear for taxi;  9 use a flexible
aircraft, 6 of these using only symmetrical modes.

Dynamic taxi design procedures have been developed and
presented in reference 22.   Firstly a simple method was suggested
to check whether or not an aircraft is taxi critical.   This consists
of considering a static 1.0g load factor, on which is superimposed
in turn a 1.0g translational load factor, a rolling acceleration
related to the roll radius of gyration, and a pitching acceleration
related to the pitch radius of gyration.   Secondly rational
deterministic criteria were proposed.   These involve deterministic
analysis of the aircraft taxiing over phased (1 - cosine) bumps,
and over runway profiles which have been amplified by suitable
roughness amplification factors, to determine limit loads, and
production of exceedance curves by deterministic analysis of the
aircraft taxiing at appropriate speeds for given percentages of its

ground movement time over profiles with different discrete roughness ranges. Finally rational statistical criteria were proposed to produce both design loads and fatigue spectra. A method of generating random runway profiles having a given power spectral density was presented; the profile could then be used with a deterministic analysis. Alternatively a set of design taxi loads which had a specified likelihood of occurrence in the life of the aircraft could be determined from taxi load spectra derived from PSD's.

Reference 27 also suggests that dynamic taxi analysis should be performed using discrete step and (1 - cosine) bumps, and a continuous runway profile. It suggests that a 2-dimensional model should be satisfactory for the majority of aircraft, but that a 3-dimensional model might be necessary for a very large flexible aircraft. However, the analysis should include non-linear shock absorber and tyre characteristics, all significant rigid body and flexural modes of vibration, aerodynamic and propulsive forces, and longitudinal forces due to tyre-ground interaction and local profile slope effects.

FIGURE 1.1
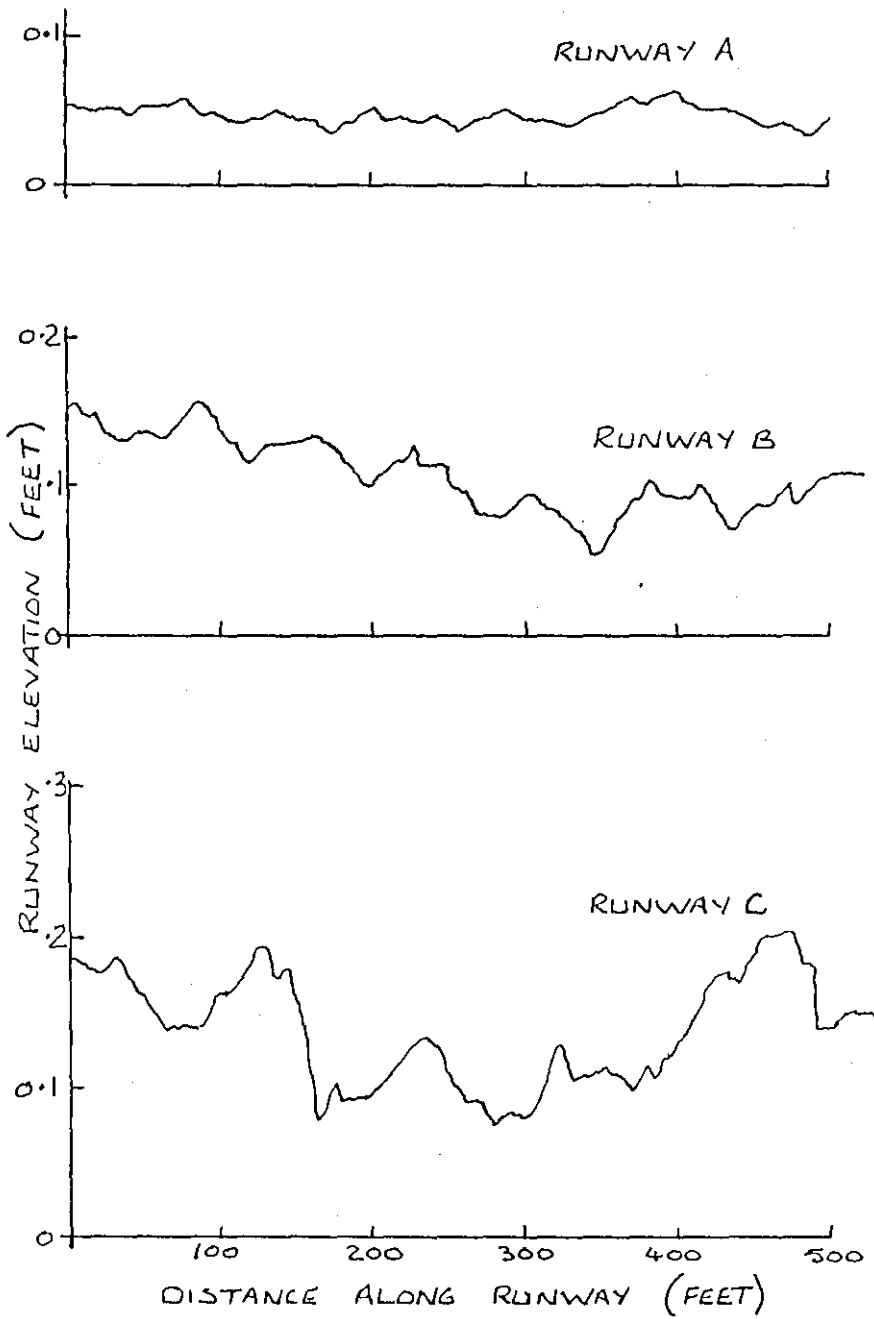
MEASURED PROFILES

FIGURE 1.2



TYPICAL SPECTRA OF RUNWAY

ELEVATION

FIGURE 1.3
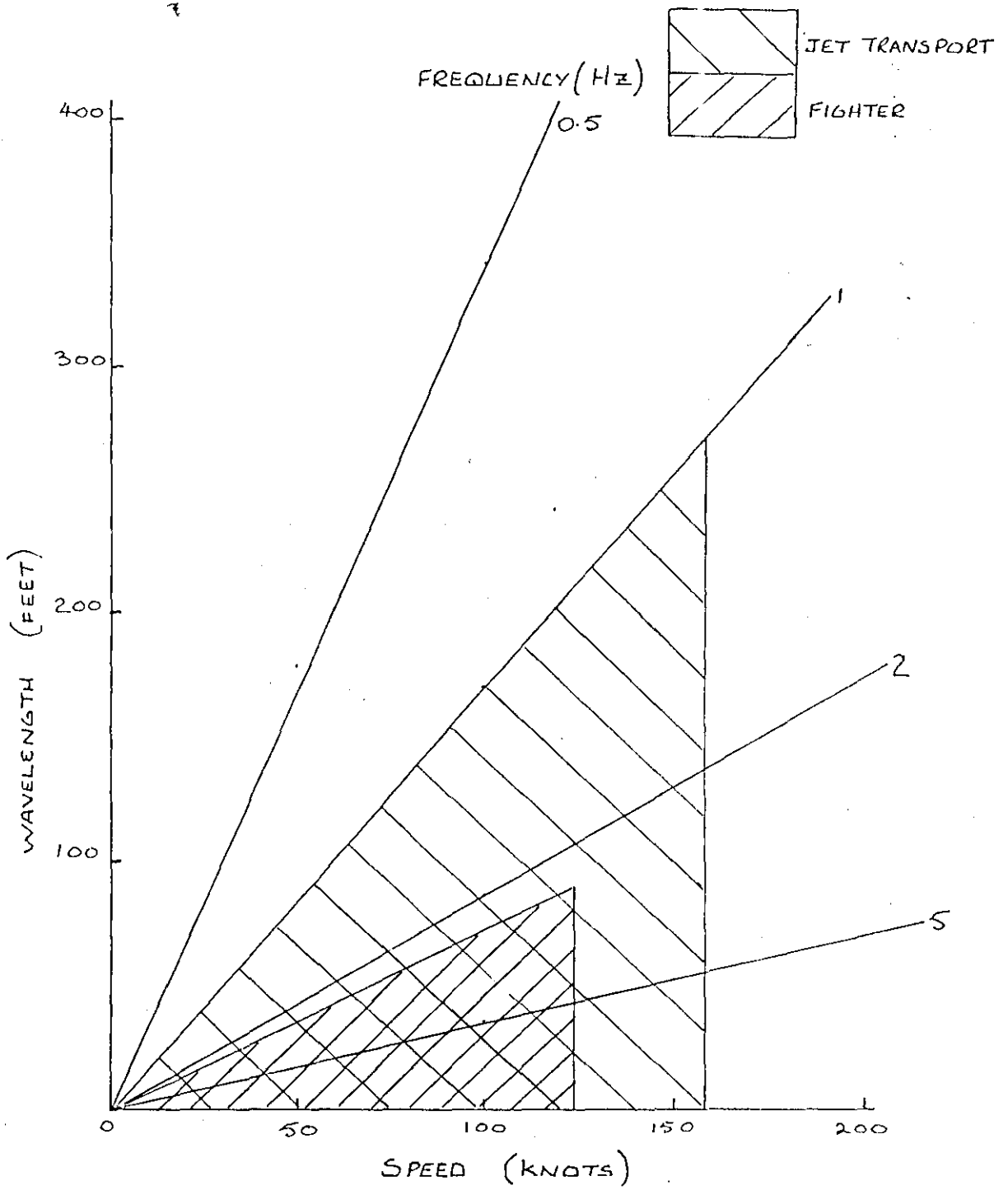
FIGURE 1.4
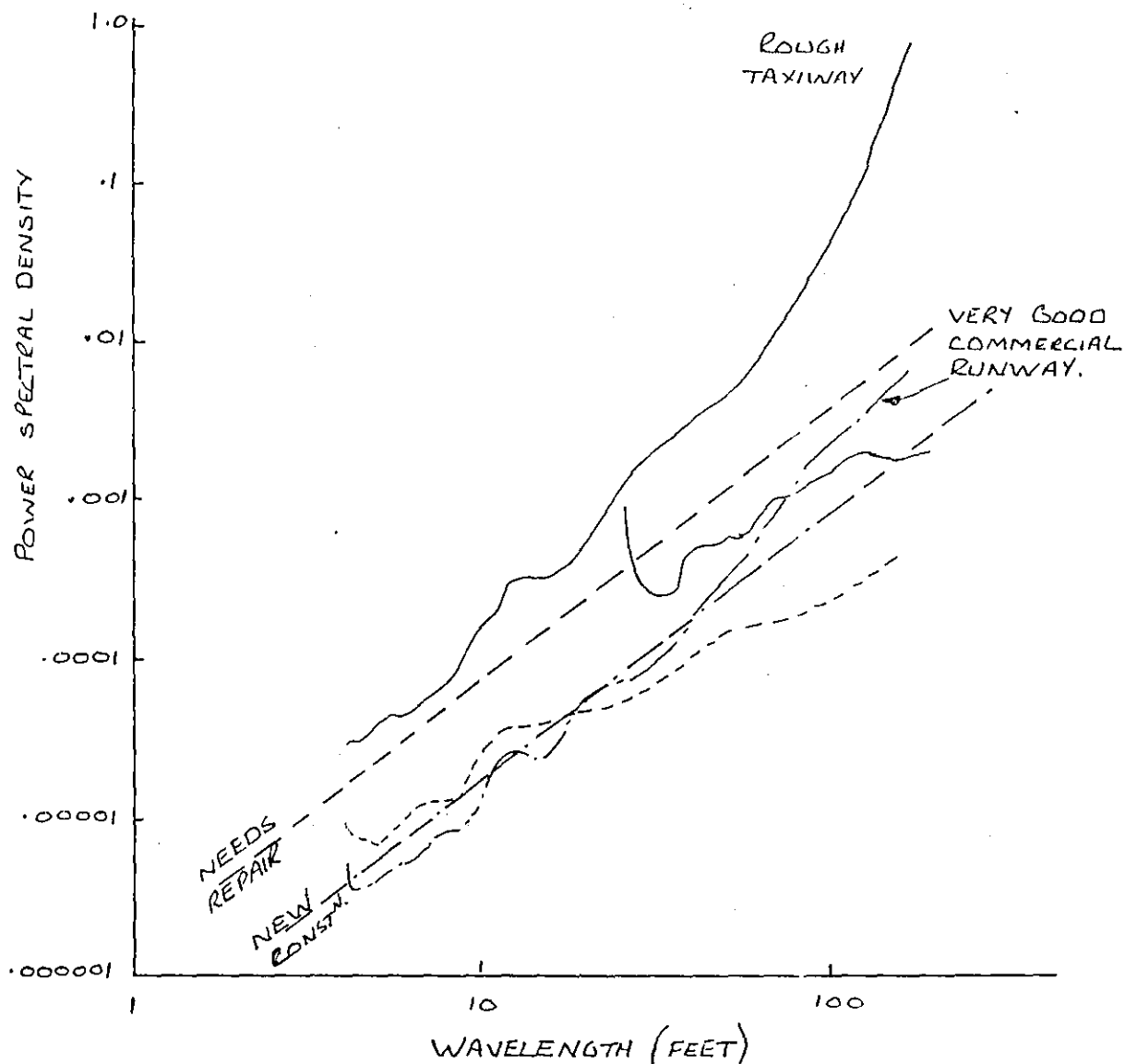


MILWITZKY'S RUNWAY UNEVENNESS

CRITERIA
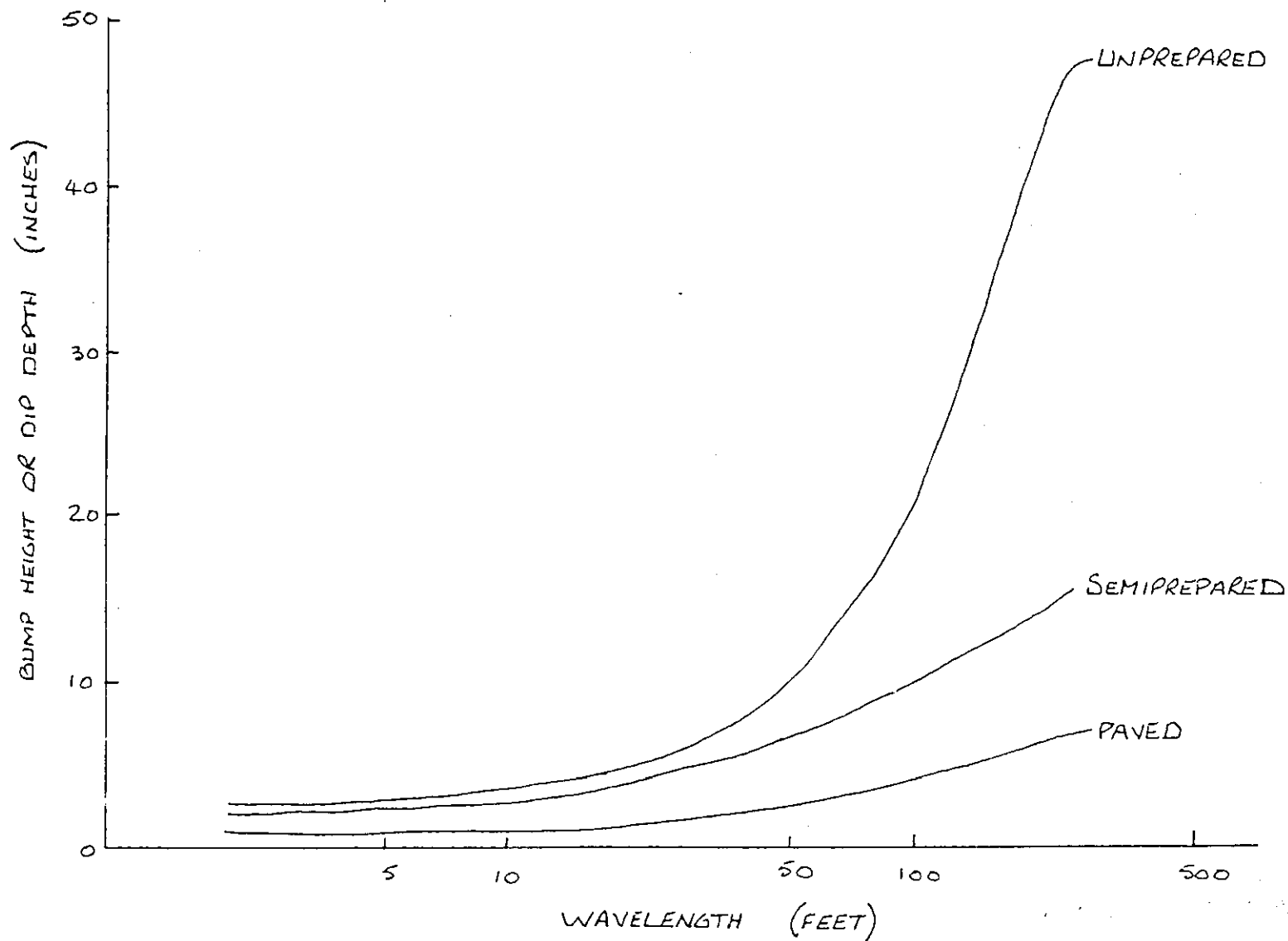
DISCRETE (1-COSINE) BUMP HEIGHTS OR (COSINE-1) DIP DEPTHS

FIGURE 1.5

54
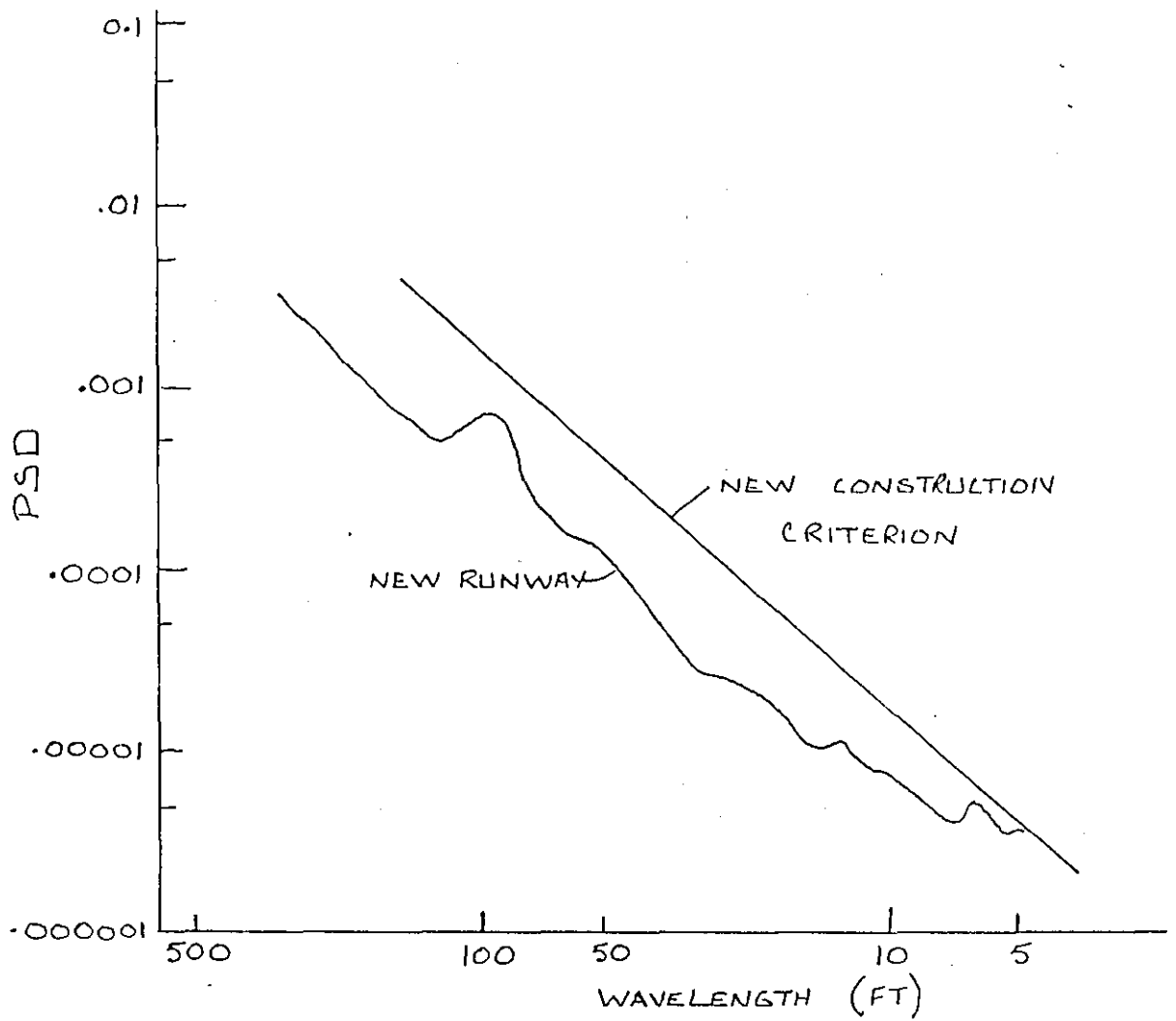
FIGURE 1.6



POWER SPECTRUM OF ROUGHNESS FOR

A NEW RUNWAY

RESPONSE ACCELERATIONS

REPRODUCED FROM REFERENCE 37

FIGURE 1.7

SECTION 2

## DERIVATION OF THE TYPICAL RUNWAY CHARACTERISTICS

The power spectral density, $\bar{\phi}_y(\Omega)$, of runway unevenness may be plotted against spacial frequency, $\Omega$, as shown in figure 2.1. If the spacial frequency, $\Omega$, is multiplied by the velocity, $V$, of traversing the runway, and the PSD, $\bar{\phi}_y(\Omega)$, is divided by $V$, a curve of PSD, $\bar{\phi}_y(\omega)$, against frequency, $\omega$, can be obtained for a particular velocity of the aircraft. Values could be taken from this latter curve to use as runway data in a computer program to compute the PSD of the displacement x of the aircraft from the relationship

$$\bar{\phi}_x(\omega) = H_{\frac{x}{y}}^2(\omega) \cdot \bar{\phi}_y(\omega) \qquad (2-1)$$

and hence the mean-square-value of aircraft displacement from

$$\bar{x}^2 = \int_{\omega_1}^{\omega_2} \bar{\phi}_x(\omega) \, d\omega \qquad (2-2)$$

Thus the response of the aircraft to an actual runway profile would be found.

However, this would detract from one of the main advantages of using statistical methods in that the response to each runway the aircraft is likely to use would have to be computed, and deterministic methods could therefore be used. Thus, an expression is usually used for PSD in terms of frequency which will give a curve approximating to actual PS$^\nu$ curves, and in which the roughness level can be varied by the adjustment of constants.

In previous work in this field it has been common to assume

that the PSD of the input from the runway is given by

$$\overline{\phi}(\Omega) = \frac{\overline{C}}{\Omega^n} \tag{2 - 3}$$

although other expressions have been used.   Common values which

have been used are n = 2, and $\overline{C}$ = 6.7 x 10$^{-6}$ rad ft for a good

runway and 20 x 10$^{-6}$ for a rough runway.   Thus, if the PSD is

plotted against the spacial frequency on log scales a straight line

will result with a slope of -2 and an intercept with the $\Omega$= 1

ordinate of 6.7 x 10$^{-6}$ or 20 x 10$^{-6}$ (fig. 2.3).

Whilst this is a very simple and straightforward approach

it is felt that it is not very representative of actual runway PSD

curves.   A more realistic expression could be deduced without

unduly increasing the complexity of the calculations, particularly

since all the calculations are made by digital computer.

Examination of the PSD curves in reference 26 suggests

that most of them could be approximated very well by fitting two

straight lines to the curve, as shown in figure 2.2.   Thus, the

PSD can be represented by two lines of the form of equation (2-3),

intersecting at some point P.   If expressions of this form are

found for several runways it should be possible to obtain mean

values of $\overline{C}$ and n to represent a runway of average roughness.

A series of numbers may of course be averaged arithmetically

or geometrically.   It is necessary therefore to decide what

properties are required of the average runway.   Runways with PSD's

derived by the two averaging methods may be defined as follows:

a. <u>Arithmetic mean runway</u>. This would be derived by taking
an arithmetic mean of the PSD's of several runways.    It
may be said that the total sample of runways would contain
as much roughness above that of the arithmetic mean runway
as below.

b. <u>Geometric mean runway</u>.   This would be derived by taking a
geometric mean of the PSD's of several runways.   It may
be said that the total sample of runways would contain
approximately as many runways with roughness above that of
the geometric mean runway as below.

The arithmetic mean runway would be much rougher than the
geometric mean runway since a very few very rough runways can boost
the value of the arithmetic mean but do not weight the geometric
mean nearly so much.   There would thus be little difference between
the arithmetic mean runway and a rough runway.   In view of this
it is felt that the geometric mean runway is the better one to
choose as a mean.

The analysis for the geometric mean runway PSD is shown
below.   The analysis for the arithmetic mean runway PSD is shown
in Appendix B, and the PSD is compared with that for the geometric
mean runway.

## 2. 1 Geometric mean runway

The PSD of a typical runway is given by

$$\phi_i(\Omega) = \frac{\overline{C_i}}{\Omega^{n_i}} \qquad\qquad (2-4)$$

It is not sufficient to merely find the mean values of $\overline{C}$ and $n$, since it is in fact the mean value of $\phi(\Omega)$ which is required.

If the geometric mean of a set of values $\dfrac{a_i}{b_i}$ is required, then

$$\text{Geometric mean} = \sqrt[m]{\frac{a_1}{b_1} \times \frac{a_2}{b_2} \times \frac{a_3}{b_3} \times \ldots\ldots\frac{a_m}{b_m}}$$

$$= \frac{\sqrt[m]{a_1 \times a_2 \times a_3 \times \ldots\ldots a_m}}{\sqrt[m]{b_1 \times b_2 \times b_3 \times \ldots\ldots b_m}}$$

$$= \frac{\text{Geometric mean of } a_i}{\text{Geometric mean of } b_i}$$

Thus the geometric mean of $\overline{C}$ and $\Omega^n$ may be found separately.

If the geometric mean of a set of values $\Omega^{n_i}$ is required, then

$$\text{Geometric mean} = \sqrt[m]{\Omega^{n_1} \times \Omega^{n_2} \times \ldots\ldots \Omega^{n_m}}$$

The value of p is required such that

$$\Omega^p = \sqrt[m]{\Omega^{n_1} \times \Omega^{n_2} \times \ldots\ldots \times \Omega^{n_m}}$$

$$\therefore p \log \Omega = \frac{1}{m}\left(n_1 \log \Omega + n_2 \log \Omega + \ldots\ldots + n_m \log \Omega\right)$$

$$= \frac{1}{m} \log \Omega \left(\sum_{i=1}^{m} n_i\right)$$

$$\therefore p = \frac{1}{m} \sum_{i=1}^{m} n_i = \text{arithmetic mean of } n_i$$

Thus to find the geometric mean of a set of PSD's given

by equation (2-4) it is necessary to calculate the geometric mean of $\overline{C}_i$ and the arithmetic mean of $n_i$

Referring to figure 2.2, two straight lines, A and B, are fitted to the PSD curve, with slopes of $n_a$ and $n_b$. Their intercepts with the $\Omega = 1$ ordinate are $\overline{C}_a$ and $\overline{C}_b$. Table 2.1 gives n and $\log \overline{C}$ for each straight line, for each runway in reference 26. Many of the PSD curves had a "bump" at the high frequency end (see figures 2.1 and 2.2). It was thought that this could be due to "aliasing" errors, and in any case always occurred at a value of $\Omega$ greater than 1.0 rad/ft, which even at an aircraft velocity of 60 ft/s represents a value of $\omega$ greater than 60 rad/s. Since it was found that PSD's in this frequency range have no significant effect on the response of the aircraft, these "bumps" were ignored.

Taking values from the table,

Arithmetic mean of $n_a = \dfrac{\sum\limits_{i=1}^{m} n_{ai}}{m}$

$$= 3.58$$

Arithmetic mean of $n_b = 2.24$

Geometric mean of $\overline{C}_a = \text{Antilog}\left[\dfrac{\sum\limits_{i=1}^{m} \log \overline{C}_{ai}}{m}\right]$

$$= 3.8 \times 10^{-7}$$

Geometric mean of $\overline{C}_b = 8.2 \times 10^{-6}$

The point of intersection of the two lines is given by

$$\frac{3.8 \times 10^{-7}}{\Omega^{3.58}} = \frac{8.2 \times 10^{-6}}{\Omega^{2.24}}$$

giving
$$\Omega = 0.101$$

Thus, the geometric mean runway PSD is given by

If $\Omega < 0.101$ rad/ft, $\phi(\Omega) = \dfrac{3.8 \times 10^{-7}}{\Omega^{3.58}}$ ft$^2$/rad/ft

If $\Omega > 0.101$ rad/ft, $\overline{\phi}(\Omega) = \dfrac{8.2 \times 10^{-6}}{\Omega^{2.24}}$ ft$^2$/rad/ft

These values are plotted in figure 2.3, where they may be compared with the two single-straight-line PSD's discussed previously.

It is more convenient, for computation, to work in terms of circular frequency, $\omega$. Since $\omega = \Omega V$, then

$$\phi(\Omega) = \frac{\overline{c}}{\Omega^n} = \frac{\overline{c}V^n}{\omega^n}$$

$$\therefore \phi(\omega) = \frac{\phi(\Omega)}{V} = \frac{\overline{c}V^n}{\omega^n V}$$

i.e. $\qquad \phi(\omega) = \dfrac{\overline{c}V^{n-1}}{\omega^n} \qquad\qquad (2-5)$

2. 2  <u>Summary of Program Data for Geometric Mean Runway</u>

| Analysis Symbol | Program Identifier | Value |
|---|---|---|
| $\bar{c}_a$ | CA | $3.8 \times 10^{-7}$ |
| $n_a$ | NA | 3.58 |
| $\bar{c}_b$ | CB | $8.2 \times 10^{-6}$ |
| $n_b$ | NB | 2.24 |
| intersection $\Omega$ | OMEGA | 0.101 rad/ft |

TABLE 2. 1

Analysis of runways in reference 26

| Fig. | $n_a$ | Log $\overline{C}_a$ | $n_b$ | Log $\overline{C}_b$ |
|---|---|---|---|---|
| 3 | 2.83 | -6 + 0.54 | 2.30 | -6 + 1.07 |
|  | 2.83 | -6 + 0.54 | 2.30 | -6 + 1.07 |
| 5 | 2.32 | -6 + 0.90 | 2.32 | -6 + 0.90 |
| 7 | 2.68 | -6 + 0.10 | 1.85 | -6 + 0.73 |
| 10 | 2.60 | -6 + 0.10 | 2.22 | -6 + 1.55 |
|  | 2.60 | -6 + 0.10 | 2.22 | -6 + 1.55 |
| 12 | 3.13 | -6 + 0.35 | 1.95 | -6 + 0.80 |
| 15 | 3.66 | -6 + 0.27 | 2.07 | -6 + 0.73 |
|  | 2.78 | -6 + 0.54 | 1.30 | -6 + 1.32 |
| 20 | 2.46 | -6 + 1.25 | 2.46 | -6 + 1.25 |
|  | 2.46 | -6 + 1.25 | 2.46 | -6 + 1.25 |
|  | 2.46 | -6 + 1.25 | 2.46 | -6 + 1.25 |
|  | 2.46 | -6 + 1.25 | 2.46 | -6 + 1.25 |
| 23 | 2.72 | -6 + 0.55 | 2.72 | -6 + 0.55 |
|  | 6.67 | -6 + 3.87 | 2.15 | -6 + 0.52 |
| 26 | 3.34 | -6 + 0.20 | 2.05 | -6 + 0.55 |
|  | 3.80 | -6 + 0.20 | 2.08 | -6 + 1.10 |
| 29 | 4.96 | -6 + 1.88 | 2.07 | -6 + 0.65 |
|  | 5.66 | -6 + 3.17 | 1.87 | -6 + 0.95 |
| 32 | 7.00 | -6 + 4.12 | 2.71 | -6 + 0.54 |
|  | 7.00 | -6 + 4.12 | 2.71 | -6 + 0.54 |
| 37 | 4.90 | -6 - 2.30 | 2.20 | -6 + 0.85 |
|  | 4.90 | -6 - 2.30 | 2.20 | -6 + 0.85 |
|  | 4.90 | -6 - 2.30 | 2.20 | -6 + 0.85 |
|  | 4.90 | -6 - 2.30 | 2.20 | -6 + 0.85 |
| 40 | 3.08 | -6 + 0.00 | 1.73 | -6 + 0.50 |
|  | 3.08 | -6 + 0.00 | 1.73 | -6 + 0.50 |
| 43 | 5.25 | -6 - 2.18 | 2.40 | -6 + 1.00 |
|  | 5.25 | -6 - 2.18 | 2.40 | -6 + 1.00 |
| 46 | 2.55 | -6 + 0.93 | 2.55 | -6 + 0.93 |
|  | 2.55 | -6 + 0.93 | 2.55 | -6 + 0.93 |
| 49 | 2.79 | -6 + 0.42 | 2.79 | -6 + 0.42 |
|  | 2.79 | -6 + 0.42 | 2.79 | -6 + 0.42 |
| 52 | 2.34 | -6 + 1.14 | 1.31 | -6 + 1.48 |
|  | 2.94 | -6 + 0.10 | 1.61 | -6 + 0.80 |
| 55 | 2.20 | -6 + 1.16 | 2.20 | -6 + 1.16 |
| 56 | 1.65 | -6 + 1.93 | 2.91 | -6 + 1.20 |
| Totals | 132.49 | -222 - 15.64 | 82.52 | -222 + 33.96 |

FIGURE 2.1
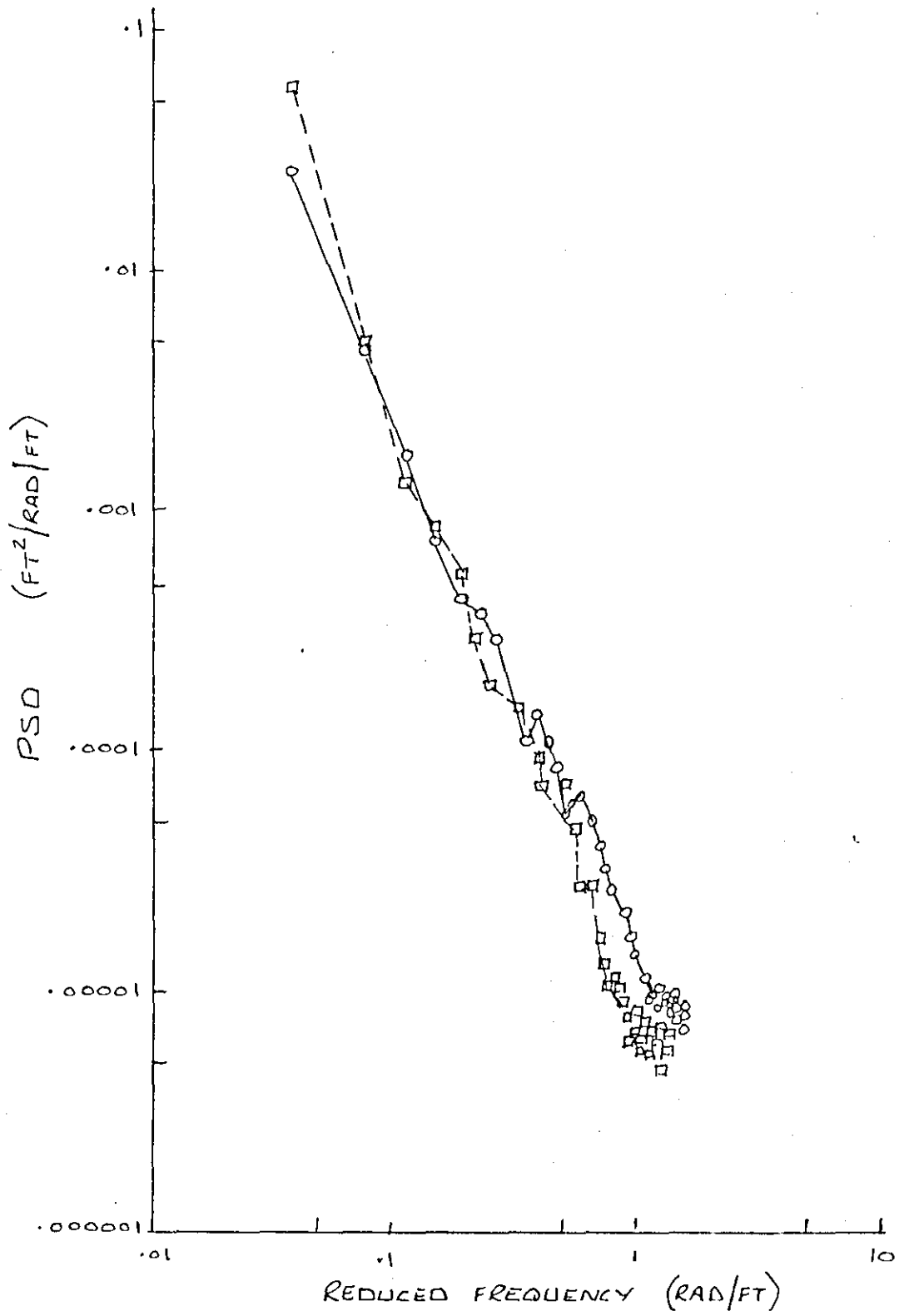


POWER SPECTRAL DENSITY FUNCTIONS

FIGURE 2.2
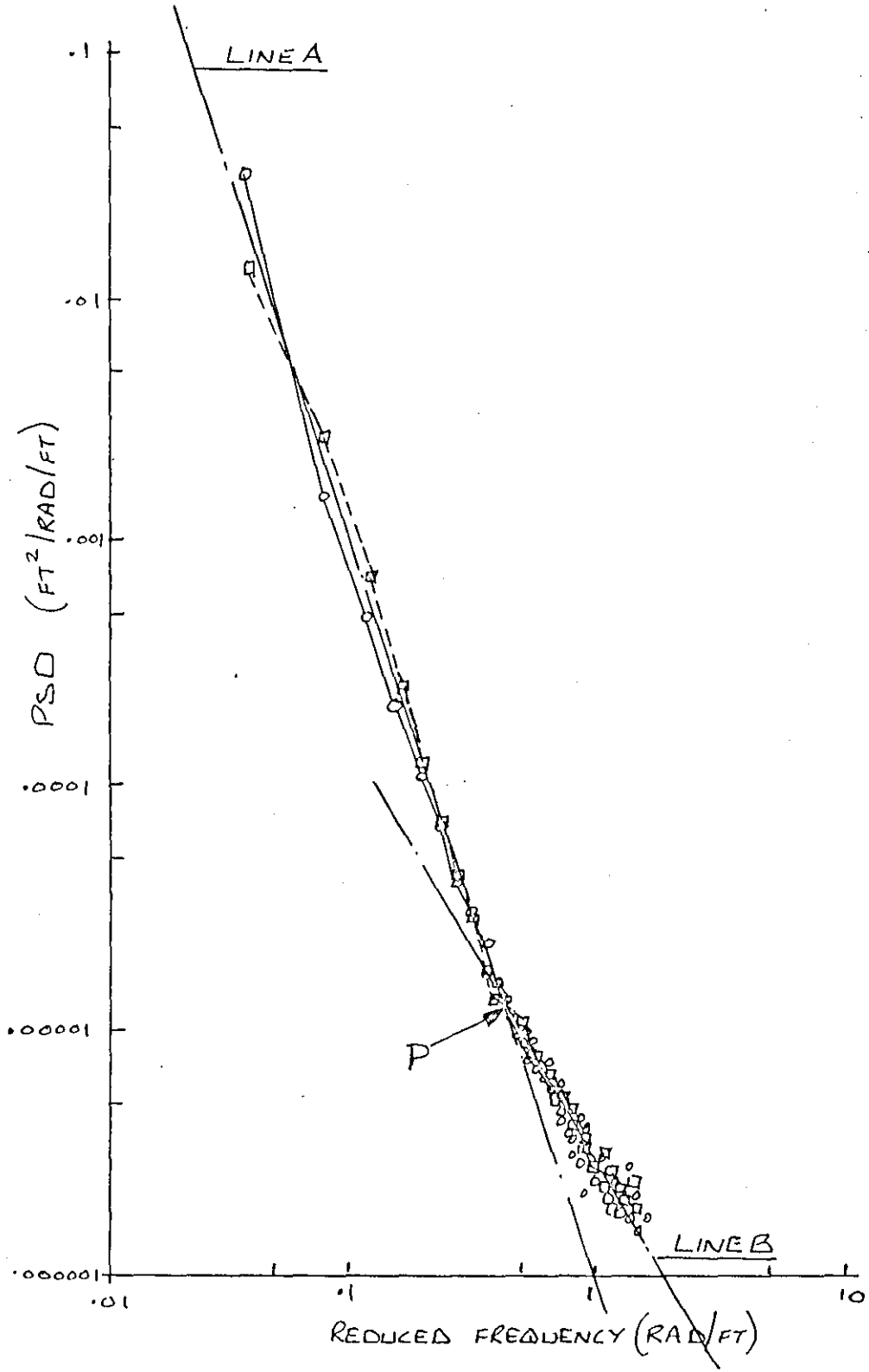


TWO STRAIGHT LINES FITTED TO PSD CURVE

FIGURE 2.3

GEOMETRIC MEAN RUNWAY

$$\bar{\phi}(\Omega) = \frac{6.7 \times 10^{-6}}{\Omega^2}$$

$$\bar{\phi}(\Omega) = \frac{20 \times 10^{-6}}{\Omega^2}$$
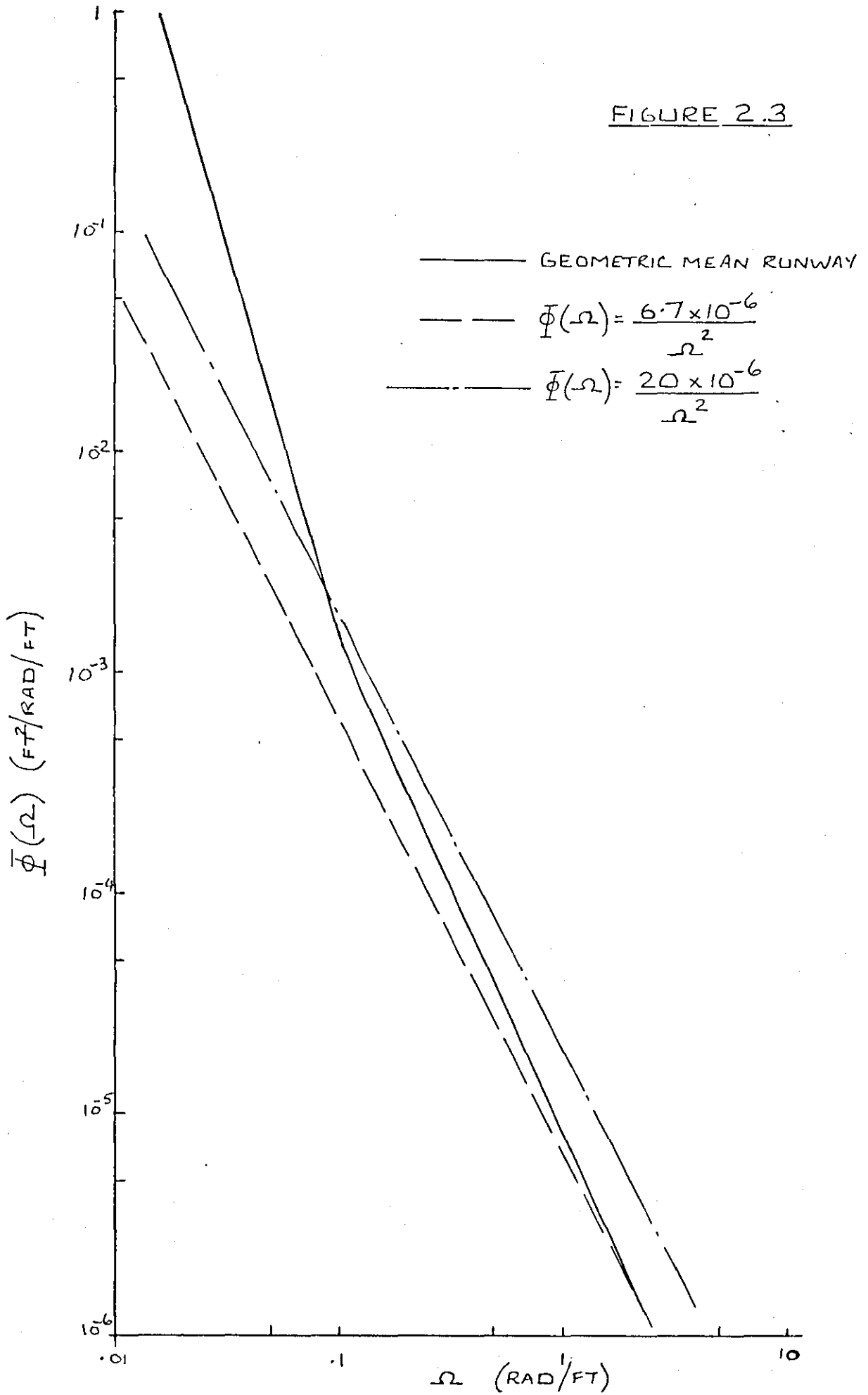
POWER SPECTRAL DENSITY FUNCTIONS

SECTION  3

THE  AIRCRAFT

3. 1  Idealisation

A diagrammatic representation of the aircraft considered
in this investigation is shown in Figure 3.1.    In the analysis
it is assumed that the runway profile elevation, h, measured from
an arbitrary datum plane, is constant across the runway.    Thus,
the dynamic response will be symmetrical about the longitudinal
axis of the aircraft.    The free-free airframe is therefore
considered to be a two dimensional elastic system, as illustrated
in Figure 3.2,  its equations of motion being formulated in terms
of the two rigid body modes (rigid body heave and pitch) and any
number of symmetric flexural normal modes of the free, unrestrained
airframe.    It is assumed that the aerodynamic lift on the aircraft
is negligible during taxiing, so that the only forces acting on
the airframe are the landing gear forces $Q_1$ and $Q_2$.

The landing gear system used is shown diagrammatically in
Figure 3.3.    It is assumed that the undercarriage leg is a linear
device, the forces being produced by a linear spring and a linear
dashpot, and friction in the undercarriage being neglected.    The
tyre is also represented by a linear spring and a linear damper.
The wheel masses plus effective masses of landing gear systems are
represented by $W_1$ and $W_2$ for the mainwheel and nosewheel
respectively.

## 3. 2  Equations of motion

### 3.2.1  Free-Free Airframe

Figure 3.2 shows the set of reference axes used in the analysis, the origin of the axes being located at the centre of gravity of the airframe.   The total vertical displacement $Z(x,y,t)$ of any point on the airframe may be expressed in terms of the rigid body heave (vertical translation), rigid body pitch (rotation about the $y$ axis), and the elastic deformation of the airframe with respect to the moving.xy plane.

Thus, the total vertical displacement of any point on the airframe from a horizontal reference plane is given by:

$$Z(x,y,t) = \sum_{j=3}^{N} \phi^{j}(x,y)X_j(t) \qquad (3 - 1)$$

where $N = N_1 + 4$, $N_1$ is the number of flexible modes considered, and the rigid heave and pitch of the x axis are represented by rigid body modes of zero frequency and generalised co-ordinates $X_3(t)$ and $X_4(t)$, so that

$$\omega_3 = \omega_4 = 0$$

$$\phi^{3}(x,y) = 1$$
$$\phi^{4}(x,y) = -X$$

The shapes, with their corresponding frequencies and normal co-ordinates, of the flexible normal modes are denoted by $\phi^{j}(x,y)$, $\omega_j$, and $X_j(t)$ where $j = 5,6$---$N$, and the elastic displacement of the airframe relative to the moving $x,y$ plane may be represented by superposition of these modes.

$X_1(t)$ and $X_2(t)$ are the vertical displacements of the undercarriage masses $M_1$ and $M_2$ respectively, and are therefore not included in equation (3-1).

Thus, the equations of motion of the elastic airframe are as follows:-

$$M_3\ddot{X}_3 = P_3(t) \qquad (3-2)$$

$$M_4\ddot{X}_4 = P_4(t) \qquad (3-3)$$

$$M_j\ddot{X}_j + C_j\dot{X}_j + M_j\omega_j^2 X_j = P_j(t) \qquad (3-4)$$

where    $M_3 = \dfrac{W}{g}$

$M_4 = J$, the moment of inertia in pitch of the aircraft about its centre of gravity

$j = 5,6,----N$

$C_j = 2\beta M_j \omega_j$

$M_j$ = generalised mass in jth mode

$\beta$ = structural damping coefficient

$P_j(t)$ = generalised forcing function of jth mode, given by

$$P_j(t) = -(Q_1 - \overline{Q}_1)\phi_1{}^j - (Q_2 - \overline{Q}_2)\phi_2{}^j \quad (3-5)$$

where $Q_1, Q_2$ represent the concentrated landing gear forces acting on the airframe from the main and nose undercarriages respectively, and $\overline{Q}_1, \overline{Q}_2$ represent the corresponding static values of Q when $V = 0$, i.e. the aircraft is stationary.

$\phi_i{}^j$ denotes the jth mode shape at the ith location where $i = 1,2$ refer to points $O_1$ and $O_2$, the main and nose undercarriage locations respectively, on Figures 3.1 and 3.2.

### 3.2.2 Undercarriage forces $Q_i$

The concentrated forces acting on the airframe from the main and nose undercarriages are represented by $Q_1$ and $Q_2$ respectively in Figure 3.2. Referring to Figure 3.3, for the ith landing gear $U_i$ represents the vertical displacement of point $O_i$, and $X_i$ represents the vertical displacement of mass $M_i$, both displacements being measured from equilibrium positions for the stationary aircraft. The displacement $U_i$ can be expressed in terms of the generalised co-ordinates $X_j$ of the rigid body and flexural modes of the airframe as follows:

$$U_i = \sum_{j=3}^{N} X_j(t) \phi_i^j \qquad (3-6)$$

If the stroke of the oleo from the static equilibrium position is $S_i$ then

$$S_i = U_i - X_i$$
$$\text{and} \quad \dot{S}_i = \dot{U}_i - \dot{X}_i$$

Thus, the nett (i.e. actual minus static equilibrium value) oleo spring force is given by :

$$F_{si} = K_i S_i = K_i(U_i - X_i) \qquad (3-7)$$

and the oleo damping force is given by :

$$F_{di} = C_i \dot{S}_i = C_i(\dot{U}_i - \dot{X}_i) \qquad (3-8)$$

where $K_i$ is the linear oleo spring stiffness and $C_i$ is the linear oleo damping constant.

Since $U_i$ is measured from the static equilibrium position,

$$(Q_i - \overline{Q}_i) = F_{si} + F_{di} \qquad (3-9)$$

i.e. $\qquad (Q_i - \overline{Q}_i) = K_i(U_i - X_i) + C_i(\dot{U}_i - \dot{X}_i) \qquad (3-10)$

Substituting for $(Q_i - \overline{Q}_i)$ in equation (3-5) gives :

$$P_j(t) = -\underline{/}K_1(U_1 - X_1) + C_1(\dot{U}_1 - \dot{X}_1)\underline{/}\phi_1{}^j$$
$$-\underline{/}K_2(U_2 - X_2) + C_2(\dot{U}_2 - \dot{X}_2)\underline{/}\phi_2{}^j \qquad (3-11)$$

where $U_1 = \sum_{j=3}^{N} X_j(t)\phi_1{}^j$

$\qquad\qquad U_2 = \sum_{j=3}^{N} X_j(t)\phi_2{}^j$

Assuming that the tyre remains in contact with the ground, the interacting force $F_{ti}$ between the ground and the tyre is given by :

$$F_{ti} = K_{ti}(\overline{X}_i + X_i + h_i) + C_{ti}(\dot{X}_i + \dot{h}_i) \qquad (3-12)$$

where $K_{ti}$ is the linear tyre stiffness

$\qquad C_{ti}$ is the linear tyre damping constant

$\qquad \overline{X}_i$ is the static downward displacement of mass $M_i$

### 3.2.3 Overall equations

The equation of motion of the mass $M_i$ is :

$$M_i\ddot{X}_i = W_i + Q_i - F_{ti} \qquad (3-13)$$

where $W_i$ = the weight of the mass $M_i$

$\qquad i = 1,2$

Substituting for $Q_i$ from equation (3-9) gives :

$$M_i\ddot{X}_i = W_i + \overline{Q}_i + F_{si} + F_{di} - F_{ti} \qquad (3-14)$$

and expanding this by equations (3-7), (3-8) and (3-12) gives:

$$M_i\ddot{X}_i = W_i + \overline{Q}_i + K_i(U_i - X_i) + C_i(\dot{U}_i - \dot{X}_i) - K_{ti}(\overline{X}_i + X_i + h_i)$$
$$- C_{ti}(\dot{X}_i + \dot{h}_i) \qquad (3-15)$$

c.f. Equations (3-2) and (3-3).

Now $W_i + \overline{Q}_i - K_{ti}\overline{X}_i = 0$ (static equilibrium conditions)

$$\text{Let } \{X_j\} = \begin{bmatrix} X_3 \\ X_4 \\ \vdots \\ X_N \end{bmatrix}$$

$$[\phi_1{}^j] = [\phi_1{}^3 \quad \phi_1{}^4 \quad ----- \quad \phi_1{}^N]$$

$$[\phi_2{}^j] = [\phi_2{}^3 \quad \phi_2{}^4 \quad ----- \quad \phi_2{}^N]$$

$$\left. \begin{aligned} \text{Then } U_1 &= [\phi_1{}^j]\{X_j\} \\ U_2 &= [\phi_2{}^j]\{X_j\} \end{aligned} \right\} \qquad (3-16)$$

Thus, equation (3-15) becomes :

$$M_i\ddot{X}_i + C_i\dot{X}_i + C_{ti}\dot{X}_i - C_i[\phi_i{}^j]\{\dot{X}_j\} + (K_{ti} + K_i)X_i$$
$$- K_i[\phi_i{}^j]\{X_j\} = -K_{ti}h_i - C_{ti}\dot{h}_i \qquad (3-17)$$

Putting $i = 1, 2$ and substituting for $h_i$ will give the first two differential equations of a simultaneous set.

From equation (3-11), if

$$\{P_j\} = \begin{bmatrix} P_3(t) \\ P_4(t) \\ \vdots \\ P_N(t) \end{bmatrix}$$

then

$$\{P_j\} = -\left[K_1(U_1 - X_1) + C_1(\dot{U}_1 - \dot{X}_1)\right]\left[\phi_1{}^j\right]^T$$
$$- \left[K_2(U_2 - X_2) + C_2(\dot{U}_2 - \dot{X}_2)\right]\left[\phi_2{}^j\right]^T \qquad (3-18)$$

Taking the first term in RHS of (3-18)

$$-\left[K_i(U_1 - X_1) + C_1(\dot{U}_1 - \dot{X}_1)\right]\left[\phi_1{}^j\right]^T$$
$$= -\left[K_1[\phi_1{}^j]\{X_j\} - K_1X_1 + C_1[\phi_1{}^j]\{\dot{X}_j\} - C_1\dot{X}_1\right]\left[\phi_1{}^j\right]^T$$

Since $\left[\phi_1{}^j\right]$ is a row and $\left\{x_j\right\}$ is a column it can easily be shown that

$$\left[\phi_1{}^j\right]\left\{x_j\right\}\left[\phi_1{}^j\right]^T = \left[\phi_1{}^j\right]^T\left[\phi_1{}^j\right]\left\{x_j\right\}$$

so that the first term in RHS of (3-18) now becomes :

$$c_1\dot{x}_1\left[\phi_1{}^j\right]^T - c_1\left[\phi_1{}^j\right]^T\left[\phi_1{}^j\right]\left\{\dot{x}_j\right\} + K_1x_1\left[\phi_1{}^j\right]^T$$

$$- K_1\left[\phi_1{}^j\right]^T\left[\phi_1{}^j\right]\left\{x_j\right\} \qquad (3-19)$$

Substituting (3-19) in equation (3-18) and forming the second term by similarity gives :

$$\left\{P_j\right\} = c_1\dot{x}_1\left[\phi_1{}^j\right]^T - c_1\left[\phi_1{}^j\right]^T\left[\phi_1{}^j\right]\left\{\dot{x}_j\right\} + K_1x_1\left[\phi_1{}^j\right]^T$$
$$- K_1\left[\phi_1{}^j\right]^T\left[\phi_1{}^j\right]\left\{x_j\right\} + c_2\dot{x}_2\left[\phi_2{}^j\right]^T - c_2\left[\phi_2{}^j\right]^T\left[\phi_2{}^j\right]\left\{\dot{x}_j\right\}$$
$$+ K_2x_2\left[\phi_2{}^j\right]^T - K_2\left[\phi_2{}^j\right]^T\left[\phi_2{}^j\right]\left\{x_j\right\} \qquad (3-20)$$

If $\ulcorner M_j\urcorner$ and $\ulcorner\omega_j\urcorner$ are diagonal matrices of the generalised masses and natural frequencies respectively in the various modes, where

$$j = 3, 4, \text{-----}N$$

and $\omega_j = 0$ for $j = 3, 4$

then equation (3-4) may be written :

$$\ulcorner M_j\urcorner\left\{\ddot{x}_j\right\} + 2\beta\ulcorner M_j\urcorner\ulcorner\omega_j\urcorner\left\{\dot{x}_j\right\} + \ulcorner M_j\urcorner\ulcorner\omega_j\urcorner\ulcorner\omega_j\urcorner\left\{x_j\right\} = \left\{P_j\right\} \qquad (3-21)$$

Substituting for $\left\{P_j\right\}$ from equation (3-20) in equation (3-21) gives :

$$\ulcorner M_j\urcorner\left\{\ddot{x}_j\right\} - c_1\dot{x}_1\left[\phi_1{}^j\right]^T - c_2\dot{x}_2\left[\phi_2{}^j\right]^T + \left[CA_j\right]\left\{\dot{x}_j\right\}$$
$$- K_1x_1\left[\phi_1{}^j\right]^T - K_2x_2\left[\phi_2{}^j\right]^T + \left[KA_j\right]\left\{x_j\right\} = \left\{0\right\} \qquad (3-22)$$

where $\left[CA_j\right]$ and $\left[KA_j\right]$ are damping and stiffness matrices respectively for the airframe given by :

$$\left[CA_j\right] = \left[2\beta\ulcorner M_j\urcorner\ulcorner\omega_j\urcorner + c_1\left[\phi_1{}^j\right]^T\left[\phi_1{}^j\right] + c_2\left[\phi_2{}^j\right]^T\left[\phi_2{}^j\right]\right] \qquad (3-23)$$

$$\left[KA_j\right] = \left[\ulcorner M_j \ulcorner \omega_j \ulcorner \dot{\omega}_j + K_1 \left[\phi_1{}^j\right]^T \left[\phi_1{}^j\right] + K_2 \left[\phi_2{}^j\right]^T \left[\phi_2{}^j\right]\right] \quad (3 - 24)$$

$$j = 3, 4 \text{ ----- } N$$

Equations (3-17) with i = 1, 2 and j = 3, 4 ----N, and

(3-22) with j = 3, 4 ----N constitute a set of N simultaneous

differential equations which may be written :

$$\ulcorner M \lrcorner \left\{\ddot{x}\right\} + \left[c\right]\left\{\dot{x}\right\} + \left[K\right]\left\{x\right\} = \left\{F(t)\right\} \quad (3 - 25)$$

where
$$\ulcorner M \lrcorner = \ulcorner M_1$$
$$M_2 \quad \bar{0}$$
$$\ulcorner \quad M_j$$
$$\bar{0} \qquad \lrcorner \quad (3 - 27)$$

$$\left\{x\right\} = \begin{bmatrix} x_1 \\ x_2 \\ \left\{x_j\right\} \end{bmatrix} \quad (3 - 28)$$

$$\left[c\right] = \begin{bmatrix} c_1 + c_{t1} & 0 & -c_1\left[\phi_1{}^j\right] \\ 0 & c_2 + c_{t2} & -c_2\left[\phi_2{}^j\right] \\ \left[-c_1\left[\phi_1{}^j\right]^T\right] & \left[-c_2\left[\phi_2{}^j\right]^T\right] & \begin{bmatrix} CA_j \\ \text{see equation} \\ (3 - 23) \end{bmatrix} \end{bmatrix} \quad (3 - 29)$$

$$\left[K\right] = \begin{bmatrix} K_1 + K_{t1} & 0 & -K_1\left[\phi_1{}^j\right] \\ 0 & K_2 + K_{t2} & -K_2\left[\phi_2{}^j\right] \\ \left[-K_1\left[\phi_1{}^j\right]^T\right] & \left[-K_2\left[\phi_2{}^j\right]^T\right] & \begin{bmatrix} KA_j \\ \text{see equation} \\ (3 - 24) \end{bmatrix} \end{bmatrix} \quad (3 - 30)$$

$$\left\{ F(t) \right\} = \begin{Bmatrix} -K_{t1}h_1 - C_{t1}\dot{h}_1 \\ -K_{t2}h_2 - C_{t2}\dot{h}_2 \\ \\ \left\{ \bar{0} \right\} \end{Bmatrix} \qquad (3 - 31)$$

Premultiplying equation (3 - 25) by $\ulcorner M \lrcorner^{-1}$ gives:

$$\left\{ \ddot{X} \right\} + \ulcorner M \lrcorner^{-1} \left[ C \right] \left\{ \dot{X} \right\} + \ulcorner M \lrcorner^{-1} \left[ K \right] \left\{ X \right\} = \ulcorner M \lrcorner^{-1} \left\{ F(t) \right\} \qquad (3 - 32)$$
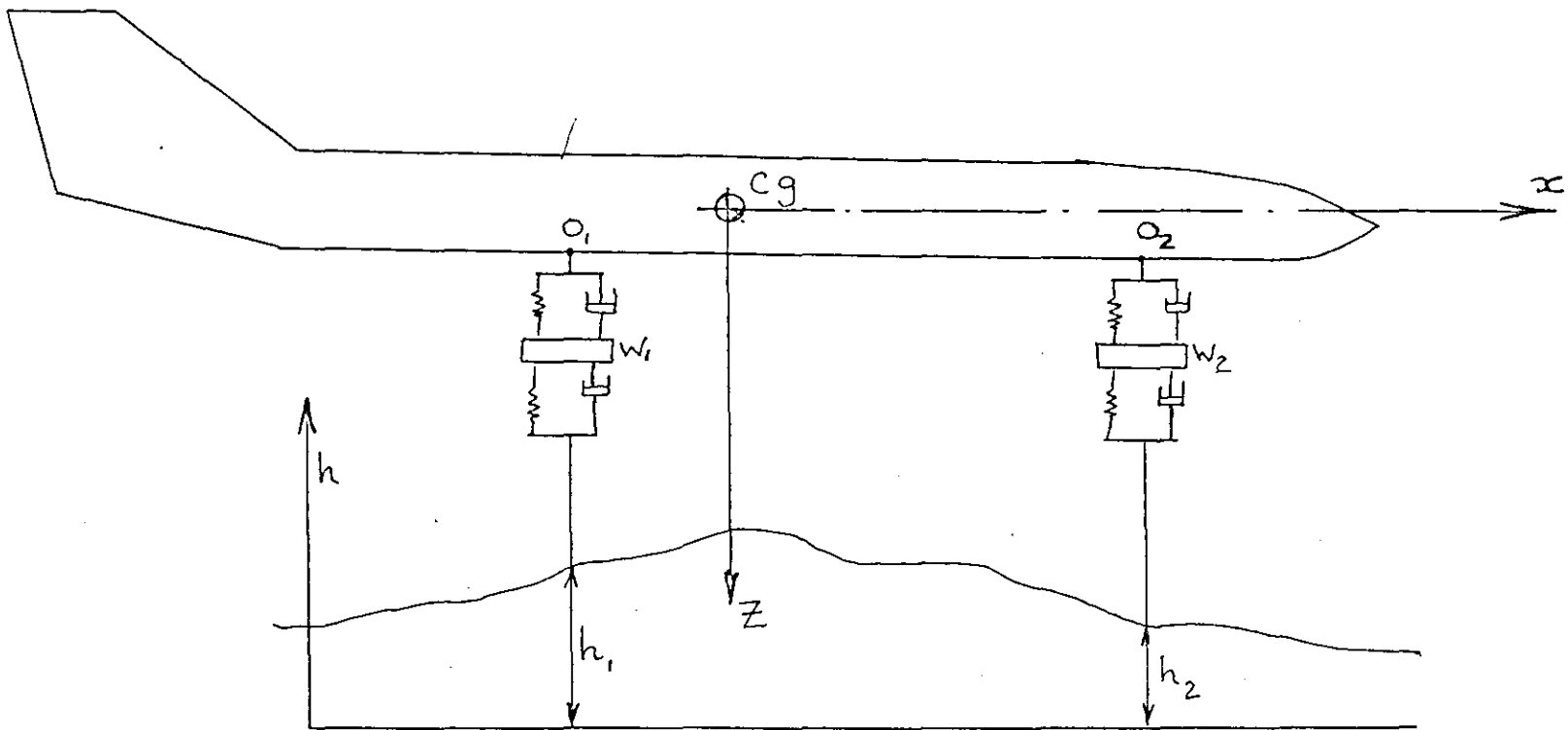
DIAGRAMMATIC  REPRESENTATION  OF  AIRCRAFT

FIGURE 3.1

77
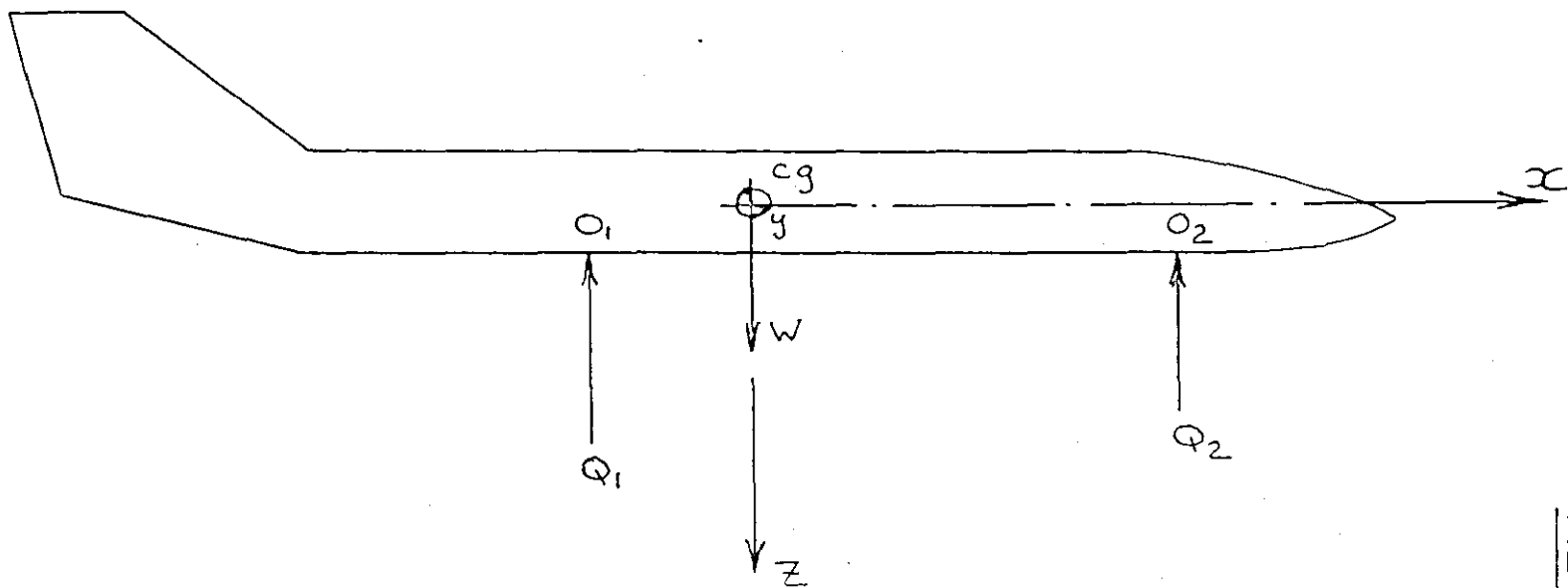
FREE-FREE AIRFRAME

FIGURE 3.2

FIGURE 3.3
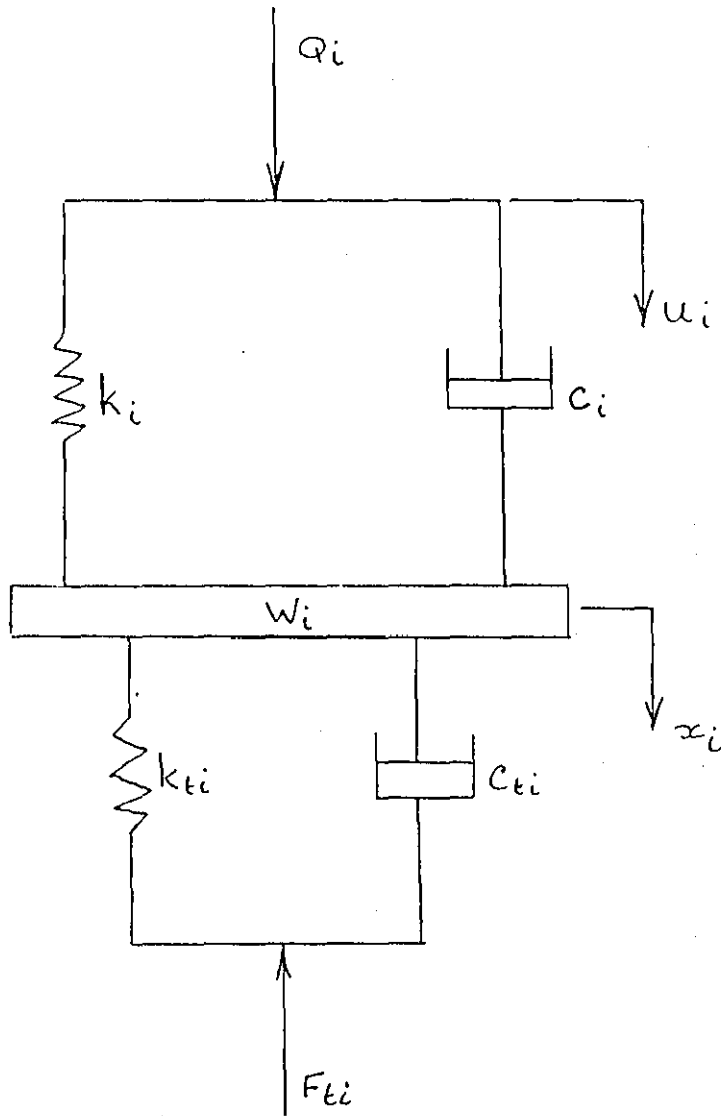


$i$ TH  UNDERCARRIAGE

## SECTION 4

## RESPONSE STUDIES

The studies of response of the aircraft to a random runway profile are based on the following relationships, which have been discussed in Section 1.

The means-square value of response acceleration is given by

$$\overline{\ddot{x}^2} = \int_{\omega_{f1}}^{\omega_{f2}} \oint_{\ddot{x}}(\omega_f) \, d\omega_f \qquad (4-1)$$

$\oint_{\ddot{x}}(\omega_f)$ is the power spectral density of the response acceleration and is given by

$$\oint_{\ddot{x}}(\omega_f) = \omega_f^4 \cdot \oint_{\ddot{x}}(\omega_f)$$

$$= \omega_f^4 \cdot H_{\frac{x}{q}}(\omega_f) \oint_q(\omega_f) \qquad (4-2)$$

## 4. 1 Frequency response function

In order to apply the above relationships, the frequency response function for the aircraft is required, that is the amplitude of the response of the aircraft due to rolling over a sinusoidal curve of frequency $\omega$, and unit amplitude. There are in effect two transfer functions to consider, since the input to the aircraft is not at one point. There is the transfer function linking the runway profile to the input to the wheels at the nose and main undercarriage locations represented by the elevations $h_1$ and $h_2$ respectively, and there is the transfer function linking the wheel input to the aircraft response. The product of these two transfer functions will give the overall transfer function linking the aircraft response to the runway profile. The two transfer functions may be treated together as follows, leading to the frequency response function.

Figure 4.1(a) shows diagrammatically the aircraft on the sinusoidal runway with runway elevations $h_1$ and $h_2$ at the main and nose undercarriages measured from some arbitrary datum. Referring to figure 4.1(b), where the datum line has been located centrally on the sinusoidal wave for convenience, the elevation $h_2$ is given by

$$h_2 = H \sin \frac{2\pi y}{L} = \sin \frac{2\pi V t}{L}$$

since $H = 1$

Since it is response functions which are required, this may be written

$$h_2 = e^{\frac{i2\pi V t}{L}} = e^{i\omega_F t} \qquad (4 - 3)$$

Similarly, $h_1$ is given by :

$$h_1 = e^{\frac{i2\pi(y+d)}{L}}$$

$$= e^{i\left(\frac{2\pi Vt}{L} + \frac{2\pi d}{L}\right)}$$

$$= e^{\frac{i2\pi Vt}{L}} \cdot e^{\frac{i2\pi d}{L}}$$

Since the aircraft velocity $V$ and the runway undulation wavelength $L$ can vary while $d$ remains constant, $\frac{2\pi d}{L}$ will vary with $\omega_f$.

Thus, $\frac{2\pi d}{L} = \frac{2\pi V}{L} \cdot \frac{d}{V} = \frac{d}{V} \cdot \omega_f$

Hence,

$$h_1 = e^{i\omega_f t} \, e^{i\frac{d}{V}\omega_f}$$

$$= (\cos \frac{d}{V}\omega + i \sin \frac{d}{V}\cdot\omega_f) e^{i\omega_f t} \qquad (4-4)$$

From equations (4-3) and (4-4),

$$\dot{h}_2 = i\omega_f e^{i\omega_f t} \qquad (4-5)$$

$$\dot{h}_1 = i\omega_f(\cos \frac{d}{V}\omega_f + \sin \frac{d}{V}\omega_f) e^{i\omega_f t} \qquad (4-6)$$

The elements of $\left\{F(t)\right\}$ in equation (3-31) may now be formed as follows:

$$-K_{t1}h_1 - C_{t1}\dot{h}_1 = -K_{t1}(\cos \frac{d}{V}\omega_f + i\sin \frac{d}{V}\omega_f) e^{i\omega_f t}$$
$$\qquad\qquad -C_{t1} i\omega_f(\cos \frac{d}{V}\omega_f + i \sin \frac{d}{V}\omega_f) e^{i\omega_f t}$$
$$= \left\{ (-K_{t1} \cos \frac{d}{V}\omega_f + C_{t1}\omega_f \sin \frac{d}{V}\omega_f) \right.$$
$$\qquad\qquad \left. -i(K_{t1} \sin \frac{d}{V}\omega_f + C_{t1}\omega_f \cos \frac{d}{V}\omega_f) \right\} e^{i\omega_f t} \qquad (4-7)$$

$$-K_{t2}h_2 - C_{t2}\dot{h}_2 = -K_{t2}e^{i\omega_f t} - C_{t2}i\omega_f e^{i\omega_f t}$$
$$= (-K_{t2} - iC_{t2}\omega_f) e^{i\omega_f t} \qquad (4-8)$$

Substituting equations (4-7) and (4-8) into equation (3-31) and pre-multiplying by $\lceil M \rfloor^{-1}$ gives

$$\lceil M \rfloor^{-1} \{F(t)\} = \lceil M \rfloor^{-1} \left\{ \begin{array}{c} \left(-K_{t1}\cos \frac{d}{V}\omega_f + C_{t1}\omega_f \sin \frac{d}{V}\omega_f \right) \\ -i\left(K_{t1}\sin \frac{d}{V}\omega_f + C_{t1}\omega_f \cos \frac{d}{V}\omega_f \right) \\ -K_{t2} - i\, C_{t2}\omega_f \\ \{\bar{0}\} \end{array} \right\} e^{i\omega_f t}$$

Equation (3-32) may now be written

$$\{\ddot{X}\} + \lceil M \rfloor^{-1}[C]\{\dot{X}\} + \lceil M \rfloor^{-1}[K]\{X\} = \lceil M \rfloor^{-1}\{G\}e^{i\omega_f t} \qquad (4-9)$$

where $\{G\}$ is a column matrix having

$$G_1 = \left(-K_{t1}\cos \frac{d}{V}\omega_f + C_{t1}\omega_f \sin \frac{d}{V}\omega_f\right) - i\left(K_{t1}\sin \frac{d}{V}\omega_f + C_{t1}\omega_f \cos \frac{d}{V}\omega_f\right)$$

$$G_2 = -K_{t2} - iC_{t2}\omega_f$$

$$G_i = 0, \quad i = 3, 4 \text{-----}N$$

In equation (4-9) the left hand side represents the aircraft system and the right hand side now represents the input to the system from a sinusoidal runway profile of unit amplitude and frequency $\omega_f$. The transfer function of a system is the Laplace transform of its impulse response. Thus, to find the transfer function of the aircraft system, the following equation may be considered:

$$\{\ddot{X}\} + \lceil M \rfloor^{-1}[C]\{\dot{X}\} + \lceil M \rfloor^{-1}[K]\{X\} = \{\delta(t)\} \qquad (4-10)$$

Taking Laplace Transforms and putting all initial values to zero gives

$$\left[ p^2 \lceil I \rfloor + p\lceil M \rfloor^{-1}[C] + \lceil M \rfloor^{-1}[K] \right] \{X(p)\} = \{1\} \qquad (4-11)$$

which may be written

$$\left[ U(p) \right] \left\{ X(p) \right\} = \left\{ 1 \right\} \qquad (4-12)$$

Premultiplying both sides by $\left[ U(p) \right]^{-1}$ gives

$$\left\{ X(p) \right\} = \left[ U(p) \right]^{-1} \left\{ 1 \right\} \qquad (4-13)$$

where $\left[ U(p) \right]^{-1}$, the aircraft system transfer function, is an

N x N complex matrix in p.

The steady-state response of a linear stable system to

an input $x = Ae^{i\omega t}$ is given by

$$y = \left| P(i\omega) \right| Ae^{i(\omega t + \Theta)}$$

where $\left| P(i\omega) \right|$ = magnitude of $P(i\omega)$

$\Theta$ = arg $P(i\omega)$

$P(i\omega)$ is determined by replacing p by $i\omega$ in the

system transfer function $P(p)$.

The input to the aircraft system under consideration is

$\left\lceil M_\rfloor^{-1} \left\{ G \right\} e^{i\omega_f t}$ from equation (4-9), and since this input is

derived from a runway profile of sinusoidal form with frequency $\omega_f$

and unit amplitude, the response to this input will be the frequency

response required for use in equation (4-2).

Thus,

$$\left\{ X(i\omega_f) \right\} = \left[ U(i\omega_f) \right]^{-1} \left\lceil M_\rfloor^{-1} \left\{ G \right\} e^{i(\omega_f t + \Theta)} \qquad (4-14)$$

The values of the elements $X_j$ of the matrix $\left\{ X(i\omega_f) \right\}$ are

therefore given by

$$\left\{ X(i\omega_f) \right\} = \left\{ \left[ U(i\omega_f) \right]^{-1} \left\lceil M_\rfloor^{-1} \left\{ G \right\} \right\} \qquad (4-15)$$

where

$$\left[ U(i\omega_f) \right] = \left[ \left\lceil M_\rfloor^{-1} \left[ K \right] - \omega_f^2 \left\lceil I_\rfloor + i\omega_f \left\lceil M_\rfloor^{-1} \left[ C \right] \right] \qquad (4-16)$$

It must be remembered that $X_j$ is the generalised co-ordinate of the jth mode. Thus, the elements of the matrix $\{X(i\omega_f)\}$ may be said to be the generalised co-ordinates of the frequency response function in the various modes, so that the actual frequency response function of the jth mode is given by $\phi_i{}^j X_j(i\omega_f)$, at frequency $\omega_f$, where $\phi_i{}^j$ is the mode shape of the jth mode at the ith position on the aircraft. The matrix of frequency response functions for the various modes at the ith point on the aircraft at frequency $\omega_f$ is therefore given by

$$\left\{\phi_i{}^j \cdot X_j(i\omega_f)\right\} = \left\{\phi_j \cdot r_j + i\phi_j \cdot s_j\right\} \qquad (4 - 17)$$

where $r_j$ and $s_j$ are the real and imaginary parts respectively of the elements of $\left\{X_j(i\omega_f)\right\}$.

The elements of the matrix in equation (4-17) give both the magnitudes, and phases relative to each other, of each mode's frequency response function. To take account of the phase differences, the real and imaginary parts must be added separately to give the real and imaginary parts of the overall frequency response function. The frequency response function required for use in equation (4-2) is therefore the modulus of this, so that

$$\frac{H_x(\omega_f)}{q} = \sqrt{Q^2 + \mathcal{G}^2} \qquad (4 - 18)$$

where $Q = \sum_{j=3}^{N} \phi_i{}^j \cdot r_j = \left[\phi_i{}^j\right]\{R\}$ $\qquad (4 - 19)$

$\mathcal{G} = \sum_{j=3}^{N} \phi_i{}^j \cdot s_j = \left[\phi_i{}^j\right]\{s\}$ $\qquad (4 - 20)$

$\{R\}$ and $\{s\}$ are column matrices of order $N - 2$ whose elements are $r_j$ and $s_j$ respectively.

$j = 3, 4 \text{ ----- } N$

NOTE    $X_1(i\omega_f)$ and $X_2(i\omega_f)$ are wheel displacements and thus

do not contribute to displacement of the aircraft.    Hence

in equations (4-19) and (4-20) the elements considered are

$j = 3, 4$, airframe rigid body heave and pitch respectively,

and $j = 5, 6$ ---N, airframe flexural modes.

4. 2  Computer Programs

4.2.1  Main Response Program, RESPONSE 12

The main response program is shown at Appendix F.  This program computes the rms values of the response acceleration at the mainwheel, nosewheel, and pilot locations of the aircraft for a constant taxiing velocity V, which is read in with the data.  The response is programmed from the equations developed in section 3 and sub-section 4.1, and the runway PSD with two straight line segments on the log scales, developed in section 2.  A "single straight line" runway PSD may be used when required simply by making both slopes and intercepts the same.

The aircraft considered in the program, therefore, has linear oleo stiffness and damping, wheel masses, linear tyre stiffness and damping, rigid body heave and pitch modes, and can have as many flexural modes as required.  The number of modes, NM, to be considered is read in with the data, together with the relevant information regarding the modes to be considered.  NM includes the rigid body heave and pitch modes, so that the number of flexural modes is (NM - 2).

The frequency response function and input PSD are calculated for a particular frequency, and used in equation (4-2) to compute the output PSD at the three required aircraft locations at that frequency.  Earlier less sophisticated programs used constant step lengths of frequency and computed the area under the output PSD v. frequency curve by a simple accumulation of height

times step length. This was found to lead to some inconsistencies and it was realised that a much more sophisticated approach to the step length was required. The procedures SIMPS and SORT were thus developed and used in conjunction with the eigen values, which are also calculated in the program, to give a much more accurate calculation of the area, whose square root is the response required. The requirement for, and development of, the method of integration, using SIMPS etc, are discussed in Appendix E.

Six procedures had been obtained, developed by Wilkinson at NPL, for computing eigenvalues and eigenvectors. These were BALANCE, ELMHES, BALBAK, ELMBAK, CDIV, HQR2. These were all used during the response studies to investigate some effects. However, for use in the integration program, BALBAK and ELMBAK are not required, since they apply only to eigenvectors, and HQR2 has been substantially shortened, the part concerned with eigenvectors being removed. A new matrix, COEFF, is formed in the program, from which the eigenvalues are computed. It can easily be shown that for a system

$$M\ddot{x} + C\dot{x} + Kx = 0$$

the eigenvalues are found from the matrix

$$COEFF = \begin{bmatrix} -M^{-1}C & -M^{-1}K \\ I & 0 \end{bmatrix}$$

The response of the aircraft with various flexural modes neglected may be obtained very easily from the above program simply by leaving out the data for the mode or modes to be neglected, and

modifying NM accordingly.

### 4.2.2 Uncoupled heave and pitch response programs, BDARBHH4 and PITCH RESPONSE 6

Programs to compute the rms value of the response acceleration at the mainwheel, nosewheel and pilot locations of the aircraft for a constant taxiing velocity in the rigid body heave mode only and the rigid body pitch mode only are shown in Appendix G.  The response is the same at all three locations of course for the heave mode.  The heave response program computes the response for a range of taxiing velocities, whilst the pitch response program computes the response for only one taxiing velocity, although this was amended to cover a range.  The aircraft considered in these programs has linear oleo stiffness and damping, but wheel masses and tyres are neglected.  The analyses leading to these programs is shown in sub-sections 4.3.2.1 and 4.3.2.2.

The choice of step length for the integration is again a critical factor in the pitch case, but is not so in the heave case.  Thus, the heave program uses constant step lengths but the pitch program uses procedures similar to those in RESPONSE 12, but differs in its method of selecting the intermediate integration limits.  This is described in Appendix E.

## 4. 3  Presentation and Interpretation of Results

### 4.3.1  Effect of neglecting various modes

The response in each mode, i.e. rigid body heave and pitch and flexural modes, was found by a simple modification to the main response program, whereby the modulus of each element of the matrix $\left\{\phi_i^{\,j}.x_j(i\omega_r)\right\}$ was found, this being the frequency response function for the jth mode.  The response for the mode was then computed as in the main response program.

This program was used to find the response in each mode at the mainwheel, nosewheel and pilot locations for the standard Boeing 707 aircraft parameters using the geometric mean runway. The values computed for a taxiing velocity of 60 ft/S are shown in table 4.1.  It was found, as might be expected, that the Rigid Body Heave mode made the largest contribution to the response at the mainwheel location and the Rigid Body Pitch mode made the largest contribution to the response at the nosewheel and pilot locations.  It was also found that, of the first 6 flexural modes, the 1st and 4th had relatively large values of response, the response from the other 4 modes being very small.  The response from the 1st flexural mode was particularly large at the mainwheel location and that from the 4th flexural mode was particularly large at the pilot location.

Table 4.2(a) confirms the above findings.  The mean square values of the second derivative of the generalised co-ordinates , $\overline{\ddot{x}^2}$ , are reproduced from results presented in reference 13.  The values of mode shape $\phi$ are also taken from the reference.  From these

values, since the mode shape is a constant for a given mode and
the generalised co-ordinates are stated in inch second units, the
rms values of response acceleration were calculated from :

$$\sigma = \sqrt{\frac{\overline{\ddot{X}^2}\,\phi^2}{12}} \quad \text{ft/s}^2$$

It will be seen that, with some slight variations, the values of
response in the modes confirm the trends discussed above.

Whilst this gives an indication of the contributions
of each mode to the overall response, it does not indicate whether
or not a particular mode may be neglected.   Since the modulus is
used for each element of the matrix in finding the frequency response
function for that mode, the final response contributions are
magnitudes only, no phase being available to enable the effect on
the overall response to be established.   Thus, although a small
response, as in flexural modes 2,3,5 and 6, will indicate that the
mode could be neglected, a large response, as in flexural modes 1 and
4, will not necessarily indicate that it cannot.   Depending on the
phase of the mode's frequency response function in the matrix
$\left\{ \phi_i^{\,j} X_j \left( i\omega_f \right) \right\}$, the neglecting of the mode could lead to either an
underestimate or an overestimate of the response by a large amount,
or indeed to very little error if the phase of the mode were
approximately at right angles to the phases of the other modes, this
assuming of course that the other modes were all in phase or 180°
out of phase, a not very likely state of affairs.

In order to estimate more accurately the effect of neglecting
various flexural modes, the main response program was used, using only

the data for the modes to be incorporated each time. Figures 4.2,
4.3 and 4.4 show the results of this for the standard Boeing 707
aircraft parameters, using the geometric mean runway, for various
taxiing velocities. It will be seen from these figures that the
indications from the response in each mode are confirmed.
Neglecting any one, or a combination, or all, of flexural modes
2, 3, 5 and 6 gives only very small errors in the estimated response
compared with that calculated using all 6 flexural modes. The
largest errors are at the main-wheel location at the higher speeds
(200, 240 ft/s) and are then only of the order of 4%. Neglecting
the 1st or 4th flexural mode, however, does, as suggested by the
previous program, give rise to substantial errors. Neglecting the
1st flexural mode leads to an overestimate of the response at the
nosewheel and pilot location by up to 25% and an underestimate of
the response at the mainwheel location by up to 25%. Neglecting
the 4th flexural mode leads to an underestimate of the response at
the nosewheel and pilot location; in the worst case, at 40 ft/s,
the predicted response neglecting this mode is less than half
that if all the modes are included. The response at the mainwheels,
however, is not so badly affected by neglecting this mode, the
result being an underestimate by up to only about 5%.

Figures 4.2, 4.3 and 4.4 also show the response estimated
by neglecting all the flexural modes, i.e. assuming a rigid aircraft.
It can be seen that this gives a closer approximation to the
response obtained using all flexural modes than was obtained by
neglecting only the 1st or 4th flexural mode. Thus it appears that

the responses in the 1st and 4th flexural modes tend to counteract each other to some extent.

The above results were obtained using an earlier less sophisticated program than the final main response program RESPONSE 12 shown at Appendix F and discussed in sub-section 4.2.1 and Appendix E, and slight differences in data from that derived in Section 2 and Appendix C (see Appendix D). The program used constant step lengths of 1 rad/s and the mid-ordinate rule for the integration of the response PSD. However, it is shown in Appendix E that this tends to give a fairly constant percentage overestimation of the response and thus, for purposes of comparison, would have been adequate. It was therefore assumed that the same results would be obtained using the more sophisticated program, and they were not repeated after the development of this program.

Figure 4.5 shows the frequency response functions at the mainwheel and pilot locations plotted against the forcing frequency, for the same aircraft and runway parameters used to produce figures 4.2, 4.3 and 4.4, including the first 6 flexural modes, for a taxiing velocity of 120 ft/s. Figure 4.6 shows the corresponding power spectral densities of the acceleration response. The values for these figures were computed as intermediate steps in response computations using the later more sophisticated program RESPONSE 12. These figures confirm that the rigid body heave and pitch, and the 1st and 4th flexural modes, contribute by far the bigger proportion of the response. Since the square root of the area under the PSD curve is the rms value of the response, it can be seen, particularly from figure 4.6, that the contributions from the 2nd,

3rd, 5th and 6th flexural modes are negligible.

Figures 4.7 and 4.8 show the frequency response functions and PSD's of acceleration response respectively for the same aircraft parameters, runway parameters, and taxiing velocity as used for figures 4.5 and 4.6, but neglecting the flexural modes. It can be seen that the two modes (rigid body heave and pitch) are very close together in this case, and each contributes to the other peak.    The eigenvalues for the cases with and without the flexural modes are shown in table 4.3, and the modes corresponding to the various frequencies given by the eigenvalues are noted on figures 4.5 to 4.8.    Since the two modes in figures 4.7 and 4.8 are so close it is not immediately obvious which is heave and which is pitch.  Close examination of the eigenvectors indicates that the higher frequency mode is the heave mode, although it also indicates considerable coupling between the modes since there is a considerable contribution to each mode from the other.    The fact that the lower frequency mode produces a much greater response at the pilot location than at the mainwheel location also indicates that this is the pitch mode.

For the case where all the flexural modes were considered (figures 4.5 and 4.6) the pitch, heave, and 1st flexural modes are close together.    This time examination of the eigenvectors did not give so clear an indication of the frequencies of the three modes, since they did not show that each frequency gave a clearly larger contribution to one mode.    This indicates that the three modes are in fact very closely coupled.    The modal frequency of the

first flexural mode is between the two frequencies found in figures 4.5 and 4.6 for heave and pitch, and thus theory would predict that this should "push apart" the pitch and heave peaks of the frequency response, so that the modes in ascending order of frequency should be pitch, 1st flexural, and heave. This appears to be confirmed by the pilot location values in table 4.1. However, examination of the damping ratios in table 4.3 indicates that the mode with frequency 6.47 rad/s is the pitch mode, and since one would not expect the heave and pitch modes to interchange order of frequencies, it is concluded that the modes in ascending order of frequency are 1st flexural, pitch and heave. This appears to be confirmed by the mainwheel location values in table 4.1. It should of course be noted that the values in table 4.1 were results for a different taxiing velocity. It is clear from the above discussion that the 1st flexural, pitch, and heave modes are very closely coupled, producing three peaks on the frequency response curve, and hence on the response PSD curve, which are extremely difficult to distinguish as separate modes.

Examination of figures 4.6 and 4.8 indicates that the area under the PSD curve, and hence the response, is decreased considerably at the pilot location for the heave and pitch modes if the 1st flexural mode is included and the peak for the 4th flexural mode is ignored. The effect on the mainwheel location is not so pronounced but in fact a small increase in area is obtained by including the 1st flexural mode. Now if the 1st flexural mode is excluded and the 4th flexural mode is included, it will be seen that the effect

will be to add the peak of the 4th flexural mode from figure 4.6

to the rigid body response on figure 4.8, giving a large increase

in response at the pilot location and in fact a small decrease

at the mainwheel location.    Thus, the effects of the 1st and

the 4th flexural modes tend to balance each other, and it will

be seen that the areas under the corresponding curves on figures

4.6 and 4.8 are approximately equal, so that for this particular

aircraft consideration of only the rigid body modes gives a

fair approximation to the response obtained by considering rigid

body plus 6 flexural modes.    The values from these figures are

| | Root mean square values of response acceleration ($ft/s^2$) | |
|---|---|---|
| | Mainwheel Location | Pilot Location |
| All modes included | 6.7064 | 9.9952 |
| Rigid body modes only included | 5.6728 | 10.5907 |

These figures confirm the earlier indications from the

less sophisticated program, shown for this particular velocity on

figure 4.3, and therefore most of the remaining investigation of

this report, and in particular the development of computer programs,

may be carried out using the rigid body modes only.    This will be

very much more economical in computer time.

The fact that neglecting the flexural modes causes

considerable modification to the response in the heave and pitch

modes may also be confirmed by reference to table 4.2.    The values

in table (b) were calculated from results presented in reference

13 in the same way as those in table (a). Comparing values in

tables 4.2(a) and (b) it will be seen that by neglecting the flexural

modes the calculated value of response in the heave mode is increased

and that in the pitch mode is decreased. If the changes are related

to areas under the response PSD curve the changes are even more

apparent, since the rms value of response is equal to the square root

of the area under this curve. Thus the changes in area would be

18.2: 29.1 for the heave mode and 35.6 : 23.4 for the pitch mode.

Each mode will of course make a contribution to the response in

the other mode due to coupling.

The damping in the various modes from the eigenvalues in

table 4.3 is worthy of note here. The damping of the nose

undercarriage mode is higher than critical, whilst the main

undercarriage mode has a damping ratio of about 0.37. These remain

essentially unchanged, whether or not the flexural modes are included

in the analysis. The damping constants obtained for these two

modes by considering the expression:

$$\beta = \frac{c}{2\sqrt{KM}}$$

where C = oleo damping constant

K = oleo stiffness

M = undercarriage mass

are $\beta$ = 3.5 and 0.48 for the nose and main undercarriage modes

respectively. Thus, coupling the undercarriage modes to the aircraft

modes causes a reduction in the modal damping of the undercarriages.

It will be shown in sub-section 4.3.2.3 that this also occurs in the

heave and pitch damping when these modes are coupled.

The heave and pitch damping ratios from table 4.3

for the case when only rigid body modes are considered are 0.046

and 0.120 respectively. When the flexural modes are included

the modal damping ratios for heave and pitch are reduced to 0.032

and 0.113 respectively. Thus the inclusion of the flexural

modes causes a reduction in modal damping in the heave and pitch

modes. However, although the damping in the heave and pitch modes

is reduced by inclusion of the flexural modes, the response from

these two modes is not increased, but is actually reduced, as has

already been shown. This is because the peaks on the response PSD

curve are now further apart and have smaller bandwidths, giving less

overlap and much narrower peaks.

The modal damping used for all flexural modes was $\beta = 0.025$.

It will thus be seen that the effect of coupling has been to increase

the damping in the flexural modes.

### 4.3.2 Variation of response with taxiing velocity

The rms values of response accleration at the mainwheels,

nosewheel and pilot locations, for a range of taxiing velocities,

were computed using an earlier, much less sophisticated version of

the response program RESPONSE 12. It was found when these were

plotted that the curves of response v. taxiing velocity, whilst

showing an increase of response with velocity, had a considerable

amount of undulation. It was in an attempt to explain this

undulation, and in particular to explain undulations in the

curves of response v. undercarriage stiffness (sub-section 4.3.3),

that the final, more sophisticated, version of the response program

was developed (see Appendix E). The results discussed in this section are therefore computed using the response program RESPONSE 12 (see sub-section 4.2.1).

Figure 4.9 shows the rms values of response acceleration at the mainwheels and pilot location plotted against taxiing velocity, using the aircraft and runway data at Appendix D. The flexural modes of the aircraft were neglected in the computation of values for this figure, as they are for the remainder of this section, and thus only rigid body data for the aircraft is used. It can be seen from the figure that peaks occur in the pilot location response curve, and to a smaller extent in the mainwheel response curve, at taxiing velocities of about 25 and 40 ft/s, but then at taxiing velocities above 60 ft/s a steady rise in response occurs with increasing velocity.

There is some similarity between figure 4.9 and the curves published in reference 37. The curves of response against velocity for the Boeing 707 showed peaks at approximately the same taxiing speeds. However, the data used in this reference for the 707 was somewhat different from that used here. In order to provide a better check of correlation between the two methods, the data used in reference 37 for the Boeing 707 and for the runway, was used with the above program. The aircraft masses were as already used, but the stiffnesses were as follows:

Main oleo stiffness, $K_1$ = 2.03 x $10^6$ lbf/ft

Nose oleo stiffness, $K_2$ = 162000 lbf/ft

Main tyre stiffness, $K_{t1}$ = 1.158 x $10^6$ lbf/ft

Nose tyre stiffness, $K_{t2}$ = 92000 lbf/ft

The main oleo damping used was $C_m = 21600$ $lbf/(ft/s)^2$, and in order to ensure no coupling between the modes it was assumed that

$$\frac{C_{em}}{C_{en}} = \frac{C_m}{C_n} = \frac{L_n}{L_m} \qquad (4 - 21)$$

where $L_n$ and $L_m$ are the distances from the Cg to the nose and main-wheels respectively. For this analysis the equivalent main oleo damping was calculated using

$$C_{em} = \frac{8}{3\pi} \cdot C_m \dot{X} \qquad (4 - 22)$$

as used to calculate the earlier data in Appendix D, and using $\dot{X}$ from Appendix C, and the equivalent nose oleo damping was calculated from equation (4-21).

Thus, the oleo damping used was

Main oleo damping, $C_1 = C_{em} = 12250$ $lbf/(ft/s)$

Nose oleo damping, $C_2 = C_{en} = 970$ $lbf/(ft/s)$

The analysis in the reference used no undercarriage masses or tyre damping, so in order to use the response program, the same values were used as for figure 4.9.

The runway used, taken from the reference, was represented by

$$\bar{\phi}(\omega) = \frac{20 \times 10^{-6} V}{\omega^2} \qquad (4 - 23)$$

Figure 4.10(a) is reproduced from reference37. Figure 4.10(b) was plotted from computer calculations using the above data in the response program RESPONSE 12. Although the analysis in reference 37 used an iterative linearisation procedure for the main

oleo damping, and used no undercarriage masses or tyre damping, the two figures show remarkably similar results. The curves in figure 4.10(a) show a slight dip at around 130 ft/s which is not evident in figure 4.10(b), and the pilot location response in figure 4.10(a) begins to decrease at velocities over about 175 ft/s, which again is not evident in figure 4.10(b). However, the peaks on the curves occur at the same taxiing velocities, and apart from the above slight differences, the curves have a very similar shape. However, in general the curves in figure 4.10(b) show responses about 20% higher than those in figure 4.10(a). This may be explained by the fact that the use of equation (4-22) gives an underestimate of the equivalent damping constant in this case, even if the value of oleo stroking velocity used (8.05 in/s in this case) were correct for all taxiing velocities. If equation (4-22) is used, $\dot{X}$ should be the peak value of oleo stroking velocity, whereas the value used was an rms value. Thus the equation should have been

$$C_{em} = \sqrt{2} \cdot \frac{8}{3\pi} \, C_m \dot{X}_{RMS} \qquad (4 - 24)$$

However, a better value would probably have been obtained by equating energy dissipated over a period of time for a random input having Gaussian distribution (see Appendix C), so that :

$$C_{em} = 2 \sqrt{\frac{2}{\pi}} \, C_m \cdot \dot{X}_{RMS} \qquad (4 - 25)$$

Using this equation, and equation (4-21) would have resulted in the following values:

$$C_{em} = 23100 \; \text{lbf/(ft/s)}$$

$$C_{en} = 1830 \; \text{lbf/(ft/s)}$$

It can be seen from sub-section 4.3.4, and in particular

figure 4.29 that an increase in main oleo damping from 12250 lbf/(ft/s) to 23100 lbf/(ft/s) gives decreases in response of approximately 8 to 10% at the pilot location and 10 to 15% at the mainwheel location. Although the figure does not show such low nose oleo damping values it may reasonably be deduced from the figure that an increase from 970 lbf/(ft/s) to 1830 lbf/(ft/s) would also give a decrease in response, this time the decrease being greater at the pilot location than the mainwheel location. The general values of response for figure 4.10(b) would therefore be reduced and correspond more closely with figure 4.10(a).

The curves of figure 4.10 show much more pronounced peaks than those of figure 4.9. This is due to the very low nose oleo damping used to produce figures 4.10. It is felt that these values are unrealistically low and that on the actual Boeing 707 the nose oleo damping is approximately half of the main oleo damping, or in fact about the same as one main oleo (see Appendix C). The corollary is, of course, that it is not realistic to assume the heave and pitch modes are uncoupled.

It will also be seen that the response at the pilot location in particular in figures 4.10 stops increasing at medium to high taxiing velocities, and indeed in figure 4.10(a) begins to decrease at taxiing velocities over 175 ft/s. This is a function of the runway profile used to produce these figures. The runway profile represented by equation (4-23) tends to underestimate the runway roughness at low frequencies. This will be discussed more fully in section 4.3.6, as it is also felt that the geometric mean runway used may in fact overestimate the roughness at low frequencies.

For completeness computations were made of response for various taxiing velocities using the standard aircraft parameters with the runway described by equation (4-23) and using the aircraft parameters from reference 37 with the geometric mean runway.

Figure 4.11 shows response acceleration at pilot and mainwheel locations for the aircraft data from reference 37, used for figure 4.10(b), running on the geometric mean runway with parameters from Appendix D. The pronounced peaks are still evident at low taxiing velocities, although not quite so high as in figure 4.10. At higher taxiing velocities, however, the response increases rapidly with increase in velocity. This is unrealistic for the following reasons. Firstly, at such high accelerations the wheels, and particularly the nosewheel, would leave the ground, and since this analysis assumes the tyres remain in contact with the ground it cannot predict any motion which occurs if this condition is not met. Secondly, if such accelerations did occur, they would be accompanied by higher stroking velocities of the oleos, and thus, the equivalent linear damping, from equation (4-24), should be increased. This in turn would compute lower accelerations. This demonstrates the requirement, with extreme responses, to calculate a new equivalent damping for each taxiing velocity, or to use an iterative technique to compute the damping and response. Lastly the high values of response are caused by a combination of the unrealistically low nose oleo damping used in this data and the possible overestimate of runway roughness at long wavelengths - i.e. low spacial frequencies - by the expression for the geometric mean runway (see section 4.3.6).

Figure 4.12 shows response acceleration at pilot and

mainwheel locations for the standard aircraft data from Appendix D, used for figure 4.9, with the runway described by equation (4-23). Again the peaks at low taxiing velocities are evident, this time slightly more pronounced than using the same parameters on the geometric mean runway (figure 4.9), but not so pronounced as using the parameters from reference 37 (figures 4.10 and 4.11). At higher taxiing velocities, however, the response at the pilot location increases by only 1 $ft/s^2$ between taxiing velocities of 100 ft/s and 240 ft/s, whilst the main wheel location response increases by only 2.75 $ft/s^2$ over the same range. Comparing this with figure 4.9 it can be seen that the corresponding increase is 12 $ft/s^2$ when the same aircraft parameters are used on the geometric mean runway.

It became clear during the development of the final response program (RESPONSE 12), that unlike the case of variation of response with main oleo stiffness, the peaks on the curves of response v. taxiing velocity were not caused by too large a step length being used in the integration of the response PSD curve (see sub-section 4.3.3 and Appendix E). The final program, using a varying step length, which is smaller at critical sections of the curve, still produces the peaks, as already seen at figures 4.9 to 4.12.

In order to investigate and explain the peaks the heave and pitch motions of the aircraft have been simplified and investigated separately as completely independent and uncoupled motions. It is assumed that the aircraft has linear oleo stiffness

and damping, no undercarriage masses, and no tyres. To find the frequency response functions for heave and pitch the aircraft is assumed to traverse a runway profile of sinusoidal form with frequency $w_f$ and unit amplitude. Figure 4.13 shows this in diagrammatic form.

### 4.3.2.1 Heave response

Referring to figure 4.13 the heave input, h, to the undercarriage system is given by

$$h = h_2 - \frac{b}{d}(h_2 - h_1)$$

$$= h_2\left(1 - \frac{b}{d}\right) + h_1\left(\frac{b}{d}\right) \qquad (4-26)$$

From figure 4.13, $a + b = d$, so that $1 - \frac{b}{d} = \frac{a}{d}$.

Using this, and substituting for $h_2$ and $h_1$ from equations (4-3) and (4-4) gives

$$h = e^{i w_f t}\left(\frac{a}{d} + \frac{b}{d}\left(\cos\phi + i\sin\phi\right)\right) \qquad (4-27)$$

where $\phi = \frac{d \cdot w_f}{V}$

The equation of motion for the uncoupled heave motion is

$$M\ddot{z} + (C_n + C_m)(\dot{z} - \dot{h}) + (k_n + k_m)(z - h) = 0$$

i.e. $M\ddot{z} + C\dot{z} + Kz = C\dot{h} + Kh \qquad (4-28)$

where $C = C_n + C_m$

$K = k_n + k_m$ $\qquad (4-29)$

If the runway elevation is denoted by the suffix r, the input displacement to the undercarriage system by h, and the aircraft response displacement by x, then the frequency response function

relating the aircraft response displacement to the runway elevation may be written

$$\left| H(i\omega)_{\frac{x}{r}} \right| = \left| H(i\omega)_{\frac{h}{r}} \right| \times \left| H(i\omega)_{\frac{x}{h}} \right| \qquad (4-30)$$

Now

$$H(i\omega)_{\frac{x}{h}} = \frac{1}{M(i\omega_f)^2 + C(i\omega_f) + K} = \frac{1}{(K-M\omega_f^2) + i(C\omega_f)^2}$$

$$\therefore \left| H(i\omega)_{\frac{x}{h}} \right| = \frac{1}{\sqrt{(K-M\omega_f^2)^2 + (C\omega_f)^2}} \qquad (4-31)$$

and

$$H(i\omega)_{\frac{h}{r}} = \frac{C\dot{h} + Kh\cdot}{e^{i\omega_f t}}$$

$$= i\omega_f C\left( \frac{a}{d} + \frac{b}{d}(\cos\phi + i\sin\phi) \right)$$

$$+ K\left( \frac{a}{d} + \frac{b}{d}(\cos\phi + i\sin\phi) \right)$$

$$= \left( \frac{a}{d} + \frac{b}{d}(\cos\phi + i\sin\phi) \right)\left( K + i(C\omega_f) \right)$$

$$\therefore H(i\omega)_{\frac{h}{r}} = \sqrt{\left( \frac{a}{d} + \frac{b}{d}\cos\phi \right)^2 + \left( \frac{b}{d}\cos\phi \right)^2} \times \sqrt{K^2 + (C\omega_f)^2}$$

Now

$$\left( \frac{a}{d} + \frac{b}{d}\cos\phi \right)^2 + \left( \frac{b}{d}\cos\phi \right)^2$$

$$= \left( \frac{a}{d} \right)^2 + 2\left( \frac{a}{d}\frac{b}{d} \right)\cos\phi + \left( \frac{b}{d}\cos\phi \right)^2 + \left( \frac{b}{d}\sin\phi \right)^2$$

$$= \frac{1}{d^2}\left( a^2 + b^2 + 2ab\cos\phi \right)$$

$$= \frac{1}{d^2}\left( a^2 + 2ab + b^2 - 2ab + 2ab\cos\phi \right)$$

$$= \frac{(a+b)^2}{d^2} - \frac{2ab}{d^2}(1 - \cos\phi)$$

$$= 1 - \frac{2ab}{d^2}(1 - \cos\phi)$$

Thus

$$\left| H(i\omega)_{\frac{h}{r}} \right| = \sqrt{K^2 + (C\omega_f)^2} \times \sqrt{1 - \frac{2ab}{d^2}(1 - \cos\phi)} \qquad (4-32)$$

Hence

$$H(i\omega)_{\frac{x}{r}} = \sqrt{\frac{K^2 + (C\omega_f)^2}{(K-M\omega_f^2)^2 + (C\omega_f)^2}} \times \sqrt{1 - \frac{2ab}{d^2}(1-\cos\frac{d.\omega_f}{V})} \quad (4-33)$$

From equations (4-1) and (4-2) the mean square value of response acceleration is given by

$$\overline{\ddot{x}^2} = \int_{\omega_1}^{\omega_2} \omega^4 \left(H(i\omega)_{\frac{x}{r}}\right)^2 \times \phi_r(\omega)d\omega \quad (4-34)$$

From equation (2-8) the PSD of the runway profile is given by

$$\overline{\phi}_r(\omega) = \frac{\overline{C}V^{n-1}}{\omega^n}. \quad (4-35)$$

Substituting from (4-33) and (4-35) in (4-34) gives

$$\overline{\ddot{x}^2} = \int_{\omega_{f1}}^{\omega_{f2}} \left(\frac{K^2 + (C\omega_f)^2}{(K-M\omega_f^2)^2 + (C\omega_f)^2}\right)\left(1 - \frac{2ab}{d^2}(1 - \cos\frac{d\omega_f}{V})\right)\left(\frac{\overline{C}V^{n-1}\omega_f^4}{\omega_f^n}\right) d\omega_f \quad (4-36)$$

A computer program (BDARBHH4) was written to compute the root-mean-square value of response acceleration from equation (4-36) (see sub-section 4.2.2 and Appendix G) for a range of taxiing velocities. Computations were made using the aircraft parameters derived from reference 37 and the runway profile PSD from the same reference. The results are shown on figure 4.14. Undulations are still apparent on this curve, but are not nearly so pronounced as on figures 4.10. Thus it would appear that the heave motion, whilst possibly making some small contribution to the peaks on the curve of response v. taxiing velocity, is not completely responsible. In order to further understand the effect of this motion, equation (4-36) is now examined more closely.

Figure 4.15 shows the parts of equation (4-36) which have

to be multiplied together before integrating. Curves (a) and
(d) are independent of the taxiing velocity except insofar as $\omega_f$
is dependent on V. Curve (C), for the simple runway profile
used for figure 4.14, is directly dependent on V, and thus
magnitudes on the curve will increase directly as V increases.
Curve (b) however is a sinusoidal wave given by

$$F(\omega_f) = 1 - \frac{2ab}{d^2}(1 - \cos\frac{d}{V}\cdot\omega_f) \qquad (4 - 37)$$

Thus the number of peaks of the curve within a given range of
$\omega_f$ will be dependent on the taxiing velocity V.

The peaks on the curve will occur when

$$\cos\frac{d}{V}\cdot\omega_f = 1$$

i.e.
$$\frac{d}{V}\cdot\omega_f = n\pi, \quad n = 0,2,4,6\text{----} \qquad (4 - 38)$$

The troughs on the curve will occur when

$$\cos\frac{d}{V}\cdot\omega_f = 1$$

i.e.
$$\frac{d}{V}\cdot\omega_f = n\pi, \quad n = 1,3,5,7\text{----} \qquad (4 - 39)$$

It may reasonably be deduced from figure 4.15 that when
the rms values of response, computed from equation (4-36) for a
range of taxiing velocities, are plotted against taxiing velocity,
local maxima will occur at velocities at which a peak of figure
4.15(b) coincides in frequency with the peak of figure 4.15(a),
and that local minima will occur at velocities at which a trough
of (b) coincides in frequency with the peak of (a). It is
therefore required to find the value of $\omega_f$ at which $f(\omega_f)$ is a
maximum, where

$$f(\omega_f) = \frac{K^2 + (C\omega_f)^2}{(K-M\omega_f^2)^2 + (C\omega_f)^2}$$

Now $f(\omega_f)$ will be a maximum when $\frac{\partial f}{\partial \omega_f} = 0$.

If $f = \frac{A}{B}$ then $\frac{\partial f}{\partial \omega_f} = \frac{B\frac{\partial A}{\partial \omega_f} - A\frac{\partial B}{\partial \omega_f}}{B^2}$

Thus, f will be a maximum when

$$B\frac{\partial A}{\partial \omega_f} = A\frac{\partial B}{\partial \omega_f}$$

where $A = K^2 + C^2\omega_f^2$

$B = K^2 - 2KM\omega_f^2 + M^2\omega_f^4 + C^2\omega_f^2$

i.e. for maximum $f(\omega_f)$,

$$\left(K^2 - 2KM\omega_f^2 + M^2\omega_f^4 + C^2\omega_f^2\right)\left(2C^2\omega_f\right)$$
$$= \left(K^2 + C^2\omega_f^2\right)\left(-4KM\omega_f + 4M^2\omega_f^3 + 2C^2\omega_f\right)$$

$$2C^2K^2\omega_f - 4C^2KM\omega_f^3 + 2C^2M^2\omega_f^5 + 2C^4\omega_f^3$$
$$= -4K^3M\omega_f + 4K^2M^2\omega_f^3 + 2C^2K^2\omega_f - 4C^2KM\omega_f^3$$
$$+4C^2M^2\omega_f^5 + 2C^4\omega_f^3$$

i.e. $2C^2M^2\omega_f^5 + 4K^2M^2\omega_f^3 - 4K^3M\omega_f = 0$

from which $\omega_f = 0$

or $C^2M\omega_f^4 + 2K^2M\omega_f^2 - 2K^3 = 0$

i.e. $\omega_f^2 = \frac{-2K^2M \pm \sqrt{4K^4M^2 + 8K^3C^2M}}{2C^2M}$

$$= -\left(\frac{K}{C}\right)^2 \pm \sqrt{\left(\frac{K}{C}\right)^4 + 2\left(\frac{K}{C}\right)^4 \frac{C^2}{KM}}$$

Taking the positive root,

$$\omega_1^2 = \left(\frac{K}{C}\right)^2\left(\sqrt{1 + \frac{2C^2}{KM}} - 1\right) \qquad (4-40)$$

where K and C are given by equations (4-29)

Substituting the values of aircraft parameters used to produce figure 4.14 in equation (4-40) gives

peak frequency, $\omega = 14.84$ rad/s

As a check on this value, if low damping is assumed, it can be said that the peak will occur at approximately the undamped natural frequency,

$$\text{i.e. } \omega_n = \sqrt{\frac{K}{M}} = \sqrt{\frac{k_m + k_n}{M}}$$

$$= \sqrt{\frac{2.03 \times 10^6 + .162 \times 10^6}{9912}}$$

$$= 14.9 \text{ rad/s}$$

This indicates that the damping used is very low, which can also be shown from the fact that

$$\text{Damping ratio, } \beta = \frac{C}{C_{crit}} = \frac{C}{2\sqrt{KM}}$$

$$= \frac{12250 + 970}{2\sqrt{(2.03 + .162)10^6 \times 9912}}$$

$$\text{i.e. } \beta = 0.0448$$

Putting the above frequency into equation (4-38) and using the wheelbase, d, of 59 feet indicates that local maxima should occur at velocities of

140, 70, 46.6, 35, 28, 23.3, 20, 17.5 ---- ft/s

Similarly, from equation (4-39) local minima should occur at velocities of

280, 93.3, 56, 40, 31.1, 25.4, 21.6, 18.7 ----ft/s

These values are plotted on figure 4.14 and clearly coincide with the peaks and troughs of the undulations on the curve for the higher velocities. In order to demonstrate the

coincidence for the lower velocities it is clear that many computer
runs would have had to be done with very small increments in
taxiing velocity, and it was not considered that any further value
could be gained from this.

It is clear from figure 4.14 that the peaks and troughs
are only small undulations on a gradually increasing response.   If
equation (4-37) is examined further it will be seen that the maximum
value of $F(\omega_f)$ is

$$F(\omega_f) \; =, \; 1 - \frac{2ab}{d^2}(1 - 1) \; = \; 1$$

whilst the minimum value is

$$F(\omega_f) \; = \; 1 - \frac{2ab}{d^2}(1 + 1) \; = \; 1 - \frac{4ab}{d^2}$$

$$= \; 1 - \frac{4(4.33 \times 54.67)}{(59)^2} \; = \; 0.73$$

Thus, referring to figure 4.15, the ratio of the values
of the peak of the final curve to be integrated for the two cases
(i) when the peak of (a) coincides with a peak of (b) and (ii) when
the peak of (a) coincides with a trough of (b) will be 1:0.73, i.e.
a reduction of 27% between maximum and minimum peak values.  This
of course neglects the effect of curve (c) which will give a
steadily increasing value of the peak with V.  Since in case (i)
some lower values to each side of the peak will be decreased and in
case (ii) some lower values to each side of the peak will be
increased, the effect will be that the area under the final curve
for case (ii) will be somewhat greater than 73% of that for case (i),
and since the rms value of response is a function of the square root
of this area, the rms value for case (ii) will be somewhat greater
than 85% of that for case (i).   This indicates that the graph of

variation of rms value of response with taxiing velocity should show a steadily increasing response on which is superimposed undulations of less than 7% from the mean. Figure 4.14 shows that this is in fact the case.

### 4.3.2.2 Pitch Response

Referring to figure 4.13 the pitch input, $\Theta_o$, to the undercarriage system is given by

$$\Theta_o = \sin^{-1}\left(\frac{h_2 - h_1}{d}\right) \qquad (4 - 41)$$

Since $(h_2 - h_1)$ is very small compared with d it may be said that

$$\Theta_o = \frac{h_2 - h_1}{d} \qquad (4 - 42)$$

Substituting for $h_2$ and $h_1$ from equations $(4-3)$ and $(4-4)$ gives

$$\Theta_o = \frac{e^{i\omega_f t}}{d}\left(1 - \cos\phi - i\sin\phi\right) \qquad (4 - 43)$$

The equation of motion for the uncoupled pitch motion is

$$I\ddot{\Theta} + b^2 C_n(\dot{\Theta} - \dot{\Theta}_o) + a^2 C_m(\dot{\Theta} - \dot{\Theta}_o) + b^2 k_n(\Theta - \Theta_o)$$
$$+ a^2 k_m(\Theta - \Theta_o) = 0$$

i.e. $I\ddot{\Theta} + C_e\dot{\Theta} + K_e\Theta = C_e\dot{\Theta}_o + K_e\Theta_o \qquad (4 - 44)$

$$\text{where } C_e = b^2 C_n + a^2 C_m \left.\right\}$$
$$K_e = b^2 k_n + a^2 k_m \left.\right\} \qquad (4 - 45)$$

Equation $(4-30)$ applies to the pitch case if x is replaced by $\Theta$ and h by the angular input, $\Theta_o$, to the undercarriage system. Proceeding from this equation,

$$\left|H(i\omega)_{\frac{\Theta}{\Theta_o}}\right| = \frac{1}{\sqrt{(K_e - I\omega_f^2)^2 + (C_e\omega_f)^2}} \qquad (4 - 46)$$

and

$$H(i\omega)_{\frac{\Theta_o}{r}} = \frac{C_e\dot{\Theta}_o + K_e\Theta_o}{e^{i\omega_f t}}$$

$$= \frac{1}{d}\left(i\omega_f C_e(1 - \cos\phi - i\sin\phi) + K_e(1 - \cos\phi - i\sin\phi)\right)$$

$$= \frac{1}{d}\left((K_e + i\omega_f C_e)(1 - \cos\phi - i\sin\phi)\right)$$

$$\therefore \left|H(i\omega)_{\frac{\theta}{r}}\right| = \frac{1}{d}\sqrt{\left(K_e^2 + (C_e\omega_f)^2\right)\left((1 - \cos\phi)^2 + (\sin\phi)^2\right)}$$

$$= \frac{1}{d}\sqrt{\left(K_e^2 + (C_e\omega_f)^2\right)\left(1 - 2\cos\phi + \cos^2\phi + \sin^2\phi\right)}$$

$$= \frac{\sqrt{2}}{d}\sqrt{\left(K_e^2 + (C_e\omega_f)^2\right)\left(1 - \cos\phi\right)} \qquad (4-47)$$

Thus

$$\left|H(i\omega)_{\frac{\theta}{r}}\right| = \frac{\sqrt{2}}{d}\sqrt{\frac{K_e^2 + (C_e\omega_f)^2}{(K_e - I\omega_f^2)^2 + (C_e\omega_f)^2}} \cdot \sqrt{(1 - \cos\phi)} \qquad (4-48)$$

Hence, in the same way as the heavecase,

$$\overline{\ddot{\theta}^2} = \int_{\omega_{f1}}^{\omega_{f2}} \frac{2}{d^2}\left(\frac{K_e^2 + (C_e\omega_f)^2}{(K_e - I\omega_f^2)^2 + (C_e\omega_f)^2}\right)\left(1 - \cos\frac{d \cdot \omega_f}{V}\right)\left(\frac{CV^{n-1}\omega_f^4}{\omega_f^n}\right)d\omega_f \qquad (4-49)$$

A computer program (PITCH RESPONSE 6) was written to compute the root-mean-square value of response from equation (4-49) (see sub-section 4.2.2 and Appendix G). The angular response was computed, and from this the linear response at the mainwheel, nosewheel, and pilot locations. The program was run for a range of taxiing velocities using the same aircraft parameters and runway profile PSD as for the heave case. The results for the pilot location are shown on figure 4.16. Very pronounced undulations are apparent on this curve, which indicates that it is the pitch motion that is responsible for the peaks on the curves of response v. taxiing velocity (figures 4.9 to 4.12). Equation (4-49) is examined in the same way as the heave equation was examined.

Figure 4.17 shows the parts of equation (4-49) except for the term $2/d^2$ which is a constant for a given aircraft configuration.

The curve of interest is again curve (b) which is a sinusoidal wave given by

$$F(\omega_f) = 1 - \cos \frac{d}{V} \cdot \omega_f \qquad (4 - 50)$$

The number of peaks of the curve within a given range of $\omega_f$ is again dependent on the taxiing velocity $V$, but this time the peaks on the curve will occur when

$$\cos \frac{d \omega_f}{V} = -1$$

i.e.

$$\frac{d \omega_f}{V} = n\pi, \quad n = 1,3,5,7 \text{ ---} \qquad (4 - 51)$$

and the troughs will occur when

$$\cos \frac{d \omega_f}{V} = 1$$

i.e.

$$\frac{d \omega_f}{V} = n\pi, \quad n = 0,2,4,6 \text{ ---} \qquad (4 - 52)$$

Referring to figure 4.17, it is again required to find the frequency at which the peak occurs on (a). Equation (4-40) may be used for the pitch case if $K$, $C$ and $M$ are replaced by $K_e$, $C_e$ and $I$ respectively. However, the damping is again low, since

$$\beta = \frac{C_e}{2\sqrt{K_e I}} = \frac{(4.33)^2 \cdot 12250 + (54.67)^2 \cdot 970}{2\sqrt{\left((4.33)^2 \times 2.03 \times 10^6 + (54.66)^2 \times 162000\right) 5.325 \times 10^6}}$$

$$= 0.0295$$

Hence it can be said that the peak occurs at the undamped natural frequency given by

$$\omega_n = \sqrt{\frac{K_e}{I}} = \sqrt{\frac{(4.33)^2 \times 2.03 \times 10^6 + (54.667)^2 \times 162000}{5.375 \times 10^6}}$$

$$= 9.86 \text{ rad/s}$$

Putting this frequency into equations (4-51) and (4-52) indicates that local maxima on figure 4.16 should occur at taxiing velocities of

185, 61.5, 37, 26.4, 20.5, 16.8 ----- ft/s

and local minima should occur at

92.5, 46.4, 30.9, 23.2, 18.5, 15.5 ---- ft/s

These values are plotted on figure 4.16 and clearly coincide with the peaks and troughs of the undulations on the curve for the higher velocities except that there is not a local maximum at the highest taxiing velocity of 185 ft/s. The form of the curve has been estimated at the lower taxiing velocities, where the computed points were not sufficiently close to show the actual effect, and it will be seen that the computed points do agree with the estimated velocities of peaks and troughs. Again it was considered that no further value could be gained by making the many computer runs which would be required to accurately plot the curve at the lower taxiing velocities.

Referring to figure 4.17 it will be seen that without curve (b) the response would gradually increase with increase in taxiing velocity, since the only curve directly dependent cn V would be (c) whose magnitudes increase directly as V (for this particular runway PSD). Hence the rms values of response would increase as $\sqrt{V}$. Thus, the effect of the coincidence of the peak of (a) with the peaks and troughs of (b) will be to give maximum deviations above and below this steadily increasing curve. A curve is drawn on figure 4.16 to represent this. The significance of the velocity of 185 ft/s may now be seen more clearly. Although it does not

show a local maximum it does give a maximum deviation above the mean line. Referring again to equation (4-50) it will be seen that the mean value of $F(\omega_f)$ occurs when

$$\cos \frac{d.\omega_f}{V} = 0$$

i.e. $\frac{d.\omega_f}{V} = n\pi$, $n = 0.5, 1.5, 2.5, 3.5, 4.5---$ (4 - 53)

giving in this case taxiing velocities of :

370, 123.5, 74, 53, 41.2, 33.7, 28.5 ----ft/s

It will be seen that the two curves on figure 4.16 cross at approximately these velocities, although it is thought that this will not be exactly so since curve (a) on figure 4.17 is not symmetrical about the peak. However, the above values indicate that the curves will again cross at a taxiing velocity of approximately 370 ft/s. This is born out by the fact that there should be another local minimum at infinite taxiing velocity, corresponding to n = 0 in equation (4-52). The explanation of this can be seen by referring to figure 4.17. The final peak at 185 ft/s occurs when the 1st peak of (b) coincides with the peak of (a). Thereafter the value on (b) which coincides with the peak of (a) is always decreasing with increase in taxiing velocity. The two curves on figure 4.16 cross at approximately the taxiing velocity when the point A on figure 4.17(b) coincides with the peak on (a) and after that the two curves on figure 4.16 diverge, the actual curve always decreasing relative to the mean curve.

In the pitch case the peaks and troughs on figure 4.16 are large undulations on the gradually increasing response. Examining equation (4-50) further, it will be seen that the maximum

value of $F(\omega_p)$ is 2, whilst the minimum value is 0. In the same way as in the heave case this does not of course mean that the ratio of the areas under the final curves to be integrated will be 2:0. A number of peaks and zeros will occur on the final curve to be integrated, depending on the taxiing velocity. Figure 4.18 shows the final curve to be integrated (i.e. the PSD of the pitch response, the area under which is the mean square value of response acceleration), using aircraft parameters of :

$$k_m . = 2.4 \times 10^6 \text{ lbf/ft}$$

$$k_n = 187000 \text{ lbf/ft}$$

$$C_m = 6540 \text{ lbf/(ft/s)}$$

$$C_n = 3438 \text{ lbf/(ft/s)}$$

The remaining aircraft parameters are as Appendix D. The taxiing velocity used for this figure was 120 ft/s, giving the first peak of $(1-\cos\phi)$ at 6.39 rad/s and the following zero at 12.78 rad/s as marked on the figure. The peak for the aircraft parameter dependent part of the equation (i.e. the natural frequency) was calculated to be at 10.6 rad/s. It can be seen therefore that the effect of $(1-\cos\phi)$ has been to slightly lower the peak, put a value of zero at $\omega = 12.78$ rad/s, and double the values at $\omega = 6.39$ and 19.2 rad/s. If the taxiing velocity had been such that $(1-\cos\phi)$ = 0 at $\omega = 10.6$ rad/s the curve would have looked completely different.

Figure 4.19 is plotted for the same parameters as figure 4.18, but using a taxiing velocity of 10 ft/s thus giving many peaks and zeros on the $(1-\cos\phi)$ curve which clearly show through on the final curve. This time there is a zero very near to the natural frequency of 10.6 rad/s.

Figure 4.20 shows the PSD of the pitch response using the aircraft parameters derived from reference 37 (i.e. corresponding to figure 4.16) for a velocity of 10 ft/s. The natural frequency in pitch using these parameters was 9.86 rad/s. It can be seen that the peak nearest to this value is very high compared with the other peaks, indicating that the aircraft parameter dependent part of the equation had a high narrow peak, and thus the pitch motion has very low damping. This is also verified by the fact that the height of the main peak is almost 20 times the height of those on figure 4.19.

It has already been stated that the value of nose undercarriage damping of 970 lbf/(ft/s) is felt to be unrealistcally low. Even the values of damping used for figures 4.18 and 4.19 are very low, being half of those originally calculated for the Boeing 707 (Appendix D) and only approximately a quarter of the values calculated in Appendix C. Referring to the calculation of pitch damping ratio above, it will be seen that even though the nose undercarriage damping is much smaller than the main undercarriage damping it has by far the overriding effect on the pitch damping, since the oleo damping constants are multiplied by the square of their distance from the cg of the aircraft in the calculation of pitch damping. Thus, halving or doubling the main undercarriage damping will have little effect on the pitch damping, but halving or doubling the nose oleo damping will almost halve or double the pitch damping. Thus an increase from 970 to 3438 lbf/(ft/s) as between figures 4.20 and 4.19 will give almost 4 times the damping in pitch.

It is worth pointing out here that figures 4.18, 4.19 and 4.20 are good examples of why it is necessary to use an integrating technique which varies the step length along the ω axis to give short steps at "peaky" positions (see Appendix E). The integration limits used for the segments in this case were the peaks and troughs of $(1-\cos\phi)$, and the undamped natural frequency.

### 4.3.2.3 Overall Rigid Body Response

The results of the foregoing two sub-sections may now be used to discuss and explain more fully the shape of the curves of aircraft response v. taxiing velocity (figures 4.9 to 4.12). Comparing figures 4.10(b) and 4.16 it will first of all be seen that the peaks occur at different taxiing velocities on the two graphs. This is easily explained (see below). However, it is also evident that in general, at the pilot location, the response due to uncoupled pitch alone is greater than the response due to combined heave and pitch. Thus it appears that the heave motion has the effect of damping the pitch motion in this aircraft even when the motions are uncoupled. It would appear that the heave and pitch motions must be out of phase at the pilot location (and therefore also at the nosewheel), so that the heave motion actually reduces the response. However, it must be remembered that the analysis for figure 4.10(b) included undercarriage masses and tyre stiffness and damping which probably filtered some of the runway roughness, particularly at the shorter wavelengths, thus reducing the response.

At the mainwheels, as would be expected, the pitch motion

has little effect, the response at the mainwheels due to pitch being only $7\frac{1}{2}\%$ of that at the pilot location. Thus the response at the mainwheel location in figure 4.10(b) is very similar to the heave response in figure 4.14, except again for the difference in taxiing velocities at which the peaks occur.

In the course of the computations made to produce figure 4.10(b) the eigenvalues were computed for the aircraft parameters under consideration. They were found to be as follows:

| | |
|---|---|
| Nose u/c mode: | $-42.15 \pm i\ 137.4$ |
| Main u/c mode: | $-48.92 \pm i\ 146.7$ |
| Heave mode: | $-0.1012 \pm i\ 8.933$ |
| Pitch mode: | $-0.0458 \pm i\ 5.926$ |

From these the modal damping for the nose undercarriage is 0.31 and for the main undercarriage is 0.33. Thus the nose undercarriage damping is very low compared with the considerable overdamping produced by the standard aircraft parameters from Appendix D (see sub-section 4.3.1).

It will be seen that the frequencies for the heave and pitch modes are 8.93 rad/s and 5.93 rad/s respectively. These should be compared with the 14.9 rad/s and 9.86 rad/s calculated in sub-sections 4.3.2.1 and 4.3.2.2 for the uncoupled cases; they explain why the peaks on the curves of figure 4.10(b) occur at different taxiing velocities to those on figure 4.16. The reason for the reduction in frequencies is that undercarriage masses and tyre stiffness and damping were used for the overall rigid body response case. The reduced frequencies are almost identical to those stated in reference 37, although this reference used no undercarriage masses or tyre

damping.   Thus these had no effect on the frequency, as would be expected since the masses were very small and the damping extremely low.   Hence the oleos and tyres were effectively springs in series, giving a lower stiffness and thus a lower natural frequency.   This helps to explain the fact that the response at the pilot location for pitch only (without tyres and hence with higher natural frequency) was higher than that for overall rigid body modes.

The values of taxiing velocity at which the peaks and troughs occur on the pitch and heave response curves, from these reduced frequencies, are

Pitch

    Peaks :   111.1, 37.1, 22.3, 15.9, 12.4 --- ft/s

    Troughs : 55.5, 27.8, 18.5, 13.9, 11.1 --- ft/s

Heave

    Peaks :   84, 42, 28, 21, 16.8 --- ft/s

    Troughs:  168, 56, 33.6, 24, 18.7 --- ft/s

The values of taxiing velocity for the pitch case confirm those found in reference 37.   However, this reference discussed only the peaks on the curve for the pilot location, making no attempt to produce similar results for heave or to relate the admittedly small peaks on the mainwheel response curve.   It also stated that the expected peak at 111 ft/s was absent or not noticeable.   It will be shown below however that the peak at 111 ft/s can be explained and is indeed apparent on the response curve.

Referring to figure 4.10(b) it will be seen that the peaks and troughs on the pilot location response curve coincide

extremely well with the velocities calculated above for pitch, and those on the mainwheel location curve with those calculated for heave. This suggests, as would be expected, that the response at the pilot location comes predominantly from pitch, and that at the mainwheel location predominantly from heave.  The points on the curves at low velocities were not computed sufficiently closely to give the true shape of the curves, and it was felt that no useful purpose would be served by going back and computing more points, since the shape of the curves is now explained and understood.

It was shown in sub-section 4.3.2.2 that the peaks and troughs on these response curves are not strictly local maxima or minima, although this is what they constitute at medium and low velocities where they are relatively close together, but are maximum deviations above and below a steadily increasing response curve.  In the same way as in that section, it can be shown that for the pitch case the mean steadily increasing curve would cross the actual curve at taxiing velocities of approximately:

222, 74, 44.4, 32, 24.6 ----- ft/s

Such a curve is drawn on the pilot location response curve on figure 4.10(b), and it can be seen that although the taxiing velocity of 111 ft/s does not show a local maximum it does fairly clearly show a point of maximum deviation of the curve from this mean line.

It has already been shown that the reduction of the mean rate of increase of response with increase of taxiing velocity at the higher taxiing velocities is a function of the runway profile used.  This may be verified by inspecting equation (2-5), i.e. the

PSD of input from the runway, given by

$$\phi(\omega) = \frac{\overline{C}.V^{n-1}}{\omega^n}$$

Neglecting the undulations caused by the $(1-\cos\phi)$ terms of figures 4.15 and 4.17 the response PSD is proportional to the input PSD, and hence the rms value of the response is proportional to the square root of the input PSD. Thus, rms value of response acceleration, $\sigma$, is given by

$$\sigma \propto \sqrt{V^{n-1}}$$

$$\text{i.e,} \quad \sigma \propto V^{\frac{n-1}{2}}$$

$$\therefore \frac{\partial\sigma}{\partial V} \propto \frac{n-1}{2}.V^{\frac{n-3}{2}}$$

Hence, if n is less than 3, then as $V \to \infty$, $\frac{\partial\sigma}{\partial V} \to 0$ as shown in the following figure.
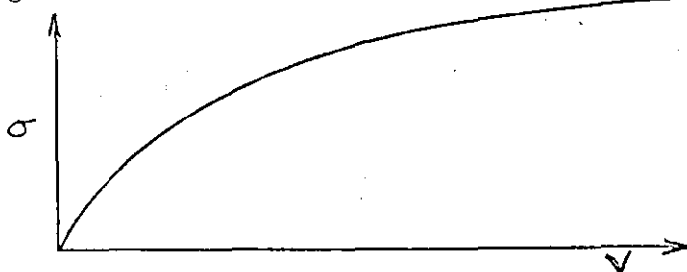


In particular, if n = 2, the case used for figure 4.10, then:

$$\frac{\partial\sigma}{\partial V} \propto \frac{1}{\sqrt{V}}$$

and the slope of the curve of response against taxiing velocity will approach zero at lower taxiing velocities than if n is equal to say 2.5. This may be clearly seen by comparing figures 4.10(b) and 4.11. The fact that the slope on these curves for the mainwheel location is actually increasing at the high velocities is of course due to the influence of the $(1-\cos\phi)$ term.

The peaks and troughs on the curves on figure 4.11 occur at the same taxiing velocities as those on figure 4.10, the same aircraft parameters having been used in both cases.

Similarly, the peaks and troughs on the curves on figures 4.9 and 4.12 occur at the same taxiing velocities, the standard aircraft parameters from Appendix D having been used for both figures.    The eigenvalues calculated during computations for these curves are as shown in table 4.3 for the case when rigid body modes only were considered.    From these the pitch and heave frequencies are 6.012 rad/s and 8.073 rad/s. respectively, giving taxiing velocities at which peaks and troughs should occur on the response curves as follows:

Pitch

   Peaks : 113, 37.6, 22.6, 16.1, 12.6 ---- ft/s

   Troughs : 56.5, 28.2, 18.8, 14.1, 11.3 ---- ft/s

Heave

   Peaks : 75.8, 37.9, 25.3, 19.0, 15.2 ---- ft/s

   Troughs : 151.6, 50.5, 30.3, 21.7, 16.8 ---- ft/s

Examination of figures 4.9 and 4.12 reveals that the peaks and troughs on the curves of pilot location response and mainwheel response occur at velocities very close to those given above for pitch and heave respectively.    Although the velocities calculated above are still an extremely good approximation to the velocities at which the peaks and troughs occur on the actual curves, they do not appear to be quite so good as were the ones for figures 4.10 and 4.11.    This may be due to coupling between the modes leading to slight modification of the curves;    it will be remembered that the aircraft

parameters from reference 37, used to produce figures 4.10 and 4.11, were chosen to produce uncoupled heave and pitch. However the correlation is so close that the method is extremely valuable in predicting velocities at which these peaks occur.

It is also important to note that since the velocities at which these peaks occur are dependent only on the frequencies of the modes of the aircraft and the aircraft wheel base, they are independent of the surface on which the aircraft is taxiing, only the magnitude of the response at these peaks being dependent on the runway surface. Thus, taxiing velocities may be calculated which should be avoided on all surfaces in order to minimise response acceleration, and thus crew and passenger discomfort and pilot fatigue. However, since the velocities at which minimum response occurs are different for the pilot and mainwheel locations, calculation of an optimum taxiing velocity will have to take into account the importance of the position on the aircraft. For a take-off or landing run of course all these velocities must be passed through in any case.

Using the aircraft parameters from table 4.3 the following damping ratios are calculated for the uncoupled heave and pitch modes:

$$\text{Heave:} \quad \beta = 0.0881$$
$$\text{Pitch:} \quad \beta = 0.2579$$

From the eigenvalues in the table, for the case when flexural modes are neglected, the damping ratios for the coupled heave and pitch modes are

$$\text{Heave:} \quad \beta = 0.0463$$
$$\text{Pitch:} \quad \beta = 0.1199$$

Similarly, although the aircraft parameters from reference 37 were chosen to produce uncoupled heave and pitch, it has been shown that when the pitch and heave responses are calculated separately the damping ratios are

$$\text{Heave: } \beta = 0.0448$$

$$\text{Pitch: } \beta = 0.0295$$

However, when the same parameters are used in the overall response program, as was done to produce fingures 4.10(b) and 4.11, the damping ratios are found to be

$$\text{Heave: } \beta = 0.0114$$

$$\text{Pitch: } \beta = 0.0077$$

Thus, for a given set of parameters, coupling tends to lower the modal damping substantially.

As an added check on the accuracy of results obtained from the main response program, an attempt was made to duplicate figures obtained in reference 13. In the reference a computer program was presented to produce the time history of response acceleration by a deterministic method of an aircraft taxiing on a given runway profile. From time histories of the response of a Boeing 707 taxiing on Runway 12, Langley Field, the root-mean-square response accelerations shown in table 4.4(a) were calculated. The profile and PSD curves of this runway are presented in reference 28; the PSD curve is reproduced here as figure 4.21 for reference. A single straight line approximation to the PSD was made (line ① on the figure) and the PSD found to be given by

$$\phi(\omega) = \frac{15 \times 10^{-6} V^{1.31}}{\omega^{2.31}} \qquad (4-54)$$

This value was used in the main response program in conjunction with the standard aircraft parameters from Appendix D, using rigid body modes only and a taxiing velocity of 100 ft/s. It produced rms values of response accelerations at the pilot and mainwheel locations of 8.312 ft/s$^2$ and 4.598 ft/s$^2$ respectively. On inspection of the intermediate computer printout, however, it was found that most of the response occurred between frequency values of $\omega = 5$ to 10 rad/s ($\Omega = 0.05$ to 0.1 rad/ft at 100 ft/s), and since the estimated PSD is not a very good fit to the actual PSD curve between these values (figure 4.21) the above response values underestimated the actual response. A better approximation was therefore drawn to the curve between these frequency values (line ②) and produced a PSD of

$$\phi(\omega) = \frac{4.5 \times 10^{-6} y^{2.0}}{\omega^{3.0}} \qquad (4 - 55)$$

This was used in the program with the same aircraft parameters and produced rms values of response acceleration at the pilot and mainwheel location of 11.231 and 6.023 ft/s$^2$ respectively. These are obviously considerably higher than the values calculated in the reference. However, it has already been stated that the values of equivalent linear damping shown in Appendix D are low, and more realistic figures are those calculated in Appendix C. The program was therefore run a third time using the aircraft parameters of Appendix C, the runway profile given by equation (4-55), rigid body modes only, and a taxiing velocity of 100 ft/s. It was also run using rigid body modes plus the first 6 flexural modes. However, since in this case response was expected up to frequencies of 35 rad/s ($\Omega = 0.35$ rad/ft) or more, and since at the higher frequencies equation (4-55) underestimates the roughness of runway

12, a further line was drawn in the figure (line ③), and lines ②
and ③ used as the PSD so that at frequencies below $\Omega = 0.22$ rad/ft
($\omega = 22$ rad/s) the PSD was given by equation (4-55) and at frequencies
above this the PSD was given by

$$\bar{\phi}(\omega) = \frac{16 \times 10^{-6} v^{1.04}}{\omega^{2.04}} \qquad (4\text{-}56)$$

These latter two computer runs resulted in the root-mean-square
values of response acceleration shown in table 4.4(b).

It will be seen from the table that the values are all
greater than the values taken from the reference.   One reason for
this can be seen by referring to figure 4.21.   At frequencies
below $\Omega = 0.05$ rad/ft ($\omega = 5$ rad/s) line ② overestimates the runway
roughness.   However, this only gives a small error, since, even if
all the area under the response PSD curve is removed, the values for
the pilot location and mainwheel location when 6 flexural modes are
considered are 8.2 and 6.05 ft/s$^2$ respectively, and the respective
values when only rigid body modes are considered are 8.35 and
4.53 ft/s$^2$.

The closest correlation between values in tables 4.4(a)
and (b) is the response at the pilot location for the case when
6 flexural modes are considered.   Here the difference in values is
only 5%; less if allowance is made for the overestimate discussed
above.   The values calculated here for response at the mainwheel
location do not of course correspond directly with the value from
the reference for the cg position since the mainwheel response will
contain a contribution from the pitch mode.   If this is taken
into account the mainwheel location responses should be slightly
reduced if they are to be compared with cg responses, though this
will not be sufficient to reduce the value in table 4.4(b), for the

case when 6 flexural modes are considered, to its respective value
in table 4.4(a). However, this value in table 4.4(a) was
calculated in reference 13 simply by using the generalised
co-ordinate in the heave mode for the case when 6 flexural modes
were considered, no contribution at all being included from the
flexural modes, it apparently being assumed that the mode shape
values at the cg were zero. It is therefore felt that this
result is of little value, and indeed cannot even be used as the
cg response for the case when only rigid body modes are considered,
since it has been shown in sub-section 4.3.1 that if the flexural
modes are neglected, the response in the heave mode is considerably
modified.

The value calculated here for the response at the pilot
location, using rigid body modes only, is considerably higher than
its corresponding value from the reference.

Perhaps the major fact which emerges from the above
discussion is that if PSD methods are to be used with equivalent
linear aircraft parameters to calculate responses, then the equivalent
linear parameters and the PSD values for the runway must be chosen
very carefully.

If the values from table 4.4(b) are compared with those
for 120 ft/s and 80 ft/s for the corresponding cases on figures 4.2
and 4.3, it will be seen that whilst all the values in the table are
lower due to the increased damping, the trends between the two cases
are very similar. However, whilst the damping has had the effect, in
the case where rigid body modes only are considered, of decreasing the
response at all positions by the same proportion, this is not quite so

for the case where 6 flexural modes were considered. Here comparison shows that the value of pilot location response in the table is relatively lower and the value of mainwheel response relatively higher than in the figure. In other words the increase in damping has had the effect of reducing the relative difference between the calculated values of response at different points on the aircraft.

It is of interest to compare the computer times required to produce the values discussed above. Reference 13 used an IBM 7090 digital computer. The times required to compute the time history of the generalized co-ordinates of the system, their first and second derivatives, the tyre forces of the mainwheels and nosewheel, the peak, mean and mean-square values of all these and of the displacement, velocity, and acceleration at the pilot compartment, for the Boeing 707 aircraft operating at a constant taxiing velocity of 100 ft/s, were approximately 32 minutes for the case when 6 flexural modes were included and 10.5 minutes when only rigid body motion was considered. The times taken to compute the corresponding rms values of response acceleration at mainwheel, nosewheel, and pilot location for this report, using the Elliot 4120 computer were, exclusive of compiling time, approximately 78 minutes for the case when 6 flexural modes were included and 4.3 minutes when only rigid body modes were considered. It should be pointed out that in the latter case, although only rms response accelerations were computed, the coupled values of the generalised co-ordinates of the system were computed in the process, and thus it would have involved very little more computer time tocompute the

mean-square values of the co-ordinates and their first and second derivatives.

Investigation showed that the speed of operation of the IBM 7090 is 0.44 times the speed of "Atlas", and the speed of the Elliot 4120 is 0.06 times that of "Atlas". Thus the speed of operation of the IBM 7090 is 7.33 times that of the Elliot 4120. In order to compare the program times, therefore, one should consider the times for both programs to be run on the same computer. Using the IBM 7090 computer the programs developed here, using the values used for table 4.4(b), would require times of approximately 10.6 minutes and 35 seconds for the two cases, compared with 32 minutes and 10.5 minutes for the programs in reference 13. This assumes the times in the reference did not include compiling time.

It will thus be seen that the programs developed here give values of response using very much less computing time than the programs in reference 13. The programs used here of course use a more simple model of the aircraft, and thus the values obtained are probably not so accurate as the values in reference 13. However, for purposes of comparison of different aircraft, investigation of the effects of changes of aircraft or runway parameters, or optimisation of aircraft parameters, these programs should be of value since they show the same trends as much more computer-time consuming programs.

4.3.3  <u>Variation of response with undercarriage stiffnesses.</u>

The rms values of response acceleration at the mainwheels, nosewheel, and pilot location, for a range of main and nose undercarriage oleo stiffnesses, were computed using the same earlier version of the main response program RESPONSE 12 as that used in early computations of variation of response with taxiing velocity.    The carpet plots of response acceleration against main and nose oleo stiffnesses showed a considerable amount of undulation (see figures E1 and E2 - Appendix E).    Attempts to explain the undulations led to the conclusion that they were not caused by any physical characteristics of the aircraft or runway system, but by lack of accuracy in the integration method used in the calculation of area under the response PSD curves.    The cause of these undulations and the development of the response program to overcome this problem are discussed in Appendix E.    The results discussed in this section were obtained using the later more sophisticated response program thus developed.

Figures 4.22 and 4.23 show carpet plots of variation of response acceleration, at the main undercarriage and pilot locations respectively, with variation of main and nose oleo stiffnesses, for a taxiing velocity of 120 ft/s, the remaining data being as Appendix D, i.e. based on a Boeing 707 aircraft and a geometric mean runway. Rigid body modes only were used in computation of values for these figures as they are for the remainder of this section.    The range of stiffnesses investigated was from half to twice the values shown in Appendix D.    The general trends shown by these figures are that the response at the mainwheel location increases with increase in

main oleo stiffness, but is little affected by changes in nose oleo

stiffness, whilst the response at the pilot location increases

with increase in either main or nose oleo stiffness. There is

some slight undulation on the mainwheel location response curve

at low main oleo stiffnesses and high nose oleo stiffnesses, which

results in a minimum response value at a main oleo stiffness of

$0.6 \times 10^6$ lbf/ft and a nose oleo stiffness of about 80000 lbf/ft,

although this minimum response is only very little less than the

response at the minimum oleo stiffnesses used, i.e. $k_m = 0.6 \times 10^6$ lbf/ft,

$k_n = 46800$ lbf/ft. The minimum response at the pilot location in

fact very clearly occurs at these minimum oleo stiffnesses. The

response curve for the nose undercarriage location was very similar

in shape to that for the pilot location, the values being in general

slightly lower.

The responses at the mainwheel and pilot locations for

the linearized stiffnesses calculated for the Boeing 707 (i.e.

$k_m = 1.2 \times 10^6$ lbf/ft, $k_n = 93600$ lbf/ft) are shown on figures 4.22

and 4.23 by circles. It is clear that the better method of

decreasing the pilot location response from this value is to reduce

the nose oleo stiffness, reductions in main oleo stiffness resulting

in a lesser decrease in response. The better method of decreasing

the mainwheel location response from this value is to reduce the

main oleo stiffness, whilst a smaller decrease in response may be

achieved by an increase in nose oleo stiffness.

Figure 4.2.4 shows the PSD of the response acceleration at

the mainwheel and pilot locations for the aircraft and runway

parameters in Appendix D, and a taxiing velocity of 120 ft/s, i.e.

corresponding to the circled points on figures 4.22 and 4.23. The lower frequency peak corresponds to the pitching mode, and the higher frequency to the heaving mode. Clearly, with these parameters, most of the mainwheel location response results from vertical translation, whilst the contributions to the pilot location response from vertical translation and pitching rotation are approximately equal.

Figures 4.25 and 4.26 show the PSD of the response acceleration at the mainwheel and pilot locations for aircraft parameters corresponding to the extreme corners of figures 4.22 and 4.23. The lower frequency peak corresponds to the pitching mode in each case, as may easily be seen by referring to the eigenvalues plotted in figure E 4 (Appendix E). It is clear from figure 4.26 that with high main oleo stiffness and low nose oleo stiffness the heave mode contributes almost all the response at both mainwheel and pilot locations, whilst with low main oleo stiffness and high nose oleo stiffness almost all the response at the mainwheel location and most of that at the pilot location comes from the pitch contribution. Figure 4.25 indicates that when both main and nose oleo stiffnesses are either low or high most of the mainwheel location response is contributed by the heave mode, whilst for the pilot location response a significant contribution is also made by the pitch mode.

Although the 4 sets of curves in figures 4.25 and 4.26 have been drawn to different scales because of their great variations in height, it is clear from examination of the heights and bandwidths that reducing the oleo stiffness has the effect of

increasing the damping in the modes, the nose oleo stiffness having

by far the greatest effect on the pitch mode, and the main oleo

stiffness the greatest effect on the heave mode.

Figure 4.27 shows the variation of response acceleration

with main and nose oleo stiffnesses for the same parameters as

figures 4.22 and 4.23 except that the main and nose oleo damping

has been doubled. The outer curves only of the carpet plots have

been drawn, but it is clear that the trends are very similar to

those in figures 4.22 and 4.23. However, in general the responses

are significantly lower due to the increased damping. With the

higher damping the undulations, which appeared on figure 4.22 ,

are almost non-existant, and there is even less variation in

mainwheel location response with change in nose oleo stiffness than

there was with the lower damping.

It is of interest to note that with these high damping

values the order of the heave and pitch frequencies was reversed at

very low oleo stiffnesses. Some of the eigenvalues corresponding

to points in figure 4.27 are shown in table 4.5. It was not clear

from the computer printout for some of these eigenvalues which were

pitch values and which were heave values, since the same eigenvalue,

either pitch or heave, was not printed out first each time. In

order to decide which eigenvalues gave the pitch frequencies and

which the heave the eigenvalues were plotted on figure 4.28. The

eigenvalues clearly fall into two separate curves, which by

comparison with figure E 4 (Appendix E) may be clearly identified.

4.3. Variation of response with undercarriage damping

The rms values of response acceleration at the mainwheel, nosewheel, and pilot locations have been computed for a range of main and nose oleo damping constants, using the program RESPONSE 12. The range of damping constants considered was from approximately half to twice the values calculated in Appendix D. Again, rigid body modes only have been used for studies in this section.

Figure 4.29 shows this variation in response for the mainwheel and pilot locations at a taxiing velocity of 120 ft/s, using the data from Appendix D, i.e. based on a Boeing 707 aircraft and a geometric mean runway. The carpet plots in the figure are very "well-behaved", indicating a general trend for the response at both the mainwheel and pilot locations to decrease as either the main or nose oleo damping is increased. The minimum response obtainable over the range of damping considered is that at the highest main and nose oleo damping, i.e. $C_m$ = 26000 lbf/ft/s and $C_n$ = 14000 lbf/ft/s. Again the response curve for the nose undercarriage location was very similar in shape to that for the pilot location, the values being in general slightly lower.

The responses at the mainwheel and pilot locations for the linearized damping constants calculated in Appendix D (i.e. $C_m$ = 13080 lbf/ft/s, $C_n$ = 6876 lbf/ft/s) are shown on the figure by circles. Reductions of 17.5% and 26% in the mainwheel and pilot location responses respectively may be obtained by doubling both the main and nose oleo damping constants. However, it will be seen that as the oleo damping is increased the rate of reduction in response gradually

decreases. Hence the trend is the same as that shown by Kirk and Perry (ref. 38) that a tenfold increase in main oleo damping coefficient would be required for the Boeing 707 to decrease the cg acceleration by 58%. Kirk and Perry's analysis included only main oleo input, no pitching contribution being considered. It will be seen from figure 4.29 that the decrease in rate of reduction in response is even greater for increasing nose oleo damping.

As might be expected, the pilot location response is influenced more by the nose oleo damping than by the main oleo damping, although at high damping constants the effect of nose oleo damping is substantially reduced relative to the effect of main oleo damping. Similarly, the main oleo damping has more influence on the mainwheel location response; at high damping the effect of increase in nose oleo damping is negligible.

It will be seen that as the nose oleo damping is decreased to half the standard value calculated in Appendix D the response, particularly at the pilot location, begins to rise quite steeply. Values for nose oleo damping constants, from values used in reference 37, have been derived in sub-section 4.3.2, where it was stated that these values were felt to be unrealistically low, due to the fact that uncoupled heave and pitch modes were assumed. The values were 970 lbf/ft/s and 1830 lbf/ft/s depending on the method of calculation. It will be seen from the trends on figure 4.29 that either of these values would extend the curves much higher, giving a considerable increase in response, particularly at the pilot compartment. Figure 4.30 shows the PSD of the pilot location response

acceleration using values of $C_m$ = 12250 lbf/ft/s and $C_n$ = 970 lbf/ft/s, together with other values of aircraft and runway parameters derived from reference 37 (see sub-section 4.3.2), and using a taxiing velocity of 40 ft/s. The effect of the assumption of uncoupled modes can immediately be seen in the very clearly separated peaks, and the very low nose oleo damping is reflected in the extremely high peak of the lower frequency pitch mode. The PSD of mainwheel location response plotted for the same parameters showed an almost identical heave mode peak, but a negligible pitch mode peak. Figure 4.30 shows further evidence of the importance of the type of integrating procedure, particularly when investigating light damping.

Bearing in mind the findings of sub-section 4.3.3, i.e. that lowering the stiffness of the oleos has the effect of increasing the damping, values for the lower boundaries of the carpet plots of figure 4.29 were again plotted, this time using half the previous oleo stiffnesses, i.e. $k_m$ = 0.6 x $10^6$ lbf/ft, $k_n$ = 46800 lbf/ft. The new boundaries are shown in figure 4.31. In general large decreases in response relative to the values in figure 4.29 have been achieved. Again, the minimum response at the pilot location is with maximum damping constants, i.e. $C_m$ = 26000 lbf/ft/s, $C_n$ = 14000 lbf/ft/s. However, minimum response at the mainwheel location occurs with damping constants of $C_m$ = 26000 lbf/ft/s, $C_n$ = 5000 lbf/ft/s, although it should be noted that with $C_m$ = 26000 lbf/ft/s, variation of $C_n$ over the range 3500 to 14000 lbf/ft/s makes only about 7% difference to the response.

The eigenvalues for the cases in figure 4.31 are shown in table 4.6, where it will be seen that, when the nose oleo damping is

high, the frequencies of the pitch and heave modes are very close together. Figure 4.32 shows the PSD of response acceleration at the mainwheel and pilot location for the highest damping, together with the low stiffnesses. It will be seen that the effect of the frequencies being so close together is to produce only one peak, the frequency of the peak on the pilot location curve, which one would expect to be predominantly pitch, being at a slightly lower frequency than that on the mainwheel location curve, which one would expect to be predominantly heave.

## 4.3.5 Variation of response with undercarriage position

The rms values of response acceleration at the mainwheel, nosewheel, and pilot locations have been computed for a range of undercarriage positions. The basic runway and aircraft parameters used were those shown in Appendix D, although the undercarriage parameters were varied from these basic values in various ways. Rigid body motion only was assumed, and a taxiing velocity of 120 ft/s was used. The range of undercarriage positions investigated in general covered mainwheel to cg distances of 4.33 to 9 feet, the distance between mainwheel and nosewheel positions being kept constant at 59 feet.

Three methods of varying the undercarriage parameters with position were used. Firstly the same linear oleo parameters were assumed for every position, secondly the same non-linear oleo curves were assumed for every position, and finally the same natural frequencies for main and nose oleo stiffnesses with their proportion of the aircraft mass were assumed.

### 4.3.5.1  Same linear undercarriages

The program RESPONSE 12 was used to compute the rms values of the response accelerations, the linearized undercarriage parameters remaining constant, and only the distances of the undercarriages from the cg being varied. Figure 4.33 shows the responses at the mainwheel, nosewheel, and pilot locations. The standard position for the mainwheels on this aircraft is 4.33 feet behind the cg. Thus it will be seen that as the mainwheels are moved aft from this position the response at the mainwheel location increases, and that at the nosewheel and pilot locations decreases. This is completely opposite to the findings of Silsby (ref.12) and Kirk (ref.37).

However, it is felt that the assumption of the same linear oleo parameters in each case is unrealistic. Clearly as the mainwheels are moved aft the mass supported by them will be reduced, resulting, since the oleo stiffness remains unchanged, in an increase in heave natural frequency, and hence, from sub-section 4.3.3, in an increase in the contribution to the response from the heave mode. Similarly the natural frequency of heave of the nosewheel supported proportion of the mass on the nose oleo stiffness will decrease, resulting in a reduction in pitch natural frequency, and hence a reduction in contribution to the response from the pitch mode. These would result in the effects shown on figure 4.33.

### 4.3.5.2  Same non-linear undercarriages

The program RESPONSE 12 was again used to compute the rms values of the response accelerations, this time the same non-linear

oleo characteristics being used in each case, so that as the undercarriages were moved the linearized characteristics were changed. The linear tyre characteristics were kept constant at the values shown in Appendix D.

The linearized oleo stiffness and damping were calculated for mainwheel to cg distances of 5, 6, 7, 8 and 9 feet, as shown in Appendix C for a distance of 4.33 feet, using the oleo characteristic curves in figures C2 and C3, except that the final linearized values of damping constant were calculated using energy dissipated in a harmonic motion as shown in Appendix D. The values of stiffness and damping thus obtained were plotted, and smooth curves drawn through them, the final values then being taken from these curves. This helped to overcome any inaccuracies in values due to difficulty in measuring values and slopes from the rather small characteristic curves, and ensured undercarriage parameters giving smooth transitions from one position to the next. The curves are shown in figure 4.34, the final values of stiffness and damping used for computations being shown in table 4.7.

Figure 4.35 shows the responses at the mainwheel, nosewheel and pilot locations. This time, as the mainwheels are moved aft from their standard position, the responses at the nosewheel and pilot locations increase. This agrees with the trends shown by Silsby and Kirk, the amount of increase at the pilot location, about 88% at the most aft position, agreeing very closely with Silsby's. However, the response at the mainwheel at first decreases very slightly as the wheels are moved aft, and then with further movement

begins to increase, the minimum response being when the mainwheels
are about 5 feet behind the cg.    Although Kirk only showed values
at two discrete positions, and Silsby at three, both showed a
decrease in cg response, although only a small decrease.    This
agrees with figure 4.35  for mainwheel to cg distances of 4.33 to
6 feet.    However, since both references computed cg response,
there was no pitching contribution to this value, whilst there will
be a pitching contribution to the mainwheel response on figure 4.35.
Clearly, as the mainwheels are moved aft, the contribution from the
pitch mode will increase, since the nosewheel and pilot location
responses have increased.    Hence, an increase in the mainwheel
response at the higher distances is to be expected.

Again, the assumption of the same non-linear oleos is
not very realistic.    The change in main oleo parameters will be
small, since the proportion of load carried by the mainwheels does
not change very much, and hence the same undercarriage might be
feasible.    However, the proportion of load carried by the nose
undercarriage is more than doubled, so that, referring to table 4.7,
if the same undercarriage is used, because of the non-linear curve,
a five-fold increase in stiffness is produced.    This accounts for
the large increases in nosewheel and pilot location response.
Clearly such a large increase in stiffness is undesirable, and in
any case, with such large increases in load, a larger undercarriage
would be required, producing changes in other undercarriage
parameters.

### 4.3.5.3 Same natural frequencies

The final method of varying the oleo characteristics with distance from the cg position was to keep constant the natural frequencies calculated from the main and nose oleo stiffnesses and their proportions of the aircraft mass.   This time the tyre characteristics and the unsprung masses were also varied.

The equation of motion of a mass on a spring and damper may be written

$$\ddot{x} + \frac{c}{M}\dot{x} + \frac{k}{M}x = P(t) \qquad\qquad (4 - 57)$$

It is required to keep the natural frequency $\omega_n$ constant, so that

$$\frac{k}{M} = \text{constant,} \qquad\qquad (4 - 58)$$

and, to maintain similarity in the equation,
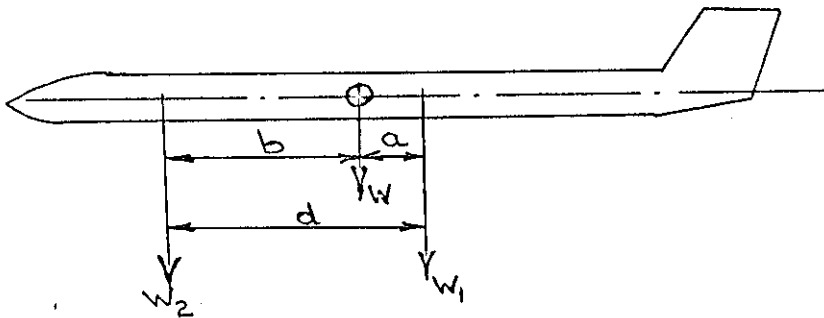
$$\frac{c}{M} = \text{constant} \qquad\qquad (4 - 59)$$



Fig. 4(i)

Referring to figure 4(i) the proportion of the weight of the aircraft supported by the mainwheels is given by

$$W_1 = \frac{W.b}{d} \qquad\qquad (4 - 60)$$

Using subscript o to denote the original aircraft parameters as calculated in Appendix D and n to denote the new parameters at the

new mainwheel distance, equation (4-58) gives

$$\frac{k_{lo}}{M_{lo}} = \frac{k_{ln}}{M_{ln}}$$

and substituting from equation (4-60)

$$\frac{k_{lo} \cdot g \cdot d_o}{W \cdot b_o} = \frac{k_{ln} \cdot g \cdot d_n}{W \cdot b_n}$$

i.e. $k_{ln} = k_{lo} \times \dfrac{b_n}{b_o} \times \dfrac{d_o}{d_n}$ \hfill (4 - 61)

Since the distance between the mainwheels and nosewheels remains constant in this analysis, equation (4-61) becomes

$$k_{ln} = k_{lo} \times \frac{b_n}{b_o} \hspace{2cm} (4 - 62)$$

Similarly, it may be shown that

$$c_{ln} = c_{lo} \times \frac{b_n}{b_o} \hspace{2cm} (4 - 63)$$

and that the nose oleo parameters are given by equations of the form

$$k_{2n} = k_{2o} \times \frac{a_n}{a_o} \hspace{2cm} (4 - 64)$$

The program RESPONSE 15 was used to compute the rms values of the response accelerations. This program is based on RESPONSE 12 but incorporates equations of the above form to vary the oleo stiffness and damping, the tyre stiffness and damping, and the unsprung mass of the main and nose undercarriages.

Figure 4.36 shows the responses at the mainwheel, nosewheel and pilot locations. This time the range of undercarriage positions has been increased slightly to cover mainwheel to cg distances of

3 to 9 feet. As the mainwheels are moved forward, from the standard position at 4.33 feet behind the cg, towards the cg, the mainwheel and nosewheel location responses increase slightly, whilst the pilot location response remains essentially unchanged. As the mainwheels are moved aft from the standard position the effect is quite similar to that using the same linear undercarriages (figure 4.33), with the slight differences that a dip occurs in the mainwheel location response, giving a minimum value when the mainwheels are located about 5.33 feet aft of the cg, and the pilot location response only decreases by 26% as opposed to the 51% on figure 4.33.

This final method of varying the undercarriage characteristics is probably the most realistic, since an increase in load carried by the undercarriage results in a proportionate increase in the characteristics, and in the weight of the undercarriage. It is also to some extent the most effective; moving the main undercarriage 1 foot aft from the standard position results in slight decreases in response at the mainwheel, nosewheel and pilot locations, whereas with both the other methods, at least one of the responses always increases as the undercarriages are moved.

4.3.6. <u>Comments on runways used</u>

The runway profile used for most of the response studies has been the geometric mean runway whose parameters are specified in Appendix D, whilst for some comparison purposes a profile of the form of equation (4-23) has been assumed. The PSD's of these profiles are shown in figure 4.37, together with the PSD of the profile of a rough runway reproduced from reference 26. It should

be noted that at frequencies below $\Omega$ = 0.101 rad/ft the PSD of

the geometric mean runway shown overestimates that of the actual

geometric mean runway calculated in Section 2, from values obtained

from reference 26, by a factor of about 1.5, as shown in Appendix

D.

Referring to figure 4.37 it will be seen that the

geometric mean runway PSD curve is very similar in shape to that

of the actual runway, but with lower values, as would be expected,

since the actual runway is one of the roughest runways from

reference 26. However, the profile described by equation (4-23),

which should describe a rough runway (ref. 20), also has lower

values than the actual runway at all frequencies, and very

substantially lower at the lower frequencies.

It appears from this, and from similar inspection of all

runway PSD's published in reference 26, that the assumption of a

"single straight line" PSD curve with a slope of -2 will badly

underestimate the roughness at low spacial frequencies. However,

it has been shown (ref. 21) that many of the published spectra

may be in error. The error consists of an overestimate of the

PSD at long wavelengths (low spacial frequencies) due to the

contaminating effect of very long wavelengths such as runway grades.

Figure 4.38 (reproduced from reference 4) illustrates this error.

The circles show the individual values of PSD computed by use of

the method which has been used for the computation of many of the

published spectra. This method is described in reference 26. The

solid line shows the spectrum computed by modifying this method to

produce a better estimate of the true spectrum at long wavelengths.

The effect of the above modification on the actual PSD curve in figure 4.37 would be to reduce the value of the PSD at a wavelength of 160 feet ($\Omega = 0.039$ rad/ft) thus reducing the slope of the curve at frequencies below that of the next point, $\Omega = 0.075$ rad/ft. Hence, a PSD curve with three straight line segments on the log scales may be a more realistic approximation. Since the geometric mean runway was derived from the actual curves in reference 26, it will overestimate the roughness at low frequencies in the same way as the actual curves.

Hence, whilst the "single straight line" PSD with a slope of -2 probably underestimates the roughness at long wavelengths, the geometric mean runway described in this thesis probably overestimates it.

Referring to figure 4.37 it will be seen that at spacial frequencies less than 0.1 rad/ft the geometric mean runway contains more roughness than the "single straight line" runway produced by equation (4-23). The effect of this may be seen by examining the response of an aircraft at two velocities on the two runways. If it is assumed that frequencies up to 13 radians per second may excite response in the aircraft (this has been shown to be reasonable when rigid body modes only are considered), then at a taxiing speed of 240 ft/s spacial frequencies up to only 0.05 rad/ft will be important, and thus the geometric mean runway will be considerably rougher over all the important range. Hence the geometric mean runway will produce considerably more response at this speed. However, at a taxiing speed of 20 ft/s spacial frequencies up to 0.65 rad/ft will be important, and thus the "single

straight line" PSD runway will be rougher over most of the
important range (0.1 to 0.65 rad/ft). Hence this runway will
produce a greater response at a taxiing speed of 20 ft/s. This
may be verified by comparing figures 4.9 and 4.12. The same
aircraft parameters were used for both figures, 4.9 using the
geometric mean runway, and 4.12 using the runway described by
equation (4-23). It will be seen that the geometric mean runway
produces less response up to about 70 ft/s, but greater response
at greater taxiing velocities, the difference at high taxiing
speeds being considerable.

Since most of this thesis is concerned with comparisons,
and the effects of parameter variations, the actual PSD function
used is not critical, so long as it is reasonably representative
of a practical runway profile.

TABLE 4.1

Response in each mode for parameters in Appendix D

| Mode | Response (ft/s$^2$) | | |
|---|---|---|---|
| | Mainwheel Location | Nosewheel Location | Pilot Location |
| Rigid body heave | 2.2412 | 2.2412 | 2.2412 |
| Rigid body pitch | .3394 | 4.2822 | 5.0590 |
| 1st Flexural | 1.5490 | .3809 | .7110 |
| 2nd " | .1460 | .3512 | .4065 |
| 3rd " | .0128 | .3817 | .4905 |
| 4th " | .9936 | 2.4191 | 3.4559 |
| 5th " | .5833 | .1389 | .2778 |
| 6th " | .0841 | .1074 | .2070 |

Rigid body + 6 flexural modes considered.

V = 60 ft/s.

TABLE 4.2

Root-mean-square values of response acceleration calculated

from generalized co-ordinates presented in reference 13.

| (a) Case where 6 flexural modes are included | | | | | |
|---|---|---|---|---|---|
| Mode | $\overline{\ddot{x}^2}$ | $\phi_m$ | $\phi_p$ | $\sigma_m$ ft/s$^2$ | $\sigma_p$ ft/s$^2$ |
| Mainwheel | 38820 | | | | |
| Nosewheel | 33720 | | | | |
| Rigid body heave | 2645 | 1 | 1 | 4.27 | 4.27 |
| Rigid body pitch | .01192 | 52 | -656 | .473 | 5.96 |
| Flexural modes ( 1 | 94040 | -0.122 | 0.056 | 3.12 | 1.43 |
| ( 2 | 6930 | 0.037 | 0.103 | .256 | .714 |
| ( 3 | 477 | -0.010 | 0.383 | .018 | .697 |
| ( 4 | 9336 | 0.230 | -0.800 | 1.850 | 6.43 |
| ( 5 | 5193 | -0.168 | 0.080 | 1.008 | .480 |
| ( 6 | 8863 | -0.065 | 0.160 | .507 | 1.250 |

| (b) Case where rigid body modes only are considered | | | | | |
|---|---|---|---|---|---|
| Mode | $\overline{\ddot{x}^2}$ | $\phi_m$ | $\phi_p$ | $\sigma_m$ ft/s$^2$ | $\sigma_p$ ft/s$^2$ |
| Mainwheel | 53770 | | | | |
| Nosewheel | 27470 | | | | |
| Rigid body heave | 4186 | 1 | 1 | 5.39 | 5.39 |
| Rigid body pitch | .007819 | 52 | -656 | .383 | 4.83 |

TABLE 4.3

Eigenvalues for aircraft parameters in Appendix D

|  | Rigid body modes only considered | | Rigid body + 6 flexural modes considered | |
|---|---|---|---|---|
| Mode | Eigenvalue | $\beta$ | Eigenvalue | $\beta$ |
| Nosewheel | -617.8 or -37.0 | | -622.9 or -35.6 | |
| Mainwheel | -44.79 ± i 114.97 | .365 | -45.78 ± i 114.96 | .370 |
| Rigid body heave | 0.374    8.073 | .046 | 0.326    10.101 | .032 |
| Rigid body pitch | 0.721    6.012 | .120 | 0.731    6.471 | .113 |
| 1st flexural | | | 0.178    5.016 | .035 |
| 2nd    " | | | 0.508    18.172 | .028 |
| 3rd    " | | | 0.718    24.073 | .030 |
| 4th    " | | | 1.304    32.546 | .040 |
| 5th    " | | | 1.037    39.097 | .0265 |
| 6th    " | | | 1.409    55.121 | .0255 |

TABLE 4.4

Rms values of response acceleration for BOEING 707 aircraft

taxiing at 100 ft/s on Runway 12, Langley Field

(a)  From reference 13

|  | Rigid body + 6 Flexible Modes considered | Rigid Body Modes only considered |
|---|---|---|
| Pilot Location response (ft/s$^2$) | 8.14 | 7.28 |
| cg response (ft/s$^2$) | 4.27 | |

(b)  Calculated by Program RESPONSE 12

|  | Rigid body + 6 Flexible Modes considered | Rigid Body Modes only considered |
|---|---|---|
| Pilot Location response (ft/s$^2$) | 8.605 | 8.820 |
| Nosewheel location response (ft/s$^2$) | 6.941 | 7.755 |
| Mainwheel location response (ft/s$^2$) | 6.259 | 4.749 |

TABLE 4.5

Eigenvalues for varying main and nose oleo stiffnesses

| $k_m$ lbf/ft | $k_n$ lbf/ft | Eigenvalues | | | |
|---|---|---|---|---|---|
| | | Pitch | | Heave | |
| $0.6 \times 10^6$ | 46800 | $-0.840 \pm$ i 6.234 | | $-3.634 \pm$ i 6.090 | |
| " | 80000 | 0.856 | 6.010 | 2.021 | 6.905 |
| " | 120000 | 0.652 | 5.954 | 1.485 | 7.563 |
| " | 155000 | 0.570 | 5.997 | 1.211 | 7.894 |
| " | 187200 | 0.536 | 6.036 | 1.026 | 8.123 |
| $1.0 \times 10^6$ | 187200 | 0.487 | 6.763 | 0.873 | 8.439 |
| $1.2 \times 10^6$ | " | 0.517 | 6.951 | 0.780 | 8.601 |
| $1.6 \times 10^6$ | " | 0.593 | 7.154 | 0.618 | 8.913 |
| $2.0 \times 10^6$ | " | 0.649 | 7.248 | 0.507 | 9.183 |
| $2.4 \times 10^6$ | " | 0.685 | 7.298 | 0.434 | 9.404 |

Rigid body modes only considered.

$C_m$ = 26000 lbf/ft/s, $C_n$ = 14000 lbf/ft/s, other parameters as Appendix D.

Eigenvalues for varying main and nose oleo damping

| $C_m$ lbf/ft/s | $C_n$ lbf/ft/s | Eigenvalues | | | |
|---|---|---|---|---|---|
| | | Pitch | | Heave | |
| 6500 | 14000 | $-3.647 \pm i$ 6.017 | | $-.374 \pm i$ 6.269 | |
| 9500 | 14000 | 3.646 | 6.027 | .445 | 6.262 |
| 13000 | 14000 | 3.644 | 6.038 | .527 | 6.256 |
| 17000 | 14000 | 3.641 | 6.053 | .622 | 6.249 |
| 21000 | 14000 | 3.638 | 6.069 | .718 | 6.242 |
| 26000 | 14000 | 3.634 | 6.090 | .840 | 6.234 |
| 26000 | 11000 | 2.351 | 5.174 | .910 | 6.340 |
| 26000 | 9000 | 1.709 | 4.923 | .903 | 6.452 |
| 26000 | 7000 | 1.239 | 4.771 | .843 | 6.543 |
| 26000 | 5000 | .857 | 4.687 | .762 | 6.597 |
| 26000 | 3500 | .599 | 4.653 | .700 | 6.618 |

Rigid body modes only considered.

$k_m$ = 0.6 x 10$^6$ lbf/ft, $k_n$ = 46800 lbf/ft, other parameters as Appendix D.

TABLE 4.7

Values of oleo stiffness and damping using some non-linear

undercarriages

| Distance from cg to mainwheels ft | Oleo stiffnesses (lbf/ft) | | Oleo damping (lbf/ft/s) | |
|---|---|---|---|---|
| | $k_m$ | $k_n$ | $C_m$ | $C_n$ |
| 4.33 | $1.2 \times 10^6$ | 93600 | 13080 | 6876 |
| 5.0 | $1.18 \times 10^6$ | 115000 | 12900 | 7550 |
| 6.0 | $1.145 \times 10^6$ | 165000 | 12630 | 8520 |
| 7.0 | $1.115 \times 10^6$ | 238000 | 12360 | 9350 |
| 8.0 | $1.083 \times 10^6$ | 328000 | 12100 | 9850 |
| 9.0 | $1.05 \times 10^6$ | 450000 | 11840 | 10170 |

FIGURE 4.1
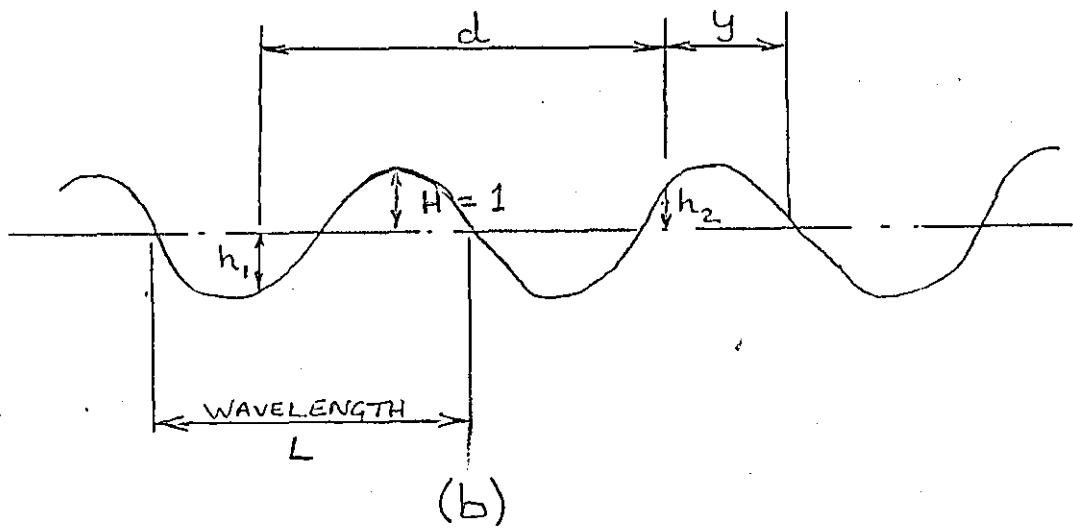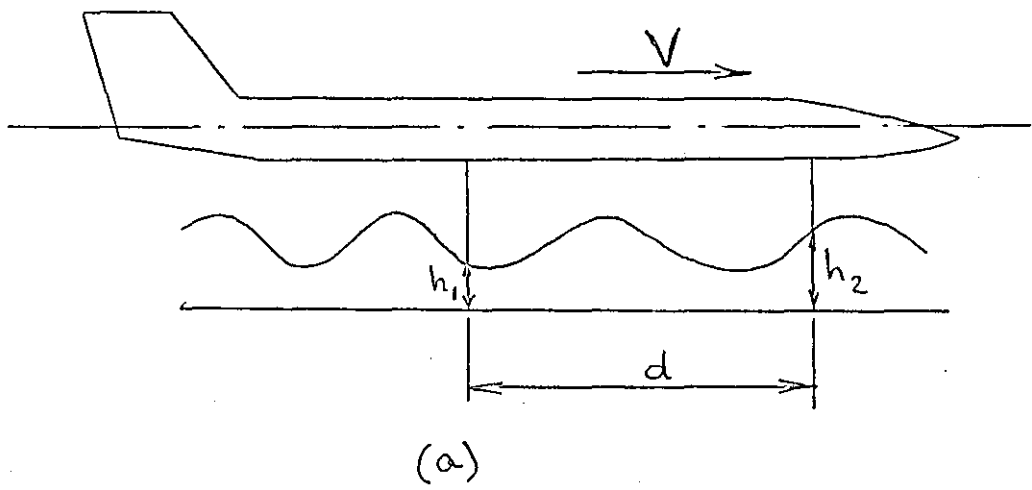
AIRCRAFT ON SINUSOIDAL RUNWAY
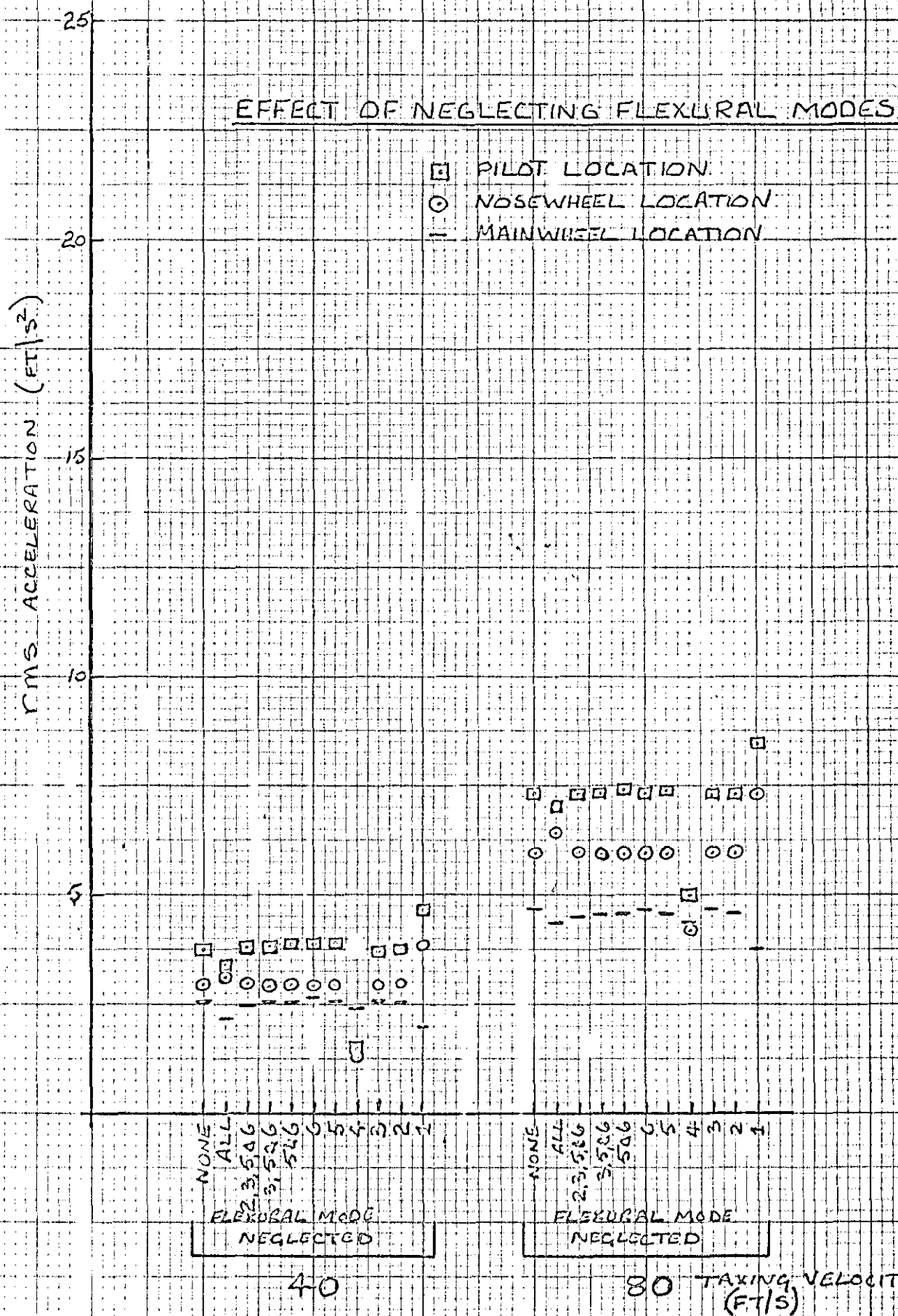
FIGURE 4.2

EFFECT OF NEGLECTING FLEXURAL MODES

FIGURE 4.3

EFFECT OF NEGLECTING FLEXURAL MODES

PILOT LOCATION
NOSEWHEEL LOCATION
MAINWHEEL LOCATION

FIGURE 4.4

EFFECT OF NEGLECTING FLEXURAL MODES

□ PILOT LOCATION
⊙ NOSEWHEEL LOCATION
— MAINWHEEL LOCATION

rms ACCELERATION ($FT/s^2$)

FLEXURAL MODE NEGLECTED

FLEXURAL MODE NEGLECTED

200                    240    TAXING VELOCITY ($FT/s$)
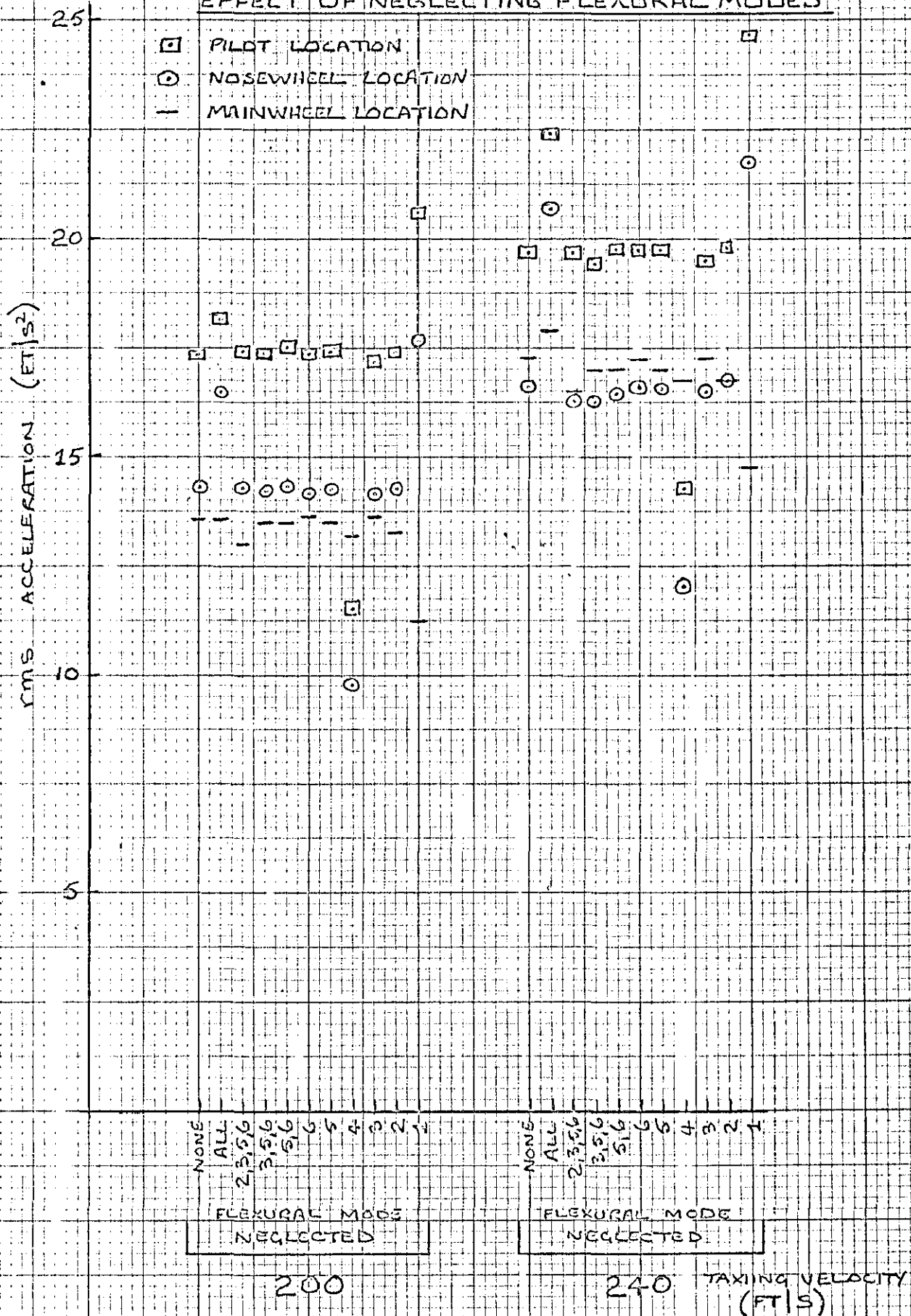
FREQUENCY RESPONSE FUNCTIONS FOR PARAMETERS IN APPENDIX D

RIGID BODY + 6 FLEXURAL MODES CONSIDERED

$V = 120$ FT/S

PILOT LOCATION

MAINWHEEL LOCATION

FIGURE 4.5

$\omega_\zeta$ (RAD/S)

PSD OF RESPONSE ACCELERATION FOR PARAMETERS IN APPENDIX D

RIGID BODY + 6 FLEXURAL MODES CONSIDERED     V= 120 FT/S

PILOT LOCATION
MAINWHEEL LOCATION
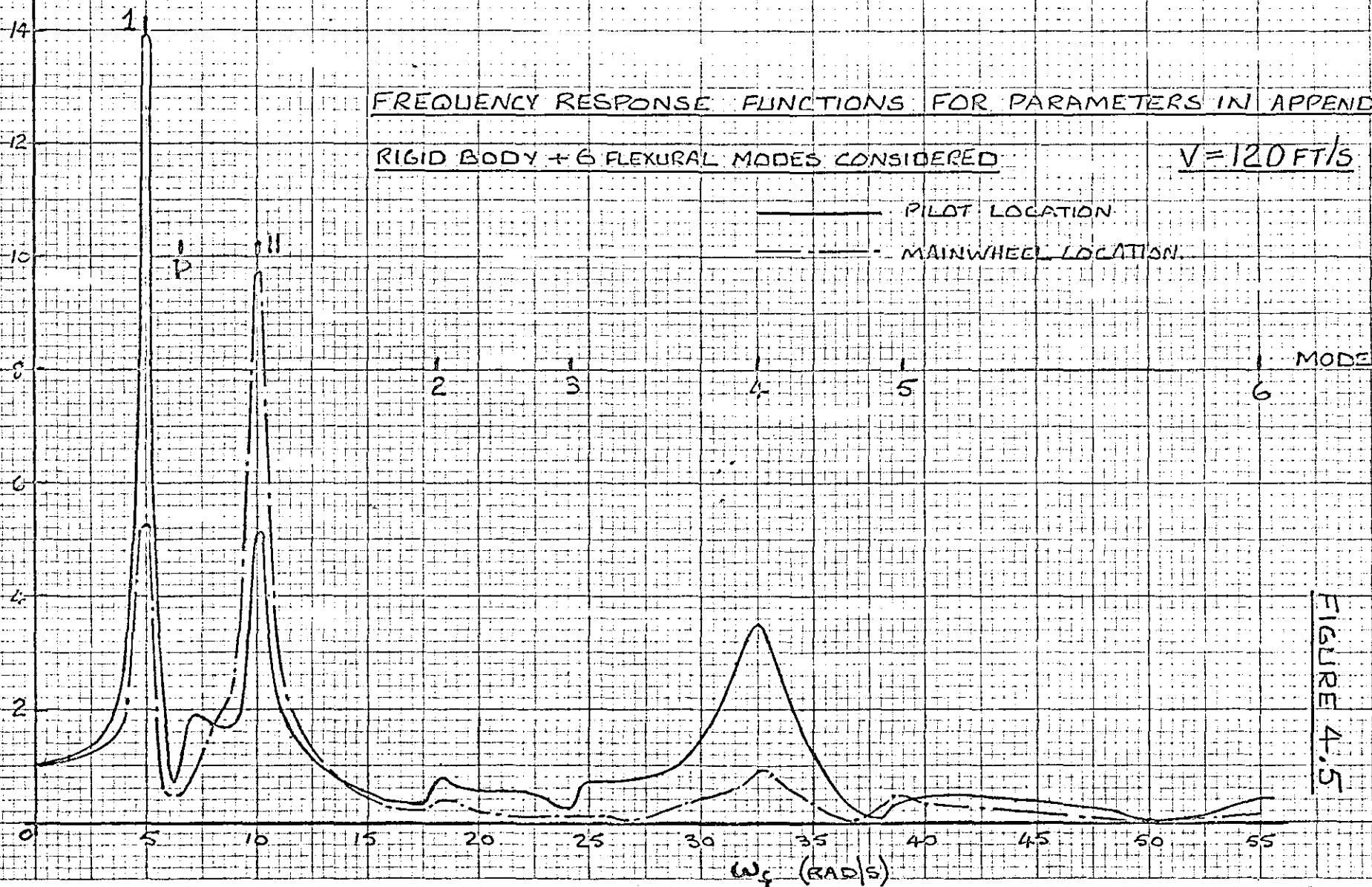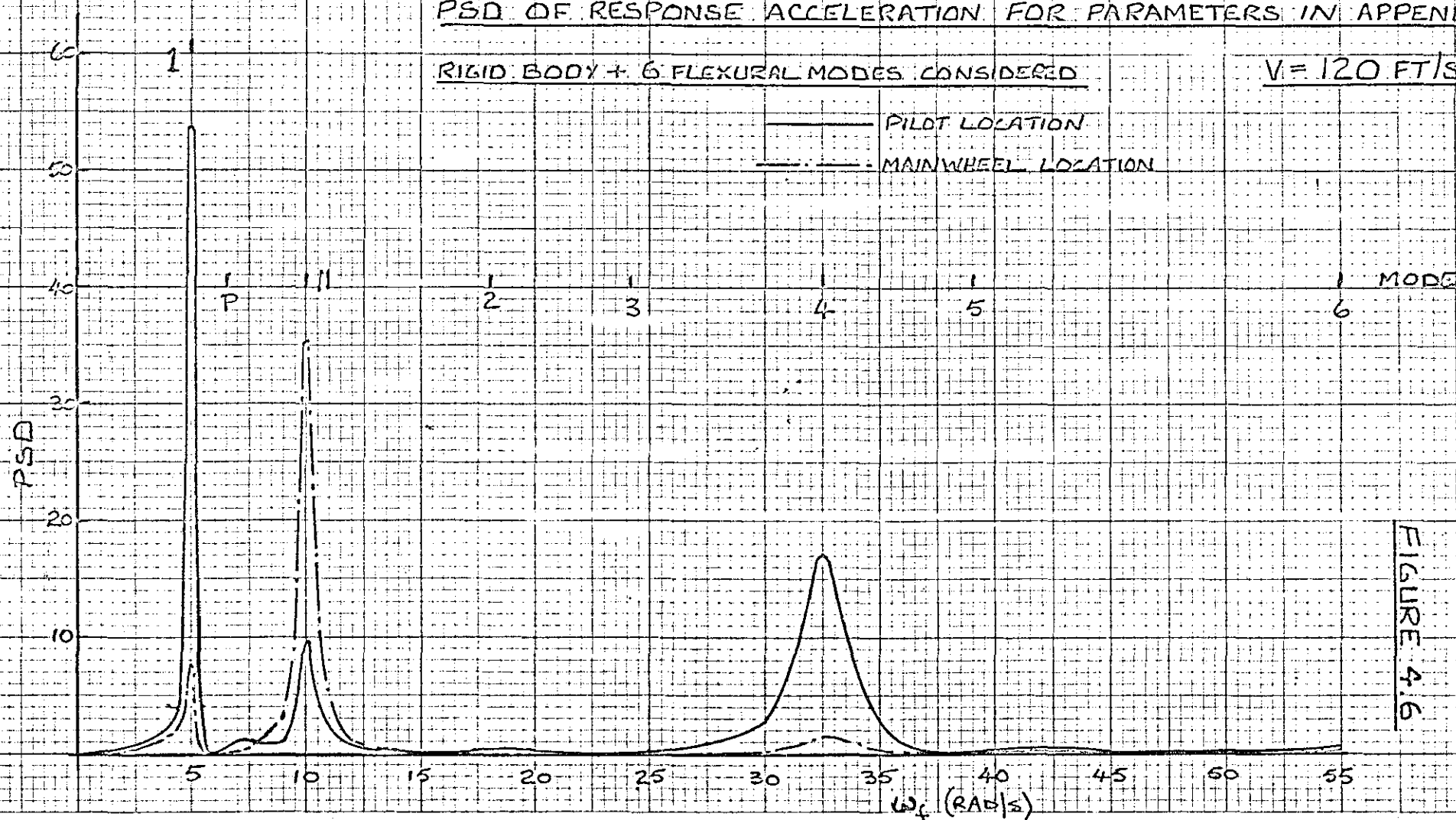
FIGURE 4.6

FIGURE 4.7

FREQUENCY RESPONSE FUNCTIONS FOR PARAMETERS

IN APPENDIX D

RIGID BODY MODES ONLY CONSIDERED    V = 120 FT/s

———————  PILOT LOCATION

—— · —— ·  MAINWHEEL LOCATION
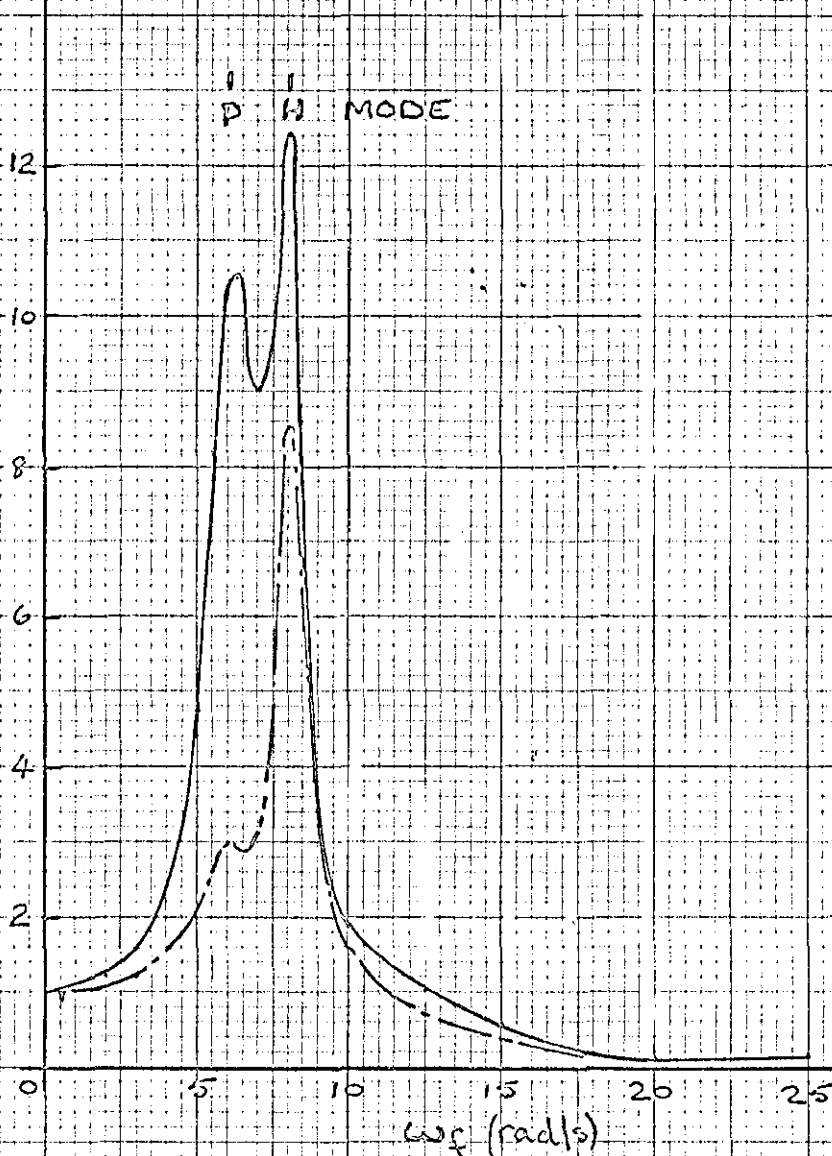
FIGURE 4.8

PSD OF RESPONSE ACCELERATION FOR PARAMETERS
IN APPENDIX D

RIGID BODY MODES ONLY CONSIDERED    V=120 FT/S

———————— PILOT LOCATION

—·—·—·— MAINWHEEL LOCATION
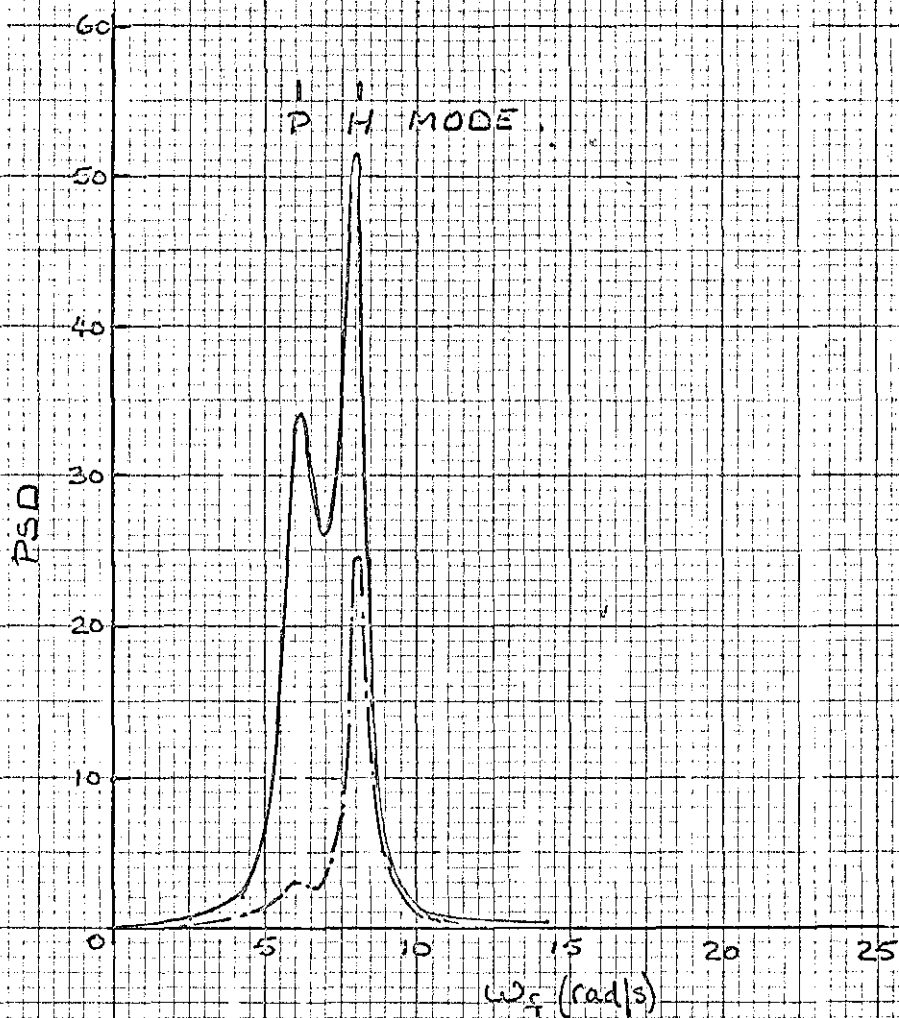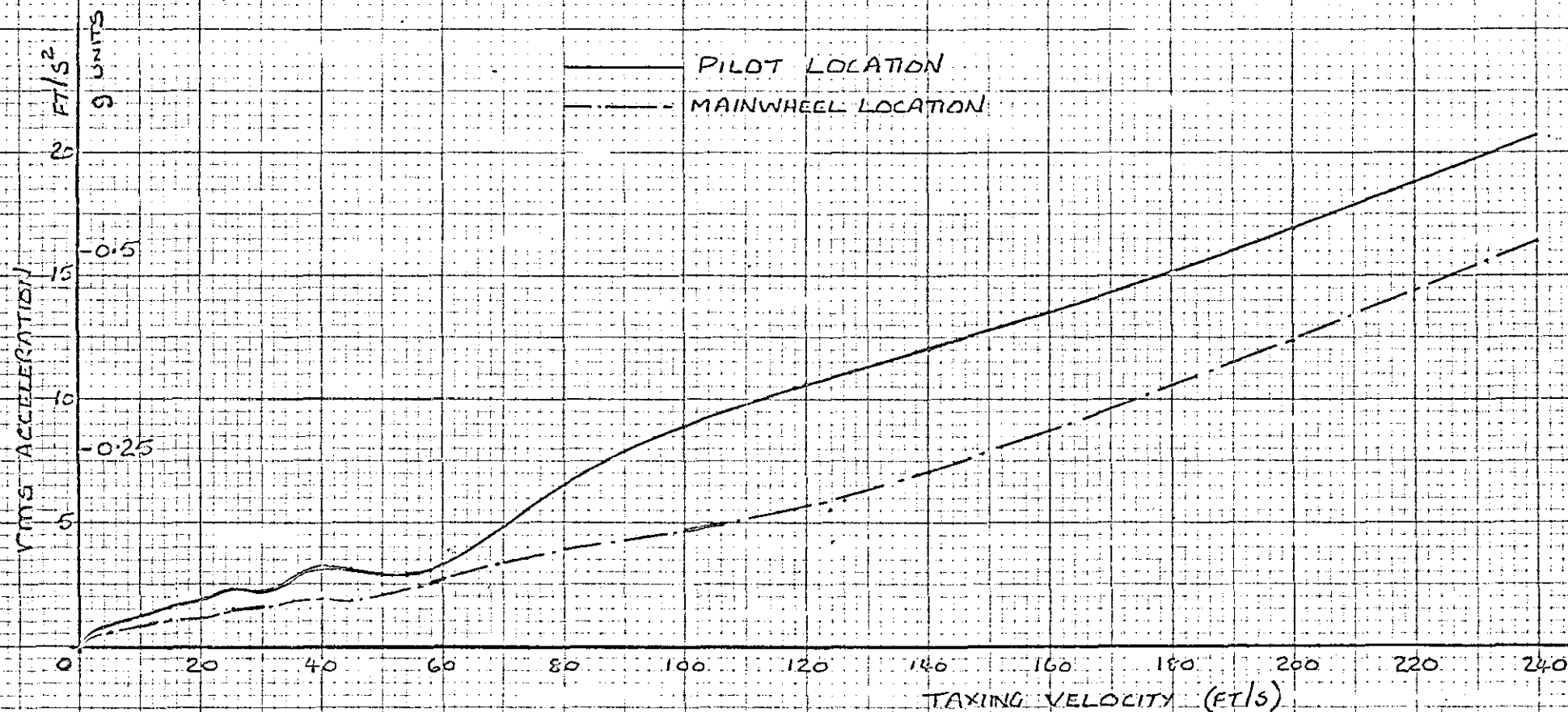
RESPONSE ACCELERATIONS FOR PARAMETERS IN APPENDIX D

RIGID BODY MODES ONLY CONSIDERED

FIGURE 4.9

FIGURE 4.10
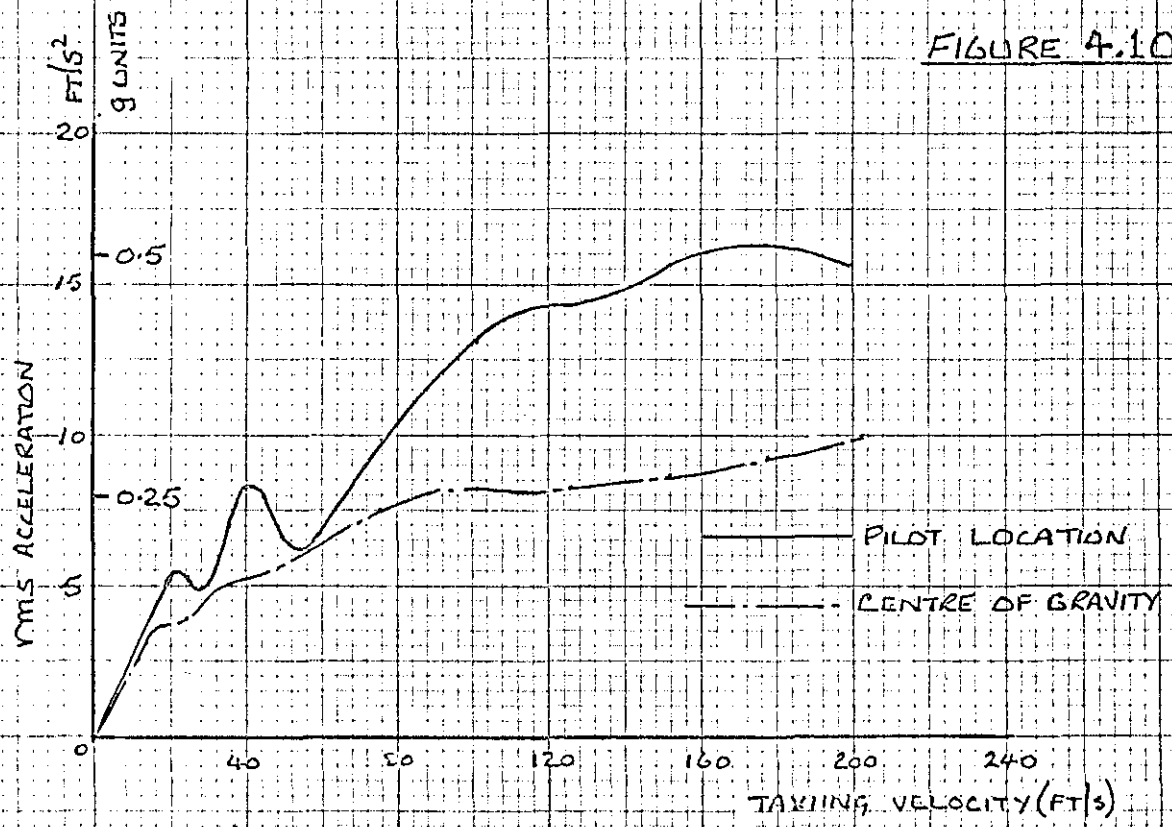
(a) REPRODUCED FROM REFERENCE 37

(b) COMPUTED FROM PARAMETERS USED IN
REFERENCE 37 USING PROGRAM RESPONSE 12

RESPONSE ACCELERATIONS

RIGID BODY MODES ONLY CONSIDERED

RESPONSE ACCELERATIONS FOR AIRCRAFT PARAMETERS USED IN REFERENCE 37

FIGURE 4.11

RIGID BODY MODES ONLY CONSIDERED

GEOMETRIC MEAN RUNWAY PARAMETERS FROM APPENDIX D USED

———————— PILOT LOCATION

— · — · — MAINWHEEL LOCATION
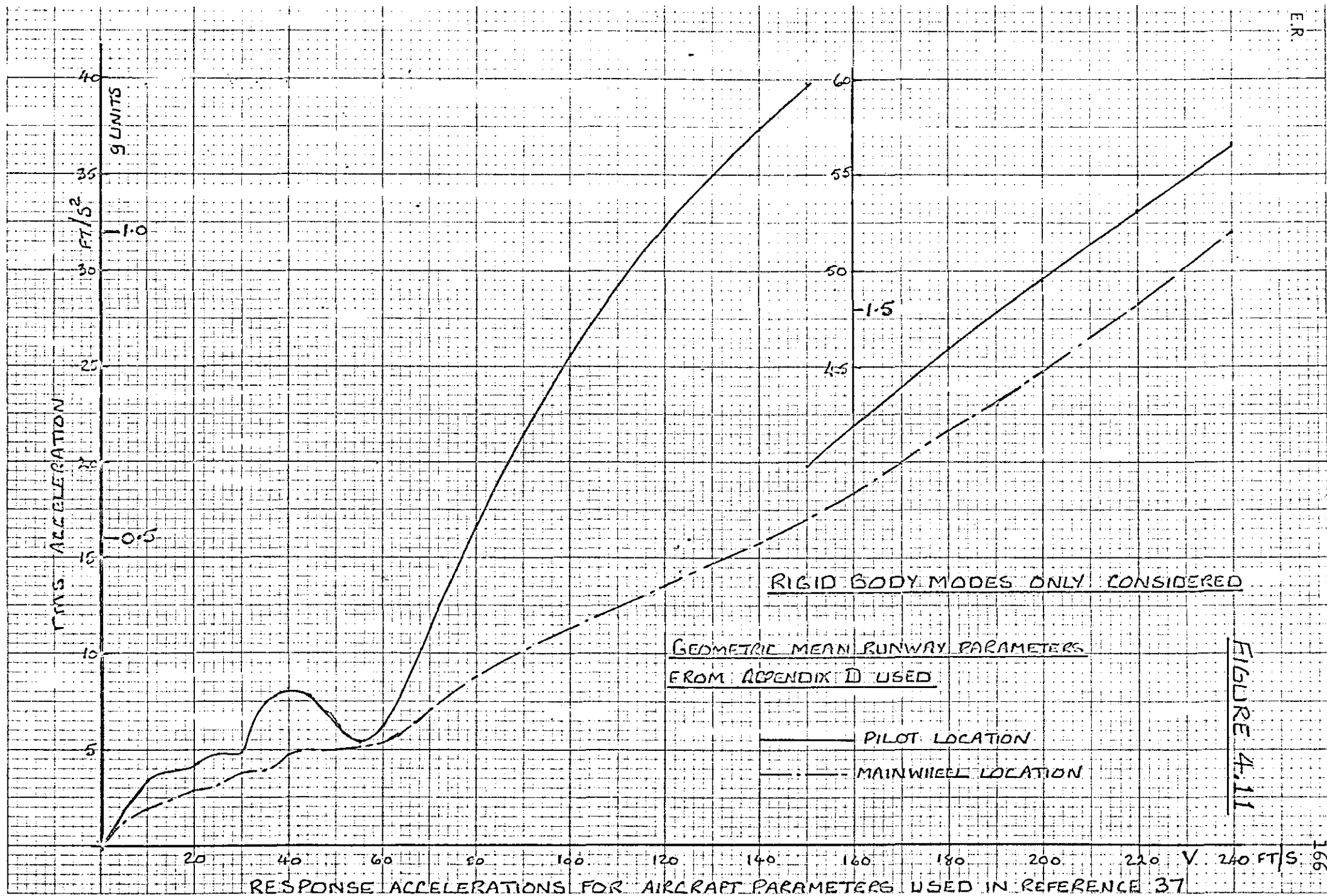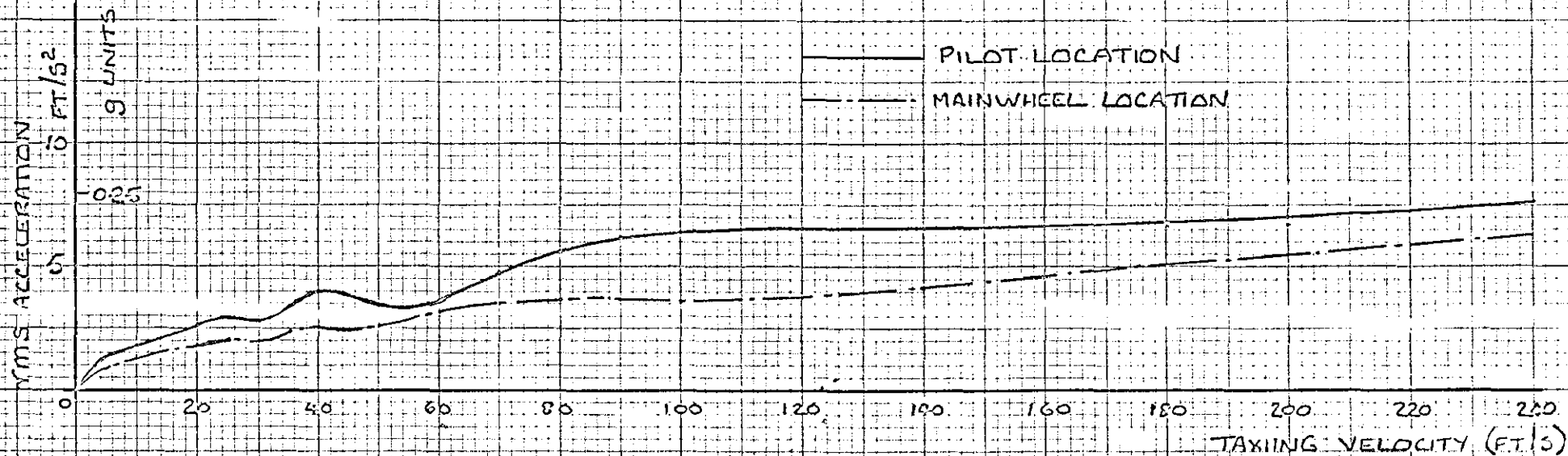
RESPONSE ACCELERATIONS FOR AIRCRAFT PARAMETERS

IN APPENDIX D WITH RUNWAY PSD $= \dfrac{20 \times 10^{-6} V}{\omega^2}$

RIGID BODY MODES ONLY CONSIDERED

FIGURE 4.12

FIGURE 4.13
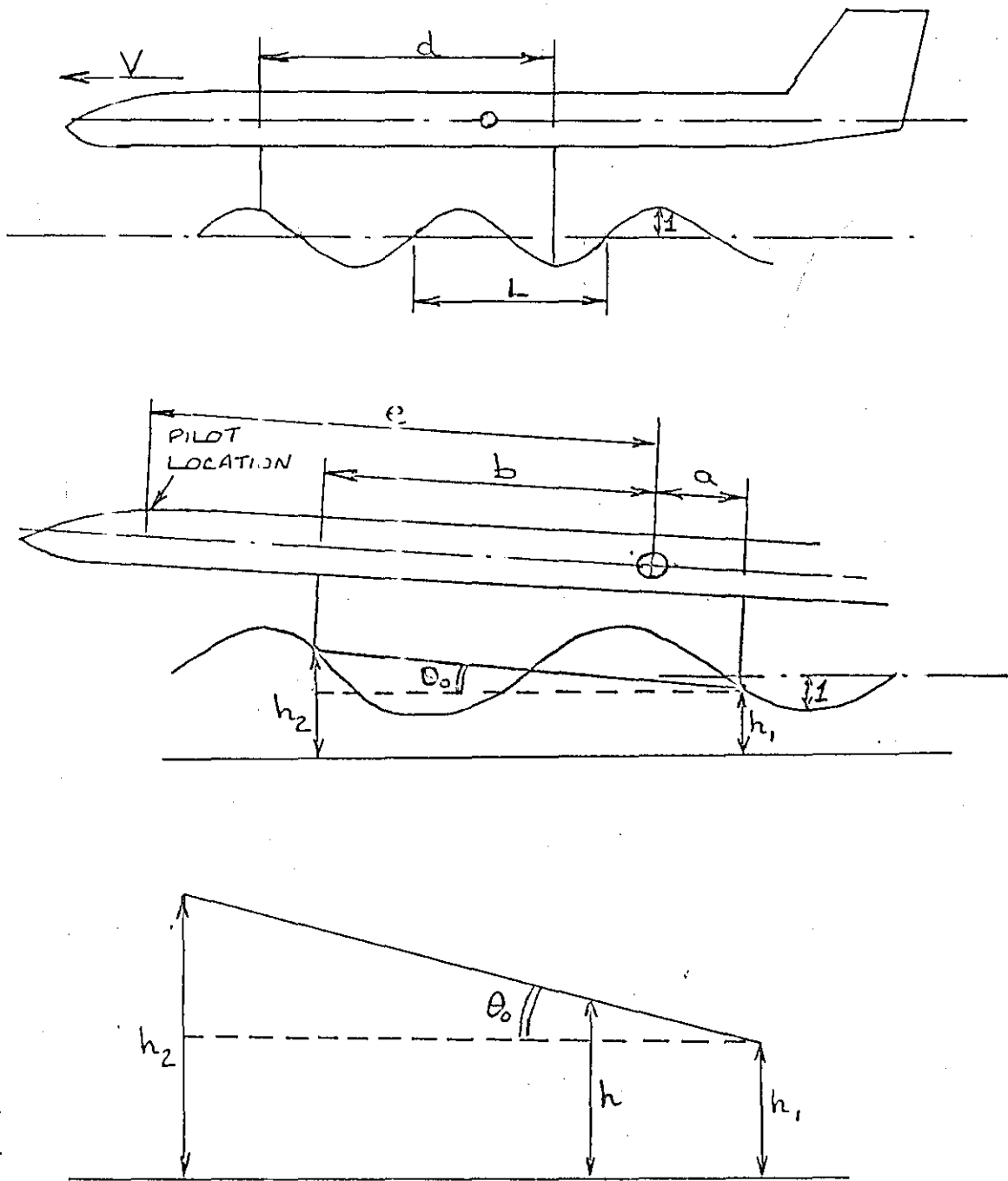


HEAVE AND PITCH INPUTS FROM
SINUSOIDAL RUNWAY
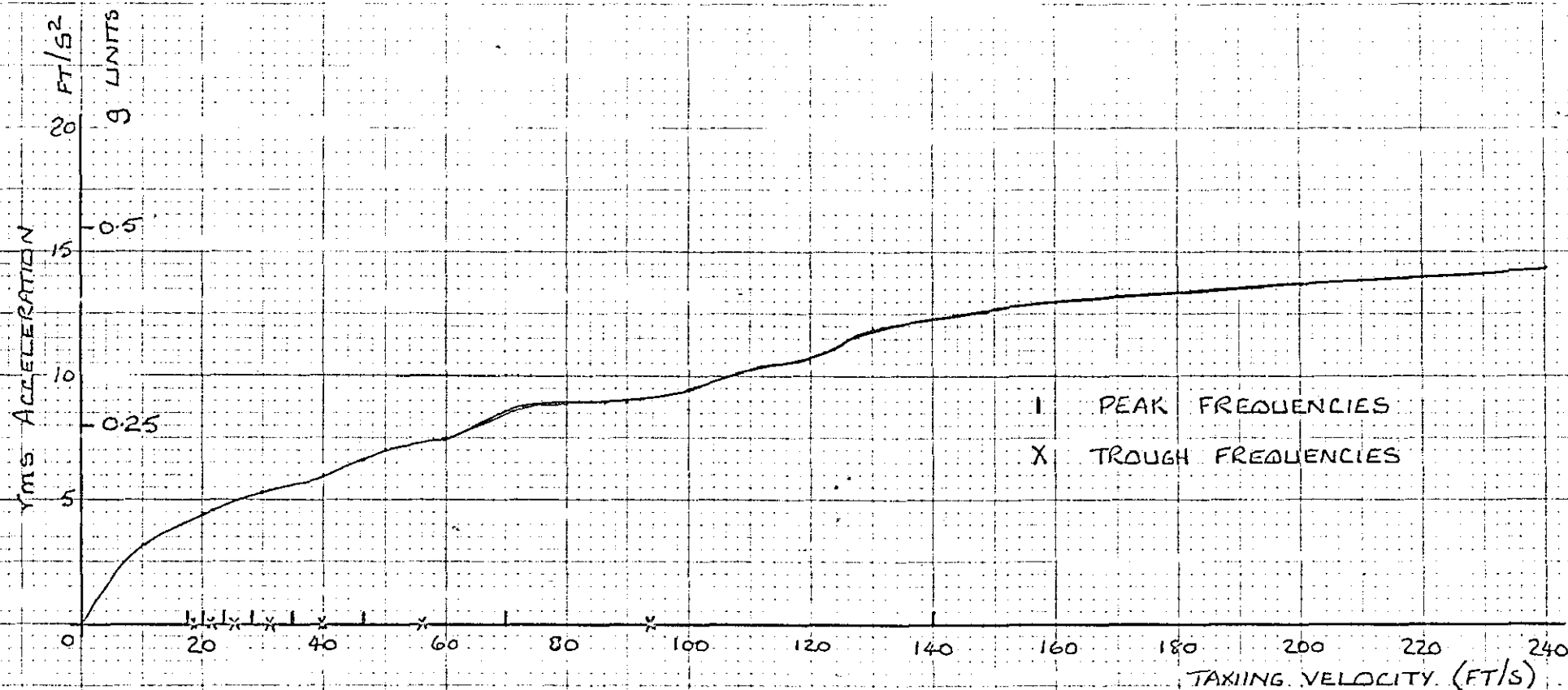
RESPONSE DUE TO UNCOUPLED HEAVE FOR PARAMETERS

USED IN REFERENCE 37

FIGURE 4.14

169

FIGURE 4.15



$$(a) \quad \frac{K^2 + (C\,\omega_f)^2}{(K - M\omega_f^2)^2 + (C\,\omega_f)^2}$$

$$(b) \quad 1 - \frac{2ab}{d^2}\left(1 - \cos\frac{d}{V}\,\omega_f\right)$$

$$(c) \quad \frac{\bar{C}\ V}{\omega_f^2}$$

$$(d) \quad \omega_f^4$$
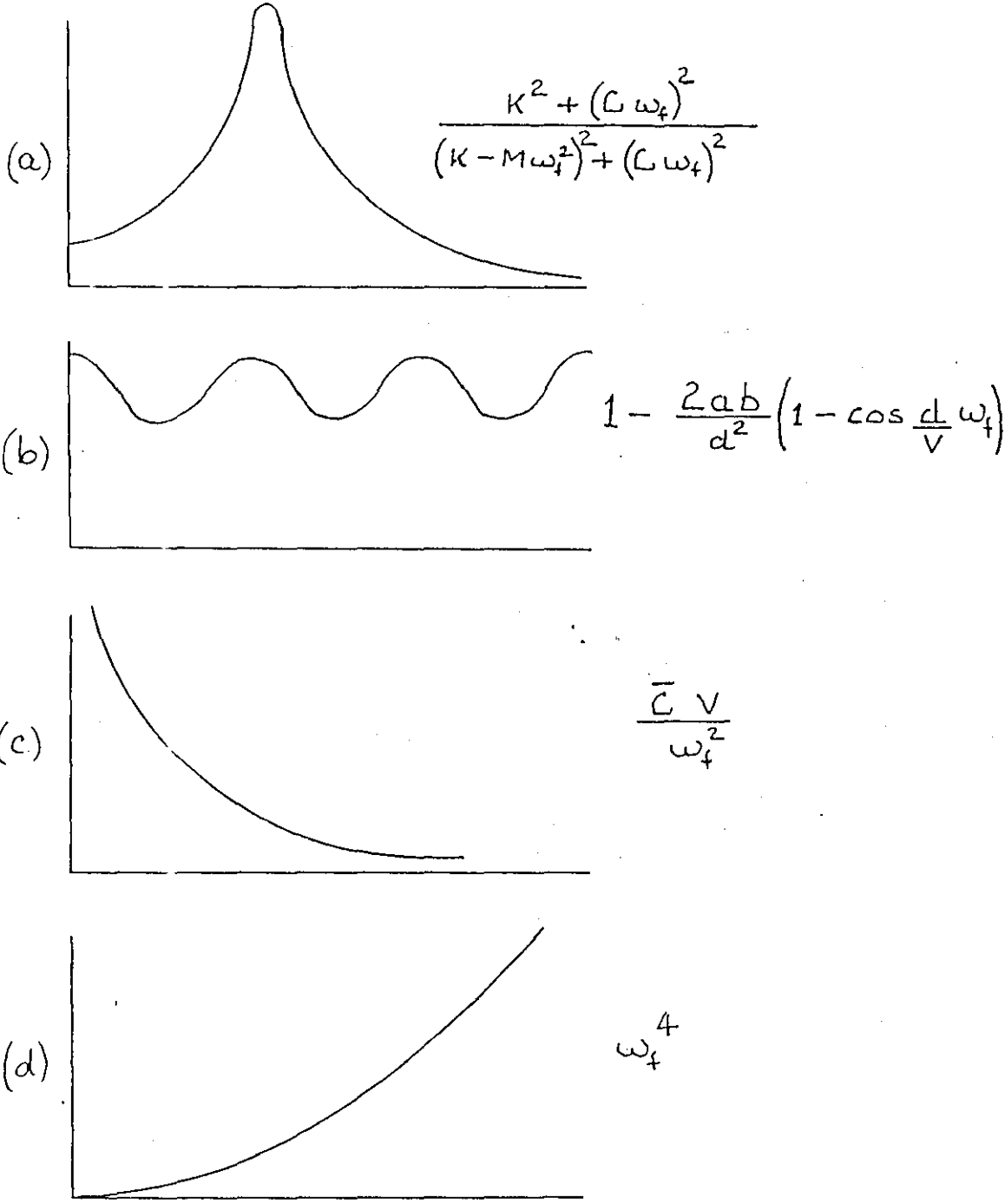
COMPONENTS OF HEAVE EQUATION
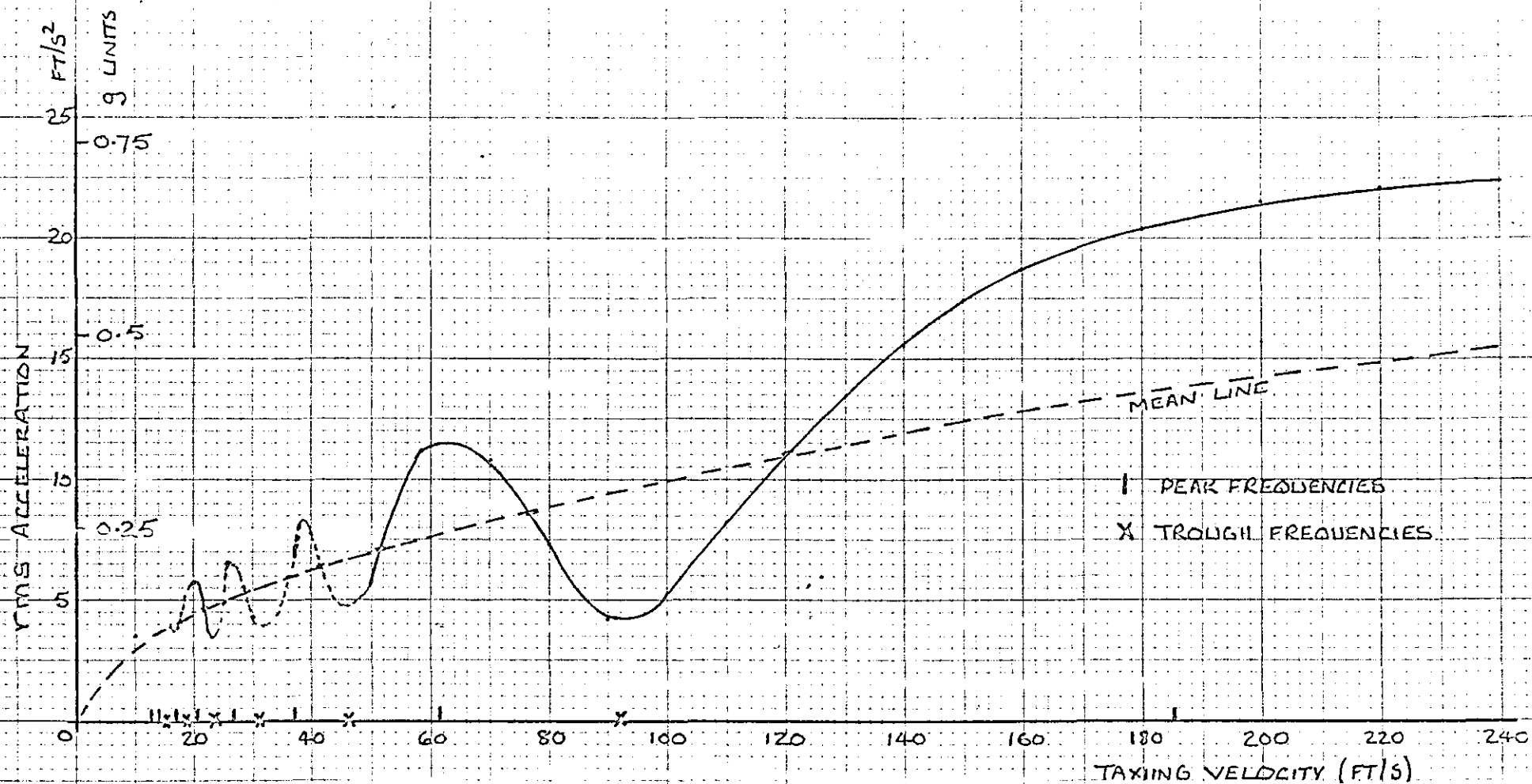
RESPONSE AT PILOT LOCATION DUE TO UNCOUPLED PITCH

FOR PARAMETERS USED IN REFERENCE 37

FIGURE 4.16

171

FIGURE 4.17

(a)
$$\frac{K_e^2 + \left(C_e \omega_f\right)^2}{\left(K_e - I \omega_f^2\right)^2 + \left(C_e \omega_f\right)^2}$$

(b)
$$1 - \cos \frac{d}{V} \omega_f$$

(c)
$$\frac{\bar{C} V}{\omega_f^2}$$

(d)
$$\omega_f^4$$
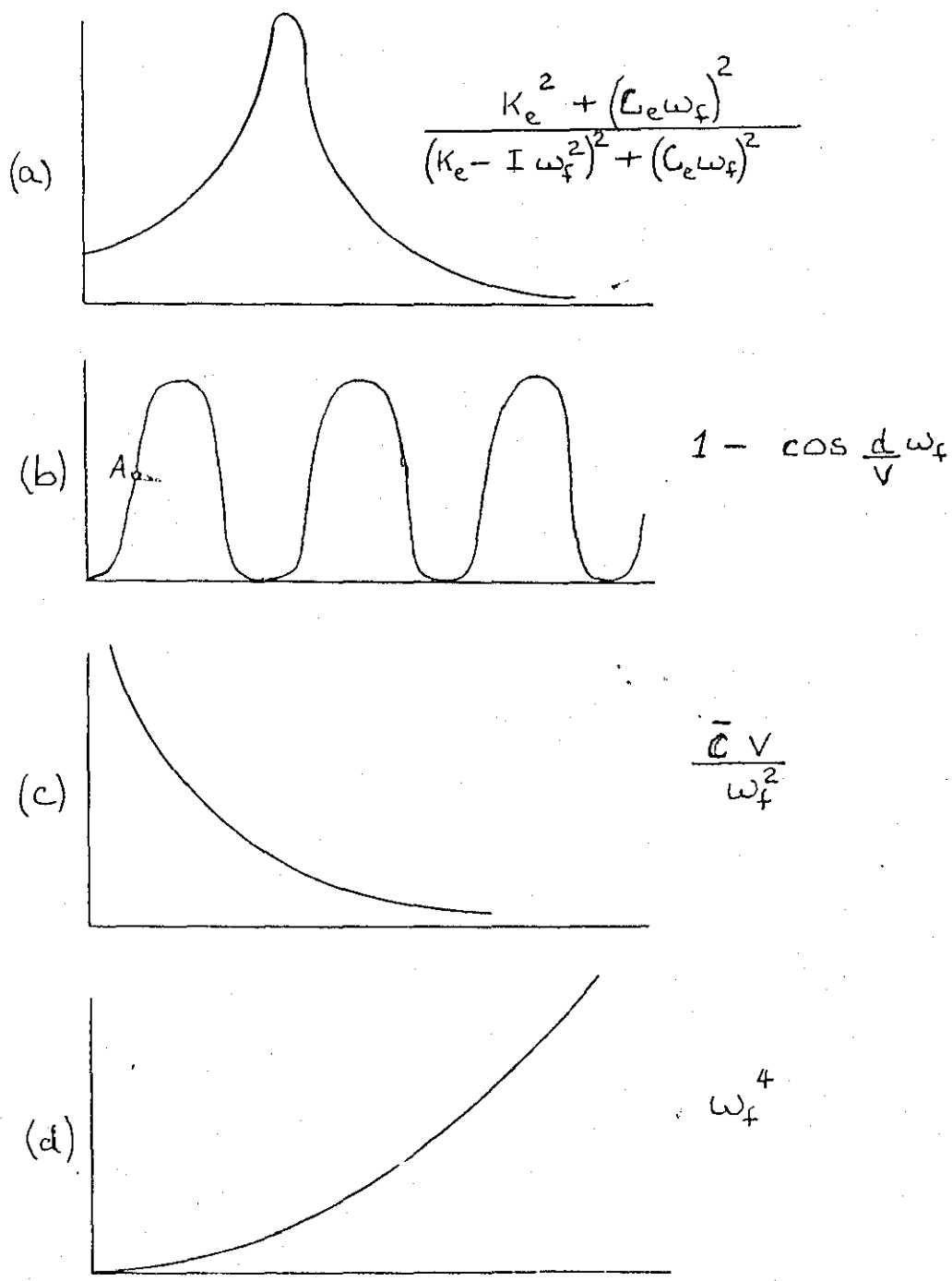
COMPONENTS OF PITCH EQUATION
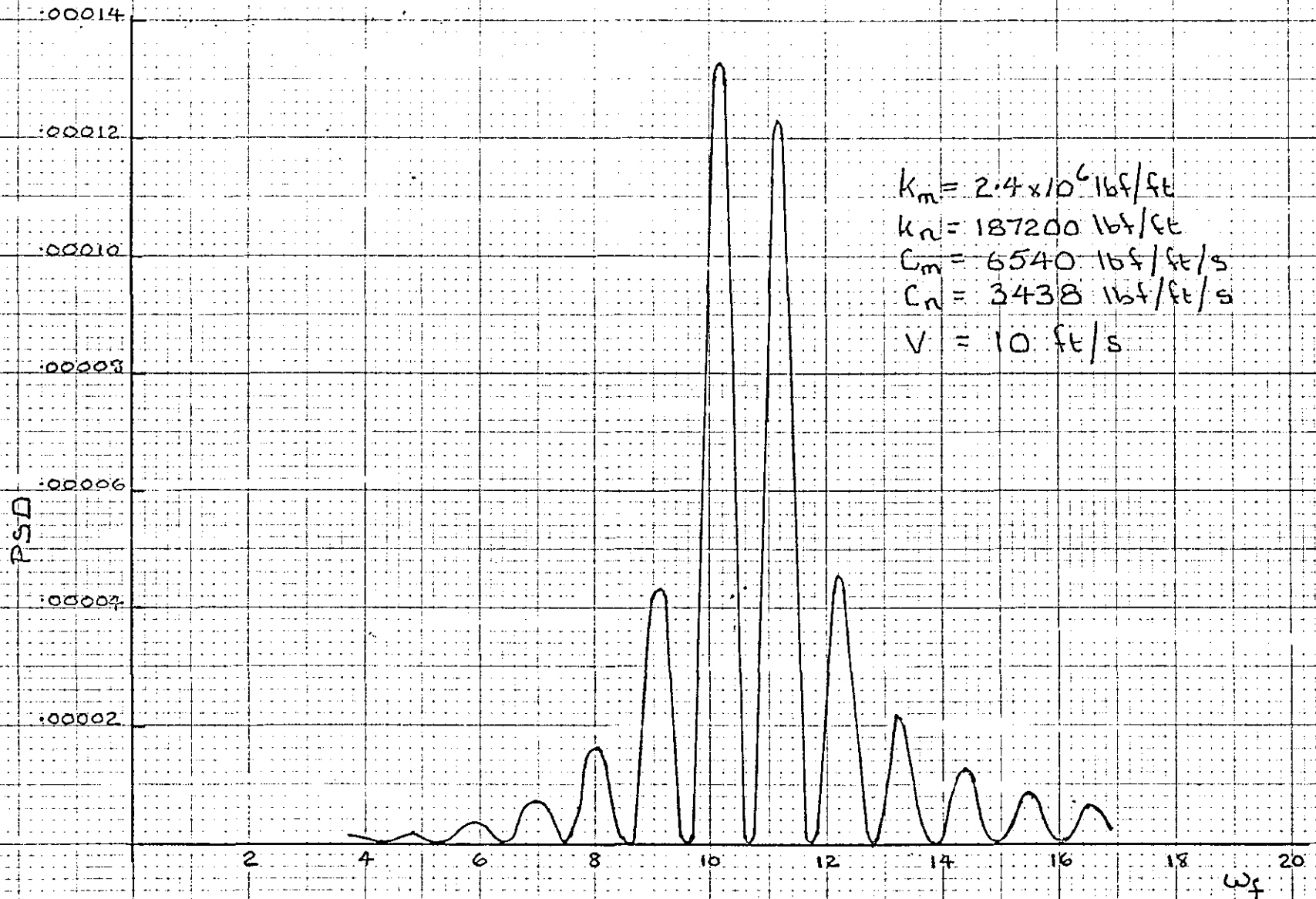
$\left| \left( 1 - \cos \frac{d}{V} \omega_t \right) \right|$

$K_m = 2.4 \times 10^6 \ lbf/ft$

$K_n = 187200 \ lbf/ft$

$C_m = 6540 \ lbf/ft/s$

$C_n = 3438 \ lbf/ft/s$

$V = 120 \ ft/s$

PSD

$\omega_t$

PSD OF PITCH RESPONSE ACCELERATION

FIGURE 4.1B

PSD OF PITCH RESPONSE ACCELERATION

$K_m = 2.4 \times 10^6 \ lbf/ft$

$k_n = 187200 \ lbf/ft$

$C_m = 6540 \ lbf/ft/s$

$C_n = 3438 \ lbf/ft/s$

$V = 10 \ ft/s$

FIGURE 4.19
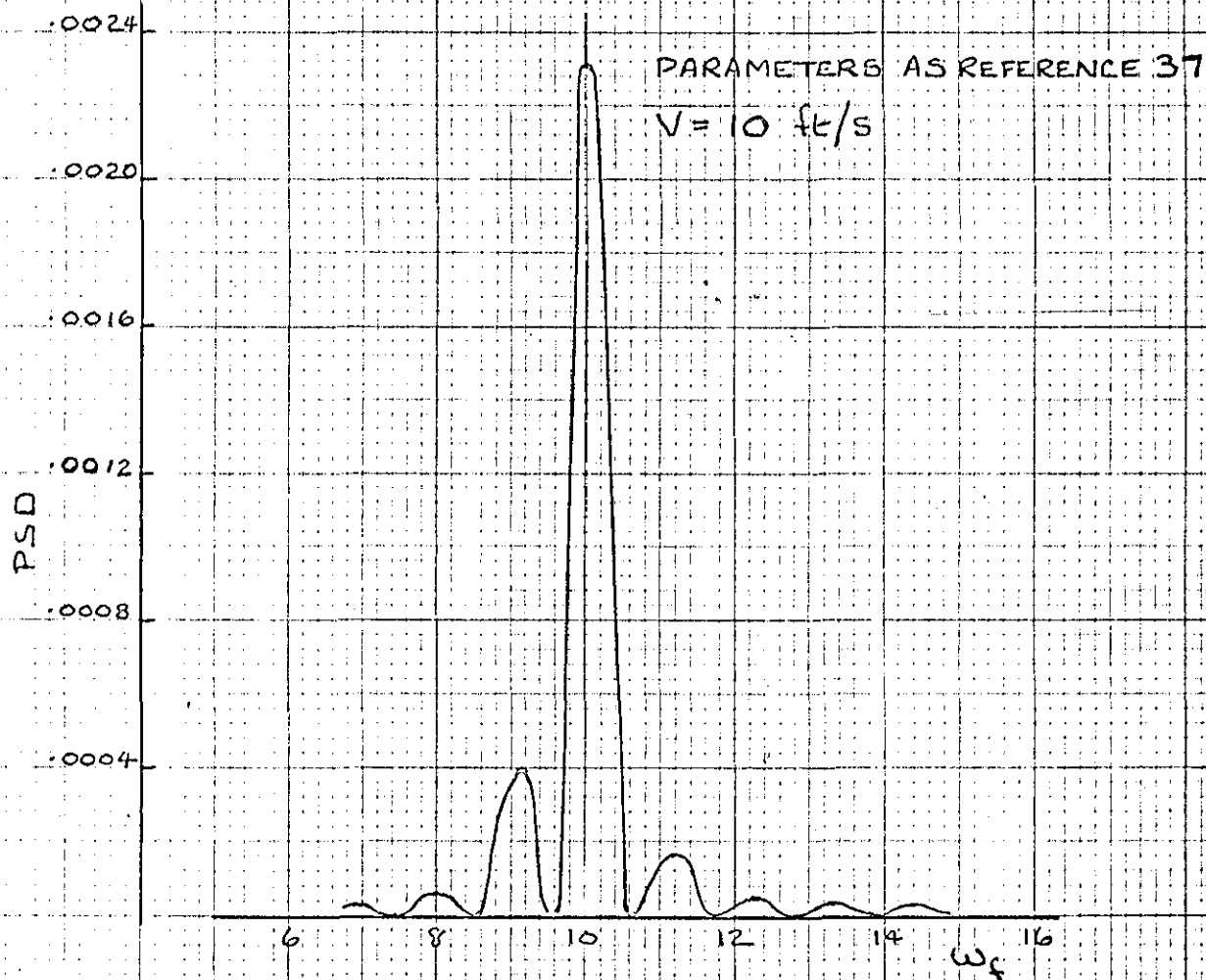
FIGURE 4.20

PSD OF PITCH RESPONSE ACCELERATION

FIGURE 4.21
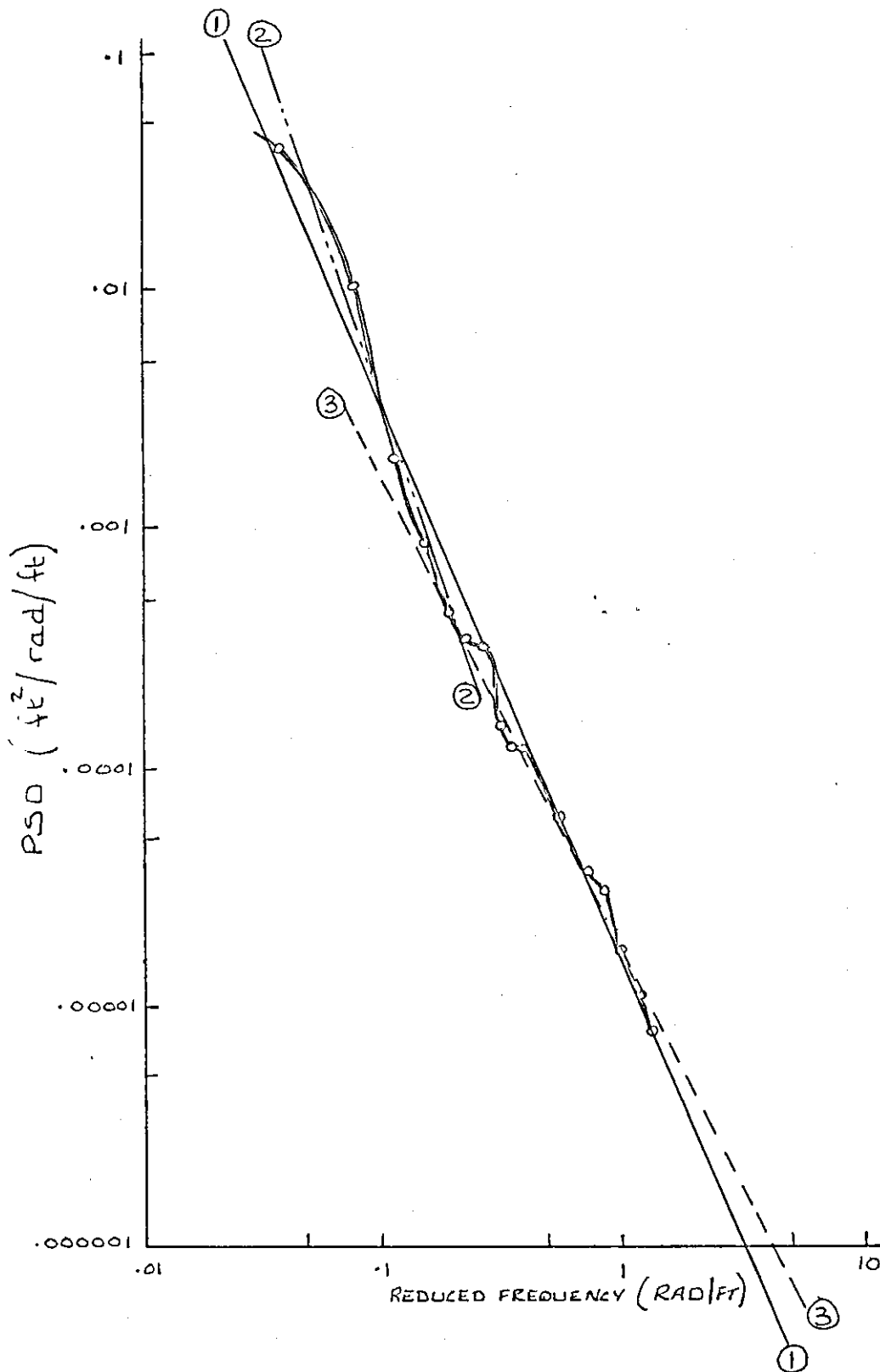
RUNWAY 12 , LANGLEY FIELD

FIGURE 4.22

VARIATION OF MAINWHEEL LOCATION RESPONSE

WITH OLEO STIFFNESS

$C_m = 13080\ lbf/ft/s \qquad C_n = 6876\ lbf/ft/s$
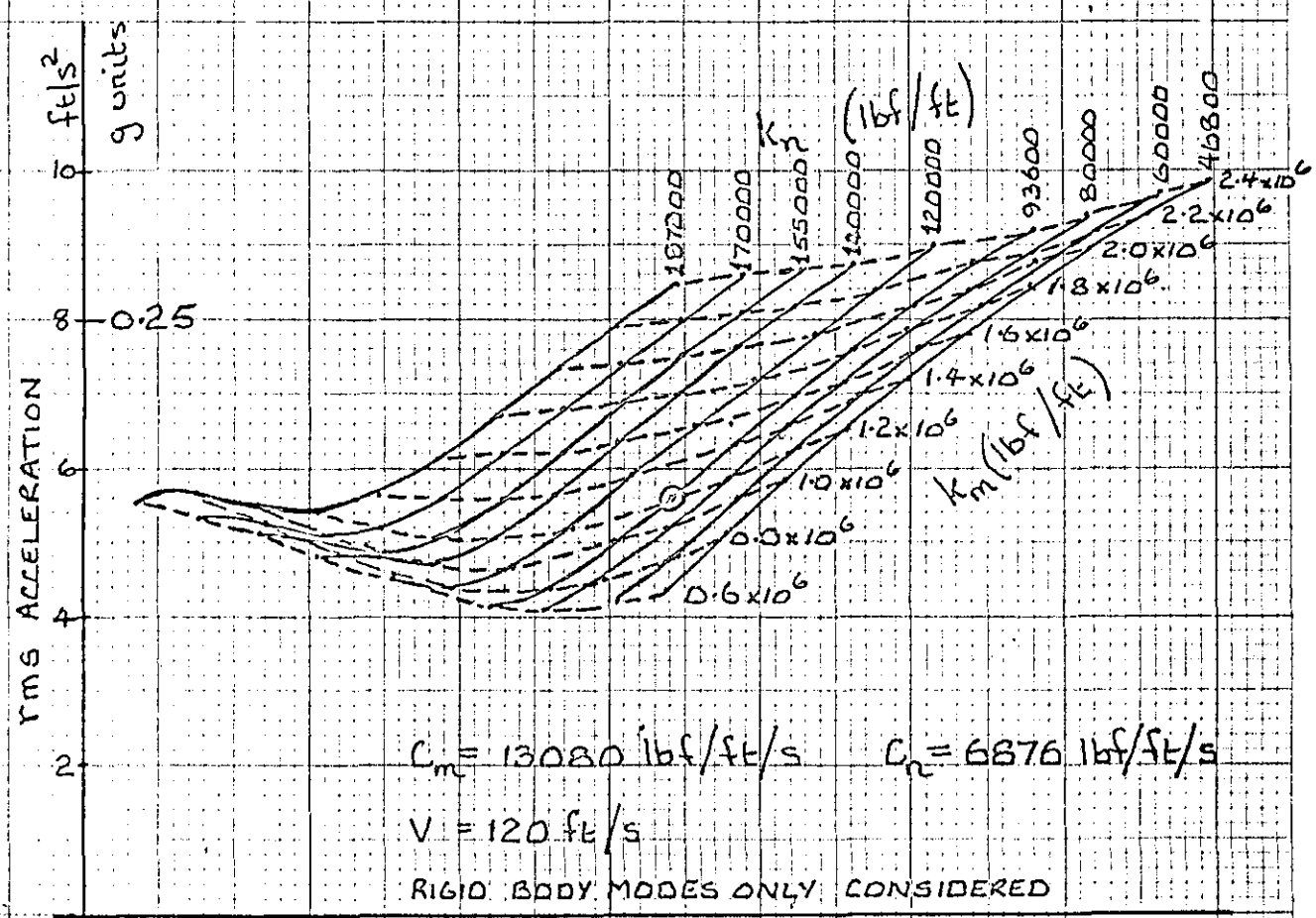
$V = 120\ ft/s$

RIGID BODY MODES ONLY CONSIDERED
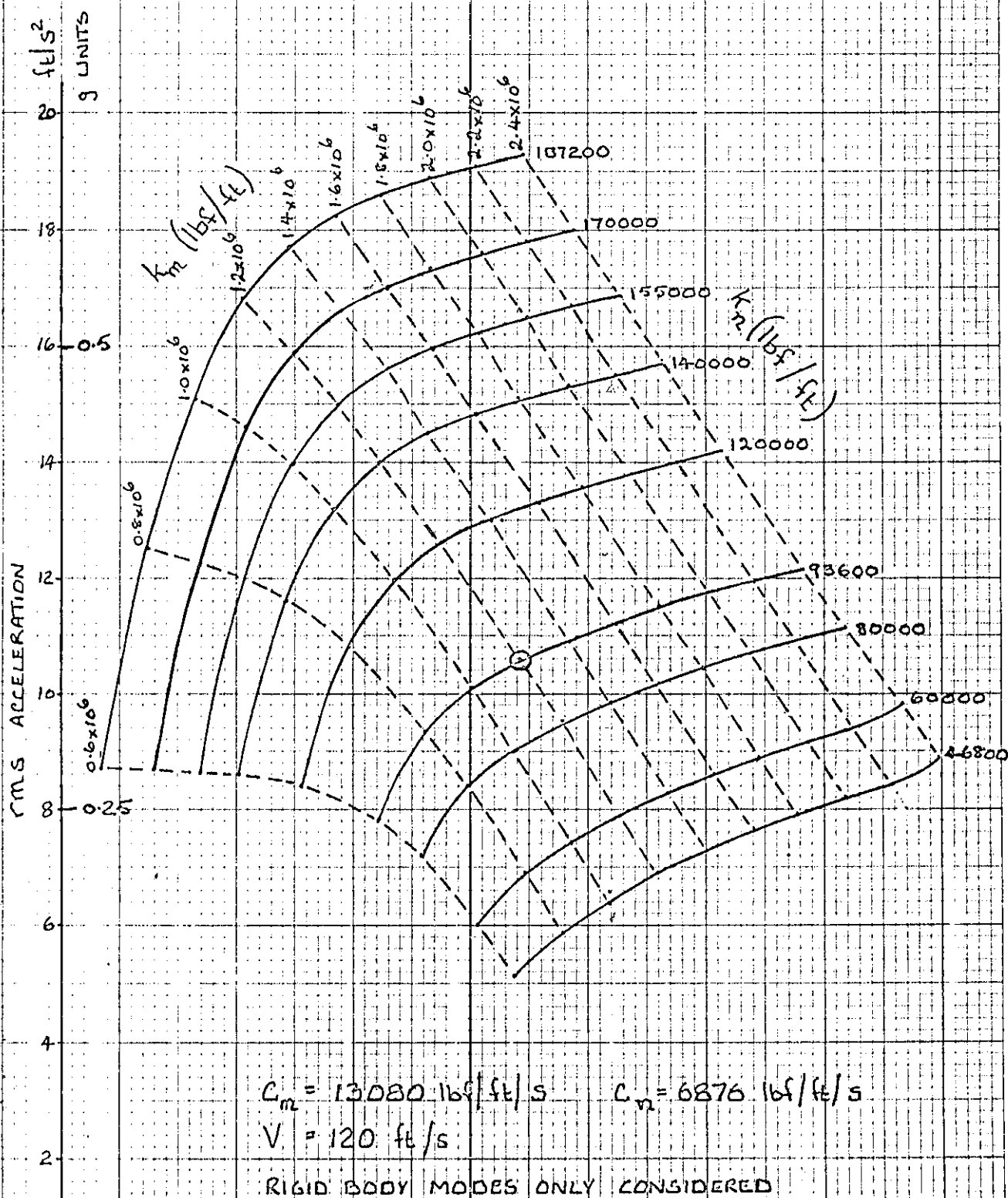
FIGURE 4.23

VARIATION OF PILOT LOCATION RESPONSE
WITH OLEO STIFFNESS
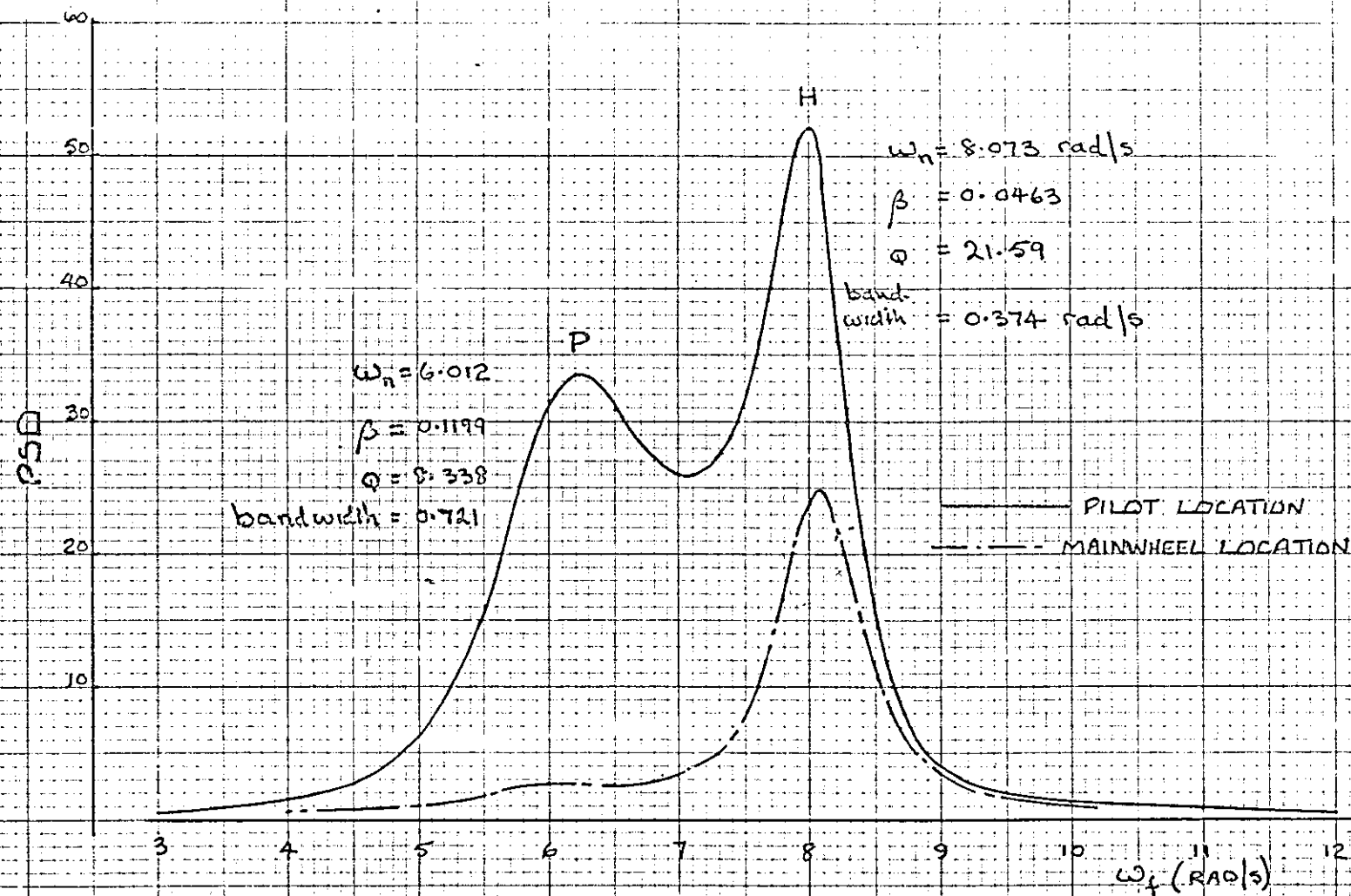
PSD OF RESPONSE ACCELERATION FOR PARAMETERS IN APPENDIX D

RIGID BODY MODES ONLY CONSIDERED     V = 120 FT/s

$\omega_n = 8.073$ rad/s
$\beta = 0.0463$
$Q = 21.59$
band width $= 0.374$ rad/s

$\omega_n = 6.012$
$\beta = 0.1199$
$Q = 8.338$
bandwidth $= 0.721$

———————— PILOT LOCATION
—·—·—·— MAINWHEEL LOCATION

$\omega_f$ (RAD/s)

PSD

FIGURE 4.24     179

(a) $k_m = 2.4 \times 10^6$ lbf/ft    $k_n = 187200$ lbf/ft    (b) $k_m = 0.6 \times 10^6$ lbf/ft    $k_n = 46800$ lbf/ft

PSD OF RESPONSE ACCELERATION FOR PARAMETERS (EXCEPT $k_m$ $k_n$) AS APPENDIX D

RIGID BODY MODES ONLY CONSIDERED    V = 120 FT/S

Figure (a) labels:

H
$\omega_n = 9.380$ rad/s
$\beta = 0.0231$
$Q = 43.22$
band width = 0.217 rad/s

P
$\omega_n = 7.122$
$\beta = 0.0501$
$Q = 19.95$
bandwidth = 0.357

Figure (b) labels:

PILOT LOCATION
MAINWHEEL LOCATION

$\omega_n = 4.788$
$\beta = 0.2543$
$Q = 3.931$
bandwidth = 1.218

$\omega_n = 6.502$ rad/s
$\beta = 0.0824$
$Q = 12.13$
b/w = 0.536 rad/s

FIGURE 4.25

F R.

180
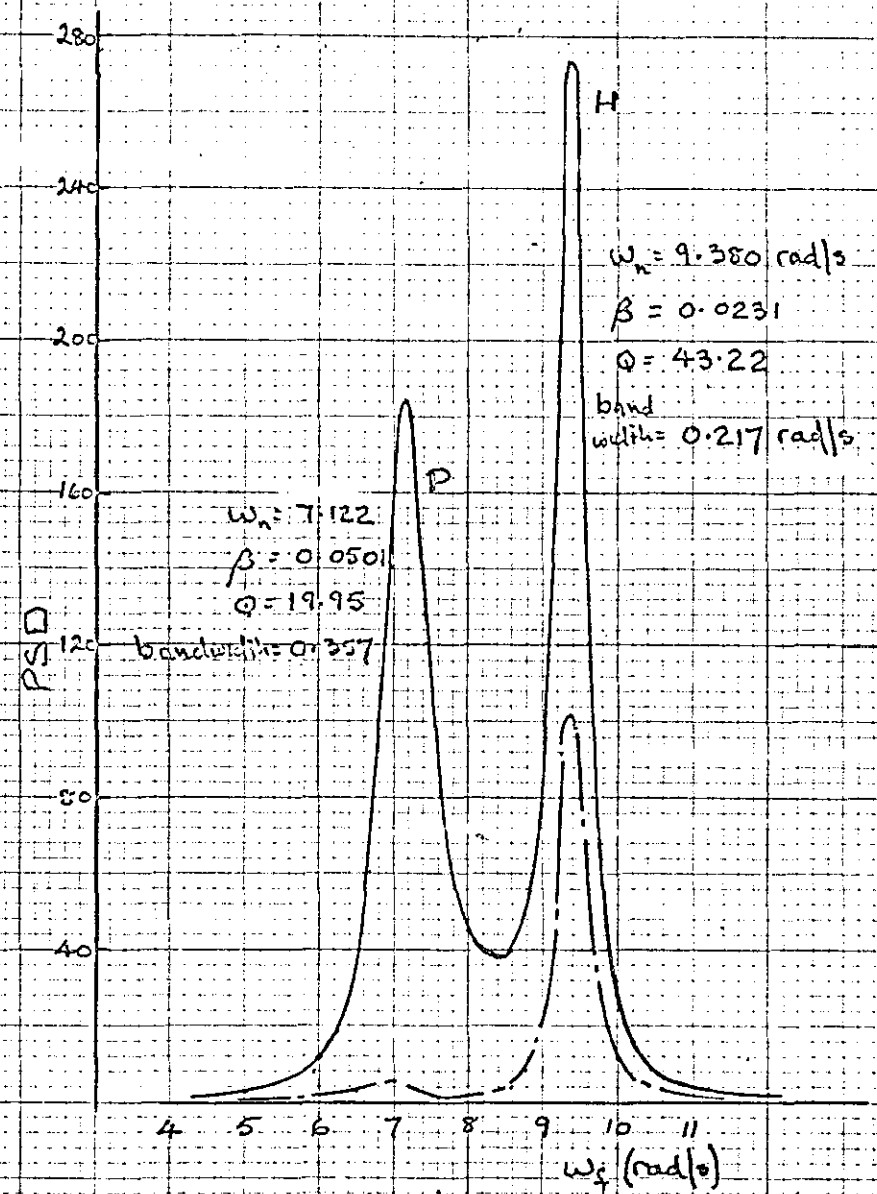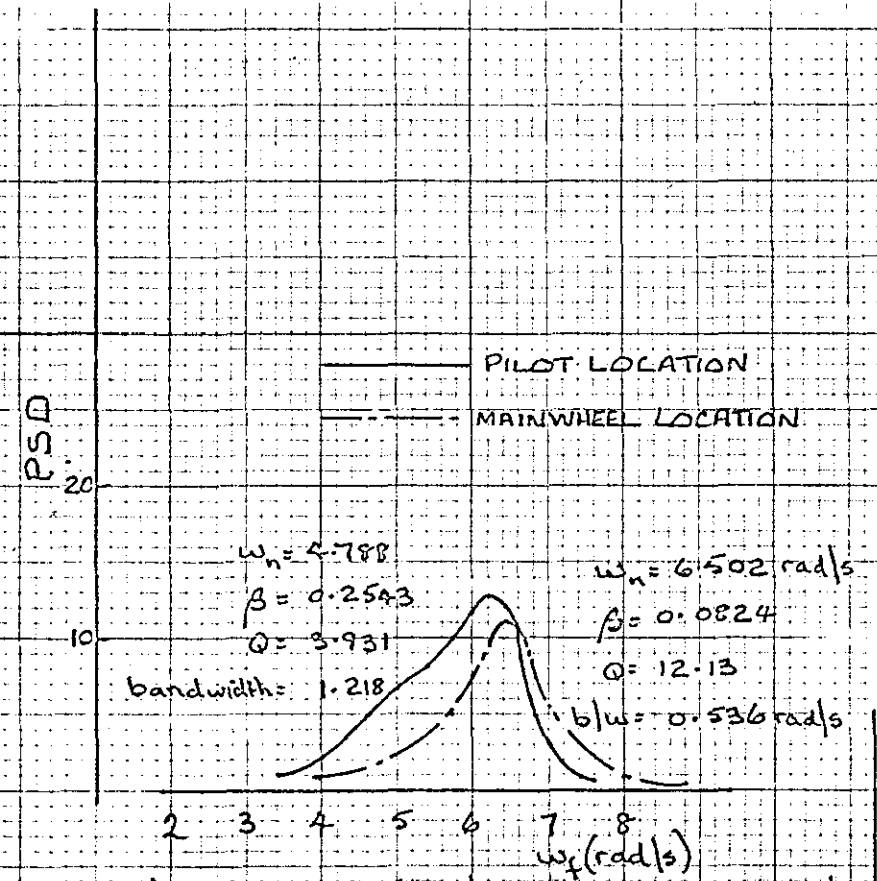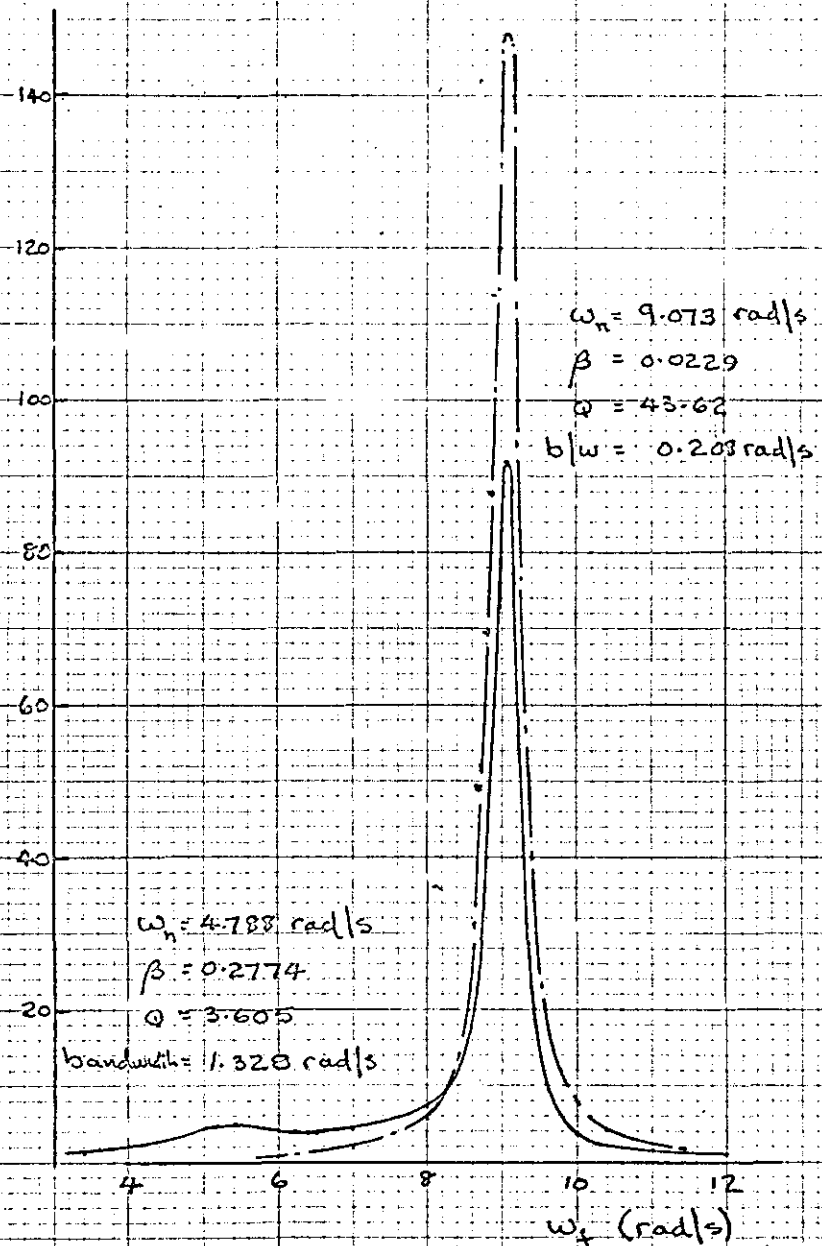
(a)  $k_m = 2.4 \times 10^6$ lbf/ft    $k_n = 46800$ lbf/ft

(b)  $k_m = 0.6 \times 10^6$ lbf/ft    $k_n = 187200$ lbf/ft

PSD OF RESPONSE ACCELERATION FOR PARAMETERS EXCEPT $(k_m, k_n)$ AS APPENDIX D

(RIGID BODY MODES ONLY CONSIDERED)    V = 120 FT/S

FIGURE 4.26    181

FIGURE 4.27

VARIATION OF RESPONSE WITH OLEO STIFFNESS

$C_m = 26000$ $lbf/ft/s$    $C_n = 14000$ $lbf/ft/s$

$V = 120$ $ft/s$

RIGID BODY MODES ONLY CONSIDERED

FIGURE 4.28

$k_m = 2.4 \times 10^6$
$k_n = 187200$    I

$k_m = 0.6 \times 10^6$
$k_n = 187200$

HEAVE

$k_m = 2.4 \times 10^6$
$k_n = 187200$

PITCH
$k_m = 0.6 \times 10^6$
$k_n = 468000$

$k_m = 0.6 \times 10^6$
$k_n = 468000$

$k_m = 0.6 \times 10^6$
$k_n = 187200$

$C_m = 26000 \; lbf/ft/s$     $C_n = 14000 \; lbf/ft/s$

R  5    4    3    2    1    0
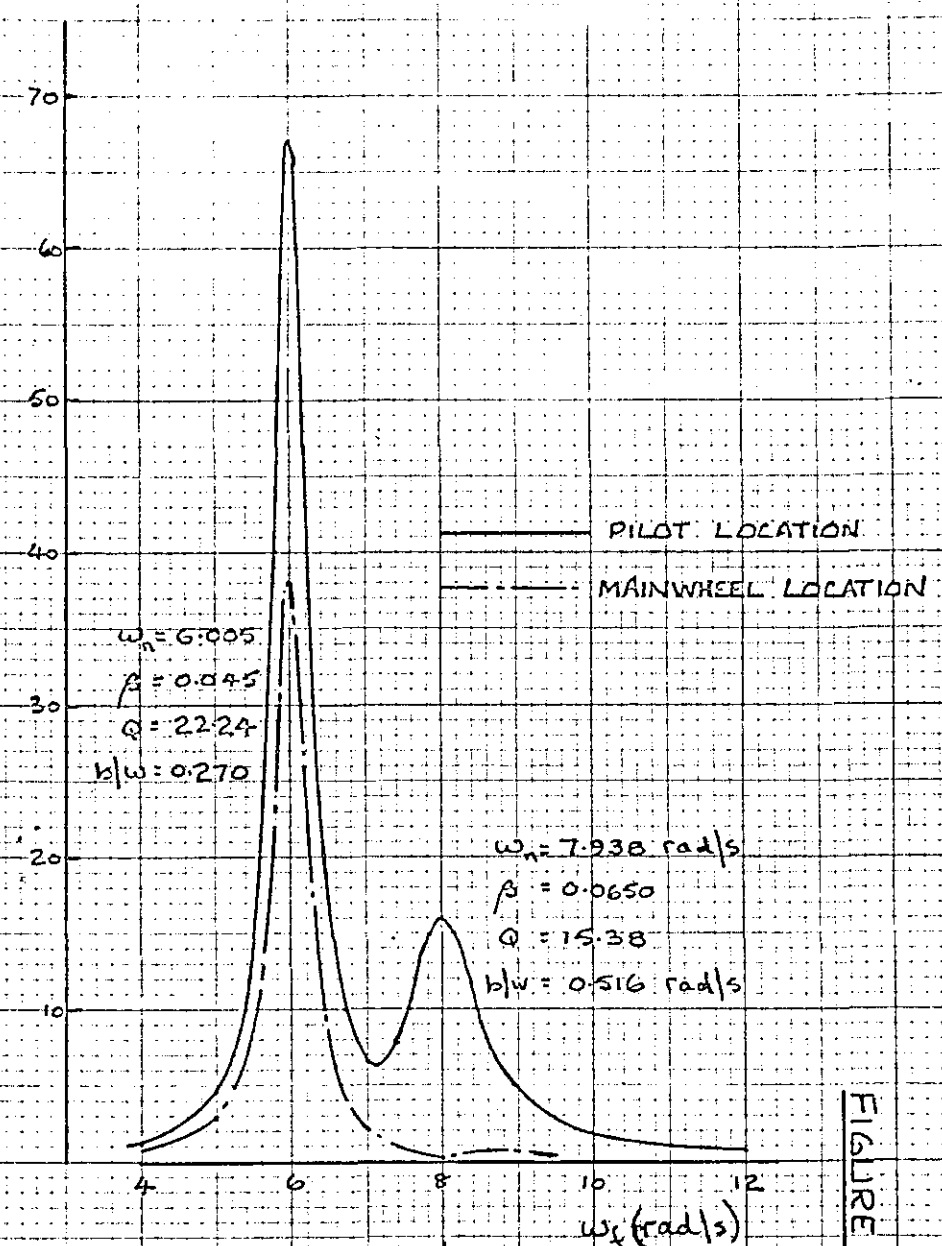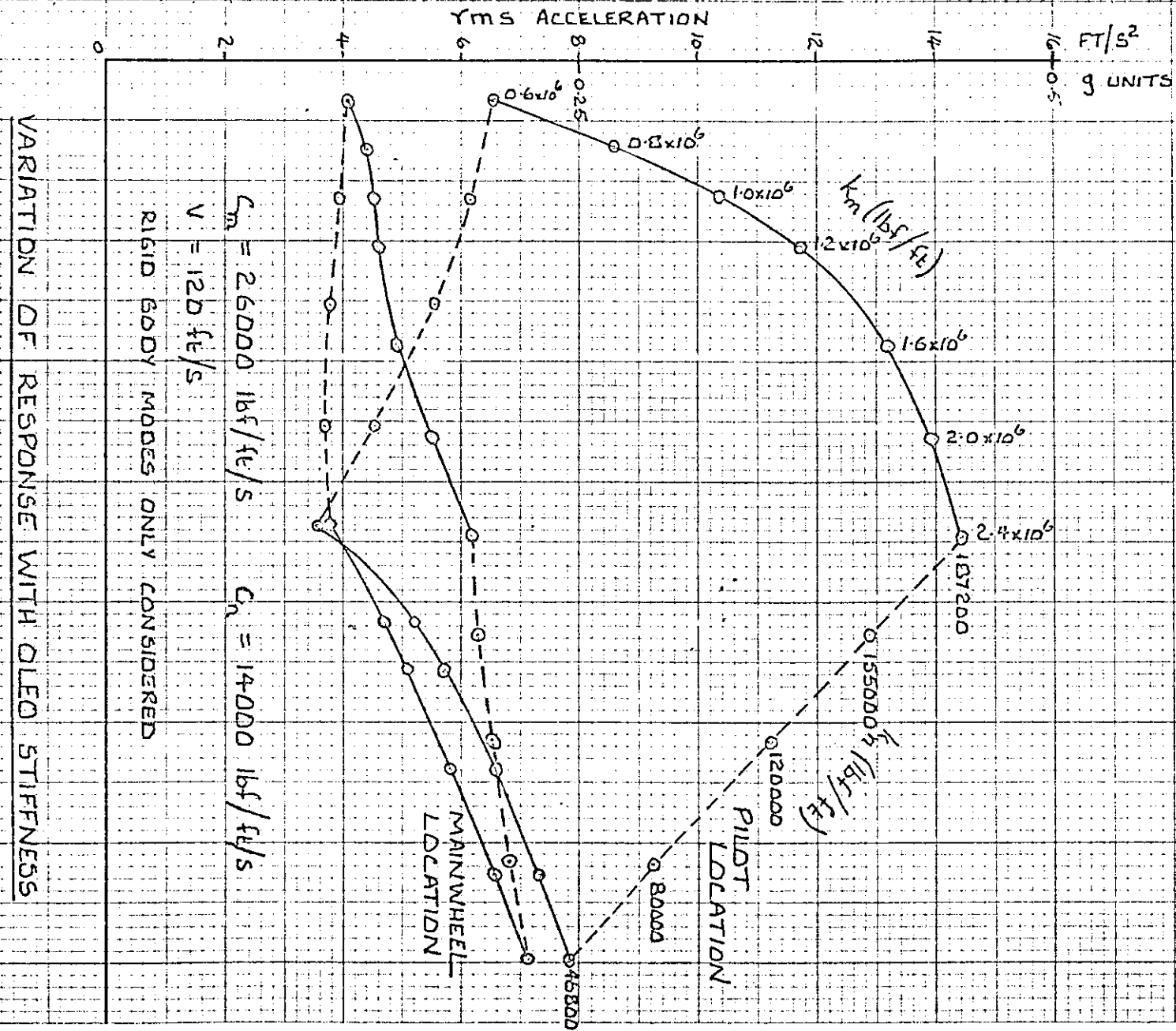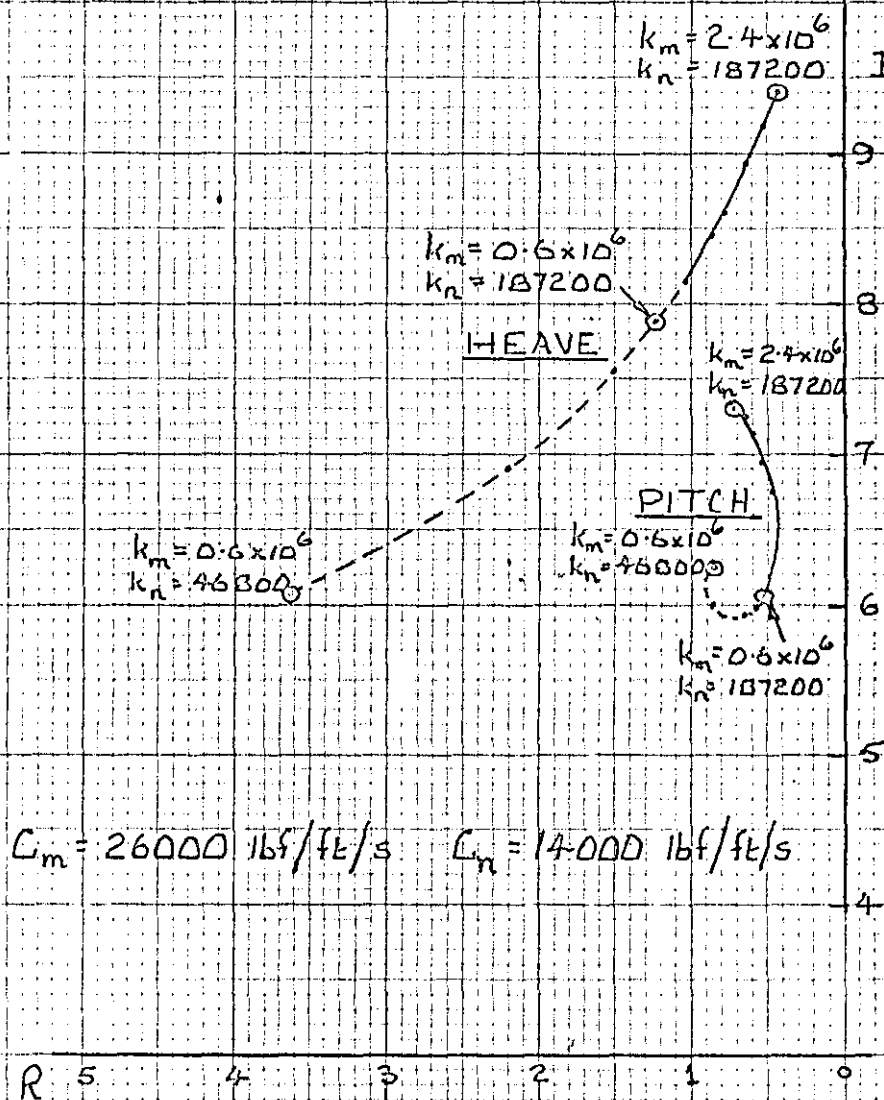
VARIATION OF EIGENVALUES WITH OLEO

STIFFNESS

RIGID BODY MODES ONLY CONSIDERED

FIGURE 4.29
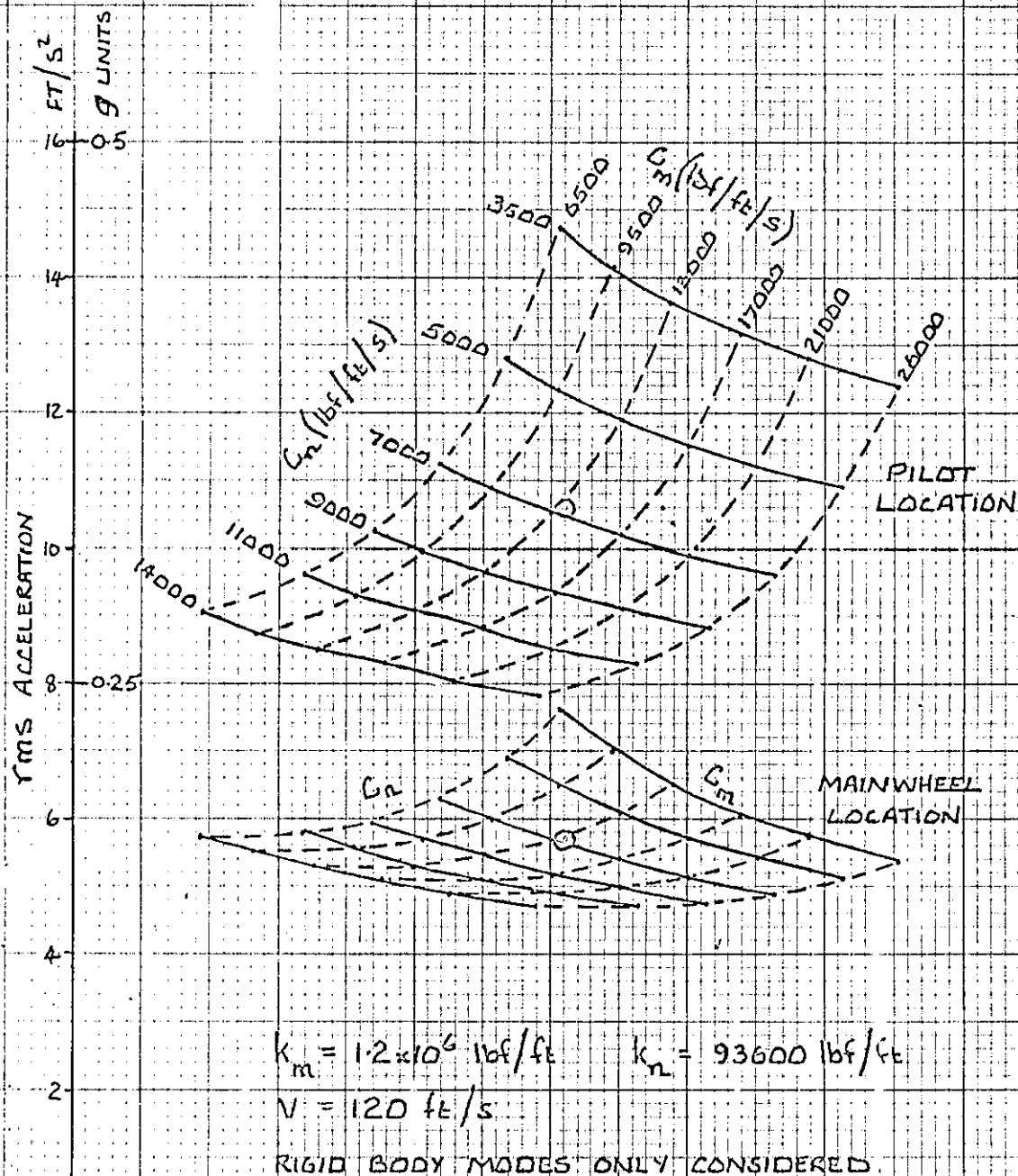
VARIATION OF RESPONSE WITH OLEO DAMPING

FIGURE 4.30
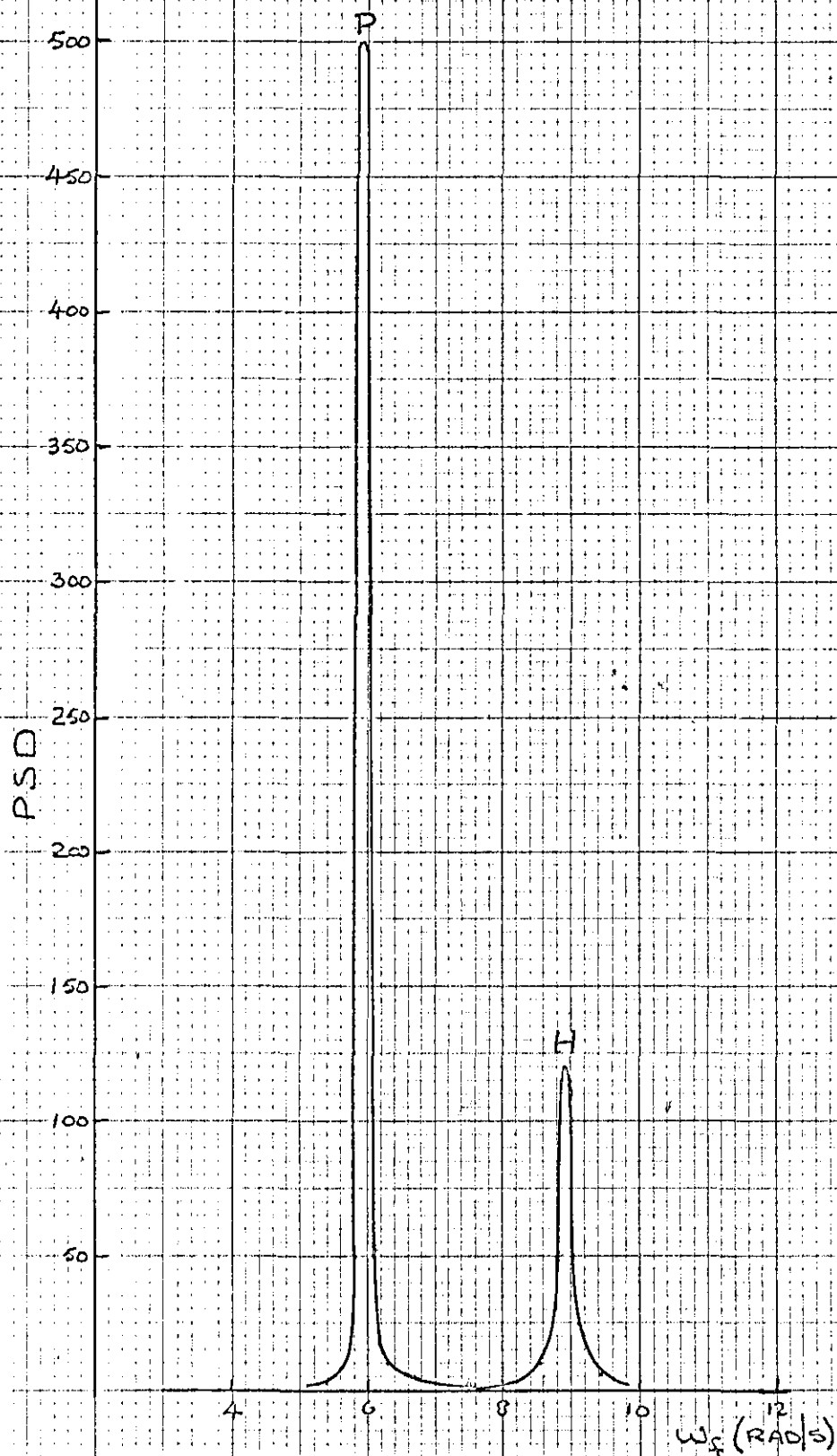
PSD OF RESPONSE ACCELERATION AT PILOT LOCATION

FOR PARAMETERS AS REFERENCE 37

RIGID BODY MODES ONLY CONSIDERED    V = 40 FT/S

FIGURE 4.31



VARIATION OF RESPONSE WITH OLEO DAMPING

$k_m = 0.6 \times 10^6 \; lbf/ft$      $k_n = 46800 \; lbf/ft$

$C_m = 26000 \; lbf/ft/s$      $C_n = 14000 \; lbf/ft/s$

REMAINING PARAMETERS AS APPENDIX D

$V = 120 \; ft/s$

——————— PILOT LOCATION

—·—·—·— MAINWHEEL LOCATION

PSD

$\omega_f$ (RAD/s)
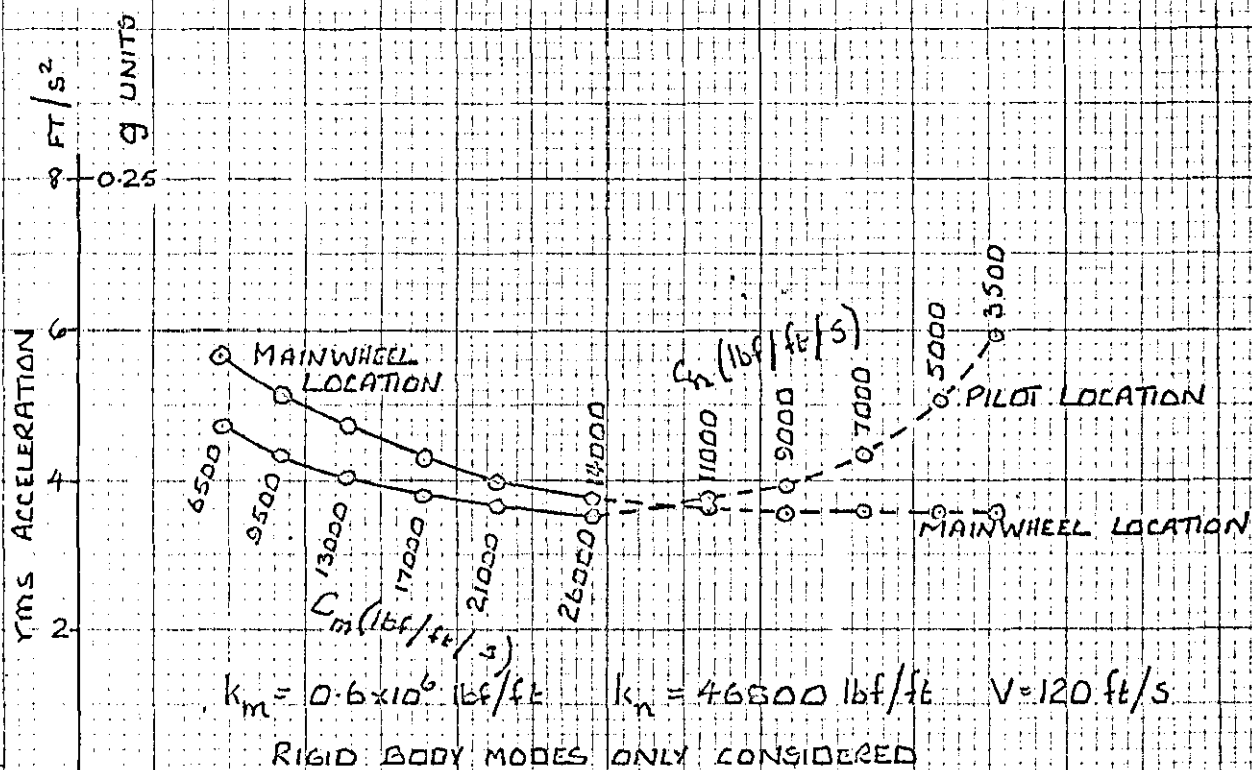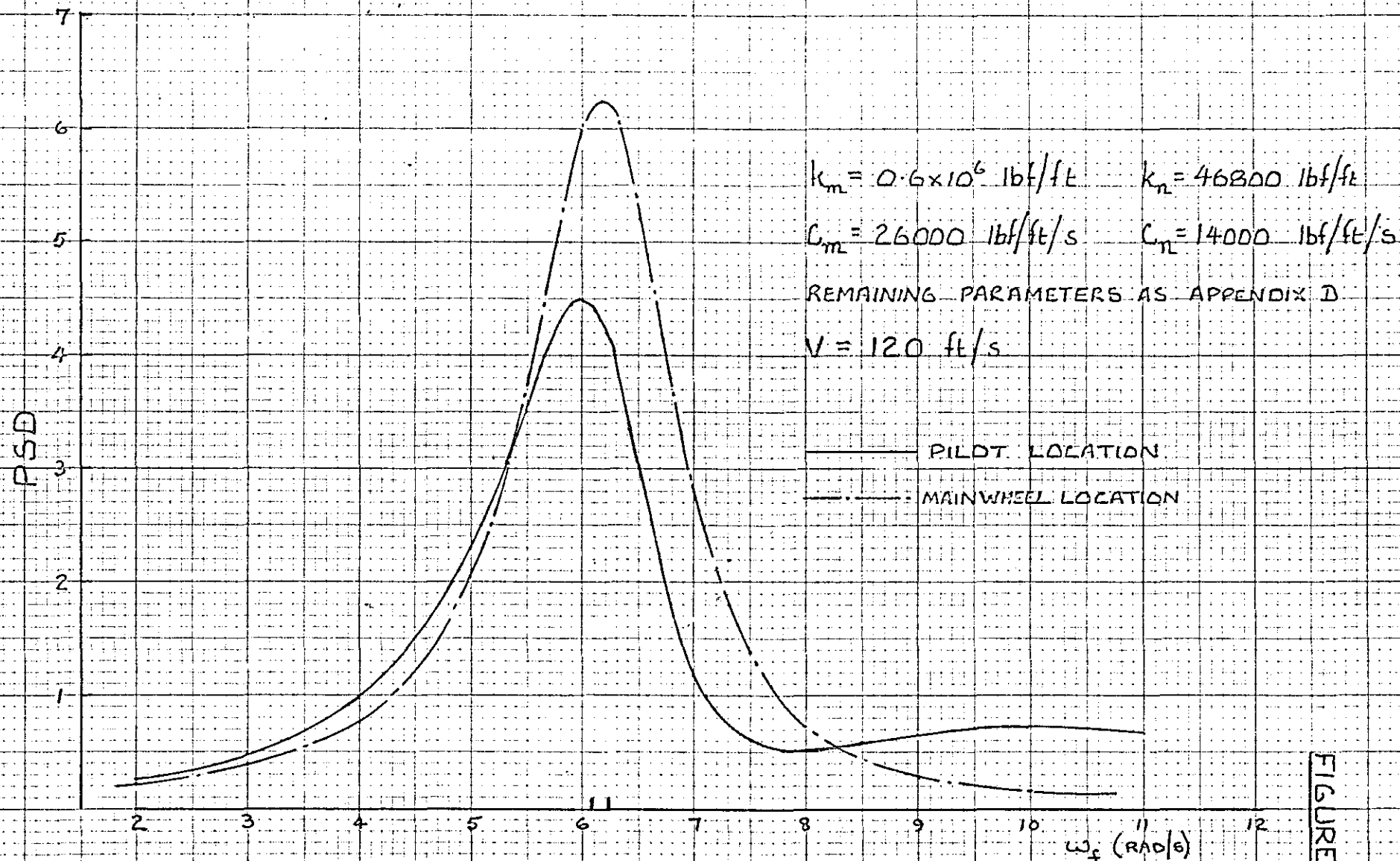
PSD OF RESPONSE ACCELERATION

RIGID BODY MODES ONLY CONSIDERED

FIGURE 4.32

FIGURE 4.33
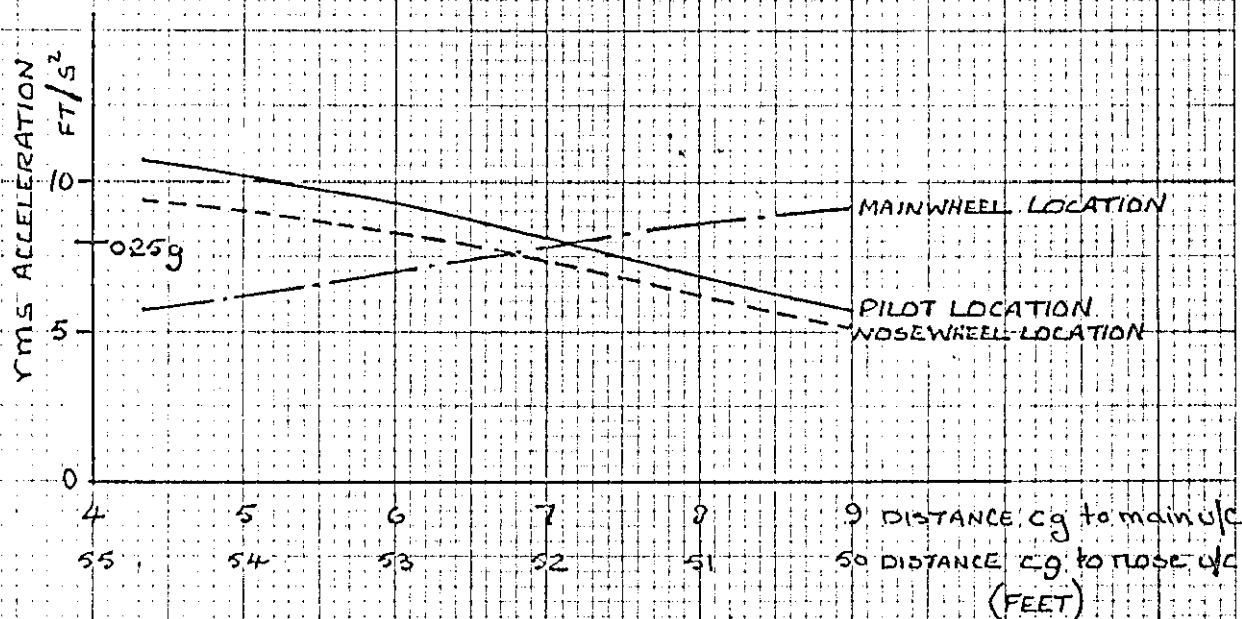


VARIATION OF RESPONSE WITH UNDERCARRIAGE
POSITION FOR SAME LINEAR UNDERCARRIAGES

RIGID BODY MODES ONLY CONSIDERED.

PARAMETERS AS APPENDIX D

FIGURE 4.34
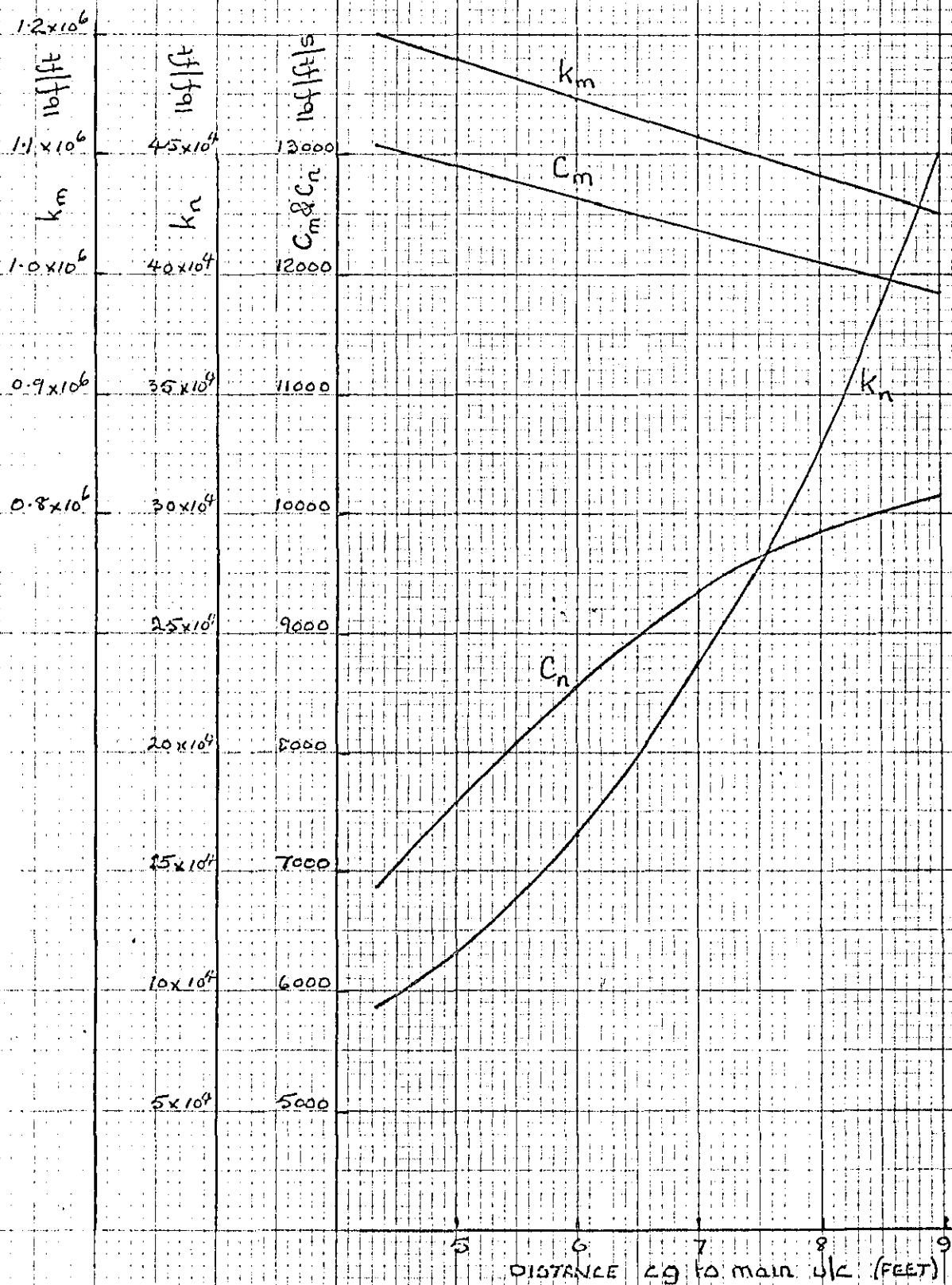
VARIATION OF OLEO PARAMETERS FOR SAME
NON-LINEAR UNDERCARRIAGES

FIGURE 4.35
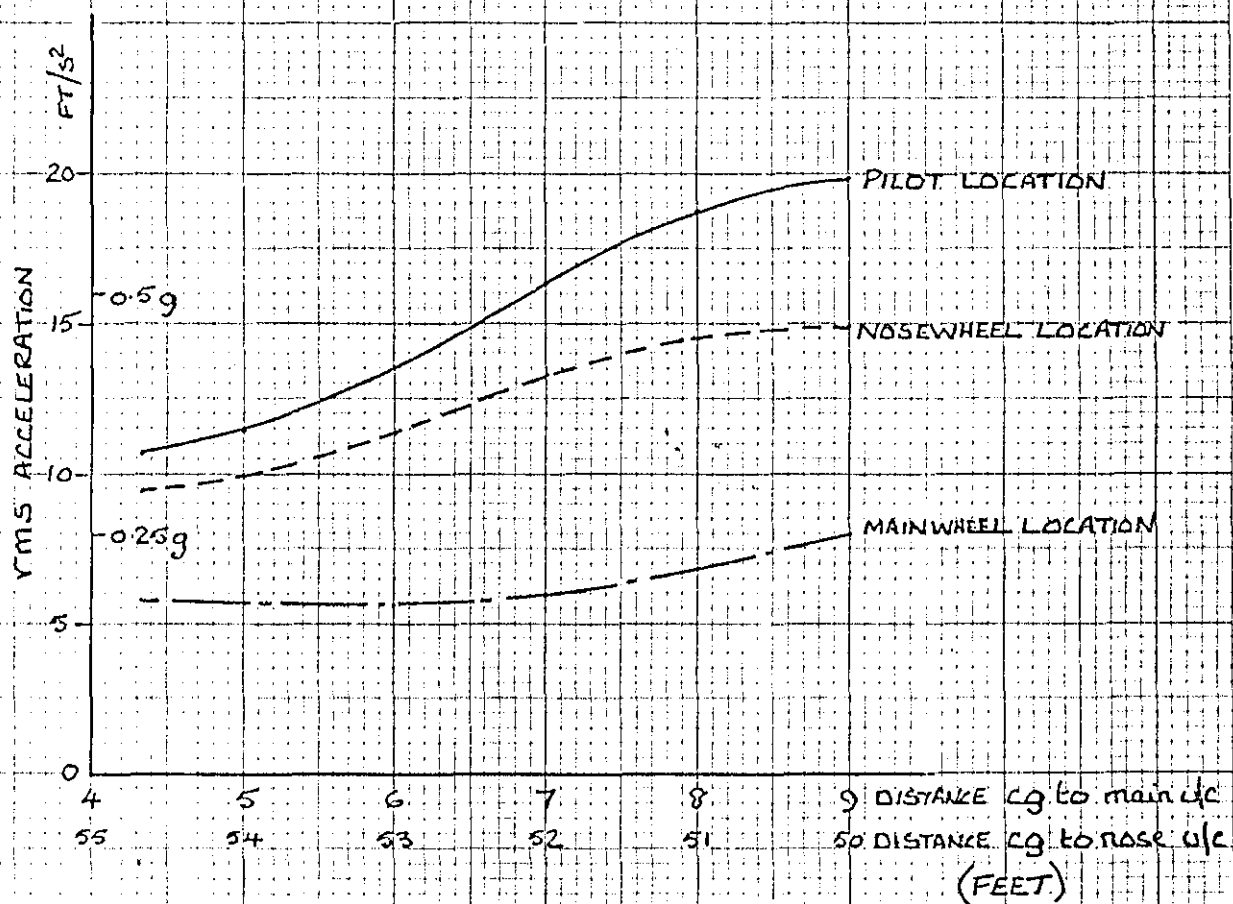


VARIATION OF RESPONSE WITH UNDERCARRIAGE
POSITION FOR SAME NON-LINEAR UNDERCARRIAGES

RIGID BODY MODES ONLY CONSIDERED

OLEO PARAMETERS AS FIGURE 4.34 OTHER PARAMETERS
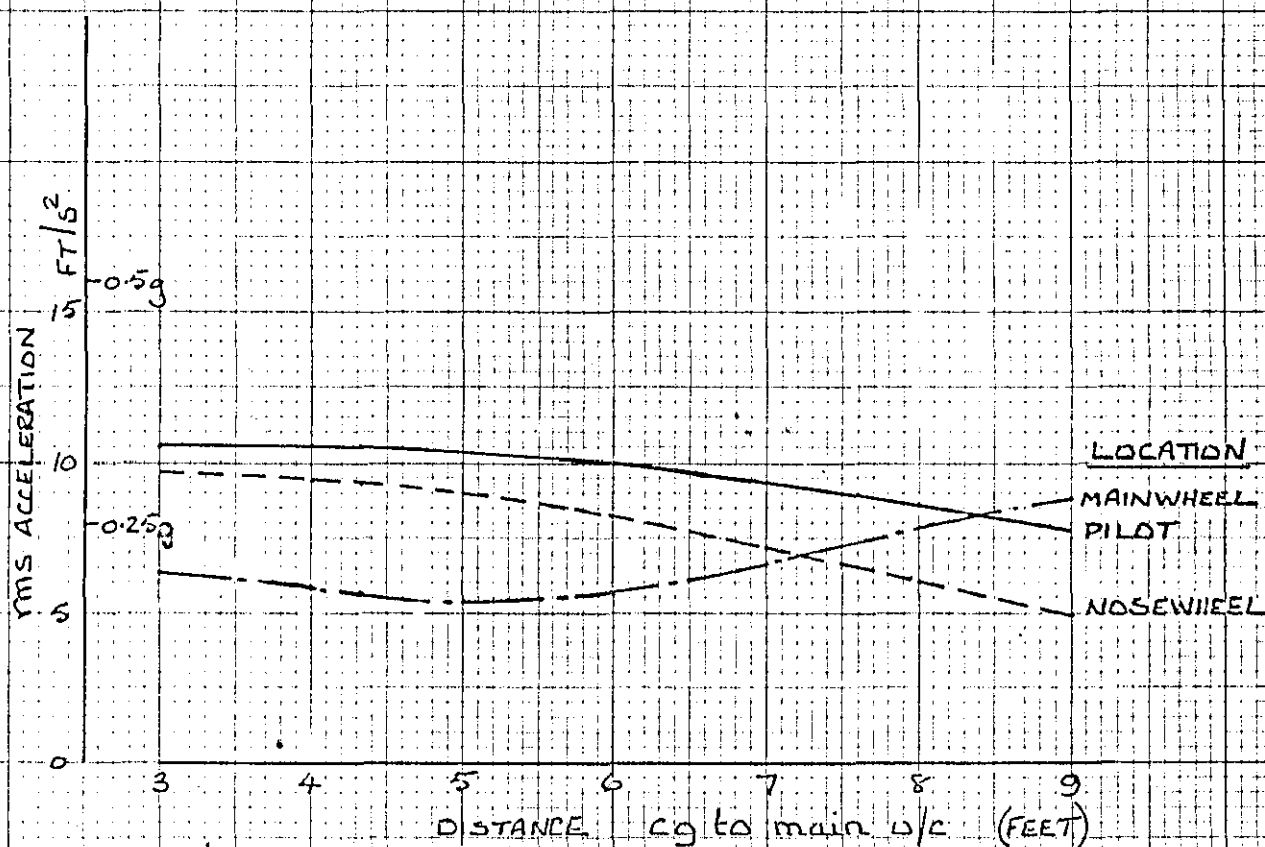
AS APPENDIX J

FIGURE 4.36

VARIATION OF RESPONSE WITH UNDERCARRIAGE
POSITION FOR SAME NATURAL FREQUENCIES

RIGID BODY MODES ONLY CONSIDERED

STARTING PARAMETERS FOR OLEOS AND TYRES (AT 4.33 FEET) AS
APPENDIX D

AIRCRAFT AND RUNWAY PARAMETERS AS APPENDIX D

FIGURE 4.37
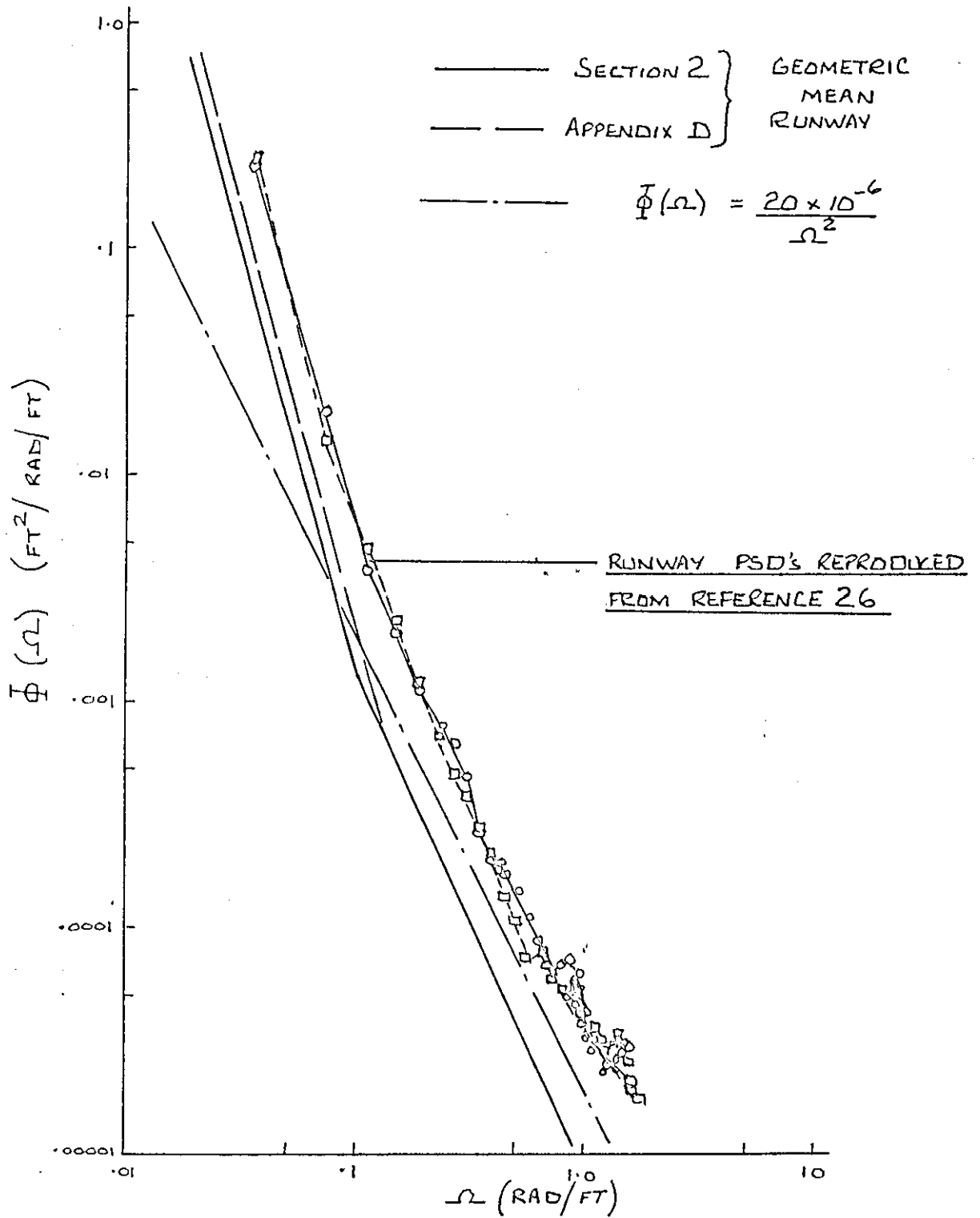
POWER SPECTRAL DENSITY FUNCTIONS

FIGURE 4.38
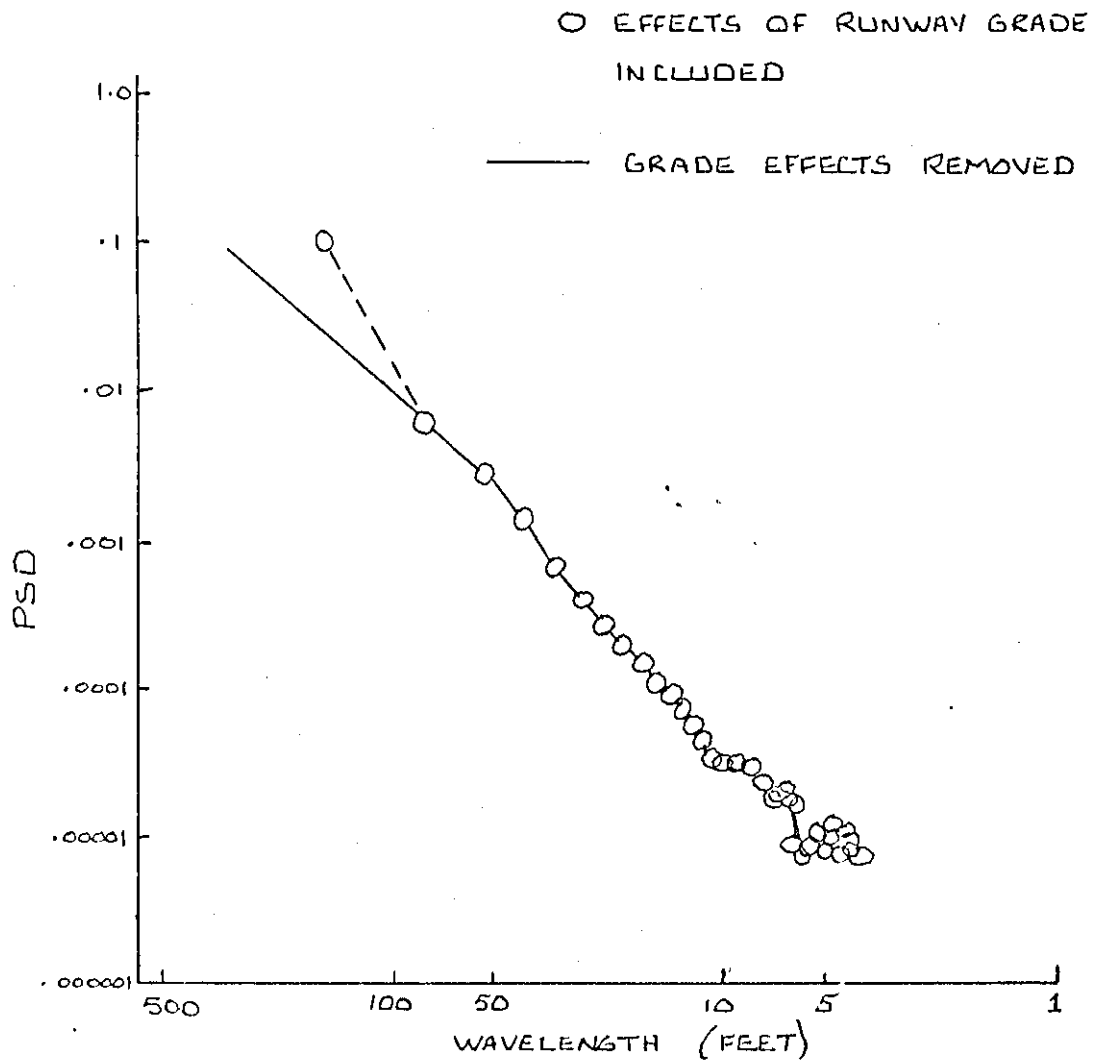
EFFECTS OF RUNWAY GRADE ON COMPUTED

ROUGHNESS SPECTRUM

(REPRODUCED FROM REFERENCE 4)

# SECTION 5

## OPTIMISATION STUDIES

### 5.1 Optimisation Techniques

It is not the object of this thesis to select a best method of optimisation for use with the aircraft taxiing problem, and no attempt whatsoever has been made to do this. The selection of such a method would be an optimisationproblem in itself, depending on many variables pertaining to the type of problem. Hence, a lengthy discussion of the various optimisation techniques would be out of place here. However, a brief summary of some of the basic optimisation methods may be advantageous.

If a system is required to fulfil a set of requirements it may be said to be optimum if it performs as well as, or better than, any other system which satisfies the requirements. If the performance can be expressed as a mathematical function of a number of variables, then optimisation may be defined as the search for the maximum or minimum value of the function. If the values of some or all of the variables are limited by constraints the optimisation process is said to be constrained; otherwise it is unconstrained. It will be assumed in this summary that the optimum value required is a minimum value. Methods of dealing with constraints will not be discussed since the only constraints likely to be met in this thesis are limitations on the maximum and minimum values of the variables, which are quite easily dealt with.

The classical mathematical approach to the optimisation of an algebraic function $f(x_i)$, $i = 1,2,----,n$, is to obtain a set of

stationary points by solving the set of equations

$$\frac{\partial f}{\partial x_i} = 0 \qquad\qquad (5-1)$$

These points may be maxima, minima or saddle points, investigation of the matrix of second derivatives (the Hessian matrix) being required to determine the minima. Although most practical problems cannot be expressed sufficiently simply to allow this form of solution, the method is useful in solving problems which are not too complex, and which have only a few variables. However, more important is the theoretical significance of the results of classical optimization theory in the development of algorithms for solving complex optimisation problems.

The remainder of this summary will be limited to a class of numerical optimisation methods generally known as search techniques. These may be broadly categorized into direct search methods, which require only function evaluation, and descent or gradient methods, which require both function and gradient evaluation. An important problem in this class is that of finding the minimum of a function of a single variable, since many n-dimensional search techniques use a sequence of one-dimensional searches.

5.1.1 Minimum along a line

Two non-sequential search methods are random search and "exhaustive" search. In the former method random values of the independent variable are generated within some pre-selected range, and the function is evaluated at each of these values. This method has the advantage that at each successive evaluation every point on

the line is equally likely to be tested.    In the latter method the

pre-selected range is subdivided into a number of equally spaced

intervals, and the function is evaluated at each point.    Both methods

are very time consuming but may be used to find the minimum of a

function which has several minima.    The minimum may be defined as

the point at which the minimum function value is calculated.

However, for further accuracy, this minimum point may be used to

locate a smaller interval over which the same, or a different,

minimization procedure may be used to establish a more accurate

value.
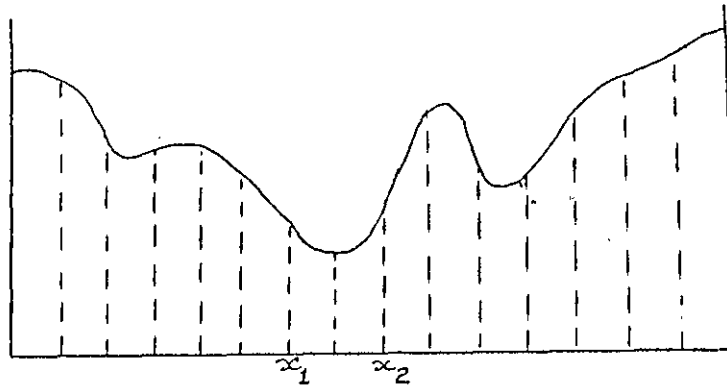


Fig. 5(i)

Figure 5(i) shows the results of an "exhaustive" search.

It will be seen that the values $x_1$ and $x_2$ bracket only one minimum

value, in this case the absolute minimum.    The curve between $x_1$ and

$x_2$ is said to be unimodal.    Several methods have been developed

to find the minimum value of such a function.    One of the simplest

of these is equal interval search.    Any number of intervals may

be chosen but Kiefer (ref. 48) has shown that the 3-point (i.e. 4

equal intervals) search is the most economical in terms of number

of function evaluations to reach a given interval of uncertainty.

The function is evaluated at $\frac{1}{4}$, $\frac{1}{2}$ and $\frac{3}{4}$ of the interval from $x_1$ to $x_2$ (figure 5(i)). Then half of the original interval is retained (i.e. the two adjacent segments containing at their centre the value of x at which the function is smallest) and the process is repeated. Part of the economy of this method is that the two extreme and the centre function values are always retained from the previous iteration, and hence after the first iteration only two function evaluations are required each time. Thus, after m iterations from figure 5(i), the minimum will be located to within an interval of uncertainty of $(\frac{1}{2})^m.(x_2 - x_1)$, and $(2m + 3)$ function evaluations will be required.

Although it might appear that rejecting half the previous interval with each iteration is the best which could be obtained this is not the case, and the more efficient methods use non-equal interval search. One very efficient method is based on Fibonacci numbers, defined by

$$F_o = F_1 = 1$$
$$F_i = F_{i-1} + F_{i-2}, \quad i \geqslant 2$$

The first few Fibonacci numbers are 1, 1, 2, 3, 5, 8, 13, 21, 34, 55, 89, 144 ------. The method is based on using a step length of

$$\triangle_{i+2} = \frac{L_{i+1}.F_{n-2-i}}{F_{n-1}}$$

measured from the end of the previous interval. It can be shown that if the original interval is of length $L_1$, then starting with $F_n$ the final interval of uncertainty will be

$$L_n = L_1\left(\frac{F_o}{F_n}\right) = L_1 . \frac{1}{F_n}$$

and this would require only n function evaluations. For example, in order to reduce the interval of uncertainty to less than 3%, 8 Fibonacci search steps are required, since $\dfrac{1}{F_8} = \dfrac{1}{34} < 3\%$. A very good explanation and example of this method is given in reference 49

The minimum of a unimodal function may also be found by assuming the function to have a simple algebraic form over the desired range, the simplest assumption being a quadratic polynomial. As an example, the function may be evaluated at three points, a quadratic polynomial fitted to it, and the minimum of the polynomial found. This point then replaces one of the initial points, and the procedure is repeated until a selected measure of accuracy is reached. An algorithm using this method has been described by Powell (ref. 50). Cubic interpolation may also be used, a notable author on this method being Davidson (ref. 51), who has produced interpolation equations using function and gradient evaluations.

## 5.1.2 Direct search methods

The great problem with the simpler search methods is that as the number of variables (or dimensions) increases, the number of function evaluations required increases enormously if the same degree of accuracy is required. Thus, a random search method can be used in several dimensions, random values of all variables being generated, or a method equivalent to the one-dimensional "exhaustive" search method may be used, now called grid search. However, if say 10 function evaluations were used for the one-dimensional case, then for the same degree of uncertainty $10^n$ function evaluations would be

required for n dimensions.    Figures 4.22 and 4.23 are in effect
examples of 2-dimensional grid search.

A way of cutting down the number of function evaluations
required is to use a univariate search method, in which only one
variable at a time is changed.    Usually the variables are changed
one by one in some sequence, the function being minimized along
each of the co-ordinate directions, and the process repeated until
some convergence criterion is reached.    This procedure is illustrated
for the 2-dimensional case in figure 5(ii).
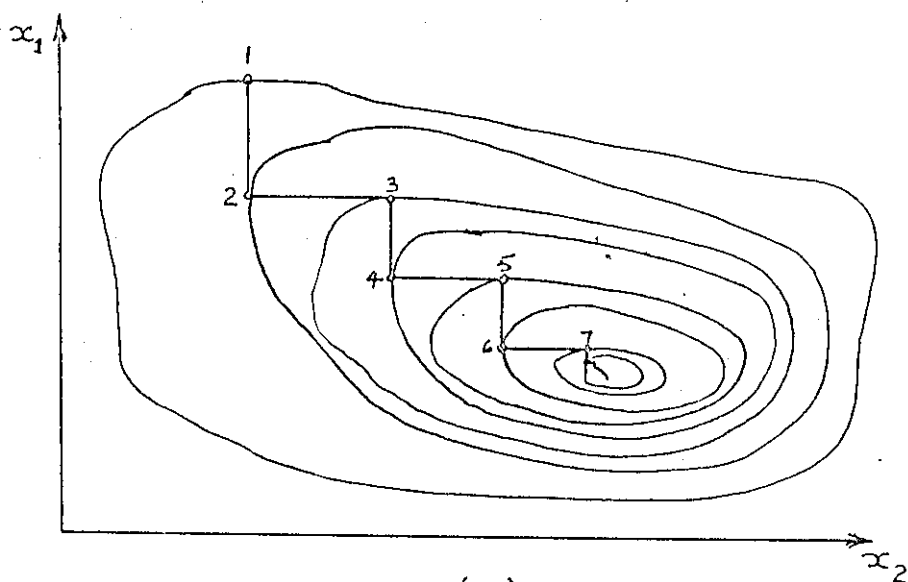


Fig. 5(ii)

It will be noted in the figure that alternate points in
the iteration (e.g.1,3; 2,4; 3,5 etc) define lines which lie in the
general direction of the minimum.    Indeed, if the function were a
quadratic the defined lines would pass through the minimum.    This
property leads to a class of methods known as "pattern move".
Exploratory moves are made from a starting point to explore the
local behaviour of the objective function.    The moves are not
necessarily intended to minimise the function along the co-ordinate

directions, so that if f(i) is the value of the function at the

ith point in figure 5(ii), and point 1 is the starting point, then

if $f(3) < f(2) < f(1)$, the pattern move can be made along the

direction of a line through points 1 and 3.   A simple method using

this principle has been developed by Hooke and Jeeves (ref. 52), a

better development of this being that of Rosenbrock (ref.33).   The

methods using this principle vary in general in the degree to which

the exploratory and pattern directions are explored.   Rosenbrock's

method has been shown in general to be very efficient for practical

problems, particularly in locating an early approximation to the

minimum.

The methods so far described have used mutually orthogonal

directions in each cycle of searches.   However, this does not

necessarily produce the quickest convergence.   Powell's method

(ref. 50) uses conjugate directions.   If a quadratic function to

be minimised is

$$f(\underline{x}) = \underline{x}^T A \underline{x} + \underline{b}^T \underline{x} + c \qquad (5-2)$$

then the directions $\underline{v}$ and $\underline{w}$ are said to be conjugate directions if

$$\underline{v}^T A \underline{w} = 0 \qquad (5-3)$$

The method may be described simply as follows:  The function is

first minimised in each of the co-ordinate directions, and then in

the associated pattern direction.   One of the co-ordinate directions is

discarded in favour of the pattern direction for all the following

iterations, since the pattern direction is likely to be a better

direction than the discarded co-ordinate direction.   Each time a

pattern direction has been generated it replaces one of the

co-ordinate directions, until at the $(n+1)^{th}$ iteration, for an

n-dimensional problem, n conjugate directions are used.   This
method produces quadratic convergence, that is it will minimise
a quadratic function in a finite number of steps - in fact the
number of variables, so that the starting point for the (n+1)st
iteration is the minimum point.

It is possible, with a non-quadratic function, for the
set of search directions to become dependent, and hence to scan
only a sub-space of the n-dimensional space.   Powell has added a
modification, extended by Zangwill (ref. 55), which ensures a
reasonable rate of convergence even when the initial approximation
is quite poor.   In fact, practical functions are usually a
reasonable approximation to a quadratic in the region of the minimum,
and Powell's method is probably one of the best of the current
search techniques not requiring gradients.

5.1.3  Gradient methods

The direct search methods have only used information
about the value of the function at various points in seeking search
directions.   If now information about the gradient of the function
is obtainable this leads to a further class of methods of choosing
search directions, potentially more efficient, than the previous
methods.   The gradient vector, $\nabla F$, of a function $F(\underline{x})$ is defined
as

$$\nabla F = \underline{g} = \left( \frac{\partial F}{\partial x_1}, \frac{\partial F}{\partial x_2}, -----, \frac{\partial F}{\partial x_n} \right) \qquad (5-4)$$

This vector lies in the direction of greatest rate of increase of
the function and has that rate of increase as its magnitude.   Thus
a move in the direction $-\nabla F$ is a move in the direction of steepest

descent, and no vector can give a greater local reduction in F.

If the function to be minimised is not readily differentiable a

discrete approximation to the gradient may be used.    The method

of steepest descent was first introduced by Cauchy in 1847, many

authors having used it since then.

The basic method uses the step

$$\underline{x}_{q+1} = \underline{x}_q - \alpha \nabla F \qquad\qquad (5 - 5)$$

where $\underline{x}_q$ is the old value of $\underline{x}$, $\underline{x}_{q+1}$ is the new value of $\underline{x}$, and $\alpha$

is a real number.    The values of $\underline{x}_{q+1}$ may be found either by

function evaluations at intervals along the direction $\nabla F$ until

there is no further decrease in F, or by minimisation of the function

along the direction $\nabla F$ using one of the previously described methods.

Although this method gives, from any position, the greatest local

decrease in F, there are better directions which may be used, and

the method is in fact relatively inefficient, particularly so when

the minimum is approached along a fairly level floor of a steep

valley, the steps then tending to oscillate from side to side of the

valley.

A further form of step which can be used is

$$\underline{x}_{q+1} = \underline{x}_q - \alpha G \nabla F \qquad\qquad (5 - 6)$$

where G is an n x n matrix.    Several forms for G have been

considered, but the potentially most efficient form of this equation

is

$$\underline{x}_{q+1} = \underline{x}_q - H^{-1} \nabla F \qquad\qquad (5 - 7)$$

where H is the Hessian matrix.    This equation is the n-dimensional

equivalent of the well known one-dimensional Newton approximation,

where if $x_q$ is an approximation to a minimum, a better approximation,

$x_{q+1}$, is given by

$$x_{q+1} = x_q - \frac{f^1(x_q)}{f^{11}(x_q)}$$

The method using equation (5-7) produces quadratic convergence, and therefore generally has a very good rate of convergence near the minimum for a practical problem. However, the method can have considerable disadvantages. It may be difficult or even impossible to compute the Hessian matrix; even for a simple function the elements of H may be extremely time consuming to compute. Furthermore, even if H can be found, computation of the vector $-H^{-1}\nabla F$ is a major computational problem for functions of many dimensions. Thus the method is impractical for large or complicated problems.

To overcome much of this complication a method has been presented by Davidon (ref. 51) and developed by Fletcher and Powell (ref. 57) which uses an approximation to the Hessian matrix. This method is variously described as a quasi-Newton method, a conjugate directions method, or a variable metric method. Basically equation (5-7) is used, but for the first step H is set to any positive definite symmetric matrix; it is common to set H = the identity matrix, I, so that the first step is in the direction of steepest descent. The function is minimised along this direction, and information gained in this iteration is used to update the matrix H for use in the next iteration. If the function to be minimised is quadratic and unimodal, then for an n-dimensional problem the Hessian matrix is constructed, and the minimum reached, after n iterations. If the function is more complicated then the

Fletcher Powell method generates an approximation to the Hessian

in the region of the minimum.  The simplification of this method,

over that using an actual Hessian, is that the matrix H is updated

using first-order information, this being achieved by calculation

of the gradient at two different points.

## 5.1.4  Scaling of variables

The convergence of most minimisation methods can be

improved by scaling the variables.  The eccentricity of the function

can be greatly influenced by the choice of scales.  Consider the

function

$$F = 144x_1^2 + 4x_2^2 - 8x_1x_2 \qquad (5-8)$$

A new form of this function may be derived using

$$G(x_1,x_2) = F\left(\frac{x_1}{12}, \frac{x_2}{2}\right) \qquad (5-9)$$

so that

$$G = x_1^2 + x_2^2 - \frac{1}{3}x_1x_2 \qquad (5-10)$$

Function contours of F and G are shown in figure 5(iii) (a) and (b),

where it will be seen that F is much more eccentric than G, so that

the gradient vector of F does not point nearly so close to the

minimum as that of G, and hence F would be harder to minimize.

The object of scaling is to make the gradients in each

direction of the same order of magnitude   It will be seen that

some eccentricity still exists in figure 5(iii)(b).  If there had

been no $x_1x_2$ term, then the contours in this figure would have

been circles, and the gradient vector would point to the minimum.

$$F = 144\,x_1^2 + 4\,x_2^2 - 8\,x_1 x_2$$

(a)

$$G = x_1^2 + x_2^2 - \tfrac{1}{3}x_1 x_2$$

(b)
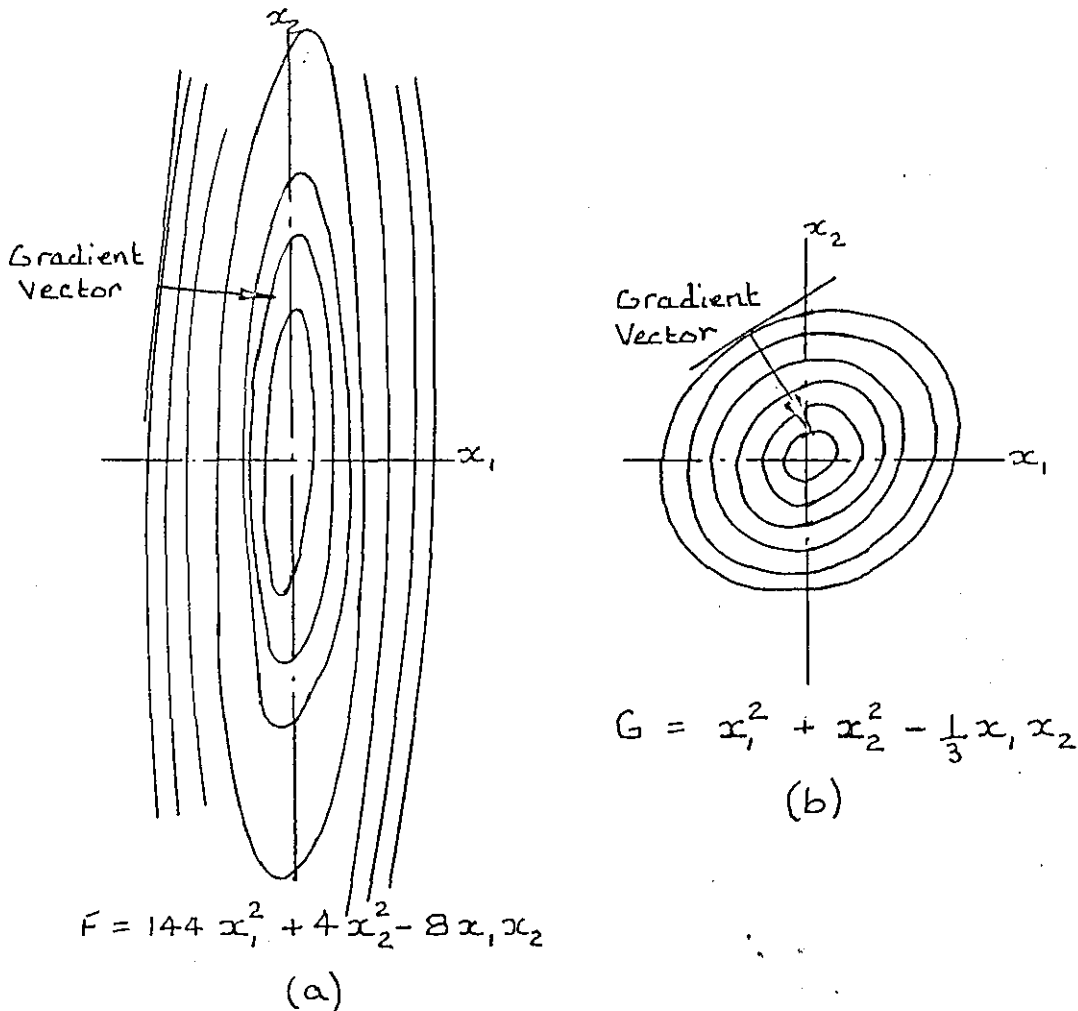
Fig. 5(iii)

On the other hand, if the coefficient of the $x_1 x_2$ term had been numerically larger, the eccentricity would have been greater. The technique of making the coefficients of the squared terms equal is not, in general, optimal scaling, even in quadratic problems, beyond the 2-dimensional case. However, considerable benefit can often be gained by this simple process.

In non-quadratic problems one method is to use a diagonal scaling matrix, whose elements are approximations to the diagonal of the Hessian matrix. The Fletcher-Powell method might be thought of in effect as a steepest descent method using a scaling matrix.

## 5.2 Method used for optimisation studies

The optimisation studies which will be described are based on a method of steepest descent. Whilst it is appreciated that this is not the most efficient method of optimisation, it has certain advantages for these studies. Firstly the algorithm chosen was easily available, and is straightforward and easy to use. Secondly it is relatively economical in terms of computer space. This latter point was quite important in these studies, since the response evaluations are quite space consuming and the computer being used was not large (Elliott 4120, 32K).

The optimisation procedure is based on a procedure STEEP 2 obtained from the mathematics department of the Royal Air Force College, Cranwell. This procedure had in turn been based on procedures STEEP 1 and STEEP 2, presented in Algorithms 203 to 205 of the Collected Algorithms of CACM. As the optimisation studies progressed it was found that certain modifications were necessary in order to improve the efficiency of the procedure for this particular application. The final version of procedure STEEP 2 is shown in Appendix H. The modifications which have been made are underlined and will be described in due course.

STEEP 2 contains two sub-routines, procedure ATIVE, for computing the partial derivatives, and procedure STEP, for computing the components of an array XSTEP $[1:NV]$, which is a new approximation of XMIN $[1:NV]$, an array of the values of the variables at the minimum value of the function, FMIN. LB(i) and UB(i) are lower and upper bounds of the independent variables,

NV is the number of variables, and XS(i) is the starting value for
XMIN(i).   FUNK(x) is the function to be minimised, in the form
of a real procedure, and hence any function evaluation program
used for optimisation, eg program RESPONSE 12, had to be written in
the form of a real procedure for use with STEEP 2.

An estimate for the derivative is

$$\frac{f(x + dx) - f(x - dx)}{2dx} \qquad\qquad (5 - 11)$$

DX was a real number in the original procedure, and hence all the
variables were increased and decreased by the same amount in the
calculation of derivatives.   It was very soon decided that, since
the values, and the derivatives, of the variables could be widely
varying in order, DX should be an array with different values for
each variable.   It was found convenient to make the starting
values of DX a direct proportion of the starting values of the
variables  XS(i).   If the derivative is very large the program
reduces the value of DX;   if the derivative is very small the
program increases the value of DX.   A maximum allowable value of
DX, DXMAX, is stipulated in the data.   DXMAX was also changed from
a real number to an array.

The significance of RELAX is to include a proportion of
the previous partial derivative in current iterations.   Thus if
RELAX = 0.5 the effect is that the new partial derivative becomes
half of the new estimate for the derivative plus half of the
previous partial derivative.

A problem encountered early in the optimisation studies
was that when the minimum occurred at an upper or lower bound the

program would not terminate, but kept oscillating at the boundary. The statements underlined with dashed lines in Appendix H were inserted to overcome this problem, the longest statement replacing FMIN: = FUNK(XMIN). This amendment had been suggested in a later comment on the Algorithm in CACM by someone who had had the same trouble.

The computation of a new estimate of the value of the ith variable at the minimum is done by

$$XSTEP(i) = XMIN(i) - Px\alpha x \ XMIN(i)$$

where $\alpha$ is the new partial derivative, and

P is a weighting factor.

P is put equal to 1 at the beginning of the program and tends to 0 at the minimum. In the original program, after a decrease of the function the step was accepted and P was multiplied by 1.5, whilst after an increase P was divided by 2. PMAX replaces P when P becomes greater than PMAX, and when P becomes less than EPS the optimisation is terminated, the choice of value of EPS therefore being a measure of the accuracy required. PMAX was set to 0.5 and EPS to $10^{-4}$ in early studies. The above values, particularly that of PMAX, were found to lead to very slow convergence to the minimum in some cases, as will be discussed later. The program was amended, the values 1.5 and 2 being replaced by PMULT and PDIV so that the weighting factor could be varied at different rates, and print statements for P were inserted so that the progress of a computer run could be easily traced.

In certain stages of the program XMIN (i) is replaced by a value ZETA if $XMIN(i) < ZETA$, and FMIN is replaced by a value

PSI if FMIN $<$ PSI. These are safeguards to prevent denominators becoming too small, and values of ZETA = PSI = 1 were used throughout these studies, which in fact meant that ZETA and PSI were never used in these minimisations since XMIN(i) and FMIN were always much greater than 1.

## 5.3. Optimisation on actual function

In the early optimisation studies the rms value of the response acceleration at the mainwheel location was minimised. These studies used the earlier version of the main response program, using equal interval integration steps, in conjunction with the early version of procedure STEEP 2. Whilst the minimum values shown on figures 4.22 and 4.29 were verified, optimising on one variable at a time, the computer time to optimise on more than one variable was prohibitive, and it was also at this time that the necessity of using the more sophisticated integration procedure was realised, particularly for low stiffness and high damping. However, during these early studies the step lengths for finding the partial derivations in the integration procedure were changed from real numbers to matrices, so that the step for each variable could be different, and the amendment to overcome cycling at the boundary was made.

All further optimisation studies minimise the sum of the rms values of response acceleration at the mainwheel and pilot locations. This is a simple attempt to decrease the general level of response along the fuselage and should prevent the response being minimised at one point at the expense of another. Figure 5.1 shows the sum of the mainwheel and pilot location responses for various values of main and nose oleo stiffnesses, keeping the oleo damping constant at the values in Appendix D. This figure is in fact the sum of the lower boundaries of figures 4.22 and 4.23. The minimum response should occur when the main and nose oleo stiffnesses are at their lower bounds.

The optimisation program BDARBH60 is shown in Appendix J. This program uses the main response program written in the form of a real procedure, in conjunction with the minimisation procedure STEEP2, to minimise the response for variable main and nose oleo stiffnesses, $K_1$ and $K_2$. Programs basically similar to this, but varying only $K_1$ or $K_2$, were used to minimise the response, the computer times required being 23 minutes for $K_1$ and 28 minutes for $K_2$. The corresponding values on figure 5.1 were verified using these programs. However, program BDARBH60, optimising on both $K_1$ and $K_2$, was found to use a prohibitive amount of computer time, the minimum not having been reached after 90 minutes, during which time 33 function evaluations had been made. Minimisation using more than the two variables would obviously be out of the question with this program, as the number of function evaluations required would increase substantially as the number of variables increased.

Clearly, modification was required before further computations could be made, the two possibilities for investigation being the computer time required for each function evaluation, and the number of function evaluations required to reach a minimum.

## 5.4 Optimisation on approximation to function

There was little possibility of reducing the computer
time required to perform an actual function evaluation.    The
computations being made at this stage only considered rigid body
modes, and the varying step integration method was required for
consistancy between results.   Hence the possibility was investigated
of using an approximation to the response function which would be
consistent for all values of the function, i.e. which would decrease
as the function decreased.
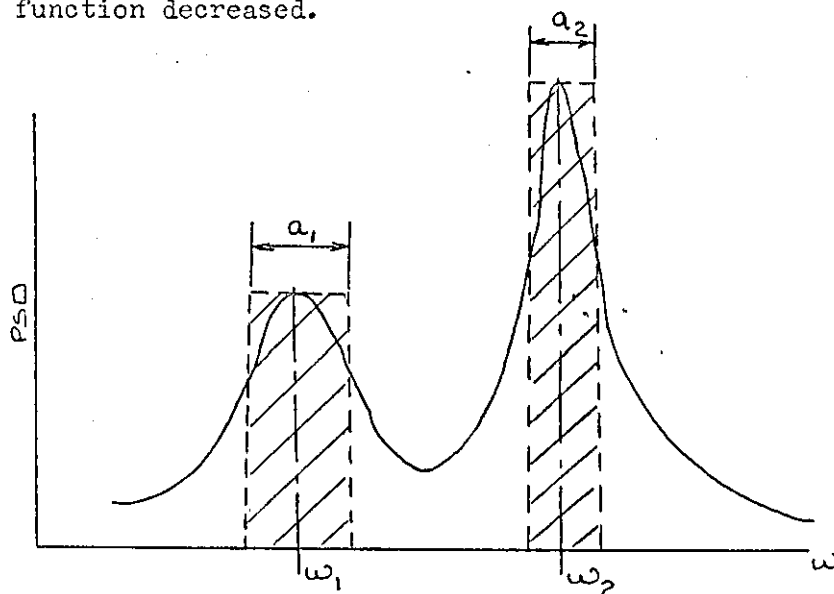
Fig.5(iv)

, One of the simplest, and most promising, possibilities
investigated is shown in figure 5(iv).   The sum of the peak heights
times the bandwidths, i.e. the shaded areas, on the curve of
response PSD v. frequency, is taken as a measure of the area under
the curve.   Thus, the PSD need only be calculated at each peak,
whose frequencies are given by the eigenvalues (i.e. two only for a
rigid aircraft), instead of at the very many points required by the
full integration routine.   Thus, if the ith eigenvalue is given by

$$\lambda_i = -a_i \pm i\omega_i \qquad\qquad (5-12)$$

and the response PSD at $\omega_i$ is $PSDM_i$ at the mainwheels and $PSDP_i$ at the pilot location, then the approximations to the rms values of response acceleration at the mainwheel and pilot locations respectively, $\sigma_m$ and $\sigma_p$, are

$$\sigma_m = \sqrt{\sum a_i PSDM_i} \qquad\qquad (5-13)$$

and $\sigma_p = \sqrt{\sum a_i PSDP_i} \qquad\qquad (5-14)$

Values for these approximations were calculated for a very wide range of stiffnesses, damping, and taxiing velocities, for rigid body modes only, using values of eigenvalues and PSD calculated in the response studies. The approximations are shown in figure 5.2 plotted against the corresponding actual computed responses, the values for mainwheel and pilot locations all being plotted on the same graph. In fact most of the lower values are mainwheel location response and most of the higher values are pilot location response. The points show that a very good correlation exists between the approximate and the actual values in general, but two distinct sets of points are seen to be diverging from the main curve. The lower set of points are in fact mainwheel location responses, and the upper set of points pilot location responses, for the same set of conditions.

Investigation of these points showed that they were all associated with high nose oleo damping; the higher the damping the further away from the curve was the point. The line of six points is in fact for the highest nose oleo damping (14000 lbf/ft/s)

with 6 values of main oleo damping ranging from 6500 lbf/ft/s to
26000 lbf/ft/s.   As the damping increased the frequencies of the
peaks came closer together, and the bandwidths increased, so that
at the higher values of damping equations (5-13) and (5-14) were
in effect including parts of the same area in both peaks.   An
increase in nose oleo damping had a much greater effect than the
main oleo damping, increasing both heave and pitch mode peak
bandwidths by a large amount.   Also, of course, for high damping,
the value of a from equation (5-12) no longer gives the bandwidth.

It was found after some trial that for the case of rigid
body modes only, that is the number of eigenvalues = 2(the eigenvalues
for the mainwheel and nosewheel movements are discarded since they
do not contribute to the response), the following modification to
equations (5-13) and (5-14) gave good correlation with actual
responses for most values of stiffness and damping.   Referring to
equation (5-12) and figure 5(iv),

$$\text{if } (a_1 + a_2) < 0.75(\omega_2 - \omega_1)$$

then equations (5-13) and (5-14) are used.   However,

$$\text{if } (a_1 + a_2) > 0.75(\omega_2 - \omega_1)$$

then equations (5-13) and (5-14) become

$$\sigma_m = \sqrt{\sum a_i \text{PSDM}_i} \cdot \sqrt{\frac{0.75(\omega_2 - \omega_1)}{a_1 + a_2}} \qquad (5-15)$$

$$\text{and} \quad \sigma_p = \sqrt{\sum a_i \text{PSDP}_i} \cdot \sqrt{\frac{0.75(\omega_2 - \omega_1)}{a_1 + a_2}} \qquad (5-16)$$

For a combination of very low stiffness (which has the
effect of increasing the damping) and very high damping even this
modification does not produce good correlation with actual responses,

since at these values the heave and pitch frequencies are almost equal for the aircraft under consideration, and even reverse position for some extreme values. Hence there is in effect only one peak, as shown in figure 4.32. Since it is not practical to produce an approximation which will give correlation with actual responses for all values of stiffness and damping, a failure criterion has been developed which ends the program if the peaks on the response PSD curve come so close together that equations (5-15) and (5-16) are in danger of giving values which are not proportional to the actual response. Thus, the approximation method fails if

$$\left| 0.75(\omega_2 - \omega_1) \right| < 0.2$$
$$\text{or if} \left| 0.75(\omega_2 - \omega_1) \right| < 0.033\omega_2$$
$$\text{or if} \left| 0.75(\omega_2 - \omega_1) \right| < 0.05(a_1 + a_2)$$

A real procedure FUNK (X) incorporating the above approximations to the response, and the failure criterion, is included in the optimisation program shown in Appendix K. The procedure is written to include any number of modes, but equations (5-15) and (5-16) and the failure criterion are incorporated in a conditional statement, only being used if the number of peaks being investigated is 2. However, it is anticipated that the procedure would only generally be used with rigid body heave and pitch, since it is a method of giving a quick estimate of the value of the parameters required for minimum response.

An initial program incorporating equations (5-13) and (5-14) was written to minimise the sum of the rms values of response acceleration at the mainwheel and pilot locations (i.e. RMSM + RMSP), varying only the main oleo stiffness, $K_1$. The minimum was found at

a value of $K_1 = 0.6 \times 10^6$ lbf/ft in only 4 minutes 54 seconds,
making 10 function evaluations.   However, when the program was
modified to vary both $K_1$ and $K_2$ the minimum had not been reached
after 53 minutes, during which time 143 function evaluations were
made (c.f. 33 function evaluations in 90 minutes for the actual
response function).

At this time the procedure STEEP2 was still using 1.5
and 2 as the multiplier and divider respectively of P, and values
of PMAX = 0.5 and EPS = $10^{-4}$ were being used.   Investigation of
the steps in the optimisation print-out showed that the value of
$K_2$ was very quickly reaching its lower bound (decreasing $K_2$ gave
the steepest slope) and the value of $K_1$ was then being decreased
very slowly along the boundary, since the value of PMAX would not
allow large steps to be taken.   Furthermore, when a minimum was
reached, the value of P had to be reduced below $10^{-4}$ before the
computations were terminated.   The value of PMAX in the data was
therefore increased to 100 and that of EPS to $10^{-1}$, and the same
program then produced a minimum at $K_1 = 0.6 \times 10^6$ lbf/ft and $K_2 =$
46800 lbf/ft in 16 minutes 5 seconds, making 43 function evaluations.

At this stage the procedure STEEP2 was modified by
replacing the values of 1.5 and 2 by PMULT and PDIV so that
different values could be used.   Increasing the values would mean
that the value of step length would be increased quicker after a
successful step and decreased quicker after an unsuccessful step, so
that when the minimum was reached the value of P would fall below
that of EPS in less iterations.   For all further optimisation

programs values of PMULT = 2, PDIV = 3, PMAX = 100, and EPS = $10^{-1}$ were used. Using these values the minimum at $K_1$ = 0.6 x $10^6$ lbf/ft and $K_2$ = 46800 lbf/ft was reached in 13 minutes 11 seconds, and 35 function evaluations were made.

Computer programs were written, incorporating all the above modifications, similar to that shown in Appendix K, but varying firstly $K_1$ and $K_2$, secondly $C_1$ and $C_2$, and thirdly $K_1$, $K_2$, $C_1$, and $C_2$. The results of optimisations using these programs are shown in table 5(i).

| Parameters varied | Computer time | Result |
|---|---|---|
| $K_1$, $K_2$ | 12m 9s | $K_1$ = 600000 lbf/ft <br> $K_2$ = 46800 lbf/ft <br> FUNK = 5.53 |
| $C_1$, $C_2$ | 10m 12s | $C_1$ = 26160 lbf/ft/s <br> $C_2$ = 13752 lbf/ft/s <br> FUNK = 6.65 |
| $K_1$,$K_2$,$C_1$,$C_2$ | 24m 49s | Response approximation failed after 64 function evaluations at <br> $K_1$ = 600000 lbf/ft <br> $K_2$ = 46800 lbf/ft <br> $C_1$ = 26160 lbf/ft/s <br> $C_2$ = 13752 lbf/ft/s <br> FUNK = 2.046 |

Table 5(i)

It should be noted that all the optimisation computer runs were started at the values in Appendix D, i.e. $K_1$ = 1.2 x $10^6$,

$K_2 = 93600$, $C_1 = 13080$, $C_2 = 6876$, and that upper and lower bounds were placed on these parameters of twice and half these values respectively. No attempt was made to start near to a possible minimum, as would generally be done in practice to cut down the computer time, since a measure of the relative efficiencies of the programs was required. Clearly the last programs are much more efficient in quickly finding optimum values than were the earliest programs using the actual function.

It will be seen that the stiffnesses have gone to the lower bound and the damping to the upper bound in seeking a minimum response. Figure 5.1 shows that for constant $C_1$ and $C_2$, at the values in Appendix D, the values of K to give minimum value of the actual response are indeed at the lower bound. The values of $K_1$ and $K_2$ found by the optimisation routine could now be used in the response program RESPONSE 12, to predict the actual response. However, since for variation of $K_1$ and $K_2$ the response approximation did not fail, the value of FUNK = 5.53 from table 5(i) used in conjunction with figure 5.2 should give an idea of the actual response. Since there is some spread on figure 5.2 the value of actual response corresponding to the approximation of 5.53 lies between 8.8 and 9.8. From figure 5.1 the actual sum of responses at the mainwheel and pilot location is in fact 9.4.

Similarly, figure 5.3, which shows the sum of the mainwheel and pilot location responses for varying $C_1$ and $C_2$, with $K_1$ and $K_2$ keeping the values in Appendix D (i.e. figure 5.3 is the sum of the lower boundaries of the curves in figure 4.29), shows that the values of damping to give minimum response are at the upper bound.

The value of FUNK = 6.65 from the table corresponds approximately

on figure 5.2 with the value of 12.5 from figure 5.3, the slight

error being due to the fact that the values of damping on figure

5.3 are slightly different from the upper bounds in the optimisation

program.

Figures 5.4 and 5.5 show the sum of the mainwheel and

pilot location response from figure 4.27, i.e. $K_1$ and $K_2$ varying,

with $C_1$ = 26000 lbf/ft/s and $C_2$ = 14000 lbf/ft/s, and from figure

4.31, i.e. $C_1$ and $C_2$ varying, with $K_1$ = 0.6 x $10^6$ lbf/ft and

$K_2$ = 46800 lbf/ft respectively. The minimum response does in

fact occur when the stiffnesses take on values at their lower bounds

and the damping takes on values at the upper bounds. Thus, although

the response approximation failed when varying $K_1$, $K_2$, $C_1$ and $C_2$

(see table 5(i)), the program had in fact found the optimum values.

The value of FUNK = 2.046 does not however correspond on figure

5.2 with the actual response value of 7.2 from figures 5.4 and 5.5,

since, as the peaks on the response PSD curve get closer together,

and the failure criterion is approached, the value of 0.75 $(\omega_2 - \omega_1)$

becomes small, and equations (5-15) and (5-16) underestimate the

response by more than the proportion indicated by figure 5.2.

Appendix K shows the optimisation program, OPTIMISATION

ON APPROXIMATE RESPONSE FUNCTION 5. This program is very similar

to the programs used above, including the better response

approximation, the failure criterion, and the better optimisation

procedure, but incorporates equations of the form of equations (4-62)

to (4-64) in order to vary the undercarriage positions whilst keeping

the heave natural frequencies constant.

The program was run, starting with values as Appendix D, and produced a minimum in 5 minutes 2 seconds, performing only 9 function evaluations. However, the minimum occurred with a distance from cg to mainwheel location of 3.91 feet, producing a minimum value of the approximation to the response acceleration of FUNK = 9.74. Figure 5.6, which shows the sum of the mainwheel and pilot locaion responses from figure 4.36, indicates that the minimum value of response should occur when the distance is about $5\frac{1}{2}$ to 6 feet. However, examination of the figure shows that the difference in response between the positions 3.91 feet and 6 feet is only $4\frac{1}{2}\%$, so that although the optimisation appears to be inaccurate when viewed in the context of undercarriage position, it has in fact produced a minimum only $4\frac{1}{2}\%$ higher than the actual minimum, the wide variation in undercarriage position occurring because the aircraft is very insensitive to changes in undercarriage position. Indeed, the variation in response over the whole range investigated is only about $8\frac{1}{2}\%$.

The value of actual response on figure 5.2 corresponding to the value of FUNK = 9.74 has a spread from 15.9 to 17.1, i.e. about $7\frac{1}{2}\%$. In view of this the production of a minimum to within $4\frac{1}{2}\%$ appears to be a very creditable performance. The effort which would be required to produce an approximation which would give a better results would be disproportionately high for the improvement which it is possible to attain. At the best only a very small decrease in response can be obtained for this particular aircraft by moving the undercarriages, and for an aircraft which was more

sensitive to undercarriage position the above method would produce
the positions to minimise the response to the same small percentage
as in this case.    The range of undercarriage positions to produce
values near to this minimum would then of course be smaller than in
this case.

The aircraft under consideration is only insensitive to
the undercarriage position, of course, so long as the optimisation
function being minimised is the sum of the mainwheel and pilot
location rms accelerations.    Reference to figure 4.36 shows that
if the response at only one position were minimised the result would
be much more determinate.    For minimisation of pilot location
acceleration for example the mainwheel should be placed 9 feet
(the upper bound) behind the cg.    However; this would increase the
mainwheel location response.    Thus, whilst the sum of the mainwheel
and pilot location responses varies only very little with
undercarriage position, responses at individual positions on the
aircraft are affected by movement of the undercarriages, and hence
a different weighting function, reflecting the relative importance
at different positions for individual cases,would produce different
results.

FIGURE 5.1
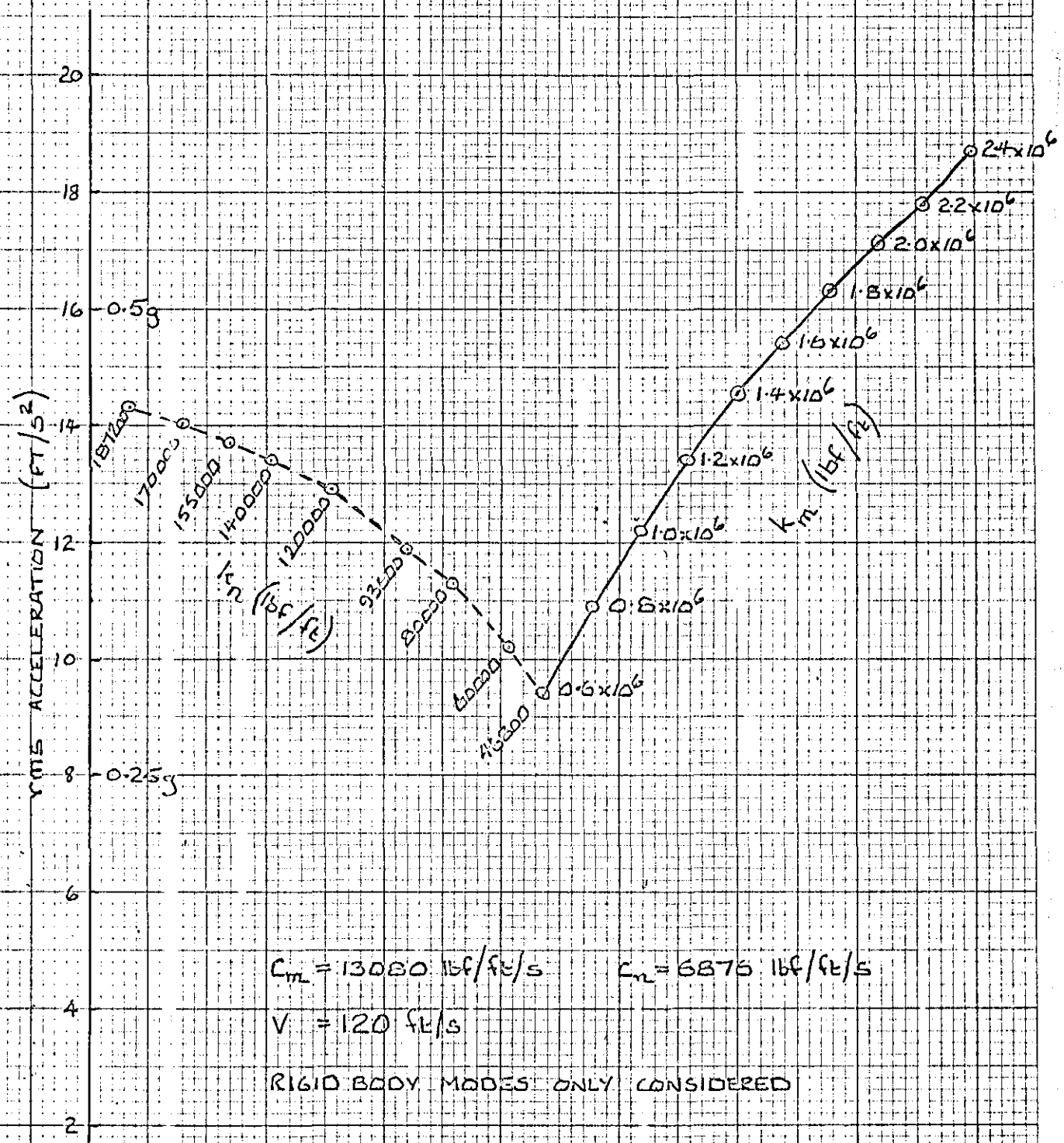


$C_m = 13080 \; lbf/ft/s \qquad C_n = 6876 \; lbf/ft/s$

$V = 120 \; ft/s$

RIGID BODY MODES ONLY CONSIDERED

VARIATION OF SUM OF MAINWHEEL AND PILOT LOCATION

RESPONSES WITH OLEO STIFFNESS
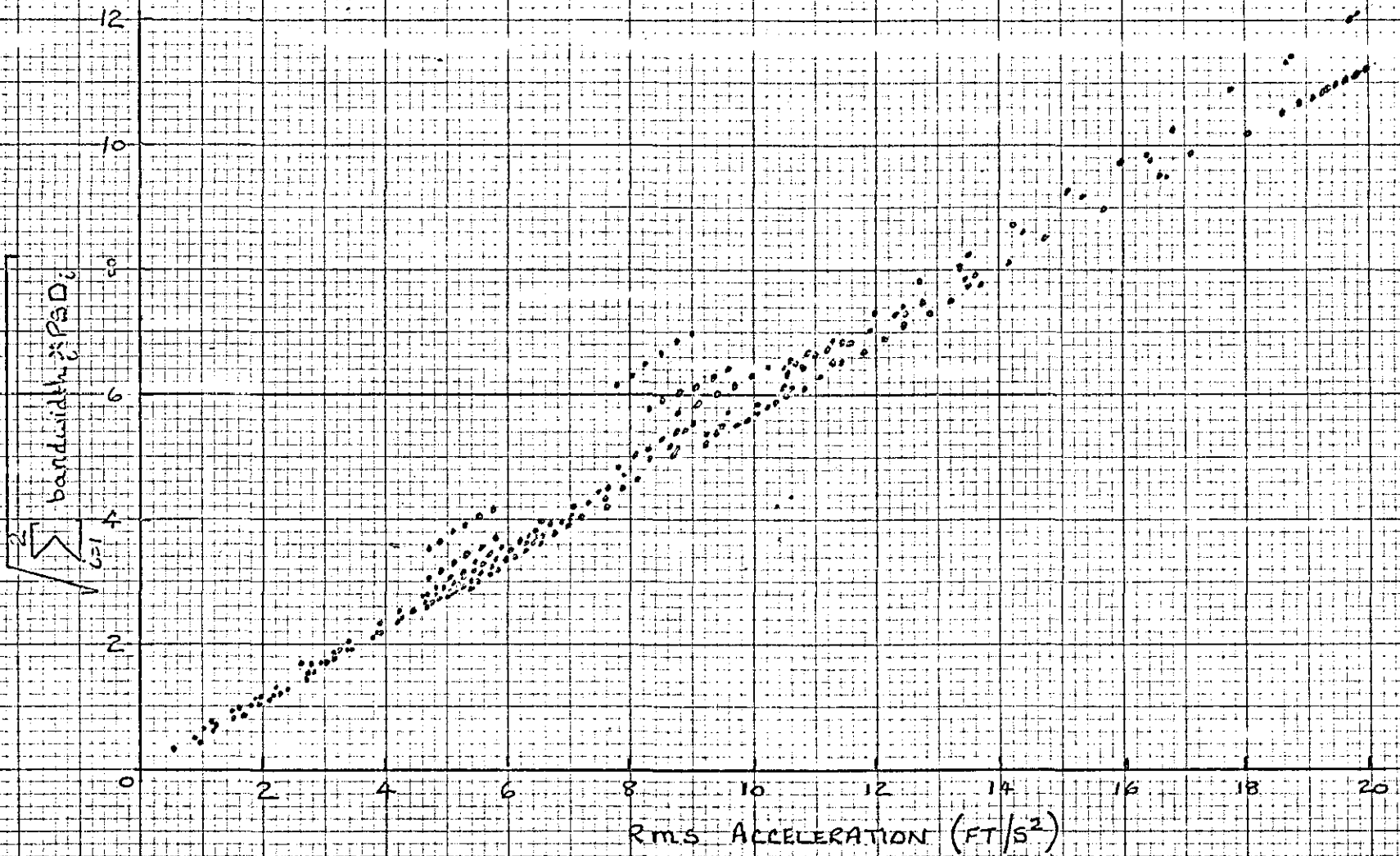
FIGURE 5.2

CORRELATION OF APPROXIMATION TO RESPONSE WITH COMPUTED RESPONSE

(RIGID BODY MODES ONLY CONSIDERED)

FIGURE 5.3
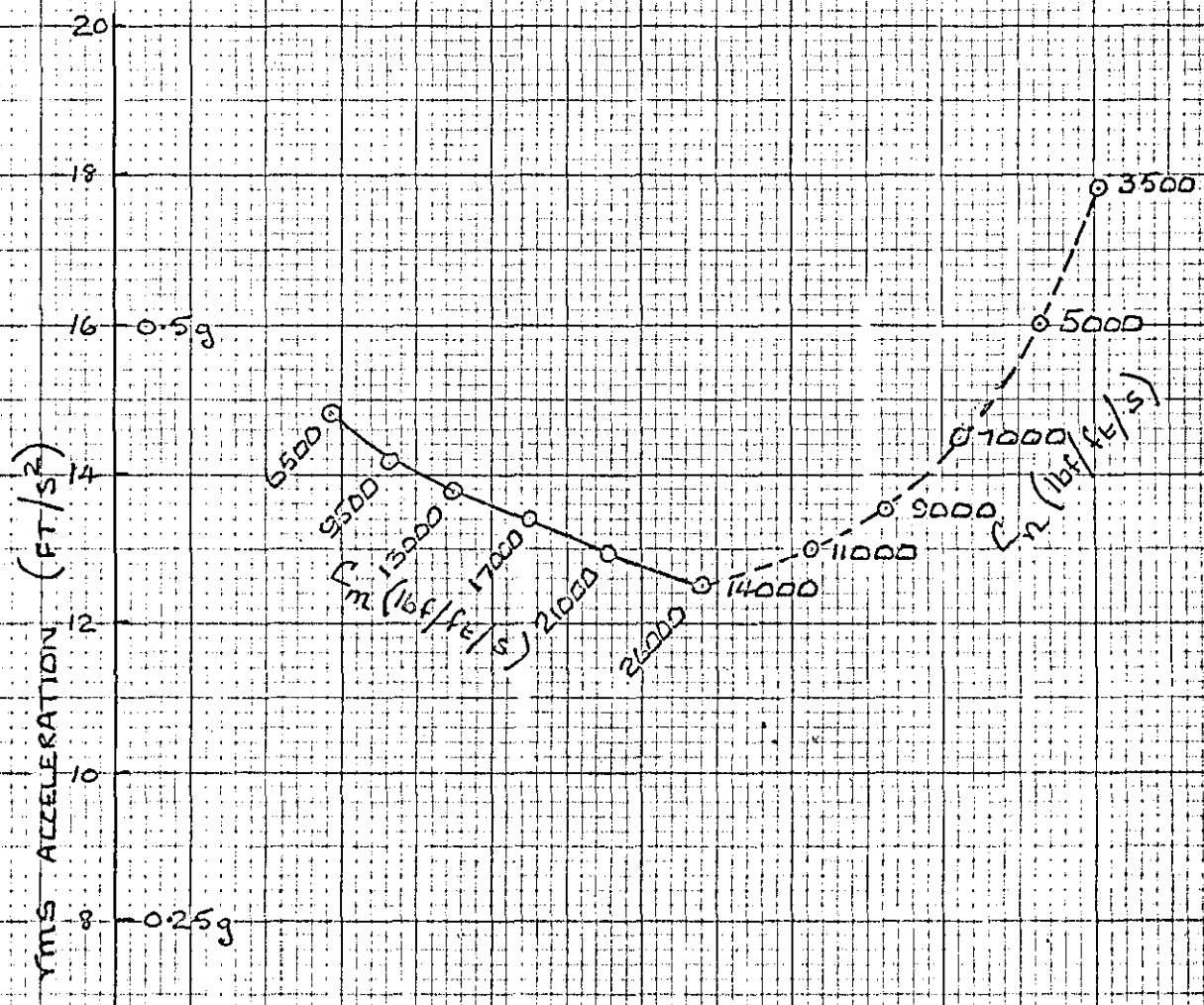


$k_m = 12 \times 10^6$ lbf/ft        $k_n = 93600$ lbf/ft

$V = 120$ ft/s

RIGID BODY MODES ONLY CONSIDERED

VARIATION OF SUM OF MAINWHEEL AND PILOT

LOCATION RESPONSE WITH OLEO DAMPING

FIGURE 5.4
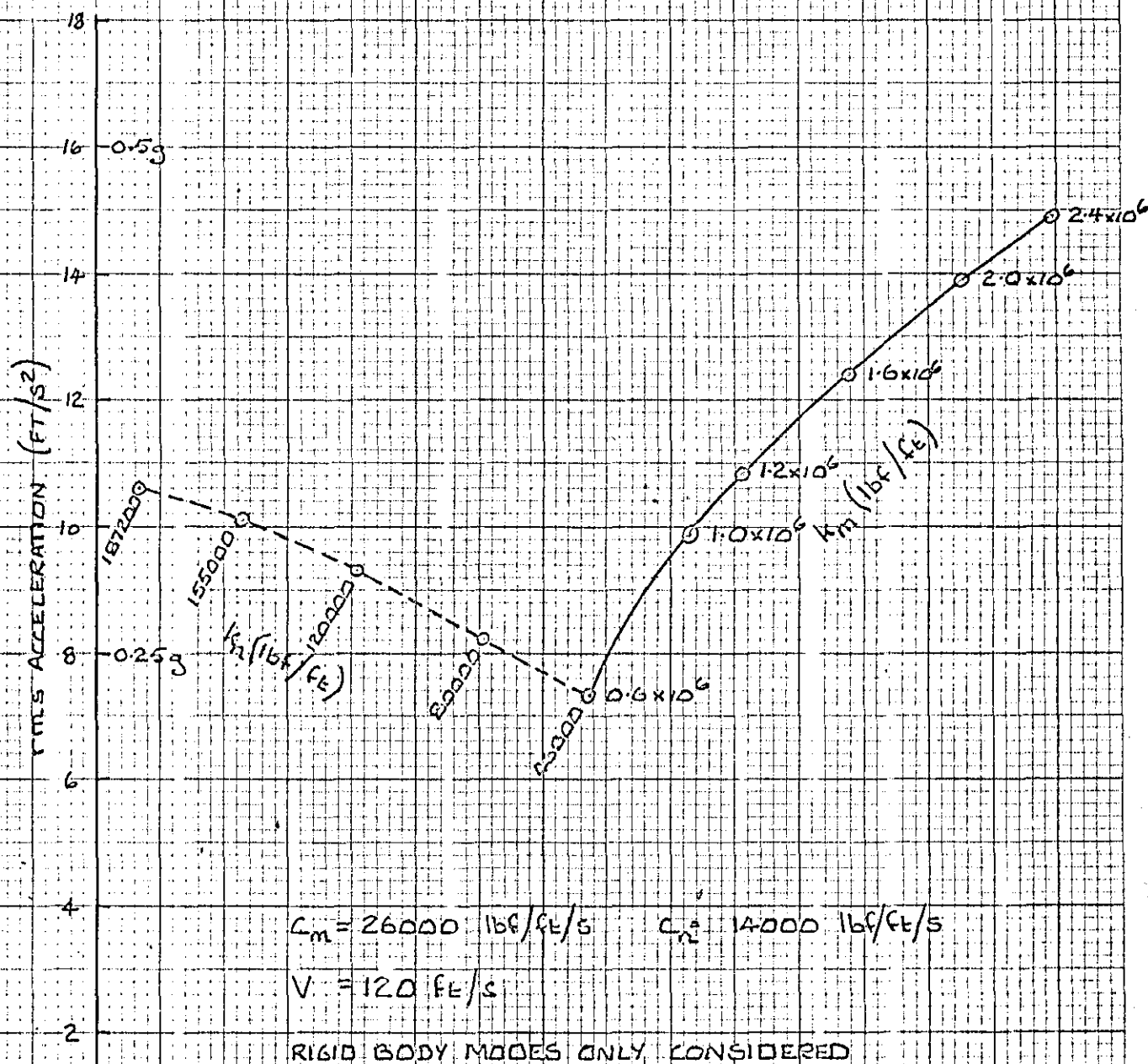
VARIATION OF SUM OF MAINWHEEL AND PILOT LOCATION

RESPONSES WITH OLEO STIFFNESS

FIGURE 5.5
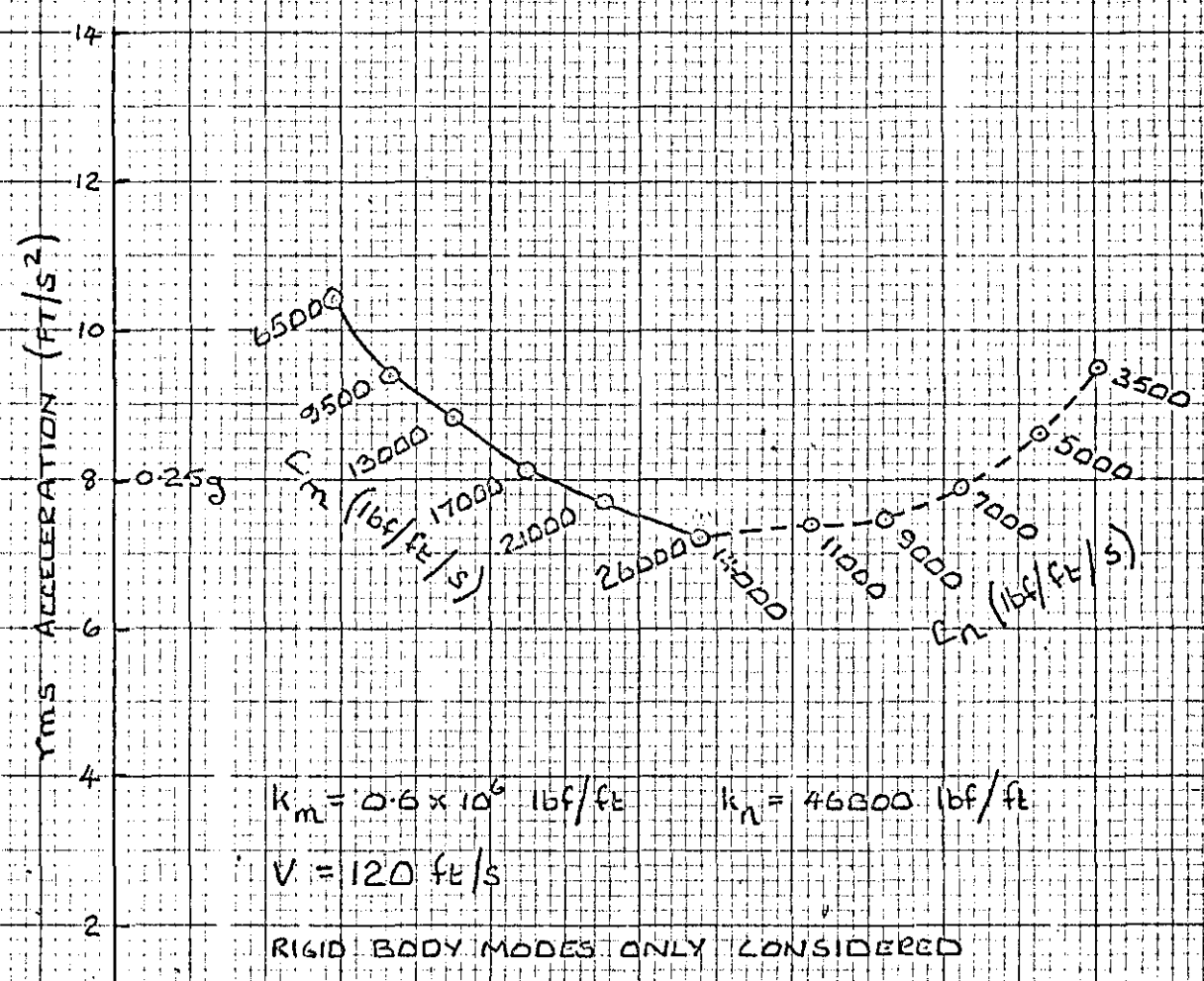
VARIATION OF SUM OF MAINWHEEL AND PILOT
LOCATION RESPONSE WITH OLEO DAMPING

FIGURE 5.6

VARIATION OF SUM OF RESPONSES AT MAINWHEEL

AND PILOT LOCATIONS WITH UNDERCARRIAGE

POSITION FOR SAME NATURAL FREQUENCIES

RIGID BODY MODES ONLY CONSIDERED

AIRCRAFT AND RUNWAY PARAMETERS AND STARTING PARAMETERS

FOR OLEOS AND TYRES (AT 4·35 FEET) AS APPENDIX D

## SECTION 6

## DISCUSSION

Computer programs have been developed, using
statistical analysis by the power spectral density method, to
investigate the response of a linearized aircraft to runway
unevenness, and to minimise this response by variation of the
undercarriage parameters.   The detailed results have been discussed
in the relevant sections.   However, further comment on some of the
results, and discussion of their overall significance, is appropriate
here.

It has generally been assumed that the higher the frequency
of the flexural mode, the less would be the response from that mode.
Hence, if say 4 flexural modes were to be included in an analysis,
the first 4 modes would be chosen, since these would be assumed to
have most effect.   However, it has been shown in sub-section 4.3.1
that this is not necessarily the case.   For the particular aircraft
analysed (the values of the parameters were based on the Boeing 707)
the 2nd, 3rd, 5th and 6th flexural modes contribute a negligible
amount to the response at the mainwheel, nosewheel and pilot
locations, and hence,for most practical purposes of computation of
fuselage accelerations,can be neglected.   The 1st and 4th modes
contribute  a significant amount to the response.   However the
contributions from these two modes appear to be of such magnitude
and phase that they counteract each other, and whilst the results may
not be representative of actual results if one of these modes is
neglected, if both modes are neglected the results give a good
indication of the actual response.   Hence for this particular aircraft,
consideration of rigid body modes only produces representative values
of fuselage acceleration.   A similar study should be performed on

any other aircraft to be analysed before it is decided which modes can be neglected.

Study of the effects of taxiing velocity on response indicates that undulations occur on the curve of response v. taxiing velocity, particularly in the case of pilot location response. These have been shown to be due predominantly to the effect of the phased undercarriage inputs on the pitching mode. The curves produced in reference 37 (see figure 4.10) are rather high, an the peaks and troughs have been shown to be rather exaggerated due to the unrealistically low nose oleo damping used in the reference, and the runway profile PSD used. A more realistic curve would be similar to that shown in figure 4.9, but with lower response at high speeds, since the runway PSD used for this figure tends to overestimate the roughness at low frequencies.

Both the response and optimisation studies have indicated that the response decreases with decreasing oleo stiffness or increasing oleo damping. These variations are in general very well behaved, the minimum response occurring at the lower boundary of stiffness and the upper boundary of damping. The only exception to this is in the case of variation of mainwheel location response with oleo stiffness. Here, for damping values of $C_1$ = 13080 lbf/ft/s and $C_2$ = 6876 lbf/ft/s, for high main oleo stiffness the response increases with decreasing nose oleo stiffness, whilst for low main oleo stiffness the response variation with nose oleo stiffness has a trough, the minimum not being at the boundary (see fig. 4.22). For low nose oleo stiffness the variation of response with main oleo

stiffness is well-behaved, but for high nose oleo stiffness the

variation of response with main oleo stiffness shows a trough,

the minimum again not occurring at a boundary.   For damping values

of twice those above (figure 4.27) the mainwheel location response

shows similar trends, although not nearly so pronounced.   In all

other cases, including all cases of variation of the sum of the

mainwheel and pilot location responses, the minimum response

occurred at lowest oleo stiffness and highest oleo damping.

For all the response and optimisation studies except

the studies of the effects of the various modes, and of course the

effect of taxiing velocity, a taxiing velocity of 120 ft/s has been

used.   The question therefore arises, "Will the values of the

parameters which give reduced response at this taxiing velocity

also reduce the response at other velocities, or could the

response be minimised at one velocity at the expense of others?"

Repeating all the studies for many velocities would of course be a

prodigious computational task.   However, in view of the fact that

the variation of response with stiffness and damping is so well-

behaved, it is anticipated that it would be so for all taxiing

velocities.   It would indeed be a great coincidence if the response

were only so well-behaved at certain velocities, and yet that this

good-behaviour coincided for all variables at the velocity chosen

for these studies.

It was shown in section 4 that the velocities at which

the peaks occur on the curve of response v. velocity are directly

proportional to the frequency of the predominant mode - the pitch

mode in the case of pilot location response.   Hence, the effect of

a reduction in oleo stiffness, for example, is not only to reduce

the response at the velocity under consideration, but to reduce

the frequencies, and hence the velocities at which the peaks and

troughs occur.    If the response at the velocity were not reduced,

the effect of squeezing the curve to the left would be to increase

the response at some velocities and decrease it at others.

However, the reduction in response due to the reduction in oleo

stiffnesses is greater than the increase in response due to

squeezing the curve to the left, at the places where the response

would be increased, i.e. on positive slopes.    The upper curve on

figure 6.1 is reproduced from figure 4.9.    Reference to figure

4.23 shows that by halving the oleo stiffnesses the response at

120 ft/s will be reduced from 10.6 ft/s$^2$ to 51 ft/s$^2$.    Reference

to figure E4 shows that this reduction in stiffness will cause

a decrease in pitch frequency from 6 rad/s to 4.9 rad/s, a decrease

of 18.4%.    Thus the position of the peaks and troughs, and any

points relative to these, will be moved to the left on figure 6.1

by 18.4%, and hence the position on the cycle which occurred at 147 ft/s

now occurs at 120 ft/s, so that in effect the point A has been moved

across to coincide with 120 ft/s and reduced to a value given by

point B.    If this same procedure, using the same proportions, is

now repeated for all taxiing velocities, a curve such as the lower

curve in figure 6.1 may be constructed.

    If these deductions are correct it will be seen that the

effect of a reduction in oleo stiffness will be to reduce the

response at all taxiing velocities, but that the reduction at some

taxiing velocities will be greater than at others.    The increase

in damping, although not changing the frequencies by the same extent, should have a similar effect. Further computations would of course be required to verify these deductions.

The most realistic method of varying the undercarriage position is to keep the same frequencies, calculated from the oleo stiffness and the proportion of the aircraft mass supported by that oleo. Using this method, as the main undercarriage moves aft from the standard position the nosewheel and pilot location responses decrease, whilst the mainwheel location response, after a slight reduction, increases. If the optimisation function is taken as the sum of the rms response accelerations at the mainwheel and pilot locations, then the aircraft under consideration is particularly insensitive to undercarriage position, and little useful purpose would be served by using this method of reducing the response.

The best reduction in response is to be gained by reducing the oleo stiffnesses. The values computed agree approximately with Wignot et al (ref. 22) who showed that a reduction of about 30% in equivalent linear stiffness of the tyre and oleo in series reduces both the passenger and crew station accelerations by 25%. However, no account has been taken of landing impacts and clearly any reduction in stiffnesses would have to take into account the energy absorption requirements of a landing impact.

The reduction to be gained in response by increasing the oleo damping is not so great as that by reducing the stiffness. Furthermore, these studies started with values of $C_1 = 13080$ lbf/ft/s

and $C_2 = 6876$ lbf/ft/s, and allowed the values to increase to twice

these values. However, the values of equivalent damping calculated

in Appendix C, i.e. $C_1 = 24650$ lbf/ft/s and $C_2 = 12900$ lbf/ft/s,

are felt to be more realistic for the Boeing 707. Reference to

figure 4.29 indicates that because of the shape of the curves at

these values, only slight reduction in response would be gained

by increasing them quite substantially. This agrees with the

findings of Wignot et al (ref. 22) who showed that for a given

configuration, varying the hydraulic damping has a negligible effect

on crew and passenger vertical accelerations.

The capability exists, in the computer programs developed,

to do a complete optimisation using the actual response program, with

all flexural modes included, and varying all the undercarriage

parameters, including tyre parameters if required. However, the

computer time required for such a task would be prohibitive.

The simplified programs developed appear to be quite

efficient in producing practically useful results quite quickly.

For example, similar results were produced, using data from reference

37, as were produced in that reference (see figure 4.10), although

the reference used an iterative technique to calculate the oleo

damping (and hence presumably more computer time), whilst the

programs used in these studies used a simply derived constant value

for damping. However, for problems where large extremes of response

are expected, an iterative technique should be used, preferably

iterating a different damping constant at each frequency step, since

increased response will produce increased oleo stroking velocity,

and hence increased damping. Hence the response at high response levels will tend to be overestimated if a constant value of damping is used (see figure 4.11). Similarly, results comparable with those in reference 13 have been produced, requiring only 33% of the computer time for the case where 6 flexural modes were included, and only $5\frac{1}{2}\%$ for the case where rigid body modes only were included.

In the optimisation studies good working results for stiffnesses and damping have been computed using only 25 minutes of computer time on a computer which is, by modern standards, very slow. /All computer times quoted in this thesis have not included compilation time./ The procedure converges very quickly onto the minimum. However, it must be remembered that in all cases except the variation of undercarriage position, the minimum being sought lay on a boundary - or more precisely at the intersection of n boundaries. Hence values of PMULT, PDIV, PMAX and EPS could be chosen which would converge this particular type of problem quickly, without loss of accuracy. If the minimum did not lie in such a position, but lay in a trough, the values would have to be chosen differently. The value of EPS would probably have to be reduced to ensure accuracy, and the other values may have to be reduced to prevent oscillation back and forth across the minimum. The fact that the method converged rapidly with only $4\frac{1}{2}\%$ error in the case of variation of undercarriage position cannot necessarily be taken as being representative of all "trough" problems without further investigation. It must be born in mind, of course, when adjusting EPS to obtain accuracy, that for the later

optimisation studies the optimisation function itself is an approximation, albeit a quite reliable one so long as the peaks are not too close together.

These studies have only considered aircraft taxiing at constant velocities. Consideration of an accelerating aircraft, such as in a take-off or landing run, is not practical by the PSD method. However, an approximation to the take-off run could be fairly simply synthesised by letting the aircraft taxi for short times at a number of discrete velocities to fit the acceleration pattern of the aircraft. The number of peak counts of acceleration could then be calculated from the response PSD's for these times; several authors have presented methods of relating peak counts to PSD's (see refs 22, 30, 58).

DEDUCED FORM OF PILOT LOCATION RESPONSE ACCELERATION CURVE

WHEN OLEO STIFFNESSES ARE HALVED FROM VALUES IN APPENDIX D

FIGURE 6.1

## SECTION 7

## CONCLUSIONS

1. The simplified system developed is useful in preliminary design, for the study of the effects of parameter variations, and for optimisation.

2. For the aircraft used for this investigation (the values are based on the Boeing 707) a good estimate of the response can be obtained by considering rigid body modes only. Of the flexural modes the 1st and 4th are by far the most predominant, but their effects tend to counterbalance each other. A similar study should be performed on any aircraft to be analysed before it is decided which modes to neglect.

3. The response acceleration at any position on the fuselage generally increases with increased taxiing velocity. However, this is not always a steady increase, particularly for pilot location response where undulations are apparent on the response curve, caused predominantly by the effect of the phased undercarriage inputs on the pitching mode. Similar, but not nearly so pronounced, undulations were apparent on the main undercarriage location response curve, caused predominantly by the same effects on the heaving mode.

4. The stiffness of the oleos would be the most rewarding parameter to vary in terms of reduction of response. The response decreases approximately linearly, in general, with decrease in equivalent linear oleo stiffness. The main oleo has most effect on the

mainwheel location response, which is predominantly due to heave, the nose oleo having almost no effect on this response. Both the main and nose oleos have a large effect on the pilot and nosewheel location responses, which have large contributions from both the pitch and heave modes.

5. Increasing the oleo damping causes a decrease in response acceleration. However, a large increase in equivalent linear damping, from what is thought to be a realistic equivalent for the Boeing 707, does not cause a very significant decrease in response.

6. As the main undercarriage location is moved aft, the distance between the two undercarriages remaining constant, the pilot and nosewheel location responses decrease, and the mainwheel location response, after a slight decrease, increases. The sum of the mainwheel and pilot location responses for the Boeing 707 remains fairly constant with change of undercarriage position. These variations assume what is thought to be the most realistic method of moving the undercarriages, i.e. keeping the frequency, calculated from the oleo stiffness and its proportion of the aircraft mass, constant.

7. The approximate optimisation function developed produces good working optima by use of very little computer time.

8. Some of the optimum parameters produced may not be realistic when viewed in the context of landing requirements (for example the oleo stiffness may be too low). However, the performance

characteristics produced should provide a useful standard with
which to compare the performance of a realizable system.

REFERENCES

1. MILWITZKY, B.
   and COOK, F.E.

   Analysis of landing gear behaviour
   NACA TR 1154                                1953

2. HUTCHINSON, B.

   Experimental investigation of undercarriage
   vibrations
   M.Sc. Thesis - College of Aeronautics,
   Cranfield                                   1969

3. MILWITZKY, B.

   Study of taxiing problems associated
   with runway roughness
   NASA Memorandum 2-21-59L          March 1959

4. COLEMAN, T.L.
   and HALL, W.H.

   Implications of recent investigations
   on runway roughness criteria
   AGARD Report 416                   January 1963

5. MORRIS, G.J.
   and HALL, A.W.

   Recent studies of runway roughness
   NASA conference on aircraft operating
   problems - Langley Research Centre   May 1965

6. MORRIS, G.J.

   Response of several turbojet airplanes to
   runway roughness .
   NASA TN D-5740                      March 1970

7. MORRIS, G.J.

   Response of a turbojet and a piston-engine
   transport airplane to runway roughness
   NASA TN D-3161                   December 1965

8. MITCHELL, C.G.B.

   Vertical acceleration in the cockpit of a
   subsonic transport aircraft during take-off
   measured during airline operation
   Ministry of Technology - Aeronautical
   Research Council. C.P.No.1120       1970

9. MITCHELL, C.G.B.

   The symmetric response of Concorde to
   uneven runways
   RAE Tech. Memo. Structures 742      March 1969

10. GUIGNARD, J.C.

    Response to low-frequency vibration
    The Chartered Mechanical Engineer   October 1968

11. GUIGNARD, J.C.

    Vibration
    A textbook of aviation physiology (ed.
    Gillies, J.A.) Chapter 29. Pergamon Press
                                        1965

12. SILSBY, N.S.

    An analytical study of effects of some airplane
    and landing-gear factors on the response to
    runway roughness with application to supersonic
    transports
    NASA TN D-1492                   December 1962

13. TUNG, C.C.,
    PENZIEN, J. and
    HORONJEFF, R.
The effect of runway unevenness on
the dynamic response of supersonic
transports
NASA CR-119                    October 1964

14. MITCHELL, C.G.B.
Some measured and calculated effects of
runway unevenness on a supersonic
transport aircraft
The Aeronautical Journal of the Royal
Aeronautical Society          .    May 1971

15. HUTTON, G.B.
Vertical cockpit accelerations measured
on an operational jet transport aircraft
during take-off and landing
RAE TR 69214                    1969

16. CALIENDI, S.C.
    and HUMPHREYS, B.
Taxiing trials on levered suspension
undercarriages
De Havilland Aircraft Co. Ltd.
Technical Note 121/59          March 1963

17. HALL, H. and
    HUTTON, G.B.
Operational and theoretical studies on
the effect of pilot action on heavy
landings
Ministry of Technology - Aeronautical
Research Council. C.P.No.1119      1970

18. MORRIS, G.J.
Response of a jet trainer aircraft to
roughness of three runways.
NASA TN D-2203                 May 1964

19. HALL, A.W. and
    KOPELSON, S.
The location and simulated repair of
rough areas of a given runway by an
analytical method
NASA TN D-1486                 October 1962

20. HOUBOLT, J.C.
Runway roughness studies in the
aeronautical field
Journal of the Air Transport Division -
Proceedings of the American Society of
Civil Engineers               March 1961

21. NEULS, G.S. et al
Optimum fatigue spectra
Technical Report No. ASD-TR-61-235(USAF)
                                April 1962

22. WIGNOT, J.E. et al
The development of dynamic taxi design
procedures
FAA Report DS-68-11            June 1968

23. MITCHELL, C.G.B.
American experience of gust and taxi
design methods and gust alleviation
RAE Tech. Memo. Structures 752    May 1969

24. MORRIS, G.J.  Three-track runway elevation profiles
measured at two United States Government
installations
NASA TN D-5545                          November 1969

25. REYNOLDS, J.,  The optimisation of undercarriage suspension
JOHNS, D.J.  characteristics by a deterministic method
and AIRD, R.J.  A paper, presented at the Symposium on Non-
linear Dynamics - University of Technology,
Loughborough                          March 1972

26. THOMPSON, W.E.  Measurements and power spectra of runway
roughness at airports of the North Atlantic
Treaty Organisation
NACA TN 4303                          July 1958

27.  Ground Manoeuvring
Joint Airworthiness Committee Paper No.
912 - RAE                          March 1972

28. WALLS, J.H.,  Some measurements and power spectra of runway
HOUBOLT, J.C.  roughness
and PRESS, H.  NACA TN 3305                          November 1954

29. PRESS, H. and  Power spectral methods of analysis and their
TUKEY, J.W.  application to problems in airplane dynamics
AGARD Flights Test Manual, Vol.IV, Part IVc

30. HOUBOLT, J.C.  Dynamic response of airplanes to atmospheric
STEINER, R.  turbulence including flight data on input and
and PRATT, K.G.  response
NASA TR R-199                          June 1964

31. ROBSON, J.D.  An introduction to random vibration
Edinburgh University Press          1963

32. BENDAT, J.S.  Principles and applications of random noise
theory
John Wiley and Sons Inc.          1958

33. HOBLIT, F.M.  Profile and power spectra of Lockheed Air
Terminal runways
Lockheed Aircraft Corporation Report
No. 10809                          September 1955

34. CRANDALL, S.H.  Perturbation techniques for random vibration
of non-linear systems
Journal of the Acoustical Society of America,
Vol. 35, No. 11.                          November 1963

35. CAUGHEY, T.K.  Equivalent linearization techniques
Journal of the Acoustical Society of America,
Vol. 35, No. 11.                          November 1963

36. ROBSON, J.D. and DODDS, C.J.
The response of vehicles components to random road-surface undulations
A paper presented at the 1970 International Automobile Safety Conference, 13th FISITA Congress

37. KIRK, C.L.
The random heave-pitch response of aircraft to runway roughness
The Aeronautical Journal of the Royal Aeronautical Society                July 1971

38. KIRK, C.L. and PERRY, P.J.
Analysis of taxiing induced vibrations in aircraft by the power spectral density method
The Aeronautical Journal of the Royal Aeronautical Society                March 1971

39. KIRK, C.L.
Analysis of taxiing induced vibrations in aircraft by the power spectral density method
Cranfield Report Aero. No. 15, Cranfield Institute of Technology                February 1973

40. COOK, F.E. and MILWITZKY, B.
Effects of interaction on landing-gear behaviour and dynamic loads in a flexible airplane structure
NACA TN 3467                August 1955

41. CAUGHEY, T.K.
Derivation and application of the Fokker-Planck equation to discrete non-linear dynamic systems subjected to white noise random excitation
Journal of the Acoustical Society of America, Vol. 35, No. 11.                November 1963

42. HOUBOLT, J.C., WALLS, J.H. and SMILEY, R.F.
On spectral analysis of runway roughness and loads developed during taxiing
NACA TN 3484                July 1955

43. HALL, H.
Some theoretical studies concerning oleo damping characteristics
Ministry of Technology - Aeronautical Research Council. C.P. No.951                1967

44. THOMPSON, A.G.
Optimum damping in a randomly excited non-linear suspension
Proceedings, Automobile Division, Institution of Mechanical Engineers, Vol.184, Part 2A                1970

45. KIRK, C.L.
Random vibration with non-linear damping
The Aeronautical Journal of the Royal Aeronautical Society                November 1973

46. HOBLIT, F.M. et al
Development of a power-spectral gust design procedure for civil aircraft
FAA Report ADS-53                1965

47. FULLER, J.R.    Contributions to the development of a
    et al          power-spectral gust design procedure for
                  civil aircraft
                  FAA Report ADS - 54               1965

48. KIEFER, J.      Optimum sequential search and approximation
                  methods under minimum regularity assumptions.
                  Journal of the Society of Industrial and
                  Applied Mathematics. 5, No.3        1959

49. COOPER, L. and
    STEINBERG, D.    Introduction to Methods of Optimisation.
                  W. B. Saunders Company         1970

50. POWELL, M.J.D.  An efficient method of finding the minimum
                  of a function of several variables without
                  calculating derivatives.
                  Computer Journal, 7.          July 1964

51. DAVIDON, W.C.   Variable metric method for minimization
                  AEC Research and Development Report,
                  ANL - 5990                   1959

52. HOOKE, R. and   Direct search solution of numerical and
    JEEVES, T.A.    statistical problems.
                  Journal of the Association for Computing
                  Machinery, 8.              April 1961

53. ROSENBROCK, H.H. An automatic method for finding the greatest
                  or the least value of a function.
                  The Computer Journal, 3.     October 1960

54. KOWALIK, J. and Methods for unconstrained optimization problems
    ORBORNE, M.R.  Elsevier                   1968

55. ZANGWILL, W.I.  Minimizing a function without calculating
                  derivatives.
                  The Computer Journal, 10.    November 1967

56. CAUCHY, A.     Méthode Générale pour la Résolution des Systémes
                  d'Équations Simultanées.
                  Comptes Rendus Hebdomadaires des Séances de
                  l'Académie des Sciences, Paris, 25.    October 1847

57. FLETCHER, R.
    and POWELL,M.J.D. A rapidly convergent descent method for
                  minimisation.
                  Computer Journal, 6.           1963

58. AUSTIN, W.H.    A summary of some recent developments in the
                  description of atmospheric turbulence used for
                  aircraft structural design.
                  USAF SEG-TR-66-45           August 1966

## IMPROVED CENTRAL DEVIATION VALUE

A.1  Houbolt's derivation of maximum deviation from the mean (ref.20)

The mean-square value of roughness that is present in a length L is given by

$$\sigma^2 = \int_{\Omega_1 = \frac{2\pi}{L_1}}^{\infty} \frac{\bar{C}}{\Omega^2} \, d\Omega = \frac{\bar{C}L}{2\pi} \qquad (A - 1)$$

Hence the root-mean-square value is given by

$$\sigma = \sqrt{\frac{\bar{C}L}{2\pi}} \qquad (A - 2)$$

Random process theory shows that the maximum deviation, $\sigma'$, in a length L can be given as

$$\sigma' = k\,\sigma$$

where k is a form factor which depends on the nature of the roughness. Experience has shown that the value of k for runway roughness is approximately the same as the value for a pure sine wave, that is $k = \sqrt{2}$.  Hence, the maximum deviation is given by

$$\sigma' = \sqrt{2}\,\sigma = \sqrt{\frac{\bar{C}L}{\pi}} \qquad (A - 3)$$

and since for new construction $\bar{C} = 6.7 \times 10^{-6}$ rad ft, then

$$\sigma' = 0.00146\sqrt{L} \text{ feet} \qquad (A - 4)$$

## A.2  Derivation of improved value of central deviation
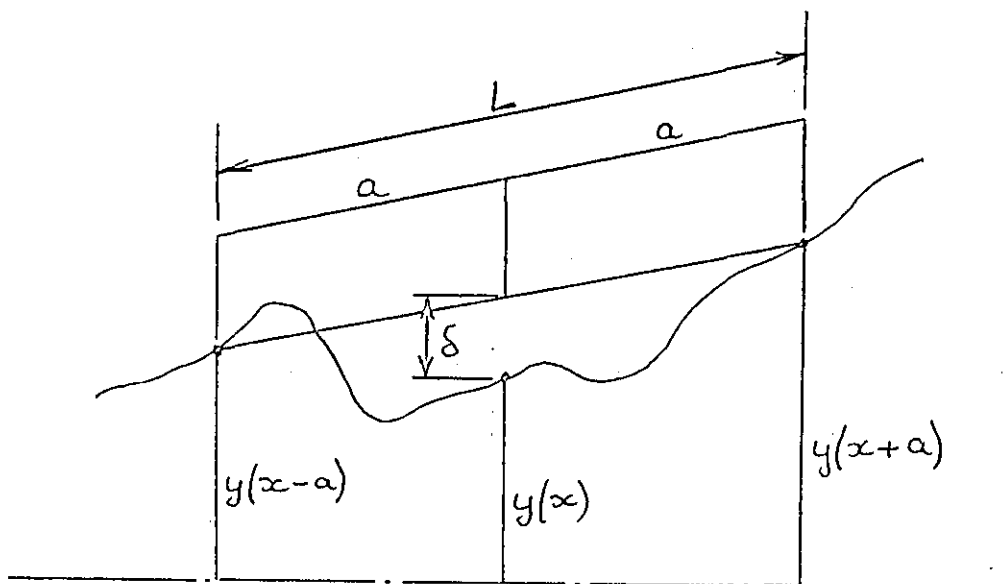


Fig. A(i)

Figure A(i) shows the central deviation $\delta$ from a straight line of length L drawn between any two points on a runway profile. Houbolt's analysis for $\delta$ is reproduced below for reference.

In terms of runway elevations, $\delta$ may be written

$$\delta = \frac{y(x + a) + y(x - a)}{2} - y(x) \qquad\qquad (A - 5)$$

The Fourier transform of $\delta$ is

$$F_\delta(\Omega) = \frac{1}{2}(e^{i\Omega a} + e^{-i\Omega a})\, F_y - F_y$$

$$= \left[\cos(\Omega a) - 1\right] F_y(\Omega) \qquad\qquad (A - 6)$$

This in turn yields the spectrum

$$\phi_\delta(\Omega) = \left[\cos(\Omega a) - 1\right]^2 \phi_y(\Omega)$$

$$= \left(4\,\sin^4\frac{\Omega a}{2}\right) \phi_y(\Omega) \qquad\qquad (A - 7)$$

The mean square value of $\delta$ is

$$\bar{\delta}^2 = \int_0^\infty \bar{\phi}_\delta(\Omega)\, d\Omega$$

$$= \int_0^\infty 4\bar{\phi}_y(\Omega)\, \sin^4\left(\frac{\Omega a}{2}\right)\, d\Omega \qquad (A - 8)$$

If the roughness spectrum is assumed to be given by the curve

$$\bar{\phi}_y(\Omega) = \frac{\bar{c}}{\Omega^2} \qquad (A - 9)$$

then equation (A-8) yields the following root-mean-square value of $\delta$

$$\sqrt{\bar{\delta}^2} = \sqrt{\frac{\pi\,\bar{c}\,a}{2}} \quad = \frac{1}{2}\sqrt{\pi\,\bar{c}\,L} \qquad (A - 10)$$

in which $L = 2a$. With a form factor of $\sqrt{2}$, as used previously, the maximum values of $\delta$ are found to be in the order of

$$\delta_{max} = \sqrt{2}\sqrt{\bar{\delta}^2} = \sqrt{\frac{\pi\,\bar{c}\,L}{2}} \qquad (A - 11)$$

For values of $\bar{c} = 6.7 \times 10^{-6}$ and $20 \times 10^{-6}$ respectively, equation (A-11) gives

$$\delta_{max} = 0.00324\sqrt{L} \text{ ft (new construction)}$$

$$\delta_{max} = 0.00561\sqrt{L} \text{ ft (needs repair)}$$

It has been stated in sub-section 1.1 that these values are felt to be suspect. Referring to equation (A-8) no reason can be seen why the lower limit of integration should be zero; since the value of $\bar{\delta}^2$ within a length L is required the lower limit should be $\Omega = \dfrac{2\pi}{L}$ as in equation (A-1)  Thus it is suggested that equation (A-8), after substitution of equation (A-9), should read

$$\bar{\delta}^2 = \int_{\Omega = \frac{2\pi}{L}}^{\infty} 4 \cdot \frac{\bar{C}}{\Omega^2} \cdot Sin^4\left(\frac{\Omega a}{2}\right) d\Omega \qquad (A - 12)$$

from which it is clear that

$$\bar{\delta}^2 < \int_{\Omega = \frac{2\pi}{L}}^{\infty} 4 \frac{\bar{C}}{\Omega^2} \qquad (A - 13)$$

Hence

$$\bar{\delta}^2 < \frac{2\bar{C}L}{\pi} \qquad (A - 14)$$

and

$$\delta_{max} = \sqrt{2} \sqrt{\bar{\delta}^2}$$

$$< 2\sqrt{\frac{\bar{C}L}{\pi}} \qquad (A - 15)$$

Thus, from equations (A-15) and (A-3)

$$\underline{\underline{\delta_{max} < 2\sigma'}}$$

In an attempt to estimate an approximate expected value of $\delta_{max}$, $Sin^4(\frac{\Omega a}{2})$ is expanded in equation (A-12) and a substitution made for $a = \frac{L}{2}$.

Thus

$$\bar{\delta}^2 = \int_{\Omega = \frac{2\pi}{L}}^{\infty} \left[ \frac{3}{2} \frac{\bar{C}}{\Omega^2} + \frac{\bar{C}}{2\Omega^2} Cos\Omega L - \frac{2\bar{C}}{\Omega^2} Cos\frac{\Omega L}{2} \right] d\Omega$$

$$= \frac{3\bar{C}L}{4\pi} + F(L) \qquad (A - 16)$$

where $F(L) = \int_{\Omega = \frac{2\pi}{L}}^{\infty} \frac{\bar{C}}{\Omega^2} \left[ \frac{1}{2} cos\Omega L - 2 cos\frac{\Omega L}{2} \right] d\Omega \qquad (A - 17)$

Now $\left| \frac{1}{2} cos\Omega L - 2 cos\frac{\Omega L}{2} \right|$ cannot exceed 2.5.

Hence

$$F(L) < \frac{5\bar{C}L}{4\pi} \qquad (A - 18)$$

confirming equation (A - 14)
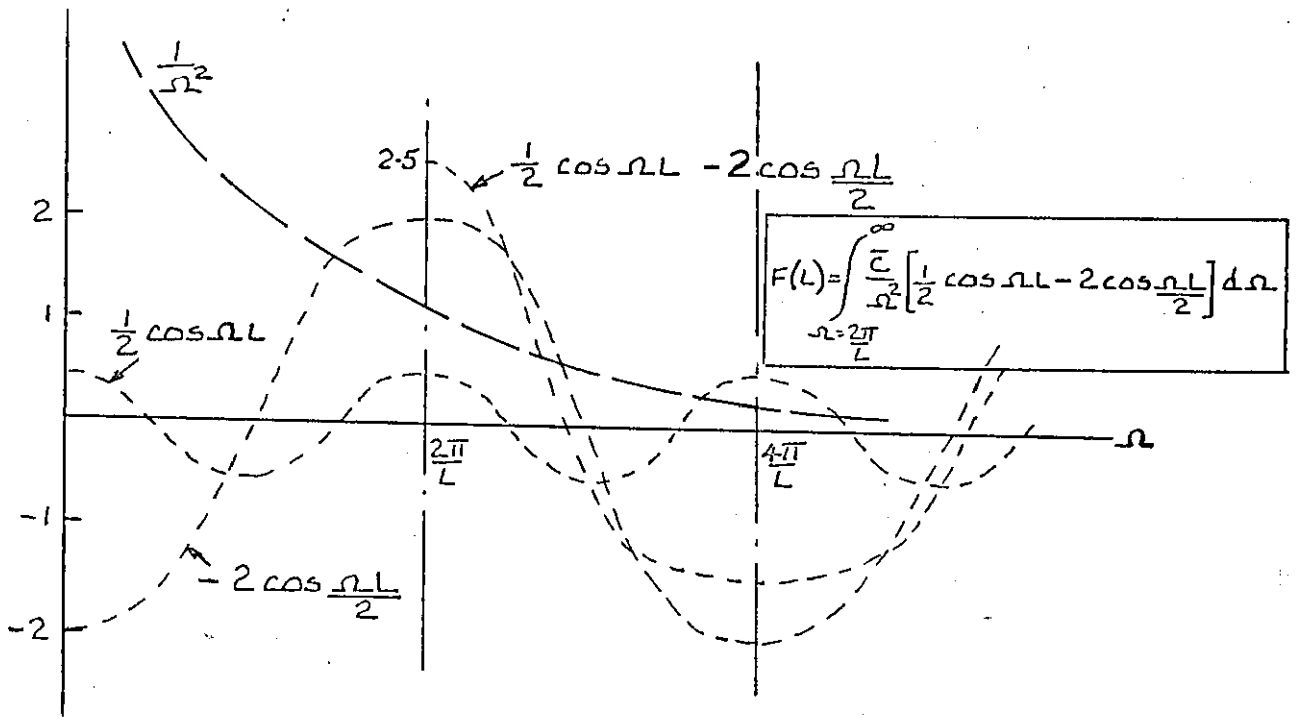
Fig. A(ii)

However, examination of figure A(ii) indicates that since the range 0 to $\frac{2\pi}{L}$ is not included in the integration for $\overline{\delta^2}$, and hence for $F(L)$, the value of $F(L)$ will be very much less than the value of $\int_{\Omega=\frac{2\pi}{L}}^{\infty} \frac{2.5\,\overline{C}}{\Omega^2}\,d\Omega$.

$$\text{i.e. } F(L) \ll \frac{5\overline{C}L}{4\pi} \qquad (A-19)$$

Similarly

$$F(L) \gg \frac{-3\overline{C}L}{4\pi} \qquad (A-20)$$

It may perhaps be concluded from equations (A - 19) and (A - 20) and from figure A(ii) that

$$F(L) \sim \frac{\overline{C}L}{4\pi}$$

so that

$$\overline{\delta^2} \sim \frac{\overline{C}L}{\pi}$$

and hence

$$\delta_{max} = \sqrt{2}\sqrt{\overline{\delta^2}}$$

$$\frac{\Omega}{} \sqrt{\frac{2\overline{C}\overline{L}}{\pi}}$$

from which

$$\delta_{max} \overset{\Omega}{=} \sqrt{2}\,\sigma'$$

$(A - 21)$

Thus, suggested values of central deviation from a straight line of length L drawn between any two points on a runway profile, to replace Houbolt's values (ref. 20) are

$$\delta_{max} = 0.00206\sqrt{L} \text{ ft (new construction)}$$

$$\delta_{max} = 0.00356\sqrt{L} \text{ ft (needs repair)}$$

DERIVATION OF ARITHMETIC MEAN RUNWAY

The PSD of a typical runway is given by

$$\phi_i(\Omega) = \frac{\bar{c}_i}{\Omega^{a_i}}$$

If the arithmetic mean of a set of values $\frac{a_i}{b_i}$ is required then

$$\text{Arithmetic mean} = \frac{\sum_{i=1}^{m} \frac{a_i}{b_i}}{m}$$

$$= \frac{1}{m} \left[ \frac{a_1(b_2 \cdot b_3 \cdot b_4 --) + a_2(b_1 \cdot b_3 \cdot b_4 --) + a_3(b_1 \cdot b_2 \cdot b_4 --) +--}{b_1 b_2 b_3 b_4} \right]$$

Thus it is not sufficient to find the mean of the numerator and denominator separately.

Referring to figure 2.2 the PSD curves can be defined by stating values of PSD at two points on each of the two straight lines. Table B1 gives the values of PSD at $\Omega = 0.05$ and $\Omega = 1.0$ for line A and at $\Omega = 0.1$ and $\Omega = 1.0$ for line B for each runway in reference 26.

Taking values from the table,

Line A

Arithmetic mean of $\bar{\phi}(\Omega)$ at $\Omega = 0.05$ is

$$\bar{\phi}_A(0.05) = \frac{\sum_{i=1}^{m} \bar{\phi}_i}{m} = \frac{100.486 \times 10^{-2}}{37}$$

$$= 2.72 \times 10^{-2}$$

Arithmetic mean of $\bar{\phi}(\Omega)$ at $\Omega = 1.0$ is

$$\bar{\phi}_A(1.0) = \frac{239.79 \times 10^{-6}}{37} = 6.49 \times 10^{-6}$$

<u>Line B</u>

Arithmetic mean of $\bar{\phi}\,(\Omega)$ at $\Omega = 0.1$ is

$$\bar{\phi}_B(0.1) = \frac{88.470 \times 10^{-3}}{37} = 2.39 \times 10^{-3}$$

Arithmetic mean of $\bar{\phi}\,(\Omega)$ at $\Omega = 1.0$ is

$$\bar{\phi}_B(1.0) = \frac{398.61 \times 10^{-6}}{37} = 10.78 \times 10^{-6}$$

These values are plotted on figure B1.

<u>Slopes</u>

a. <u>Line A</u>

$\text{Log } 2.72 \times 10^{-2} = -2 + .4346$

$\text{Log } 6.49 \times 10^{-6} = -6 + .8122$

$\text{Log } 0.05 = -2 + .6990$

$\text{Log } 1.0 = 0$

Thus, slope of line A $= \dfrac{(-6 + .8122) - (-2 + .4346)}{0 - (-2 + .6990)}$

$$= -2.79$$

b. <u>Line B</u>

Similarly, slope of line B $= -2.35$

<u>Intersection</u>

The point of intersection of the two lines is given by

$$\frac{6.49 \times 10^{-6}}{\Omega^{2.79}} = \frac{10.78 \times 10^{-6}}{\Omega^{2.35}}$$

Thus the PSD of the arithmetic mean runway is given by

If $\Omega < 0.32$ rad/ft, $\phi(\Omega) = \dfrac{6.49 \times 10^{-6}}{\Omega^{2.79}}$ ft$^2$/rad/ft

If $\Omega > 0.32$ rad/ft, $\phi(\Omega) = \dfrac{10.78 \times 10^{-6}}{\Omega^{2.35}}$ ft$^2$/rad/ft

Analysis of runways in reference 26

| Fig. | LINE A | | LINE B | |
|---|---|---|---|---|
| | $\phi$ at $\Omega$ = 0.05 | $\phi$ at $\Omega$ = 1.0 | $\phi$ at $\Omega$ = 0.1 | $\phi$ at $\Omega$ = 1.0 |
| | $10^{-2}$ | $10^{-6}$ | $10^{-3}$ | $10^{-6}$ |
| 3 | 1.738 | 3.47 | 2.239 | 11.75 |
| | 1.738 | 3.47 | 2.239 | 11.75 |
| 5 | 0.794 | 7.94 | 1.549 | 7.94 |
| 7 | 0.398 | 1.26 | 0.363 | 5.37 |
| 10 | 9.120 | 1.26 | 5.623 | 35.48 |
| | 9.120 | 1.26 | 5.623 | 35.48 |
| 12 | 2.692 | 2.24 | 0.550 | 6.31 |
| 15 | 2.754 | 0.54 | 0.661 | 5.37 |
| | 1.349 | 3.47 | 0.417 | 20.89 |
| 20 | 2.951 | 17.78 | 5.248 | 17.78 |
| | 2.951 | 17.78 | 5.248 | 17.78 |
| | 2.951 | 17.78 | 5.248 | 17.78 |
| | 2.951 | 17.78 | 5.248 | 17.78 |
| 23 | 1.318 | 3.55 | 1.995 | 3.55 |
| | 3.981 | 0.00015 | 0.398 | 3.31 |
| 26 | 1.413 | 0.631 | 1.318 | 3.55 |
| | 4.266 | 0.631 | 3.311 | 12.59 |
| 29 | 2.818 | 0.013 | 0.525 | 4.47 |
| | 1.122 | 0.00068 | 0.661 | 8.91 |
| 32 | 10.00 | 0.00007 | 1.778 | 3.47 |
| | 10.00 | 0.00007 | 1.778 | 3.47 |
| 37 | 1.445 | 0.00501 | 1.202 | 7.08 |
| | 1.445 | 0.00501 | 1.202 | 7.08 |
| | 1.445 | 0.00501 | 1.202 | 7.08 |
| | 1.445 | 0.00501 | 1.202 | 7.08 |
| 40 | 0.933 | 1.00 | 0.166 | 3.16 |
| | 0.933 | 1.00 | 0.166 | 3.16 |
| 43 | 2.951 | 0.0066 | 2.818 | 10.00 |
| | 2.951 | 0.0066 | 2.818 | 10.00 |
| 46 | 1.698 | 8.51 | 3.090 | 8.51 |
| | 1.698 | 8.51 | 3.090 | 8.51 |
| 49 | 1.259 | 2.63 | 1.820 | 2.63 |
| | 1.259 | 2.63 | 1.820 | 2.63 |
| 52 | 1.585 | 13.80 | 0.631 | 30.20 |
| | 0.794 | 1.26 | 0.234 | 6.31 |
| 55 | 1.072 | 14.45 | 2.399 | 14.45 |
| 56 | 1.148 | 85.11 | 12.590 | 15.85 |
| TOTALS | 100.486 | 239.79 | 88.470 | 398.61 |

FIGURE B1
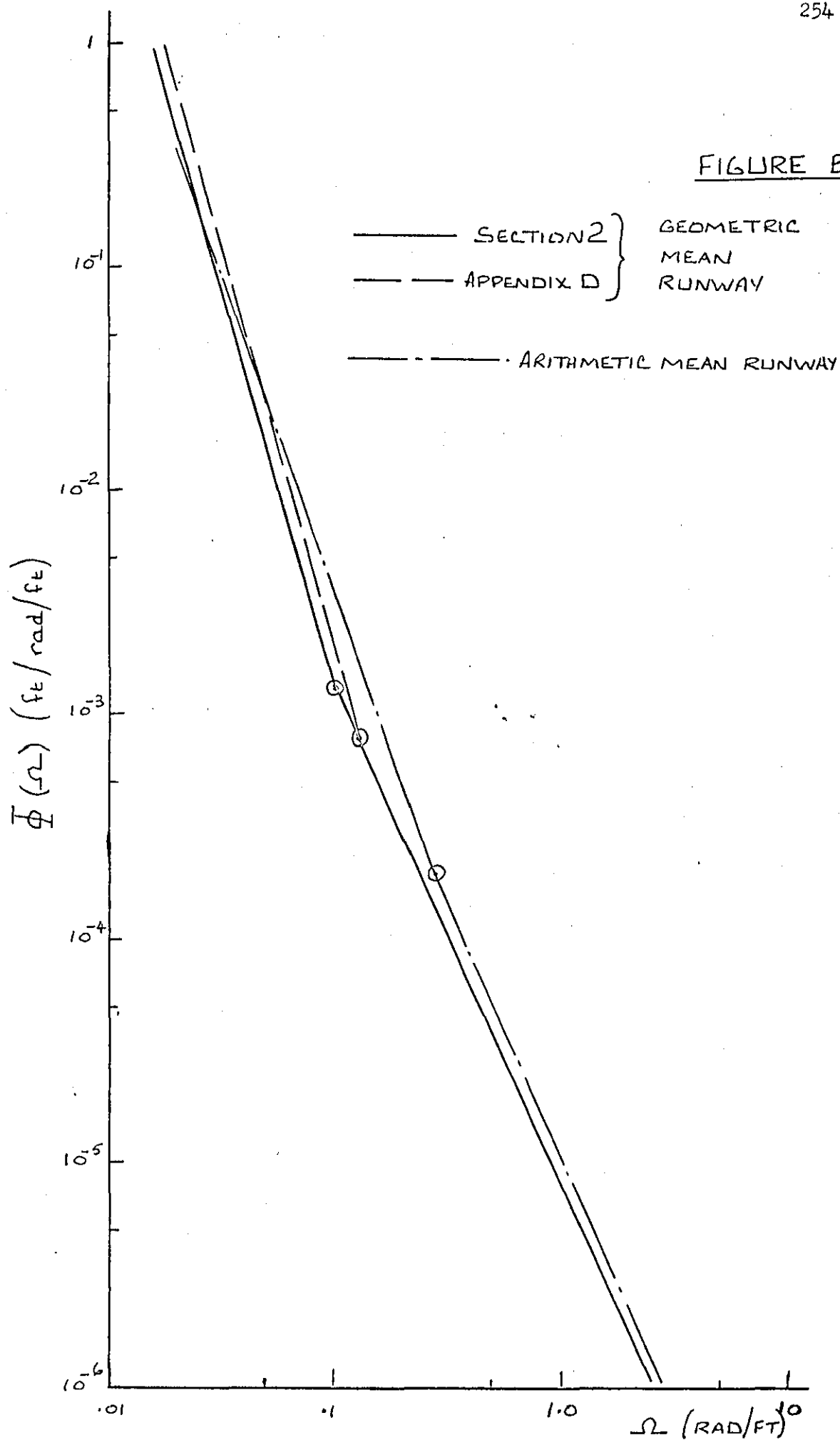
POWER SPECTRAL DENSITY FUNCTIONS

BOEING 707 DATA AND EQUIVALENT LINEAR UNDERCARRIAGE CHARACTERISTICS

The basic data from which the following data and linearised undercarriage characteristics are derived is taken from reference 13.

C.1  Undercarriage and pilot positions

The dimensions required for use in this analysis are shown in figure C 1.

C.2  Masses and Inertias

Gross weight of aircraft  =  324040 lbf

$\therefore$ Mass of aircraft  =  10078 slug

Unsprung weight of two
main undercarriages, $W_1$  =  4992 lbf

$\therefore$ Unsprung mass, $M_1$  =  155 slug

Unsprung weight of nose
undercarriage, $W_2$  =  342 lbf

$\therefore$ Unsprung mass, $M_2$  =  10.6 slug

$\therefore$ Total sprung mass of aircraft, $MJ[1,1]$

$$= 10078 - (155 + 10.6)$$

$$= 9912 \text{ slug}$$

Aircraft Moment of Inertia in pitch about centre of
gravity, $J$  =  $0.645 \times 10^8$ lbf in $s^2$

i.e. $J$  =  $MJ[2,2] = 5.375 \times 10^6$ slug ft$^2$

C.3  Modal frequencies, generalised masses, and damping for first

6 flexible modes

| Flexible Mode No. | Modal Frequency rad/s | Generalised Mass Slug |
|---|---|---|
| 1 | 7.22 | 369.36 |
| 2 | 18.00 | 278.29 |
| 3 | 23.85 | 701.23 |
| 4 | 31.0 | 635.84 |
| 5 | 38.8 | 742.54 |
| 6 | 55.0 | 192.46 |

Damping ratio of airframe, assumed the same in each mode, $\beta = 0.025$

## C. 4 Mode shapes for first 6 flexible modes

| Flexible Mode No. | Location on Fuselage | | |
|---|---|---|---|
| | Main u/c | Nose u/c | Pilot Location |
| 1 | -0.122 | 0.030 | 0.056 |
| 2 | 0.037 | 0.089 | 0.103 |
| 3 | -0.010 | 0.298 | 0.383 |
| 4 | 0.230 | -0.560 | -0.800 |
| 5 | -0.168 | 0.040 | 0.080 |
| 6 | -0.065 | 0.083 | 0.160 |

## C. 5 Undercarriage stiffnesses

The spring force curves for the main and nose undercarriages shown in figure C2 are reproduced from reference 13. The values of spring stiffnesses used for initial response calculations in this investigation are the stiffnesses (i.e. slopes of curves) at the static equilibrium position with the aircraft at its maximum all-up-weight.

Sprung weight of aircraft at max. AUW

$$= 324030 - (4992 + 342)$$

$$= 318700 \text{ lbf}$$

$\therefore$ Sprung weight on two mainwheels

$$= 318,700 \times \frac{656}{708} = 295,300 \text{ lbf}$$

Sprung weight on nosewheel $= 318700 \times \frac{52}{708}$

$$= 23400 \text{ lbf}$$

Thus, drawing tangents to the curves at these values in figure C2 gives the following approximate values:

$$k_{main} = k_1 = \frac{500000}{20} \times \frac{9.6}{2.4} = 100000 \text{ lbf/in}$$

$$= 1.2 \times 10^6 \text{ lbf/ft}$$

$$k_{nose} = k_2 = \frac{39000}{10} \times \frac{8}{4} = 7800 \text{ lbf/in}$$
$$= 93600 \text{ lbf/ft}$$

## C.6 Undercarriage damping

The damping coefficient curves for the main and nose undercarriages shown in figure C3 are reproduced from Reference 13. The values of equivalent linear damping coefficients to correspond to non-linear damping coefficients may be calculated by two main methods. One is to equate the damping force of the two coefficients; the other is to equate the energy absorbed per cycle using the two coefficients. Both methods require a knowledge of the non-linear damping coefficient, and a stroking velocity for the oleo. The non-linear damping coefficients may be obtained from the curves in figure C3 by using strokes at static equilibrium position obtained from the curves in figure C2. The velocities are a little more difficult. There are available, in reference 13, mean square values, $\overline{\dot{x}_i^2}(t)$, of the generalised co-ordinates of response velocity of the aircraft in the various modes. These may be used to calculate an approximate rms response velocity at the main and nose undercarriages which will be used as an approximate rms oleo stroking velocity.

If a quantity $V(t) = V_1(t) + V_2(t) + \text{---} + V_n(t)$, then the mean-square value of V is given by

$$\overline{V^2}(t) = \frac{1}{T} \int_o^T V^2 dt$$
$$= \frac{1}{T} \int_o^T (V_1 + V_2 + V_3 + \text{-----} V_n)^2 dt$$
$$= \frac{1}{T} \int_o^T \left[ (V_1^2 + V_2^2 + \text{-----} + V_n^2) + (2\sum V_i V_j) \right] dt$$

For a large number of modes $2\sum V_i V_j$ will approach zero, so that it can be said that

$$\overline{V^2}(t) \simeq \frac{1}{T}\int_0^T (V_1^2 + V_2^2 + \text{----} V_n^2)\, dt$$

$$= \frac{1}{T}\int_0^T V_1^2 dt + \frac{1}{T}\int_0^T V_2^2 dt + \text{----} + \frac{1}{T}\int_0^T V_n^2 dt$$

$$= \overline{V_1^2}(t) + \overline{V_2^2}(t) + \text{---} + \overline{V_n^2}(t)$$

Thus

$$\text{rms value of } V \simeq \sqrt{\text{Sum of mean-square values of } V_i}$$

Using the mode shapes given in C.4, remembering that $\phi^3 = 1$ (rigid body heave) and $\phi^4 = -X$ (rigid body pitch) where $X$ is the horizontal distance from the c.g. (sub-section 3.2.1), and taking values of $\overline{\dot{X}_j^2}(t)$ from Table 3 (p.92) of Reference 13 gives

| Mode j | $\overline{\dot{X}_j^2}(t)$ | $\phi_1^j$ | Main undercarriage $(\phi_1^j)^2$ | $(\phi_1^j)^2(\dot{X}_j)^2$ | Nose undercarriage $\phi_2^j$ | $(\phi_2^j)^2$ | $(\phi_2^j)^2(\dot{X}_j)^2$ |
|---|---|---|---|---|---|---|---|
| 3 | 43.33 | 1 | 1 | 43.33 | 1 | 1 | 43.33 |
| 4 | .0004354 | 52 | 2704 | 1.178 | -656 | 430000 | 187.3 |
| 5 | 1318 | -.122 | .0149 | 19.6 | .030 | .009 | 11.87 |
| 6 | 27.08 | .037 | .00137 | .037 | .089 | .00792 | .215 |
| 7 | 1.04 | -.010 | .0001 | .0001 | .298 | .0887 | .092 |
| 8 | 12.66 | .230 | .0529 | .670 | -.560 | .314 | 3.97 |
| 9 | 3.882 | -.168 | .0282 | .109 | .040 | .0016 | .0045 |
| 10 | 3.184 | -.065 | .00423 | .0135 | .083 | .0069 | .022 |
| | | | | 64.94 | | | 246.8 |

Root-mean-square value of vertical velocity at main undercarriage

$$\text{location} = \sqrt{\sum (\phi_1^j)^2 (\dot{X}_j)^2}$$

$$= \sqrt{64.94}$$

$$= 8.05 \text{ in/s}$$

Similarly, rms value of vertical velocity at nose undercarriage

$$\text{location} = 15.7 \text{ in/s}$$

If these values are assumed to be the oleo stroking velocities they will at the best be only approximations as they take no account of the vertical velocity of the wheel, it being assumed that the wheel remains still relative to the runway. Whilst the mean and mean-square values of main and nose wheel velocities are available in reference 13, it is felt that since

$$\dot{s} = \dot{u} - \dot{x}$$

where $\dot{s}$ = stroking velocity

$\dot{u}$ = airframe velocity

$\dot{x}$ = wheel velocity

it cannot be said that

$$\overline{\dot{s}^2}(t) = \overline{\dot{u}^2}(t) + \overline{\dot{x}^2}(t)$$

since, with only two values, it cannot be assumed that

$$\frac{2}{T} \int_0^T \dot{u}\dot{x}dt = 0$$

However, the above velocities give an idea of the order of the velocities, and thus will give an initial estimate of the order of the equivalent linear damping coefficient which should be used. Since the ultimate aim is optimisation of the undercarriage characteristics, all that is required is a starting value. However, it will be useful if this is as accurate as possible from the available data, for the purpose of comparing response values for the aircraft with those obtained by previous authors.

From figure C2(a), for the main undercarriage at static equilibrium position,

Stroke position = 20 in

From figure C3(a) $C_{Nm}$ = 160 lbf/(in/s)$^2$

Similarly, for the nose undercarriage, from figures C2(b) and C3(b)

$$\text{Stroke position} = 14 \text{ in}$$

$$C_{Nn} = 43 \text{ lbf}/(\text{in/s})^2$$

where $C_{Nm}$ and $C_{Nn}$ are the non-linear (i.e. $V|V|$) damping coefficients for the main and nose undercarriage oleos respectively.

The equivalent linear damping coefficient $C_e$ may now be calculated using one of the methods mentioned above. The first method would be to equate damping forces caused by the two damping coefficients, so that

$$C_e.\dot{X} = C_N.\dot{X}^2$$

giving 
$$C_e = C_N.\dot{X}$$

It is felt that the better method is to calculate $C_e$ by assuming the same energy absorption by the two types of damping over a given period. It can be shown (ref. 38) that for a harmonic input, equating energy dissipated per cycle gives

$$C_e = \frac{8}{3\pi}.C_N \, S \, \omega$$

where S is the stroke amplitude

$\omega$ is the input frequency

Thus, since the motion is harmonic, $S\omega$ is the maximum stroking velocity and therefore equal to $\sqrt{2} \, \dot{S}$ where $\dot{S}$ is the rms value of the stroking velocity.

Hence, 
$$C_e = \frac{8\sqrt{2}}{3}.C_N\dot{S} = 1.2 \, C_N\dot{S}$$
$$= 1.2 \, C_N\dot{X}$$

However, since the value of $\dot{X}$ obtained is calculated from the results of a random input it is better to equate the energy absorptions in such a process. It can be shown (ref. 38) that for a random input having Gaussian distribution, equating energy dissipated over a period of time gives

$$C_e = 2\sqrt{\frac{2}{\pi}}\, C_N.\dot{X} = 1.593\, C_N.\dot{X}$$

It can be seen that, of the above methods, the last one will give the greatest values for $C_e$.

For main oleo, equivalent linear damping

$$\text{coefficient, } C_{em} = 1.593 \times 160 \times 8.05$$

$$= 2055 \text{ lbf/in/s}$$

$$\text{i.e.} C_{em} = 24650 \text{ lbf/ft/s}$$

For nose oleo, equivalent linear damping

$$\text{coefficient, } C_{en} = 1.593 \times 43 \times 15.7$$

$$= 1075 \text{ lbf/in/s}$$

$$\text{i.e.} C_{en} = 12900 \text{ lbf/ft/s}$$

## C. 7 Tyres

### C.7.1 Stiffnesses

Total Main Undercarriage tyre stiffness, $k_{t1} = 1.158 \times 10^6$ lbf/ft

Total Nose Undercarriage tyre stiffness, $k_{t2} = 162000$ lbf/ft

### C.7.2 Damping

It is assumed that the damping in the tyres is 2.5% of the critical damping for the wheel mass on the tyre.

Now $C_{crit} = 2M\omega_n = 2M\sqrt{\dfrac{k}{M}} = 2\sqrt{kM}$

∴ Mainwheel tyre damping coefficient,

$$C_{t1} = .025 \times 2\sqrt{k_{t1}M_1}$$

$$= .025 \times 2\sqrt{1.158 \times 10^6 \times 155}$$

$$= 670.8 \text{ lbf/ft/s}$$

Nosewheel tyre damping coefficient,

$$C_{t2} = .025 \times 2\sqrt{162000 \times 10.6}$$

$$= 65.6 \text{ lbf/ft/s}$$

## C.8 Summary of program data for aircraft with 6 flexible modes for initial response studies and as starting data for optimisation studies

| Analysis Symbol | Program Identifier | Value |
|---|---|---|
| $k_1$ | K1 | $1.2 \times 10^6$ lbf/ft |
| $k_2$ | K2 | 93600 lbf/ft |
| $c_1, c_{cm}$ | C1 | 24650 lbf/ft/s |
| $c_2, c_{en}$ | C2 | 12900 lbf/ft/s |
| $k_{t2}$ | KT1 | $1.158 \times 10^6$ lbf/ft |
| $k_{t2}$ | KT2 | 162000 lbf/ft |
| $c_{t1}$ | CT1 | 670.8 lbf/ft/s |
| $c_{t2}$ | CT2 | 65.6 lbf/ft/s |
| $d$ | WBASE | 59 ft |
| $\beta$ | BETA | 0.025 |
| $M_1$ | M1 | 155 slug |
| $M_2$ | M2 | 10.6 slug |
| $\lceil M_j \rfloor$ | MJ[i,i] | $[9912, \ 5.375 \times 10^6, \ 369.36, \ 278.29$ $701.23, \ 635.84, \ 742.54, \ 192.46]$ |
| $\lceil \omega_j \rfloor$ | WJ[i,i] | $[0, \ \ 0, \ \ 7.22, \ \ 18.0,$ $23.85, \ \ 31.0, \ \ 38.8, \ \ 55.0]$ |

| Analysis Symbol | Program Identifier | Value |
|---|---|---|
| $\left[\phi_1{}^j\right]$ | PHI1 | $\begin{bmatrix} 1.0, & 4.333, & -0.122, & 0.037, \\ -0.010, & 0.230, & -0.168, & -0.065 \end{bmatrix}$ |
| $\left[\phi_2{}^j\right]$ | PHI2 | $\begin{bmatrix} 1.0, & -54.667, & 0.030, & 0.089, \\ 0.298, & -0.560, & 0.040, & 0.083 \end{bmatrix}$ |
| $\left[\phi_p{}^j\right]$ | PHIP | $\begin{bmatrix} 1.0, & -64.583, & 0.056, & 0.103, \\ 0.383, & -0.800, & 0.080, & 0.160 \end{bmatrix}$ |
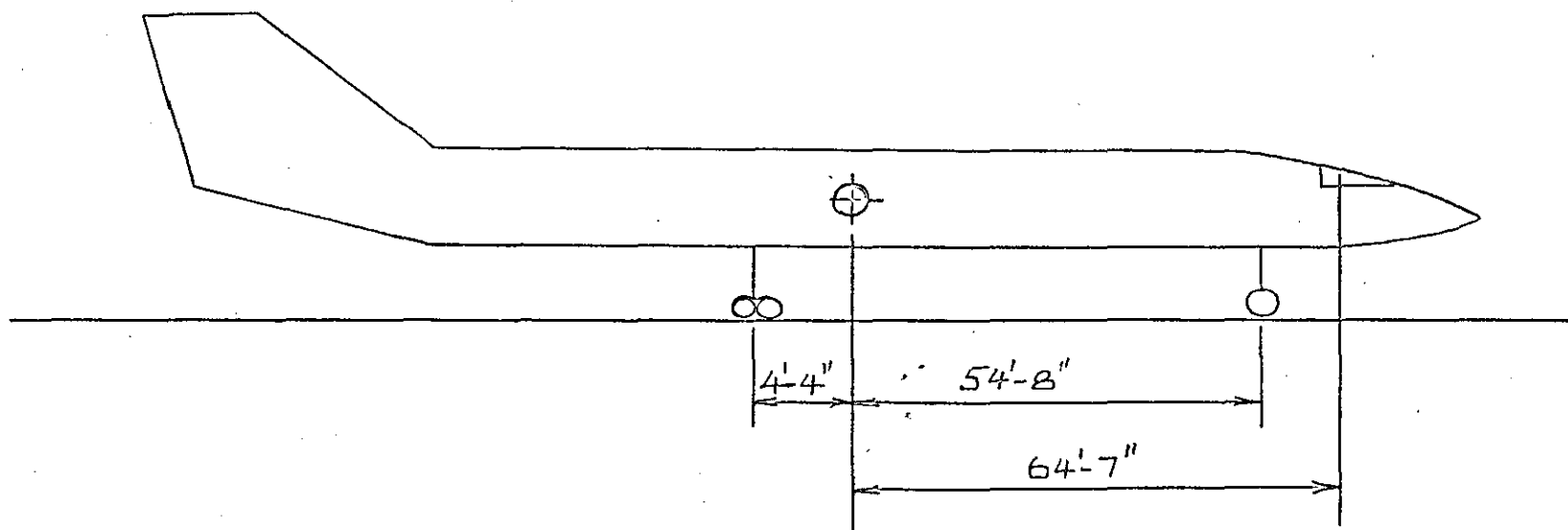
UNDERCARRIAGE AND PILOT LOCATIONS

FIGURE C2

(a) MAIN OLEO SPRING FORCE

(b) NOSE OLEO SPRING FORCE
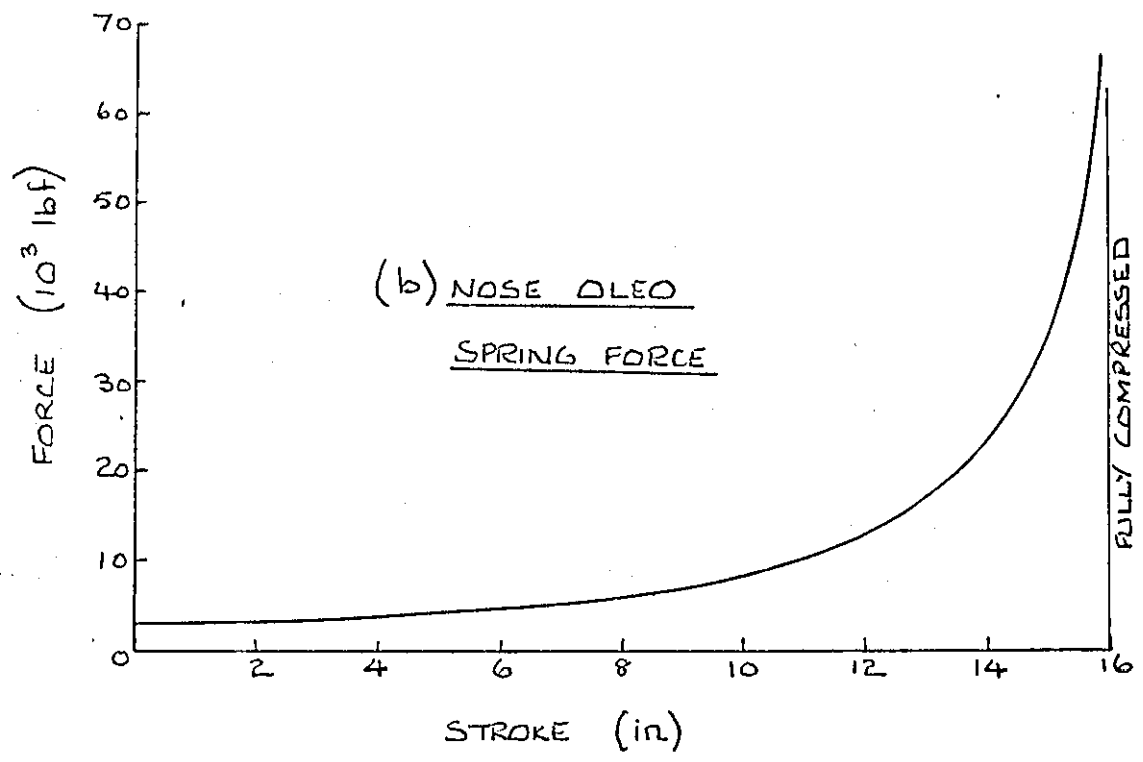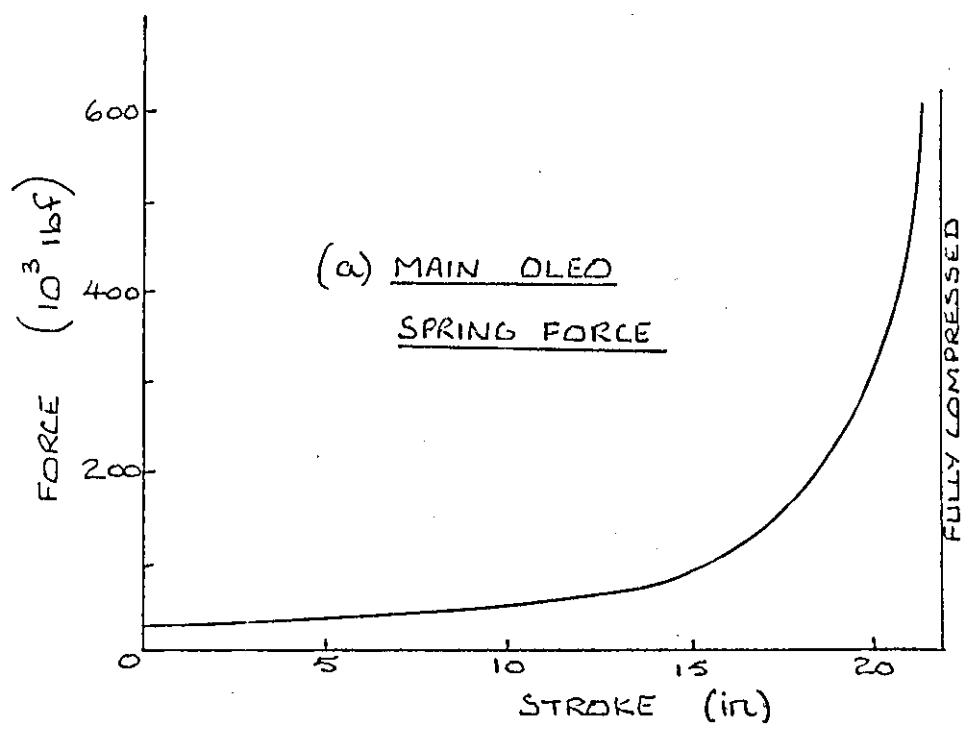
OLEO SPRING FORCES FOR BOEING 707

FIGURE G3
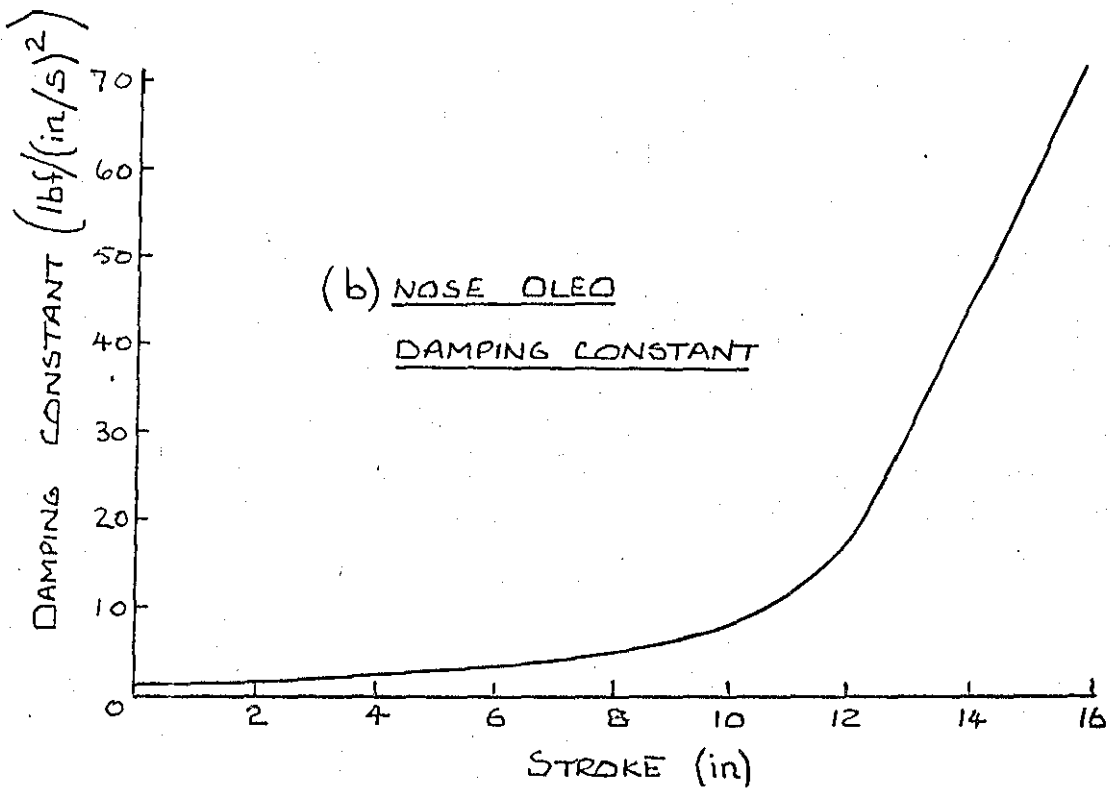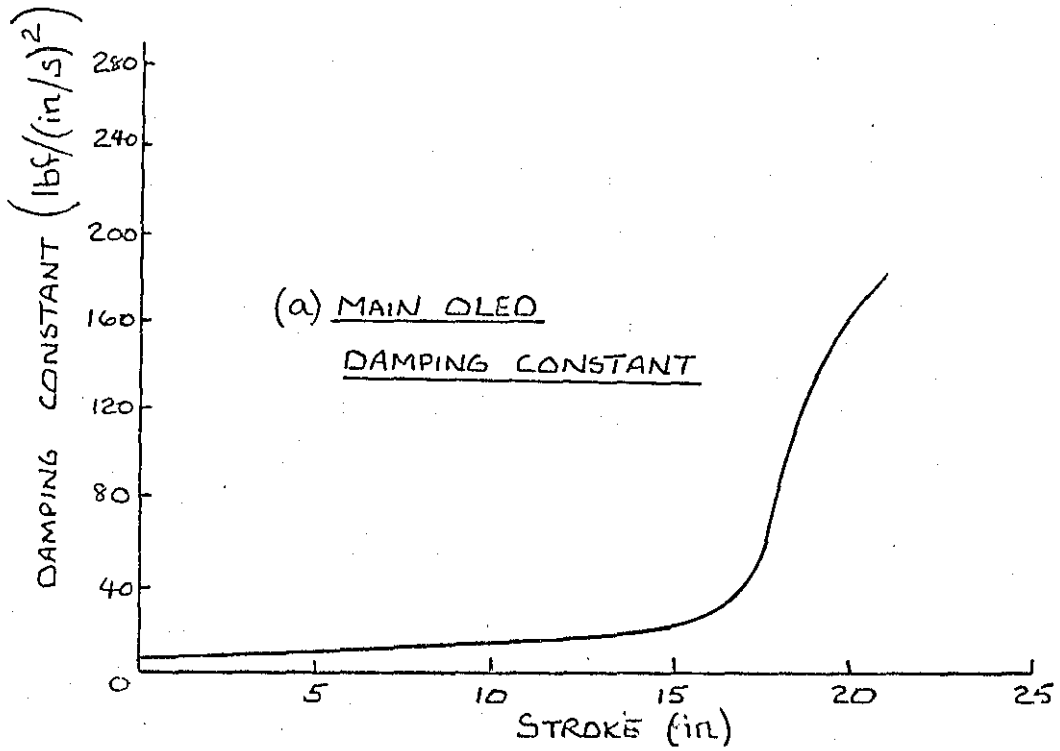
OLEO DAMPING CONSTANTS FOR BOEING 707

AIRCRAFT AND RUNWAY DATA USED FOR MOST OF THE WORK IN THIS REPORT

Due partly to some numerical error in early calculations
and partly to some modification in thoughts on equivalent.damping
as the work progressed, some of the values derived in Section 2
and Appendix C are modifications of values which were actually
used for most of the computer work in this report.   This Appendix
shows the actual values which were used for this work.

### D.1 Runway characteristics

Referring to the summary in sub-section 2.2 it will be
seen that the value of $\overline{C}_a$ calculated for the geometric mean runway
is $3.8 \times 10^{-7}$.   Due to a numerical error in earlier calculations
the original value calculated for $\overline{C}_a$ was $6.1 \times 10^{-7}$.   The values
of $n_a$, $\overline{C}_b$ and $n_b$ remain unchanged.   By the analysis shown in
sub-section 2.1 these values led to a value of $\Omega$ at the intersection
of the two lines representing the PSD curve of 0.15.   The values
used for most of the computer work are summarised in table D1.

These values are plotted on figure B1 in Appendix B.
At spacial frequencies in excess of 0.15 rad/ft of course the
line coincides with that plotted from the values in section 2.
However, at frequencies below 0.101 rad/ft it will be seen that
the runway derived here contains approximately 1.5 times the power
contained by the runway derived in Section 2.

### D.2 Aircraft characteristics

Referring to Appendix C it will be seen that the values
of main and nose oleo damping constant calculated from the values

in reference 13 were 24650 and 12900 lbf/ft/s respectively.    These
were calculated by equating energy dissipated over a period of time
by linear and non-linear dampers subjected to a random input having
Gaussian distribution.

An earlier method used was to equate the energy dissipated
per cycle for a harmonic input, so that

$$C_e = \frac{8}{3\pi} C_N \dot{S}$$

where  $C_e$  =  equivalent linear damping coefficient

$C_N$  =  non-linear $(V|V|)$ damping coefficient

$\dot{S}$  =  oleo stroke velocity

However, due to an error, the rms value of $\dot{S}$ was used instead of the
peak value so that, referring to Appendix C

$$C_{em} = \frac{8}{3\pi} \times 160 \times 8.05 = 1090 \ \text{lbf/in/s}$$

$$\text{i.e. } C_{em} = 13080 \ \text{lbf/ft/s}$$

$$\text{and } C_{en} = \frac{8}{3\pi} \times 43 \times 15.7 = 573 \ \text{lbf/in/s}$$

$$\text{i.e. } C_{en} = 6876 \ \text{lbf/ft/s}$$

For ease of reference all the standard aircraft parameters
used for most of the computer work are summarized in table D2,
although all values except oleo damping are the same as in Appendix C.

Program Data for Geometric Mean Runway

| Analysis Symbol | Program Identifier | Value |
|---|---|---|
| $\bar{c}_a$ | CA | $6.1 \times 10^{-7}$ |
| $n_a$ | NA | 3.58 |
| $\bar{c}_b$ | CB | $8.2 \times 10{-6}$ |
| $n_b$ | NB | 2.24 |
| Intersection $\Omega$ | OMEGA | 0.15 rad/ft |

Summary of program data for aircraft with 6 flexible modes for

initial response studies and as starting data for optimisation studies

| Analysis Symbol | Program Identifier | Value |
|---|---|---|
| $k_1$ | K1 | $1.2 \times 10^6$ lbf/ft |
| $k_2$ | K2 | 93600 lbf/ft |
| $c_1, c_{em}$ | C1 | 13080 lbf/ft/s |
| $c_2, c_{em}$ | C2 | 6876 lbf/ft/s |
| $k_{t1}$ | KT1 | $1.158 \times 10^6$ lbf/ft |
| $k_{t2}$ | KT2 | 162000 lbf/ft |
| $c_{t1}$ | CT1 | 670.8 lbf/ft/s |
| $c_{t2}$ | CT2 | 65.6 lbf/ft/s |
| d | WBASE | 59 ft |
| $\beta$ | BETA | 0.025 |
| $M_1$ | M1 | 155 slug |
| $M_2$ | M2 | 10.6 slug |
| $\lceil \overline{M}_j \rfloor$ | MJ[i,i] | $\begin{bmatrix} 9912, & 5.375 \times 10^6, & 369.36, & 278.29 \\ 701.23, & 635.84, & 742.54, & 192.46 \end{bmatrix}$ |
| $\lceil \omega_j \rfloor$ | WJ[i,i] | $\begin{bmatrix} 0, & 0, & 7.22, & 18.0 \\ 23.85, & 31.0, & 38.8, & 55.0 \end{bmatrix}$ |
| $\lceil \phi_{1}{}^{j} \rfloor$ | PHI1 | $\begin{bmatrix} 1.0, & 4.333, & -0.122, & 0.037, \\ -0.010, & 0.230, & -0.168, & -0.065 \end{bmatrix}$ |
| $\lceil \phi_{2}{}^{j} \rfloor$ | PHI2 | $\begin{bmatrix} 1.0, & -54.667, & 0.030, & 0.089, \\ 0.298, & -0.560, & 0.040, & 0.083 \end{bmatrix}$ |
| $\lceil \phi_{p}{}^{j} \rfloor$ | PHIP | $\begin{bmatrix} 1.0, & -64.583, & 0.056, & 0.103, \\ 0.383, & -0.800, & 0.080, & 0.160 \end{bmatrix}$ |

REQUIREMENT FOR AND DEVELOPMENT OF INTEGRATION METHOD

E.1 Requirement

Early versions of the Main Response Program RESPONSE 12 used a constant step length method to calculate the area under the response PSD curve. The response PSD was calculated at intervals of 1 rad/s and the values added together, in effect being multiplied by the strip width of 1 rad/s. Thus the instruction "FOR" WF: = 1 "STEP" 1 "UNTIL" 50 was in effect a mid-ordinate rule, integrating the curve from $\omega = 0.5$ to $50.5$ rad/s.

Using this method of integration to produce rms values of response acceleration, figures E1 and E2 were produced to show the variation of response at the mainwheel and pilot locations respectively with variation of main and nose oleo stiffnesses. The curves of response at the nosewheel location were very similar to those for the pilot location but generally slightly lower. The aircraft parameters other than oleo stiffnesses and the runway parameters used to produce these curves were as in Appendix D. The method was also used to calculate values to produce figure E3(a), which shows variation of rms response acceleration at mainwheel and pilot location with taxiing velocity. Again the values at the nosewheel location were slightly lower than those at the pilot location. The parameters used to produce these curves were those described in sub-section 4.3.2 taken from reference 37. Flexural modes were neglected in the production of all the above figures.

There is a considerable amount of undulation on all three figures described above. In attempts to explain these undulations the eigenvalues and eigenvectors were investigated for rigid body heave and pitch modes, curves of PSD of response acceleration against frequency were plotted, and the responses in uncoupled rigid body heave and pitch were investigated. The eigenvalues are plotted in figure E4 for the same parameters used for figures E1 and E2. It will be seen that they give no indication of any trends which should lead to the undulations. The eigenvectors too gave no such indication. Investigation of the uncoupled heave and pitch modes however led to large changes of response with velocity in an apparently inconsistent manner, particularly for the pitch case.

Figures E5 to E7 (copies of figures 4.25, 4.26 and 4.30 for ease of reference) show the PSD's of response acceleration for some extreme cases of oleo stiffness. Figures E5 and E6 use the parameters from Appendix D except that, instead of the standard oleo stiffnesses, four combinations of twice and half the main and nose oleo stiffnesses are used. The taxiing velocity for both figures is 120 ft/s. Figure E7 uses the parameters taken from reference 37 and a taxiing velocity of 40 ft/s. It is shown in sub-section 4.3.2 that the nose oleo damping in these parameters is unrealistically low. This is evidenced here by the extremely high narrow peak of the pitch mode.

It can immediately be seen from figures E5 to E7 that to use constant step lengths of 1 rad/s to integrate these curves is

quite useless, particularly in cases such as figures E6(a) and
E7. Figure 4.6 shows that the same problem will exist when the
flexural modes are considered. For the case of variation in
oleo-stiffnesses, as the stiffness increases the frequency at which
the peak on the response curve, pertaining to the affected mode,
occurs increases, and thus will sometimes coincide with a frequency
at which the PSD is calculated, and sometimes fall between two PSD
calculations. If the peak is narrow this will lead to peaks and
troughs on the response curve. Thus, the step length must be
sufficiently small to give several steps within the frequency span
of each peak. In the case of variation of response with taxiing
velocity of course, the eigenvalues remain constant as the velocity
changes, and hence the peaks do not change frequency. Thus the
undulations on the curves of figure E3(a) are not caused by this,
and in fact have a physical cause as discussed in sub-section 4.3.2.
However, figureE3(b), reproduced from figure 4.10(a) for ease of
reference, shows the correct curves of response acceleration with
varying taxiing velocity. Comparing this with figure E3(a)
indicates that the effect of using too big a step length has been
to give an overestimate of the response over the entire range. A
little thought suggests that if any of the aircraft parameters were
changed, thus changing the eigenvalues, the degree of this
overestimate would change, possibly becoming an underestimate,
depending on how close the peaks were to a frequency at which the
PSD was calculated.

Another point which emerges from examination of figures E5
to E7 is that for the case where rigid modes only are considered most

of the power in the response PSD is within a small frequency range of about 6 rad/s, so that there is little point in integrating over a range of say 50 rad/s.

Reference to figures 4.18 to 4.20, discussed in section 4.3.2.2, shows that here again, for the case of uncoupled pitch response, there is a clear requirement for a more selective integration method.

E.2  Development

Clearly a much more accurate method of integration was required in order to give correct results for the rms values of response acceleration.  Two main methods could be employed in order to achieve the desired accuracy.  Firstly very small step lengths could be used over the whole range of the integration, and secondly very small step lengths could be used at the critical frequencies (i.e. at the peaks) only.

The first of these two methods was quickly discarded as being too lengthy.  Although by far the simplest method, it would require step lengths of the order of .01 rad/s, which, even for the case where rigid body modes only were considered, would require several hundred steps.  For the case where several flexural modes were considered, requiring integration up to perhaps 60 rad/s, several thousand steps would have to be employed.  The problem would still remain of course of how to choose the step length in order to minimise the computer time required.

The second method, then, appeared potentially far more attractive in terms of minimising the computer time used. It was thus decided to use small step lengths at and near to the peaks.

The first method considered was to compute the slope of the curve at each step and shorten the step lengths as the slope increased. This is a perfectly reasonable method for what might be called more well behaved curves, but in the case of a curve such as that on figure E6(a) or 7, with very narrow high peaks, a step from A to B (fig.E(i)) would sense a small, and inaccurate, slope. In order to avoid this the program would have to start with step lengths short enough to be sure of sensing the correct slope at the peak, and thus would use smaller steps than necessary for much of the time.

Fig. E (i)
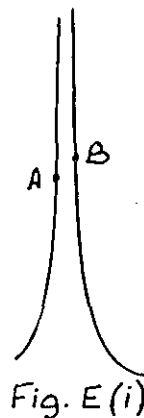
It was therefore considered necessary to find the frequencies at which the peak values occurred, and use small step lengths for a range of frequencies on either side of the peak frequencies. Brief consideration was given to scanning the frequency response function in order to find the frequencies of the peaks. This would require either a knowledge of the peak widths, or very small scanning step lengths, in order to avoid missing a peak. One method would be to scan with smaller steps over any range where the frequency response function was found to be greater than a given value, say 3.

It was finally decided that the eigenvalues should be calculated, from which the values of the frequencies at the peaks could be found. The problems thus remained of how far either side of a peak to integrate in small steps, and how small to make the steps in these regions. However, since the eigenvalues were being calculated, the bandwidths of the peaks could be found. Now the highest damping of the curves on figures E5 to E7 is that of the first peak on figure E6(a), which it will be seen is a very "flat" peak, whose eigenvalue is given by

$$\lambda = -1.328 \pm i4.788 \qquad (E - 1)$$

From this

$$\omega_d = \omega_n \sqrt{1 - \beta^2} = 4.788 \qquad (E - 2)$$

$$\beta \omega_n = 1.328 \qquad (E - 3)$$

where $\omega_d$ = damped natural frequency

$\omega_n$ = undamped natural frequency

$\beta$ = damping ratio

giving
$$\omega_n = 4.970 \text{ rad/s}$$
$$\beta = 0.2672$$

Now from the eigenvalue in equation (E-1), the damping ratio may be calculated approximately by

$$\beta = \frac{1.328}{4.788} = 0.2774$$

Thus, comparing the values of damping calculated above, and noting the very small difference between the damped and undamped natural frequencies, it may be considered that even for such a "flat" peak as this, the damping is low enough for it to be considered a high Q case, so that

$$\text{Bandwidth} \ = \ \frac{\omega_n}{Q} \ = \ \omega_n \beta \ = \ 1.328$$

The peak of course occurs at the damped natural frequency, $\omega_d$

Thus, for most damping cases considered in this report, if the eigenvalue is given by

$$\lambda = -a \pm ib$$

then

Frequency of peak $= b$ rad/s

$$\beta = \frac{a}{b}$$

$$Q = \frac{1}{\beta} = \frac{b}{a}$$

Bandwidth $= a$ rad/s

A method considered for determining the size of integrating steps, and the frequency band over which to use them, was to make both of these functions of the bandwidth, so that, for example, the width over which small steplengths were to be used would be given by

$$\Delta\omega = n \ \text{x bandwidth}$$

and the size of the steps by

$$\delta\omega = m \ \text{x} \ \frac{\text{bandwidth}}{\text{peak height}}$$

where n and m are constants.

This did not lead to a reliable method of obtaining an accurate value for the integration, and it was finally decided that a method should be used whereby an integration was done, and was successively repeated, halving the step length each time, until two successive integrations were within a given small percentage, say 1%. This could of course be done over the whole range of integration as one integration, but this would mean that however small the final step

length required at the peaks, this step length would be used over the whole integration, steps thus being unnecessarily small at non-critical parts of the curve, leading to a lrge and wasteful usage of computer time.   After much experimentation the method below was developed for the main  response program RESPONSE 12.   During this development the mid-ordinate method of integration was discarded, and a method substituted using Simpson's Rule.

### E.3 Method for Main Response Program

Figure E8 represents a curve of PSD of response acceleration against frequency.   The curve is shown for the case where rigid body heave and pitch and 1 flexural mode are considered, but the method, of course, applies to any number of modes.

The eigenvalues are calculated and the 3 frequencies $\omega_B$, $\omega_C$, and $\omega_D$ of the peaks are selected by taking the imaginary parts of the eigenvalues and discarding the negative values and the high frequencies of the nosewheel and mainwheel modes.   The three frequencies are then sorted into ascending order by the procedure SORT and put into the 2nd, 3rd and 4th spaces of a 5th order one dimensional array, the 1st and 5th spaces being reserved for $\omega_A$ and $\omega_E$ where

$$\omega_A = 0.5 \; x \, \omega_B$$
$$\omega_E = 1.4 \; x \, \omega_D$$

This array now gives 4 sets of integration limits.   These in turn are divided into sub-sets for the actual integration as follows: If $\omega_{n+1} - \omega_n < 2$ then the limits for the actual integration are $\omega_{n+1}$ and $\omega_n$.   However, if $\omega_{n+1} - \omega_n \geqslant 2$ then the limits for the actual

integration depend on whether the range being considered is a
peak to peak range (e.g. $\omega_C$ to $\omega_D$) or a range at one end of the curve
being considered (e.g. $\omega_A$ to $\omega_B$ or $\omega_D$ to $\omega_E$). The limits in these
cases are shown on figure E 8.

Thus, if $\omega_B$ = 5 rad/s, $\omega_C$ = 6.5 rad/s, $\omega_D$ = 10 rad/s,
then $\omega_A$ = 2.5 rad/s and $\omega_E$ = 14 rad/s, and the sub-sets of integration
limits are

$$\omega_A \text{ to } \omega_B - 0.5 = 2.5 \text{ to } 4.5$$
$$\omega_B - 0.5 \text{ to } \omega_B = 4.5 \text{ to } 5.0$$
$$\omega_B \text{ to } \omega_C = 5.0 \text{ to } 6.5$$
$$\omega_C \text{ to } \omega_C + 0.5 = 6.5 \text{ to } 7.0$$
$$\omega_C + 0.5 \text{ to } \omega_D - 0.5 = 7.0 \text{ to } 9.5$$
$$\omega_D - 0.5 \text{ to } \omega_D = 9.5 \text{ to } 10.0$$
$$\omega_D \text{ to } \omega_D + 0.5 = 10.0 \text{ to } 10.5$$
$$\omega_D + 0.5 \text{ to } \omega_E = 10.5 \text{ to } 14.0$$

The procedure SIMPS is now called for each sub-set of
integration limits. Procedure SIMPS uses Simpson's rule to
integrate between the two sets of limits. Now Simpson's rule
calculates the area under the curve by

$$\text{Area} = \frac{h}{3}(1\text{st} + \text{Last} + 2 \times \text{odds} + 4 \times \text{evens}) \qquad (E - 4)$$

where h is the step length

1st is the height of the first ordinate

Last is the height of the last ordinate

odds is the sum of the heights of the odd
numbered ordinates

and evens is the sum of the heights of the even
numbered ordinates

SIMPS starts by using two steps, and successively uses 4, 8 etc

until two consecutive iterations are within TOLP%, for the

responses at the mainwheel, nosewheel, and pilot locations, where

TOLP is read in with the data.    Thus,

referring to figure E(ii), it will be

seen that at each successive iteration

all the intermediate ordinates from

the previous iteration now become

odd ordinates.    Thus, to keep computer

time to a minimum for each iteration

the 1st, Last, and sum of all

intermediate ordinates are stored, to
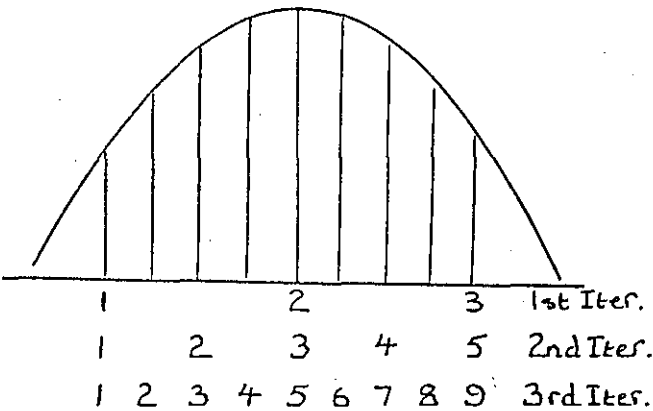
be used in the next iteration as 1st,                    Fig. E(ii)

Last and sum of odd ordinates.    Hence at each iteration only the

new even ordinates need be calculated and then used in equation

(E-4) together with previously stored values.    Procedure SIMPS

calls procedure POSPDY to calculate the height of each ordinate, and

POSPDY in turn calls procedure TRAFUN to calculate the frequency

response function at the ordinate frequency.

### E.4  Method for Uncoupled Pitch Response program

The method of integration of the response PSD curve for

uncoupled pitch response is broadly similar to the method described

above, differing only in the method of selection of the sub-sets

of integration limits.

Referring to figures 4.18 to 4.20 (Section 4), comparison

of figures 4.18 and 4.19 shows how vastly the response PSD curve

varies for taxiing velocities of 120 and 10 ft/s, using the same

aircraft parameters.    Similarly comparison of figures 4.19 and 4.20

shows how the response PSD curve varies for the same taxiing

velocity using different aircraft parameters.    Thus, using

only the damped natural frequency as a starting point for

calculating the sub-sets would be a satisfactory method for figure

4.18, but not for figures 4.19 and 4.20.

It was briefly considered that an accurate estimate of

the area could be obtained by replacing each peak by a superimposed

triangle as shown in figure E(iii).    This would of course give an
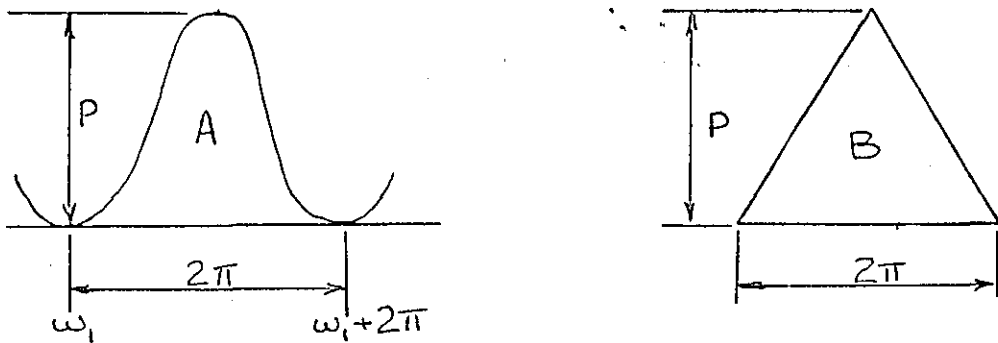


Fig. E(iii)

exact value for a sinusoidal peak, since

$$\text{Area A} = \int_{\omega_i}^{\omega_i + 2\pi} \frac{P}{2}(1 - \cos\omega)\,d\omega = P\pi$$

and

$$\text{Area B} = \frac{2\pi \times P}{2} = P\pi$$

It will be seen from figure 4.19 that for very low taxiing

velocities the peaks are approximately sinusoidal, and hence this

method would give a good approximation to the area.    However,

reference to figure 4.18 shows that the method would be grossly

inaccurate here. Thus the method of sub-section E.3 is used, the method of selecting the sub-sets of integration limits being as follows:

The damped natural frequency, $\omega_d$, is found from the pitch equivalent of equation (4-40) (Section 4). This gives the peak of the aircraft parameter dependent part of the expression for the mean-square value of pitch response acceleration, equation (4-49). The bottom and top integration limits are then set at 0.5 rad/s and $2 \times \omega_d$ rad/s, and all the values of $\omega_f$ found within this range such that

$$1 - \cos \frac{d}{V}\omega_f = 0 \text{ or } 2$$

$$\text{i.e. } \cos \frac{d}{V}\omega_f = \pm 1$$

Thus

$$\frac{d}{V}\omega_f = n\pi, \quad n = 1,2,3,4 \text{ ----}$$

giving

$$\omega_f = \frac{n\pi V}{d}$$

where  $V$ = taxiing velocity

  $d$ = longitudinal distance between nosewheel and mainwheel locations

These values give the frequencies of the peaks and troughs (zero) of the response PSD curve for the lower taxiing velocities (figure 4.19). However, for higher taxiing velocities where the first trough frequency (other than $\omega_f = 0$),

$$\text{i.e. } \omega_f = \frac{2\pi V}{d} \text{ rad/s,}$$

is greater than $\omega_d$, the first peak of $(1 - \cos \frac{d}{V}\omega_f)$,

$$\text{i.e. } \omega_f = \frac{\pi V}{d} \text{ rad/s,}$$

does not show as a peak on the response PSD curve (see figure 4.18).
Hence it is important, in order to cut down the range over which
small steps are used in the integration, toinclude $\omega_d$ in the sub-sets
of integration limits.

Thus, the sub-sets of integration limits for the uncoupled
pitch response case are given by 0.5, $\omega_d$, 2 x $\omega_d$, and the
frequencies of all the peaks and troughs of $(1 - \cos \frac{d}{V} \omega_f)$ between
0.5 and 2 x $\omega_d$.
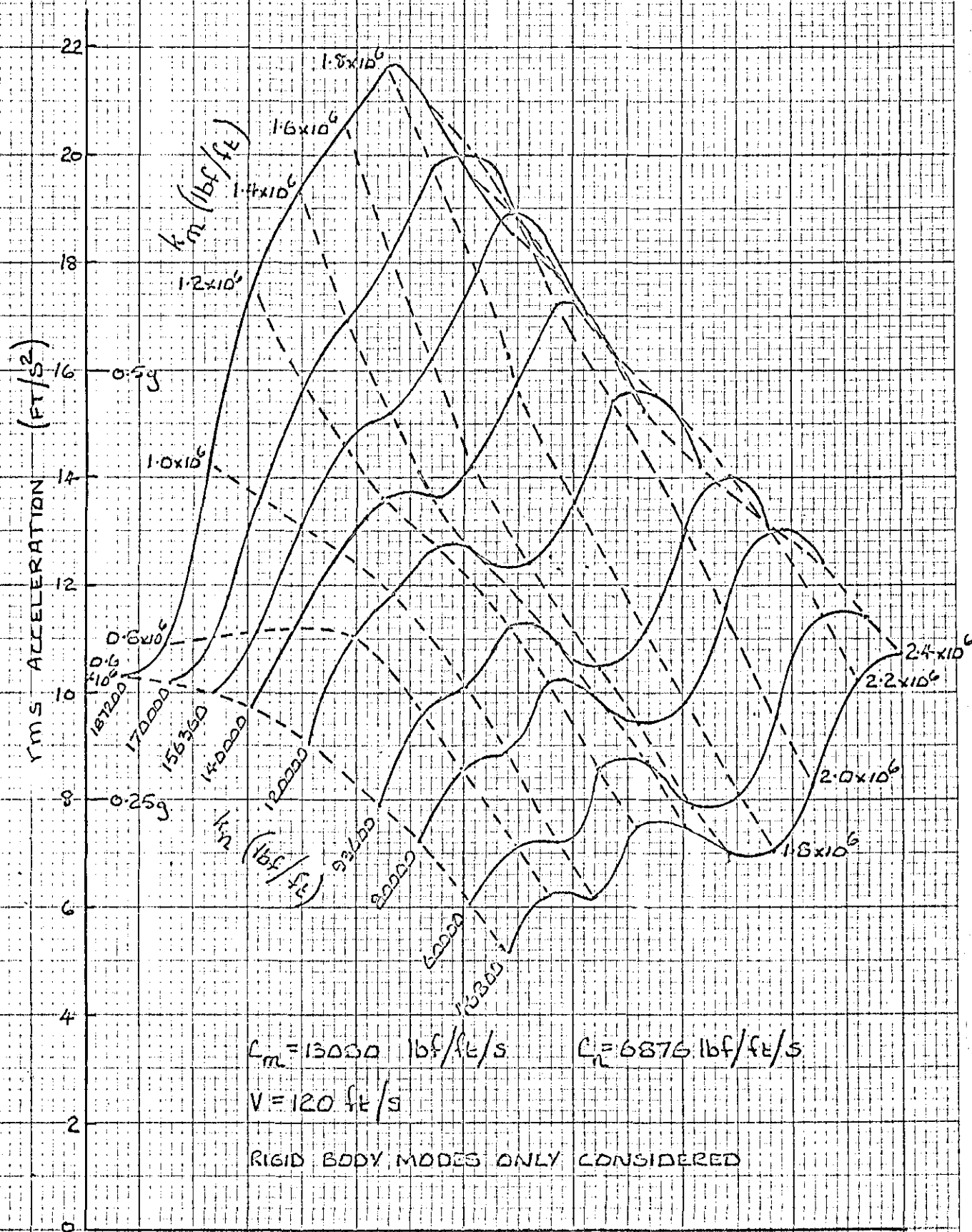
FIGURE E1

$C_m = 13080$ lbf/ft/s    $C_n = 6876$ lbf/ft/s

$V = 120$ ft/s

RIGID BODY MODES ONLY CONSIDERED

VARIATION OF MAINWHEEL LOCATION RESPONSE USING

EARLIER CONSTANT STEP LENGTH INTEGRATION PROGRAM

(c.f. figure 4.22)

FIGURE E2



$k_m \, (lbf/ft)$

rms ACCELERATION — $(Ft/S^2)$

$1.8 \times 10^6$
$1.6 \times 10^6$
$1.4 \times 10^6$
$1.2 \times 10^6$
$1.0 \times 10^6$
$0.8 \times 10^6$
$0.6 \times 10^6$
$0.6 \times 10^6$

0.5g
0.25g

181200
170000
156350
140000
120000

$k_n \, (lbf/ft)$

92400
80000
60000
40360

$2.4 \times 10^6$
$2.2 \times 10^6$
$2.0 \times 10^6$
$1.8 \times 10^6$

$C_m = 13030 \ \ lbf/ft/s \qquad C_n = 6876 \ lbf/ft/s$

$V = 120 \ ft/s$

RIGID BODY MODES ONLY CONSIDERED

VARIATION OF PILOT LOCATION RESPONSE USING

EARLIER CONSTANT STEPLENGTH INTEGRATION PROGRAM

(cf. figure 4.23)

FIGURE E 3
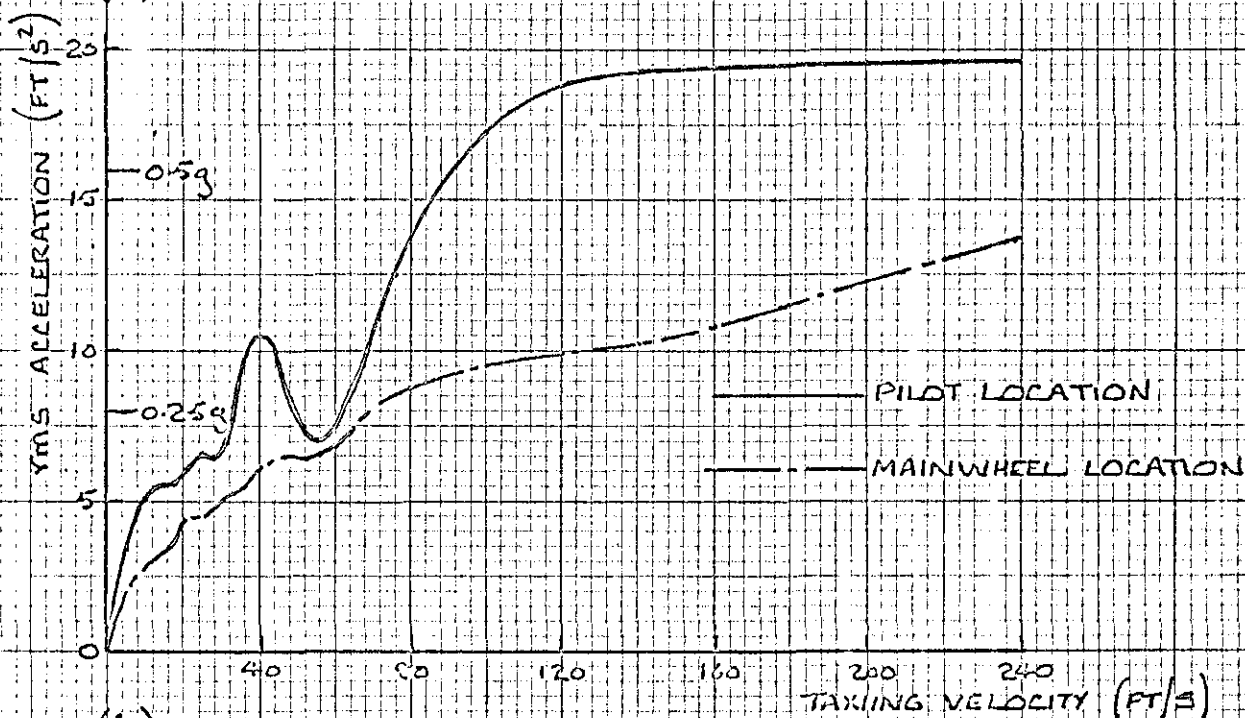
RIGID BODY MODES ONLY CONSIDERED



(a) USING EARLIER CONSTANT STEP LENGTH INTEGRATION PROGRAM

(b) USING RESPONSE 12

RESPONSE ACCELERATIONS FOR PARAMETERS IN REF.37

RIGID BODY HEAVE MODE

187200

$k_n (lbf/ft)$

140000

93600

60000

30000

45000

RIGID BODY PITCH MODE

$2.0 \times 10^6$

$1.6 \times 10^6$

$1.2 \times 10^6$

$1.0 \times 10^6$

$k_m$

$2.4 \times 10^6$

$1.6 \times 10^6$

$1.0 \times 10^6$

$k_m$

$0.6 \times 10^6$

$k_n (lbf/ft)$

60000

93600

120000

140000

156350

187200

-1.3  -1.2  -1.1  -1.0  -0.9  -0.8  -0.7  -0.6  -0.5  -0.4  -0.3
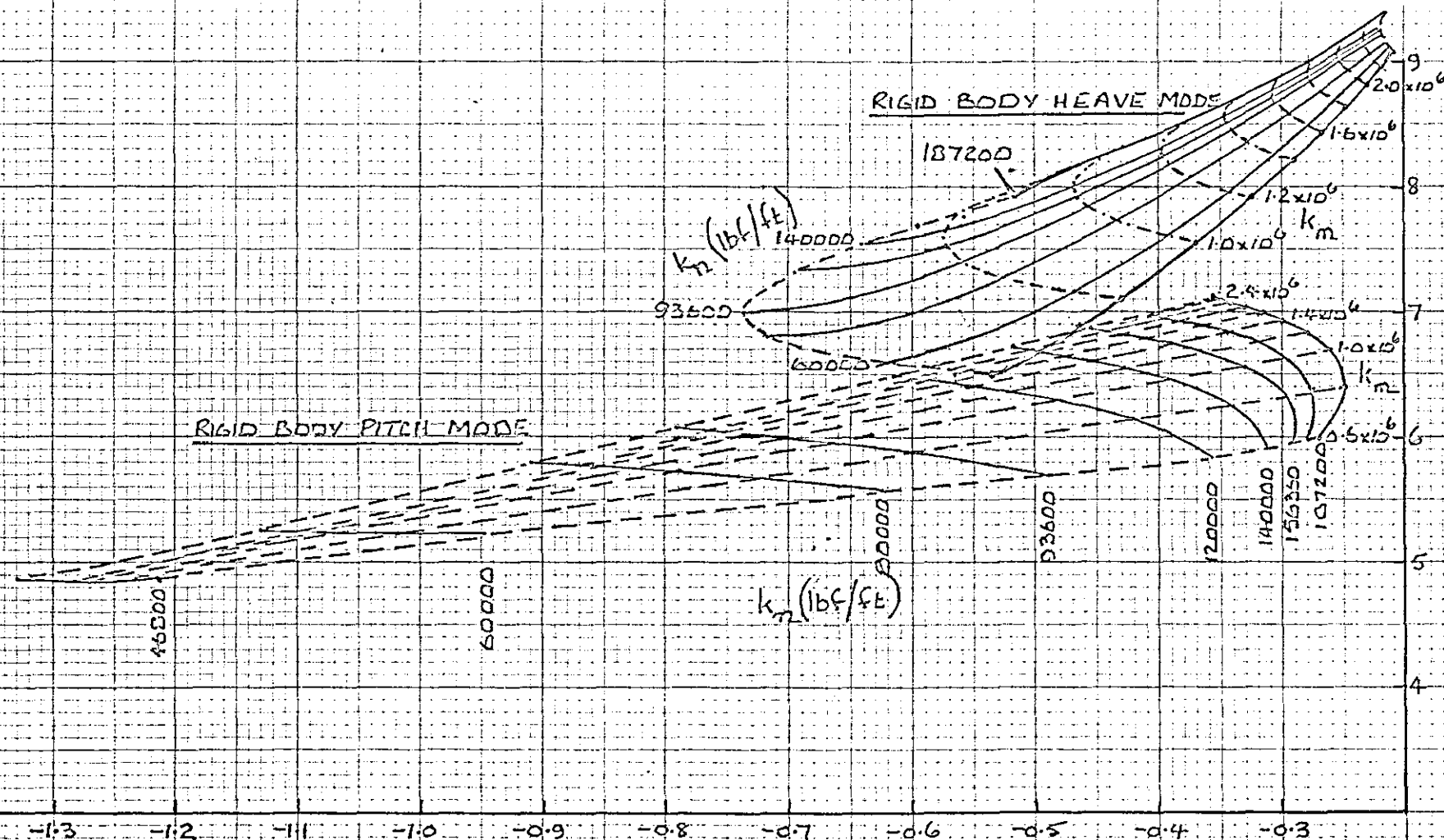
VARIATION OF EIGENVALUES WITH OLEO STIFFNESS

OTHER PARAMETERS AS APPENDIX D

RIGID BODY MODES ONLY CONSIDERED

$\omega_n = 9.380$ rad/s

$\beta = 0.0231$

$Q = 43.22$

band width $= 0.217$ rad/s.

$\omega_n = 7.122$

$\beta = 0.0501$

$Q = 19.95$

bandwidth $= 0.357$

$\omega_n = 4.788$

$\beta = 0.2543$

$Q = 3.931$

bandwidth: $1.218$

$\omega_n = 6.502$ rad/s

$\beta = 0.0824$

$Q = 12.13$

b/w $= 0.536$ rad/s

—————— PILOT LOCATION

—·—·— MAINWHEEL LOCATION

(a) $k_m = 2.4 \times 10^6$ lbf/ft      $k_n = 187200$ lbf/ft

(b) $k_m = 0.6 \times 10^6$ lbf/ft      $k_n = 46800$ lbf/ft

PSD OF RESPONSE ACCELERATION FOR PARAMETERS (EXCEPT $k_m, k_n$) AS APPENDIX D

RIGID BODY MODES ONLY CONSIDERED

$V = 120$ FT/S

(a) Graph details:

$\omega_n = 9.073 \text{ rad/s}$

$\beta = 0.0229$

$Q = 43.62$

$b/w = 0.208 \text{ rad/s}$

$\omega_n = 4.788 \text{ rad/s}$

$\beta = 0.2774$

$Q = 3.605$

bandwidth $= 1.328 \text{ rad/s}$

$\omega_f \text{ (rad/s)}$

(a)  $k_m = 2.4 \times 10^6 \text{ lbf/ft}$   $k_n = 46800 \text{ lbf/ft}$

(b) Graph details:

——— PILOT LOCATION

—·—·— MAINWHEEL LOCATION

$\omega_n = 6.005$

$\beta = 0.045$

$Q = 22.24$

$b/w = 0.270$

$\omega_n = 7.938 \text{ rad/s}$

$\beta = 0.0650$

$Q = 15.38$

$b/w = 0.516 \text{ rad/s}$

$\omega_f \text{ (rad/s)}$
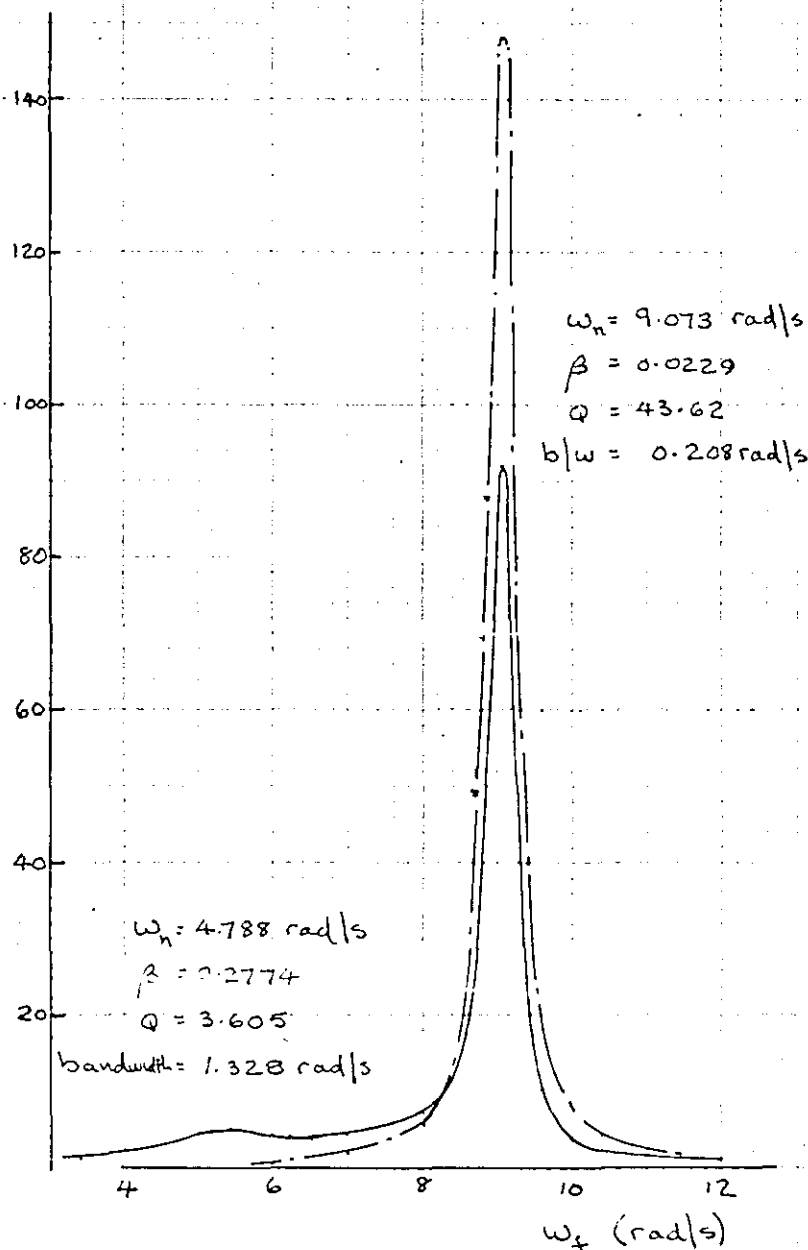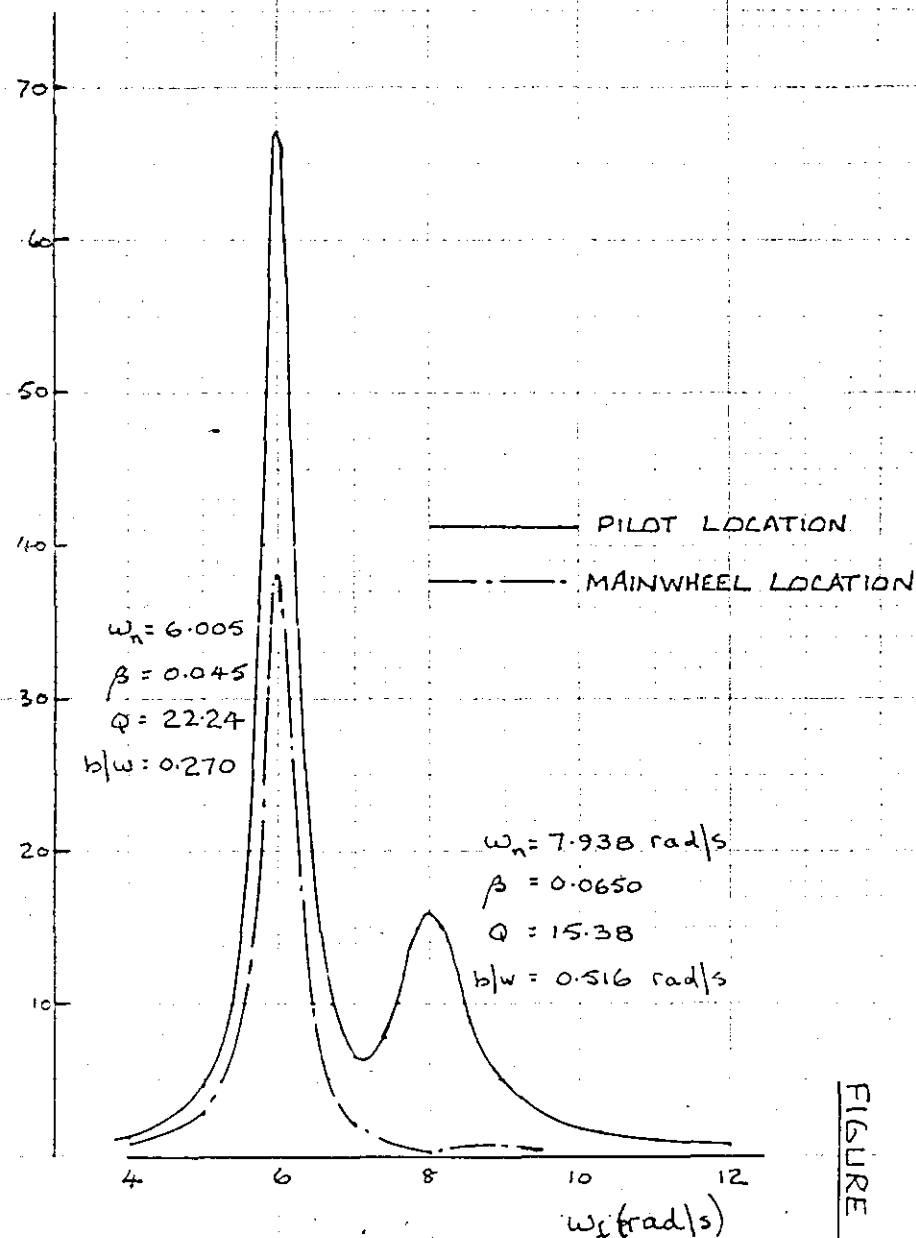
(b)  $k_m = 0.6 \times 10^6 \text{ lbf/ft}$   $k_n = 187200 \text{ lbf/ft}$

PSD OF RESPONSE ACCELERATION FOR PARAMETERS EXCEPT $(k_m, k_n)$ AS APPENDIX D

(RIGID BODY MODES ONLY CONSIDERED)    V = 120 FT/S

FIGURE E.6

289

E.R.

PSD OF RESPONSE ACCELERATION AT PILOT LOCATION

FOR PARAMETERS AS REFERENCE 37

RIGID BODY MODES ONLY CONSIDERED        V = 40 FT/S

FIGURE E8

INTERMEDIATE INTEGRATION LIMITS

291

```
RESPONSE 12;
"BEGIN" "INTEGER" NM;
       "READ" NM;
"BEGIN" "COMMENT" THIS PROGRAM COMPUTES RMS
                  ACCELERATIONS OF THE AIRCRAFT AT
                  MAINWHEELS, NOSEWHEEL AND PILOT LOCATION FOR ONE
                  TAXIING VELOCITY;
       "INTEGER" I,J,NSTEPS,SS,LOW,HI,NNEGO,JE,IE,NEIG;
       "REAL" BETA,C1,C2,K1,K2,KT1,KT2,M1,M2,CT1,CT2,
WBASE,OMEGA,V,CA,NA,CB,NB,PSDMTOT,PSDNTOT,PSDPTOT,IM1,IM2,IN1,IN2,IP1,IP2,TOLP,
       WF,WFMIN,WFMAX,WFFIN,Z1,Z2,ZP,PSDIN,PSDMOUT,PSDNOUT,PSDPOUT,RMSM,
       RMSN,RMSP,WFSTART,WFSTEP,MACHEPS;
       "REAL" "ARRAY" MJ,WJ,XW,YW,UW,VW,A,B,SMC5,SMK5[1:NM,1:NM],PHI1,
              PHI2,SMC1,SMC2,SMK1,SMK2,PHIP[1:1,1:NM],PHI1T,
              PHI2T,SMC3,SMC4,SMK3,SMK4[1:NM,1:1],C,K,MI,
              STFMX,DMPMX,UNIT[1:NM+2,1:NM+2],CMI,U[1:NM+2,1:NM+2,1:2],
              G,X[1:NM+2,1:1,1:2],XJ[1:NM,1:1,1:2],F,COEFF[1:2*(NM+2),1:2*(NM+2)],D,WR,WI[1:2*(NM+2)]
       "INTEGER" "ARRAY" CNT,INT[1:2*(NM+2)];


       "PROCEDURE" BALANCE(N,B,A,LOW,HI,D);

       "PROCEDURE" ELMHES(N,K,L,A,INT);

       "PROCEDURE" CDIV(XR,XI,YR,YI,ZR,ZI);

       "PROCEDURE" HQR2(N,LOW,UPP,MACHEPS,H,WR,WI,CNT,F,FAIL);
```

```
"PROCEDURE" TRAFUN(ARRX,ARRPHI,M,MOD);
          "VALUE" M;
          "INTEGER" M;
          "REAL" MOD;
          "ARRAY" ARRX,ARRPHI;
          "BEGIN"
                "INTEGER" Q;
                "REAL" SUMR,SUMI;
                SUMR:=SUMI:=0.0;
                "FOR" Q:=1 "STEP" 1 "UNTIL" M "DO"
                 "BEGIN"
                        SUMR:=ARRX[Q,1,1]*
                        ARRPHI[1,Q]+SUMR;
                        SUMI:=ARRX[Q,1,2]*
                        ARRPHI[1,Q]+SUMI;
                   "END";
                   MOD:=SQRT(SUMR*SUMR+SUMI*SUMI);
               "END" TRAFUN;
"PROCEDURE" SORT(ARREIG,NVAL);
"INTEGER" NVAL;
"ARRAY" ARREIG;
"BEGIN" "INTEGER" QE;
        "REAL" VALEIG;
        "BOOLEAN" INTERCHANGE;
SCAN AGAIN:   INTERCHANGE:="FALSE";
        "FOR" QE:=1 "STEP" 1 "UNTIL" NVAL-1 "DO"
        "BEGIN" "IF" ARREIG[QE]>ARREIG[QE+1] "THEN"
                "BEGIN" VALEIG:=ARREIG[QE];
                        ARREIG[QE]:=ARREIG[QE+1];
                        ARREIG[QE+1]:=VALEIG;
                        INTERCHANGE:="TRUE";
                "END";
        "END";
        "IF" INTERCHANGE "THEN" "GOTO" SCAN AGAIN;
   "PRINT" ''L2S5'NATURAL FREQUENCIES IN ASCENDING ORDER';
   "FOR" QE:=1 "STEP" 1 "UNTIL" NVAL "DO"
   "PRINT" ALIGNED(4,6),''LS19'',SAMELINE,ARREIG[QE];
"END" SORT;
```

```
"LIBRARY" FORMMX,READMX,MXTRANS,MXPROD,MXCOPY,SCPROD,
          MXSUM,CMXFORM,CMXPROD,CMXCOP,CMXINV;
"PROCEDURE" POSPDY;
        "BEGIN"                    CMXFORM(U,STFMX[I,J]-WF*WF*
        UNIT[I,J],WF*DMPMX[I,J],I,J);
        CMXFORM(G,0.0,0.0,I,J);
        G[1,1,1]:=-KT1*COS(WBASE*WF/V)+CT1*WF*SIN(WBASE*WF/V);
        G[2,1,1]:=-KT2;
        G[1,1,2]:=-KT1*SIN(WBASE*WF/V)-CT1*WF*COS(WBASE*WF/V);
        G[2,1,2]:=-CT2*WF;
        CMXPROD(X,CMI,G);
        CMXCOP(G,X);
        CMXINV(U);
        CMXPROD(X,U,G);
        "FOR" I:=1 "STEP" 1 "UNTIL" NM "DO"
        "BEGIN" XJ[I,1,1]:=X[I+2,1,1];
                XJ[I,1,2]:=X[I+2,1,2];
        "END";
        TRAFUN(XJ,PHI1,NM,Z1);
        TRAFUN(XJ,PHI2,NM,Z2);
        TRAFUN(XJ,PHIP,NM,ZP);
        "IF" WF<OMEGA*V "THEN" PSDIN:=CA*V↑(NA-1)/WF↑NA "ELSE"
        PSDIN:=CB*V↑(NB-1)/WF↑NB;
        PSDMOUT:=Z1*Z1*PSDIN*WF↑4;
        PSDNOUT:=Z2*Z2*PSDIN*WF↑4;
        PSDPOUT:=ZP*ZP*PSDIN*WF↑4;
        "END" POSPDY;
"PROCEDURE" SIMPS;
"BEGIN"
"REAL" IM2FIRST,IN2FIRST,IP2FIRST,IM2LAST,
IN2LAST,IP2LAST,IM2ODD,IN2ODD,
IP2ODD,MODDTOT,NODDTOT,PODDTOT,
IM2EVEN,IN2EVEN,IP2EVEN,MEVENTOT,
NEVENTOT,PEVENTOT;
```

```
      "FOR" NSTEPS:=2,4,2*NSTEPS "WHILE"
            TOLP<100*ABS(IM1/IM2-1) "OR"
            TOLP<100*ABS(IN1/IN2-1) "OR"
            TOLP<100*ABS(IP1/IP2-1) "DO"
      "BEGIN" "IF" NSTEPS "NE" 2 "THEN"
            "BEGIN" IM1:=IM2;
                    IN1:=IN2;
                    IP1:=IP2;
            "END";
        WFSTEP:=(WFFIN-WFSTART)/NSTEPS;
      "IF" NSTEPS=2 "THEN"
      "BEGIN" WF:=WFSTART;
            POSPDY;
            IM2FIRST:=PSDMOUT;
            IN2FIRST:=PSDNOUT;
            IP2FIRST:=PSDPOUT;
            WF:=WFFIN;
            POSPDY;
            IM2LAST:=PSDMOUT;
            IN2LAST:=PSDNOUT;
            IP2LAST:=PSDPOUT;
            WF:=WFSTART+WFSTEP;
            POSPDY;
            IM2EVEN:=PSDMOUT;
            IN2EVEN:=PSDNOUT;
            IP2EVEN:=PSDPOUT;
IM2ODD:=0.0;
IN2ODD:=0.0;
IP2ODD:=0.0;
MODDTOT:=0.0;
NODDTOT:=0.0;
PODDTOT:=0.0;
"GOTO" INTSUM;
    "END";
```

```
        MODDTOT:=2*IM2ODD;
        NODDTOT:=2*IN2ODD;
        PODDTOT:=2*IP2ODD;
        IM2EVEN:=0.0;
        IN2EVEN:=0.0;
        IP2EVEN:=0.0;
"IF" NSTEPS "NE" 2 "THEN"
    "FOR" WF:=WFSTART+WFSTEP "STEP" 2*WFSTEP "UNTIL" WFFIN "DO"
    "BEGIN" POSPDY;
            IM2EVEN:=IM2EVEN+PSDMOUT;
            IN2EVEN:=IN2EVEN+PSDNOUT;
            IP2EVEN:=IP2EVEN+PSDPOUT;
    "END";
INTSUM:     MEVENTOT:=4*IM2EVEN;
    NEVENTOT:=4*IN2EVEN;
    PEVENTOT:=4*IP2EVEN;
    IM2ODD:=IM2ODD+IM2EVEN;
    IN2ODD:=IN2ODD+IN2EVEN;
    IP2ODD:=IP2ODD+IP2EVEN;
    IM2:=(IM2FIRST+IM2LAST+MODDTOT+MEVENTOT)*WFSTEP/3;
    IN2:=(IN2FIRST+IN2LAST+NODDTOT+NEVENTOT)*WFSTEP/3;
    IP2:=(IP2FIRST+IP2LAST+PODDTOT+PEVENTOT)*WFSTEP/3;
"END" OF NSTEPS LOOP;
        PSDMTOT:=PSDMTOT+IM2+(IM2-IM1)/15;
        PSDNTOT:=PSDNTOT+IN2+(IN2-IN1)/15;
        PSDPTOT:=PSDPTOT+IP2+(IP2-IP1)/15;
        "PRINT" ''L2S40'FOR WFSTART=',SAMELINE,WFSTART,
        ''S'AND WFFIN=',WFFIN,',',
        ''S'NSTEPS=',NSTEPS"DIV"2,
        ''LS40'PSDMTOT=',PSDMTOT,
        ''S4'PSDNTOT=';PSDNTOT,
        ''S4'PSDPTOT=';PSDPTOT;
        "END" SIMPS;
        FORMMX(MJ,0.0,I,J);
        FORMMX(WJ,0.0,I,J);
```

```
"FOR" I:=1 "STEP" 1 "UNTIL" NM "DO" "READ" MJ[I,I];
"FOR" I:=1 "STEP" 1 "UNTIL" NM "DO" "READ" WJ[I,I];
"READ" BETA,C1,C2,K1,K2,CT1,CT2;
READMX(PHI1);
READMX(PHI2);
"READ" KT1,KT2,M1,M2,MACHEPS,WBASE,OMEGA,V,CA,NA,CB,NB,WFMIN,WFMAX,TOLP;
MXTRANS(PHI1T,PHI1);
MXTRANS(PHI2T,PHI2);
MXPROD(XW,PHI1T,PHI1);
MXPROD(YW,PHI2T,PHI2);
MXCOPY(UW,XW);
MXCOPY(VW,YW);
SCPROD(XW,C1);
SCPROD(YW,C2);
MXSUM(A,XW,YW);
SCPROD(UW,K1);
SCPROD(VW,K2);
MXSUM(B,UW,VW);
MXPROD(XW,MJ,WJ);
MXCOPY(YW,XW);
BETA:=2*BETA;
SCPROD(XW,BETA);
MXSUM(SMC5,XW,A);
MXPROD(XW,YW,WJ);
MXSUM(SMK5,XW,B);
MXCOPY(SMC1,PHI1);
SCPROD(SMC1,-C1);
MXCOPY(SMC2,PHI2);
SCPROD(SMC2,-C2);
MXCOPY(SMC3,PHI1T);
SCPROD(SMC3,-C1);
MXCOPY(SMC4,PHI2T);
SCPROD(SMC4,-C2);
```

```
MXCOPY(SMK1,PHI1);
SCPROD(SMK1,-K1);
MXCOPY(SMK2,PHI2);
SCPROD(SMK2,-K2);
MXCOPY(SMK3,PHI1T);
SCPROD(SMK3,-K1);
MXCOPY(SMK4,PHI2T);
SCPROD(SMK4,-K2);
FORMMX(C,0.0,I,J);
C[1,1]:=C1+CT1;
C[2,2]:=C2+CT2;
"FOR" J:=1 "STEP" 1 "UNTIL" NM "DO"
"BEGIN" C[1,J+2]:=SMC1[1,J];
        C[2,J+2]:=SMC2[1,J];
"END";
"FOR" I:=1 "STEP" 1 "UNTIL" NM "DO"
"BEGIN" C[I+2,1]:=SMC3[I,1];
        C[I+2,2]:=SMC4[I,1];
"END";
"FOR" I:=1 "STEP" 1 "UNTIL" NM "DO" "FOR" J:=1 "STEP" 1
"UNTIL" NM "DO" C[I+2,J+2]:=SMC5[I,J];
FORMMX(K,0.0,I,J);
K[1,1]:=KT1+K1;
K[2,2]:=KT2+K2;
"FOR" J:=1 "STEP" 1 "UNTIL" NM "DO"
"BEGIN" K[1,J+2]:=SMK1[1,J];
        K[2,J+2]:=SMK2[1,J];
"END";
"FOR" I:=1 "STEP" 1 "UNTIL" NM "DO"
"BEGIN" K[I+2,1]:=SMK3[I,1];
        K[I+2,2]:=SMK4[I,1];
"END";
"FOR" I:=1 "STEP" 1 "UNTIL" NM "DO" "FOR" J:=1 "STEP" 1
"UNTIL" NM "DO" K[I+2,J+2]:=SMK5[I,J];
```

```
            FORMMX(MI,0.0,I,J);
            MI[1,1]:=1/M1;
            MI[2,2]:=1/M2;
            "FOR" I:=1 "STEP" 1 "UNTIL" NM "DO"
            MI[I+2,I+2]:=1/MJ[I,I];
            MXPROD(STFMX,MI,K);
            MXPROD(DMPMX,MI,C);
            FORMMX(COEFF,0.0,I,J);
            "FOR" I:=1 "STEP" 1 "UNTIL" NM+2 "DO" "FOR" J:=1 "STEP"
            1 "UNTIL" NM+2 "DO"
            "BEGIN" COEFF[I,J]:=-DMPMX[I,J];
                    COEFF[I,J+NM+2]:=-STFMX[I,J];
            "END";
            "FOR" I:=1 "STEP" 1 "UNTIL" NM+2 "DO"
             COEFF[I+NM+2,I]:=1;
             BALANCE(2*(NM+2),2,COEFF,LOW,HI,D);
             ELMHES(2*(NM+2),LOW,HI,COEFF,INT);  HQR2(2*(NM+2),LOW,HI,MACHEPS,COEFF,WR,WI,CNI,F,FAIL);
            "PRINT" ''L2S'K1=',SAMELINE,K1,''S5'K2=',K2,
      ''S5'C1=',C1,''S5'C2=',C2,
      ''L'KT1=',KT1,''S4'KT2=',KT2,
      ''S4'CT1=',CT1,''S4'CT2=',CT2,
      ''LS2'V=',V,''L2S19'EIGENVALUES';
            "FOR" I:=1 "STEP" 1 "UNTIL" 2*(NM+2) "DO"
            "BEGIN" "PRINT"SCALED(8), ''LS9'',SAMELINE,WR[I],''S4'',WI[I];
            "END";
     NNEGO:=0;
      "FOR" I:=1 "STEP" 1 "UNTIL" 2*(NM+2) "DO"
      "IF" WI[I]<WFMIN "OR" WI[I]>WFMAX "THEN" NNEGO:=NNEGO+1;
      NEIG:=2*(NM+2)-NNEGO;
```

```
"BEGIN" "REAL" "ARRAY" EIGEN[1:NEIG],LIMINT[1:NEIG+2];
        JE:=1;
        "FOR" I:=1 "STEP" 1 "UNTIL" 2*(NM+2) "DO"
        "IF" WI[I]>WFMIN "AND" WI[I]<WFMAX "THEN"
        "BEGIN" EIGEN[JE]:=WI[I];
                JE:=JE+1;
        "END";
        "PRINT" ''L2S5`NUMBER OF NATURAL FREQUENCIES WITHIN SPECIFIED RANGE=`,SAMELINE,NEIG,
        ''L2S15`NATURAL FREQUENCIES`;
        "FOR" JE:=1 "STEP" 1 "UNTIL" NEIG "DO"
        "PRINT" ALIGNED(4,6),''LS19``,SAMELINE,EIGEN[JE];
        SORT(EIGEN,NEIG);
    LIMINT[1]:=WFMIN;
    "FOR" JE:=1 "STEP" 1 "UNTIL" NEIG "DO"
     LIMINT[JE+1]:=EIGEN[JE];
     LIMINT[NEIG+2]:=EIGEN[NEIG]+5;
    "PRINT" ''L2S15`INTEGRATION LIMITS`;
    "FOR" JE:=1 "STEP" 1 "UNTIL" NEIG+2 "DO"
    "PRINT" ALIGNED(4,6),''L2S19``,SAMELINE,LIMINT[JE];
 RESPONSE: FORMMX(UNIT,0,0,I,J);
        "FOR" I:=1 "STEP" 1 "UNTIL" NM+2 "DO" UNIT[I,I]:=1;
       CMXFORM(CMI,MI[I,J],0.0,I,J);
       READMX(PHIP);
 PSDMTOT:=0.0;
```

```
PSDNTOT:=0.0;
PSDPTOT:=0.0;
"FOR" IE:=1 "STEP" 1 "UNTIL" NEIG+1 "DO"
"IF" LIMINT[IE+1]-LIMINT[IE]<2 "THEN"
"BEGIN" WFSTART:=LIMINT[IE];
WFFIN:=LIMINT[IE+1];
SIMPS;
"END"
"ELSE" "BEGIN" WFSTART:=LIMINT[IE];
               WFFIN:=LIMINT[IE]+0.5;
               SIMPS;
               WFSTART:=LIMINT[IE]+0.5;
               WFFIN:=LIMINT[IE+1]-0.5;
               SIMPS;
               WFSTART:=LIMINT[IE+1]-0.5;
               WFFIN:=LIMINT[IE+1];
               SIMPS;
        "END";
RMSM:=SQRT(PSDMTOT);
        RMSN:=SQRT(PSDNTOT);
        RMSP:=SQRT(PSDPTOT);
        "PRINT"''L3`ACCELERATIONS    RMSM=`,
               SAMELINE,RMSM,''LS16`RMSN=`,RMSN,
               ''LS16`RMSP=`,RMSP;
"END";
"END";
    "GOTO" END;
FAIL:"PRINT" ''L`HQR2 FAILURE`;
END: "END";
```

```
BDARBHH4;
"BEGIN" "COMMENT" THIS PROGRAM COMPUTES RMS ACCELERATION OF
        THE AIRCRAFT IN THE UNCOUPLED HEAVE MODE FOR A RANGE OF TAXIING
        VELOCITIES;
        "REAL" K,KM,KN,C,CM,CN,A,B,D,P,WF,WFSTART,WFSTEP,
               WFFIN,XW,YW,ZW,M,V,OMEGA,CA,NA,CB,NB,PSDIN,PSDOUT,
               PSDTOT,RMSX;
        "READ" KM,KN,CM,CN,A,B,D,M,OMEGA,CA,NA,CB,NB,WFSTART,
               WFSTEP,WFFIN;
            "FOR" V:=10 "STEP" 10 "UNTIL" 240 "DO"
             "BEGIN"
        "PRINT" ''L3S'V=',SAMELINE,V,''L2'KM=',KM,
                ''S4'KN=',KN,''S4'CM=',CM,''S4'CN=',CN;
               K:=KM+KN;
               C:=CM+CN;
               PSDTOT:=0.0;
               P:=2*A*B/(D*D);
               "FOR" WF:=WFSTART "STEP" WFSTEP "UNTIL" WFFIN "DO"
               "BEGIN" XW:=C*WF;
                       YW:=K-M*WF*WF;
                       ZW:=(K*K+XW*XW)/(YW*YW+XW*XW);
                       XW:=1.0-P*(1.0-COS(D*WF/V));
                       "IF" WF<OMEGA*V "THEN" PSDIN:=
                       CA*V↑(NA-1)/WF↑NA "ELSE" PSDIN:=
                       CB*V↑(NB-1)/WF↑NB;
                       PSDOUT:=ZW*XW*PSDIN*WF↑4;
                       PSDTOT:=PSDTOT+PSDOUT*WFSTEP;
                             "END";
               RMSX:=SQRT(PSDTOT);
               "PRINT" ''L2'HEAVE ACCELERATION    RMSX=',
                       SAMELINE,RMSX;
    "END";
    "END";
```

```
PITCH RESPONSE 6;
"BEGIN" "COMMENT" THIS PROGRAM COMPUTES RMS ACCELERATION OF THE AIRCRAFT
        IN THE UNCOUPLED PITCH MODE AND THE RESULTING LINEAR ACCELERATIONS
        AT THE MAINWHEEL, NOSEWHEEL, AND PILOT LOCATIONS AT ONE TAXIING
        VELOCITY;
        "INTEGER" J,NW;
        "REAL" KM,KN,KE,CM,CN,CE,A,B,D,E,WF,WFSTART,WFSTEP,WFFIN,XW,YW,
        ZW,I,V,OMEGA,CA,NA,CB,NB,PSDIN,PSDOUT,PSDTOT,RMSANG,RMSM,RMSN,
        RMSP,N,WD,TOLP;
        "PROCEDURE" SORT(ARRW,NVAL);
        "INTEGER" NVAL;
        "ARRAY" ARRW;
        "BEGIN" "INTEGER" QE;
            "REAL" VALW;
            "BOOLEAN" INTERCHANGE;
SCAN AGAIN:   INTERCHANGE:="FALSE";
        "FOR" QE:=1 "STEP" 1 "UNTIL" NVAL-1 "DO"
        "BEGIN" "IF" ARRW[QE]>ARRW[QE+1] "THEN"
            "BEGIN" VALW:=ARRW[QE];
                    ARRW[QE]:=ARRW[QE+1];
                    ARRW[QE+1]:=VALW;
                    INTERCHANGE:="TRUE";
            "END";
         "END";
         "IF" INTERCHANGE "THEN" "GOTO" SCAN AGAIN;
         "END" SORT;
      "PROCEDURE" POSPDY;
         "BEGIN" XW:=CE*WF;
                 YW:=KE-I*WF*WF;
                 ZW:=2*(KE*KE+XW*XW)/(D*D*(YW*YW+XW*XW));
                 XW:=1.0-COS(D*WF/V);
               "IF" WF<OMEGA*V "THEN" PSDIN:=CA*V↑(NA-1)/WF↑NA "ELSE"
                PSDIN:=CB*V↑(NB-1)/WF↑NB;
               PSDOUT:=ZW*XW*PSDIN*WF↑4;
              "PRINT" ''L2'WF=',SAMELINE,WF,''S4'PSDOUT=',PSDOUT;
       "END" POSPDY;
```

```
"PROCEDURE" SIMPS;
    "BEGIN" "REAL" I1,I2,I2FIRST,I2LAST,I2ODD,ODDTOT,I2EVEN,
            EVENTOT,NSTEPS;
    "FOR" NSTEPS:=2,4,2*NSTEPS "WHILE" TOLP<100*ABS(I1/I2-1) "DO"
    "BEGIN" "IF" NSTEPS "NE" 2 "THEN"
        I1:=I2;
        WFSTEP:=(WFFIN-WFSTART)/NSTEPS;
        "IF" NSTEPS=2 "THEN"
    "BEGIN" "PRINT" ''L3S20'WFSTART=',SAMELINE,WFSTART,''S5'WFFIN=',WFFIN;
    WF:=WFSTART;
    POSPDY;
    I2FIRST:=PSDOUT;
    WF:=WFFIN;
    POSPDY;
    I2LAST:=PSDOUT;
    WF:=WFSTART+WFSTEP;
    POSPDY;
    I2EVEN:=PSDOUT;
    I2ODD:=0.0;
    ODDTOT:=0.0;
    "GOTO" INTSUM;
    "END";
    ODDTOT:=2*I2ODD;
    I2EVEN:=0.0;
    "IF" NSTEPS "NE" 2 "THEN"
    "FOR" WF:=WFSTART+WFSTEP "STEP" 2*WFSTEP "UNTIL" WFFIN "DO"
     "BEGIN" POSPDY;
            I2EVEN:=I2EVEN+PSDOUT;
     "END";
INTSUM:          EVENTOT:=4*I2EVEN;
    I2ODD:=I2ODD+I2EVEN;
    I2:=(I2FIRST+I2LAST+ODDTOT+EVENTOT)*WFSTEP/3;
    "PRINT" ''L2S30'NSTEPS=',SAMELINE,NSTEPS,',',''S5'I2=',I2;
     "END" NSTEPS LOOP;
     PSDTOT:=PSDTOT+I2+(I2-I1)/15;
    "PRINT" ''L2S44'PSDTOT=',SAMELINE,PSDTOT;
    "END" SIMPS;
```

```
    "READ"  V,KM,KN,CM,CN,A,B,D,E,I,OMEGA,CA,NA,CB,NB,TOLP;
   "PRINT"  ''L3S'V=`,SAMELINE,V,''L2'KM=`,
            KM,''S4'KN=`,KN,''S4'CM=`,CM,
            ''S4'CN=`,CN;
   KE:=A*A*KM+B*B*KN;
   CE:=A*A*CM+B*B*CN;
   WD:=SQRT((KE/CE)*(KE/CE)*(SQRT(1.0+2*CE*CE/(KE*I))-1.0));
   N:=2*WD*D/(3.1416*V);
   NW:=ENTIER(N)+3;
   "PRINT"  ''L2'WD=`,SAMELINE,WD,''S5'N=`,N,''S4'NW=`,NW;
   "BEGIN" "REAL" "ARRAY" LIMINT[1:NW];
      LIMINT[1]:=0.5;
      LIMINT[2]:=WD;
      LIMINT[NW]:=2*WD;
   "FOR" J:=1 "STEP" 1 "UNTIL" NW-3 "DO"
      LIMINT[J+2]:=3.1416*J*V/D;
      SORT(LIMINT,NW);
   "PRINT"  ''L3S15'INTEGRATION LIMITS';
   "FOR" J:=1 "STEP" 1 "UNTIL" NW "DO"
   "PRINT"  ALIGNED(2,6),''L2S19'',
         SAMELINE,LIMINT[J];
         PSDTOT:=0.0;
         "FOR"  J:=1 "STEP" 1 "UNTIL" NW-1 "DO"
      "BEGIN" WFSTART:=LIMINT[J];
              WFFIN:=LIMINT[J+1];
              SIMPS;
       "END";
       RMSANG:=SQRT(PSDTOT);
       RMSM:=RMSANG*A;
       RMSN:=RMSANG*B;
       RMSP:=RMSANG*E;
      "PRINT"  ''L2'PITCH ACCELERATION   RMSANG=`,
               SAMELINE,RMSANG,
               ''LS6'ACCELERATIONS  RMSM  =`,
               RMSM,''LS21'RMSN  =`,
               RMSN,''LS21'RMSP  =`,RMSP;
   "END";
"END";
```

```
"PROCEDURE" STEEP2 (LB,XS,UB,DX,XMIN,FMIN,NV,EPS,RELAX,DXMAX,
ETA,PSI,PMAX,PMULT,PDIV,ZETA,FUNK);
"VALUE" DX,NV,EPS,RELAX,ETA,PSI,DXMAX,PMAX,PMULT,PDIV,ZETA;
"INTEGER" NV;
"REAL" FMIN,EPS,RELAX,ETA,PSI,PMAX,PMULT,PDIV,ZETA;
"ARRAY"LB,XS,UB,XMIN,DX,DXMAX;"REAL" "PROCEDURE" FUNK;
"BEGIN""INTEGER" J; "REAL" ALPHA,P;
"ARRAY" XSTEP,DFDX,DFPR[1:NV];
"PROCEDURE" ATIVE;
"BEGIN" "REAL" THETA,LAMBDA,X,GAMMA;"BOOLEAN"BA;
LAMBDA:=0;
"FOR" J:=1 "STEP"1"UNTIL" NV"DO"
"BEGIN" BA:="FALSE"; ALPHA:=DX[J];
"IF" XMIN[J] + ALPHA>UB[J] "THEN"
"BEGIN"XSTEP[J]:=XMIN[J];XMIN[J]:=UB[J]-ALPHA; BA:="TRUE" "END"
"ELSE" "IF"XMIN[J]-ALPHA<LB[J] "THEN"
"BEGIN"XSTEP[J]:=XMIN[J];XMIN[J]:=LB[J]+ALPHA;BA:="TRUE" "END";
        X:=XMIN[J];
        XMIN[J]:=X+DX[J];ALPHA:=FUNK(XMIN);
        XMIN[J]:=X-DX[J];THETA:=FUNK(XMIN);
         XMIN[J]:=X;"IF" BA "THEN""BEGIN" GAMMA:=FUNK(XMIN);
             "IF" FMIN "LE" GAMMA "THEN"
             XMIN[J]:=XSTEP[J] "ELSE" FMIN:=GAMMA
    "END";
        DFDX[J]:=(ALPHA-THETA)/(2*DX[J]);
        LAMBDA:=LAMBDA+DFDX[J]↑2;
"IF" ALPHA-FMIN>0"AND"THETA-FMIN>0 "THEN" "GOTO" END;
THETA:=ABS((ALPHA-THETA)/("IF"ABS(FMIN)<PSI"THEN"PSI"ELSE"FMIN));
"IF"THETA>ETA "THEN" DX[J]:=.3*DX[J] "ELSE"
"BEGIN"DX[J]:=3*DX[J];"IF"DX[J]>DXMAX[J]"THEN"DX[J]:=DXMAX[J] "END";
END:"END" FOR;
LAMBDA:=SQRT(LAMBDA);
"FOR" J:=1"STEP"1"UNTIL"NV"DO" DFDX[J]:=DFDX[J]/LAMBDA
"END" PROCEDURE ATIVE;
```

```
"PROCEDURE" STEP;
"BEGIN""FOR"J:=1"STEP"1"UNTIL"NV"DO"
"BEGIN"ALPHA:=(1-RELAX)*DFDX[J]+RELAX*DFPR[J];
XSTEP[J]:=XMIN[J]-P*ALPHA*
("IF"ABS(XMIN[J])<ZETA"THEN"ZETA"ELSE"ABS(XMIN[J]));
DFPR[J]:=ALPHA;
"IF"XSTEP[J]>UB[J]"THEN"XSTEP[J]:=UB[J]
"ELSE""IF"XSTEP[J]<LB[J]"THEN"XSTEP[J]:=LB[J]
"END"FOR;
"END"STEP;
P:=1;
"FOR" J:=1"STEP"1"UNTIL"NV"DO"
"BEGIN" XMIN[J]:=XS[J];DFPR[J]:=0 "END";FMIN:=FUNK(XMIN);
DERIV:ATIVE;
NEXT:STEP;
ALPHA:=FUNK(XSTEP);
"IF"ALPHA<FMIN"THEN"
"BEGIN"FMIN:=ALPHA;P:=PMULT*P;
      "PRINT" ''L2'P=',SAMELINE,P;
      "IF"P>PMAX"THEN"P:=PMAX;
      "FOR"J:=1"STEP"1"UNTIL"NV"DO"XMIN[J]:=XSTEP[J];
      "GOTO" DERIV "END";
P:=P/PDIV;
"PRINT" ''L2'P=',SAMELINE,P;
"IF"P>EPS"THEN" "GOTO" NEXT;
"END"STEEP2;
```

```
BDARBH60;
"BEGIN" "INTEGER" NM,NV;
        "READ" NM,NV;
"BEGIN" "COMMENT" THIS PROGRAM MINIMISES THE SUM OF THE RMS
                  ACCELERATIONS OF THE AIRCRAFT AT
                  MAINWHEELS AND PILOT LOCATION FOR ONE
                  TAXIING VELOCITY FOR VARIABLE K1 AND K2;
        "INTEGER" I,J,NSTEPS,SS,LOW,HI,NNEGO,JE,IE,NEIG,COUNT;
        "REAL" BETA,C1,C2,K1,K2,KT1,KT2,M1,M2,CT1,CT2,
WBASE,OMEGA,V,CA,NA,CB,NB,PSDMTOT,PSDNTOT,PSDPTOT,IM1,IM2,IN1,IN2,IP1,IP2,TOLP,
        WF,WFMIN,WFMAX,WFFIN,Z1,Z2,ZP,PSDIN,PSDMOUT,PSDNOUT,PSDPOUT,RMSM,
        RMSN,RMSP,WFSTART,WFSTEP,MACHEPS,FMIN,EPS,RELAX,PMAX,ZETA,PSI,ETA;
        "REAL" "ARRAY" MJ,WJ,XW,YW,UW,VW,A,B,SMC5,SMK5[1:NM,1:NM],PHI1,
        PHI2,SMC1,SMC2,SMK1,SMK2,PHIP[1:1,1:NM],PHI1T,
        PHI2T,SMC3,SMC4,SMK3,SMK4[1:NM,1:1],C,K,MI,
        STFMX,DMPMX,UNIT[1:NM+2,1:NM+2],CMI,U[1:NM+2,1:NM+2,1:2],XS,LB,UB,XMIN,DX,DXMAX[1:NV],
        G,XT[1:NM+2,1:1,1:2],XJ[1:NM,1:1,1:2],F,COEFF[1:2*(NM+2),1:2*(NM+2)],D,WR,WI[1:2*(NM+2)]
        "INTEGER" "ARRAY" CNT,INT[1:2*(NM+2)];



        "PROCEDURE" BALANCE(N,B,A,LOW,HI,D);

        "PROCEDURE" ELMHES(N,K,L,A,INT);

        "PROCEDURE" CDIV(XR,XI,YR,YI,ZR,ZI);

        "PROCEDURE" HQR2(N,LOW,UPP,MACHEPS,H,WR,WI,CNT,F,FAIL);
```

```
        "PROCEDURE" TRAFUN(APPX,ARRPHI,M,MOD);

        "PROCEDURE" SORT(ARRSIG,NVAL);

        "LIBRARY" FORMMX,READMX,MXTRANS,MXPROD,MXCOPY,SCPROD,
                  MXSUM,CMXFORM,CMXPROD,CMXCOP,CMXINV;

        "PROCEDURE" POSPDY;

        "PROCEDURE" SIMPS;



"REAL" "PROCEDURE" FUNK(X);
      "ARRAY" X;
"COMMENT" IN THIS PROCEDURE X(1)=K1,X(2)=K2;
"BEGIN" COUNT:=COUNT+1;
      "PRINT" '?L3'ENTRY TO FUNK',SAMELINE,COUNT;
          MXPROD(XW,PHI1T,PHI1);
          MXPROD(YW,PHI2T,PHI2);
          MXCOPY(UW,XW);
          MXCOPY(VW,YW);
          SCPROD(XW,C1);
          SCPROD(YW,C2);
          MXSUM(A,XW,YW);
          SCPROD(UW,X[1]);
          SCPROD(VW,X[2]);
          MXSUM(B,UW,VW);
          MXPROD(XW,MJ,WJ);
          MXCOPY(YW,XW);
          SCPROD(XW,BETA);
          MXSUM(SMC5,XW,A);
          MXPROD(XW,YW,WJ);
          MXSUM(SMK5,XW,B);
```

```
MXCOPY(SMC1,PHI1);
SCPROD(SMC1,-C1);
MXCOPY(SMC2,PHI2);
SCPROD(SMC2,-C2);
MXCOPY(SMC3,PHI1T);
SCPROD(SMC3,-C1);
MXCOPY(SMC4,PHI2T);
SCPROD(SMC4,-C2);
MXCOPY(SMK1,PHI1);
SCPROD(SMK1,-X[1]);
MXCOPY(SMK2,PHI2);
SCPROD(SMK2,-X[2]);
MXCOPY(SMK3,PHI1T);
SCPROD(SMK3,-X[1]);
MXCOPY(SMK4,PHI2T);
SCPROD(SMK4,-X[2]);
FORMMX(C,0.0,I,J);
C[1,1]:=C1+CT1;
C[2,2]:=C2+CT2;
"FOR" J:=1 "STEP" 1 "UNTIL" NM "DO"
"BEGIN" C[1,J+2]:=SMC1[1,J];
        C[2,J+2]:=SMC2[1,J];
"END";
"FOR" I:=1 "STEP" 1 "UNTIL" NM "DO"
"BEGIN" C[I+2,1]:=SMC3[I,1];
        C[I+2,2]:=SMC4[I,1];
"END";
"FOR" I:=1 "STEP" 1 "UNTIL" NM "DO" "FOR" J:=1 "STEP" 1

"UNTIL" NM "DO" C[I+2,J+2]:=SMC5[I,J];
FORMMX(K,0.0,I,J);
K[1,1]:=KT1+X[1];
K[2,2]:=KT2+X[2];
"FOR" J:=1 "STEP" 1 "UNTIL" NM "DO"
"BEGIN" K[1,J+2]:=SMK1[1,J];
        K[2,J+2]:=SMK2[1,J];
"END";
```

```
"FOR" I:=1 "STEP" 1 "UNTIL" NM "DO"
"BEGIN" K[I+2,1]:=SMK3[I,1];
        K[I+2,2]:=SMK4[I,1];
"END";
"FOR" I:=1 "STEP" 1 "UNTIL" NM "DO" "FOR" J:=1 "STEP" 1
"UNTIL" NM "DO" K[I+2,J+2]:=SMK5[I,J];
MXPROD(STFMX,MI,K);
MXPROD(DMPMX,MI,C);
FORMMX(COEFF,0.0,I,J);
"FOR" I:=1 "STEP" 1 "UNTIL" NM+2 "DO" "FOR" J:=1 "STEP"
1 "UNTIL" NM+2 "DO"
"BEGIN" COEFF[I,J]:=-DMPMX[I,J];
        COEFF[I,J+NM+2]:=-STFMX[I,J];
"END";
"FOR" I:=1 "STEP" 1 "UNTIL" NM+2 "DO"
 COEFF[I+NM+2,I]:=1;
 BALANCE(2*(NM+2),2,COEFF,LOW,HI,D);
 ELMHES(2*(NM+2),LOW,HI,COEFF,INT);   HQR2(2*(NM+2),LOW,HI,MACHEPS,COEFF,WR,WI,CNT,F,FAIL);
 "PRINT" ''L4S'K1=',SAMELINE,X[1],''S5'K2=',X[2],
''S5'C1=',C1,''S5'C2=',C2,
''L2'KT1=',KT1,''S4'KT2=',KT2,
''S4'CT1=',CT1,''S4'CT2=',CT2,
''L2S2'V=',V;
NNEGO:=0;
 "FOR" I:=1 "STEP" 1 "UNTIL" 2*(NM+2) "DO"
 "IF" WI[I]<WFMIN "OR" WI[I]>WFMAX "THEN" NNEGO:=NNEGO+1;
 NEIG:=2*(NM+2)-NNEGO;
 "BEGIN" "REAL" "ARRAY" EIGEN[1:NEIG],LIMINT[1:NEIG+2];
        JE:=1;
        "FOR" I:=1 "STEP" 1 "UNTIL" 2*(NM+2) "DO"
        "IF" WI[I]>WFMIN "AND" WI[I]<WFMAX "THEN"
        "BEGIN" EIGEN[JE]:=WI[I];
                JE:=JE+1;
        "END";
        "PRINT" ''L3S5'NUMBER OF NATURAL FREQUENCIES WITHIN SPECIFIED RANGE=',SAMELINE,NEIG;
        SORT(EIGEN,NEIG);
```

```
        LIMINT[1]:=EIGEN[1]/2;
        "FOR" JE:=1 "STEP" 1 "UNTIL" NEIG "DO"      LIMINT[JE+1]:=EIGEN[JE];
         LIMINT[NEIG+2]:=EIGEN[NEIG]*1.4;
        "PRINT" ''L3S15'INTEGRATION LIMITS';
        "FOR" JE:=1 "STEP" 1 "UNTIL" NEIG+2 "DO"
        "PRINT" ALIGNED(4,6);''L2S19'',SAMELINE,LIMINT[JE];
PSDMTOT:=0.0;
PSDNTOT:=0.0;
PSDPTOT:=0.0;
"FOR" IE:=1 "STEP" 1 "UNTIL" NEIG+1 "DO"
"IF" LIMINT[IE+1]-LIMINT[IE]<2 "THEN"
"BEGIN" WFSTART:=LIMINT[IE];
WFFIN:=LIMINT[IE+1];
SIMPS;
"END"
"ELSE" "BEGIN"

        "IF" IE=1 "THEN"
        "BEGIN" WFSTART:=LIMINT[IE];
                WFFIN:=LIMINT[IE+1]-0.5;
                SIMPS;
                WFSTART:=LIMINT[IE+1]-0.5;
                WFFIN:=LIMINT[IE+1];
                SIMPS;
        "END"
        "ELSE" "IF" IE=NEIG+1 "THEN"
        "BEGIN" WFSTART:=LIMINT[IE];
                WFFIN:=LIMINT[IE]+0.5;
                SIMPS;
                WFSTART:=LIMINT[IE]+0.5;
                WFFIN:=LIMINT[IE+1];
                SIMPS;
        "END"
```

```
                "ELSE"
                "BEGIN"  WFSTART:=LIMINT[IE];
                         WFFIN:=LIMINT[IE]+0.5;
                         SIMPS;
                         WFSTART:=LIMINT[IE]+0.5;
                         WFFIN:=LIMINT[IE+1]-0.5;
                         SIMPS;
                         WFSTART:=LIMINT[IE+1]-0.5;
                         WFFIN:=LIMINT[IE+1];
                         SIMPS;
                "END"
                "END";
     RMSM:=SQRT(PSDMTOT);
                RMSN:=SQRT(PSDNTOT);
                RMSP:=SQRT(PSDPTOT);
                "PRINT"''L3'ACCELERATIONS   RMSM=',
                         SAMELINE,RMSM,''LS16'RMSN=',RMSN,
                         ''LS16'RMSP=',RMSP;
     "END";
     FUNK:=RMSM+RMSP;
     "PRINT" ''L2S16'FUNK=',SAMELINE,RMSM+RMSP;
     "END" FUNK;


     "PROCEDURE" STEEP2 (LB,XS,UB,DX,XMIN,FMIN,NV,EPS,RELAX,DXMAX,
     ETA,PSI,PMAX,ZETA,FUNK);


        FORMMX(MJ,0.0,I,J);
        FORMMX(WJ,0.0,I,J);
        "FOR" I:=1 "STEP" 1 "UNTIL" NM "DO" "READ" MJ[I,I];
        "FOR" I:=1 "STEP" 1 "UNTIL" NM "DO" "READ" WJ[I,I];
        "READ" BETA,C1,C2,K1,K2,CT1,CT2;
        READMX(PHI1);
        READMX(PHI2);
```

```
"READ" KT1,KT2,M1,M2,MACHEPS,WBASE,OMEGA,V,CA,
NA,CB,NB,WFMIN,WFMAX,TOLP;
MXTRANS(PHI1T,PHI1);
MXTRANS(PHI2T,PHI2);
BETA:=2*BETA;
FORMMX(MI,0.0,I,J);
MI[1,1]:=1/M1;
MI[2,2]:=1/M2;
"FOR" I:=1 "STEP" 1 "UNTIL" NM "DO"
MI[I+2,I+2]:=1/MJ[I,I];
FORMMX(UNIT,0.0,I,J);
"FOR" I:=1 "STEP" 1 "UNTIL" NM+2 "DO" UNIT[I,I]:=1;
CMXFORM(CMI,MI[I,J],0.0,I,J);
READMX(PHIP);
COUNT:=0;
XS[1]:=K1;
XS[2]:=K2;

      LB[1]:=XS[1]/2;
      UB[1]:=XS[1]*2;
       LB[2]:=XS[2]/2;
       UB[2]:=XS[2]*2;
      DX[1]:=XS[1]/50;
      DX[2]:=XS[2]/50;
      DXMAX[1]:=XS[1]/5;
      DXMAX[2]:=XS[2]/5;
       "READ" EPS,PSI,ZETA,ETA,RELAX,PMAX;
       STEEP2(LB,XS,UB,DX,XMIN,FMIN,NV,EPS,RELAX,DXMAX,
              ETA,PSI,PMAX,ZETA,FUNK);
       "PRINT" ''L3'OPTIMUM VALUES ARE',
               ''L'ACCELERATION    RMSM+RMSP=',
               SAMELINE,FMIN,''LS22'K1=',
               XMIN[1],''S4'K2=',XMIN[2];
"END";
    "GOTO" END;
FAIL:"PRINT" ''L'HQR2 FAILURE';
END: "END";
```

```
OPTIMISATION ON APPROXIMATE RESPONSE FUNCTION 5;
"BEGIN" "INTEGER" NM,NV:
"REAL" SUMRW,DIFWF:
        "READ" NM,NV;
"BEGIN" "COMMENT" THIS PROGRAM MINIMISES THE SUM OF SIMPLE APPROXIMATIONS TO THE RMS
                  ACCELERATIONS OF THE AIRCRAFT AT
                  MAINWHEELS AND PILOT LOCATION FOR ONE
                  TAXIING VELOCITY FOR VARIABLE MAINWHEEL AND NOSEWHEEL POSITION;
        "INTEGER" I,J,SS,LOW,HI,NNEGO,JE,IE,NEIG,COUNT;
        "REAL" BETA,C1,C2,K1,K2,KT1,KT2,M1,M2,CT1,CT2,
            OK1,OK2,OC1,OC2,OKT1,OKT2,OCT1,OCT2,OM1,OM2,ODMAIN,ODNOSE,NDMAIN,MNMULT,NSMULT,
WBASE,OMEGA,V,CA,NA,CB,NB,PSDMTOT,PSDNTOT,PSDPTOT,BWMULT,
            WF,WFMIN,WFMAX,Z1,Z2,ZP,PSDIN,PSDMOUT,PSDNOUT,PSDPOUT,RMSM,
            RMSN,RMSP,MACHEPS ,FMIN,EPS,RELAX,PMAX,PMULT,PDIV,ZETA,PSI,ETA;
        "REAL" "ARRAY" MJ,WJ,XW,YW,UW,VW,A,B,SMC5,SMK5[1:NM,1:NM],PHI1,
            PHI2,SMC1,SMC2,SMK1,SMK2,PHIP[1:1,1:NM],PHI1T,
            PHI2T,SMC3,SMC4,SMK3,SMK4[1:NM,1:1],C,K,MI,
            STFMX,DMPMX,UNIT[1:NM+2,1:NM+2],CMI,U[1:NM+2,1:NM+2,1:2],XS,LB,UB,XMIN,DX,DXMAX[1:NV],
            G,XT[1:NM+2,1:1,1:2],XJ[1:NM,1:1,1:2],F,COEFF[1:2*(NM+2),1:2*(NM+2)],D,WR,WI[1:2*(NM+2):
        "INTEGER" "ARRAY" CNT,INT[1:2*(NM+2)];



        "PROCEDURE" BALANCE(N,B,A,LOW,HI,D);

        "PROCEDURE" ELMHES(N,K,L,A,INT);

        "PROCEDURE" CDIV(XR,XI,YR,YI,ZR,ZI);

        "PROCEDURE" HQR2(N,LOW,UPP,MACHEPS,H,WR,WI,CNT,F,FAIL);
```

```
        "PROCEDURE" TRAFUN(ARRX,ARRPHI,M,MOD);

        "LIBRARY" FORMMX,READMX,MXTRANS,MXPROD,MXCOPY,SCPROD,
                  MXSUM,CMXFORM,CMXPROD,CMXCOP,CMXINV;

        "PROCEDURE" POSPDY;



"REAL" "PROCEDURE" FUNK(X);
      "ARRAY" X;
"COMMENT" IN THIS PROCEDURE X(1)=PHI1[1,2];
"BEGIN" COUNT:=COUNT+1;
      "PRINT" ''L2S5'ENTRY TO FUNK',SAMELINE,COUNT,''S5'V=',V;
        PHI1[1,2]:=X[1];
        PHI2[1,2]:=PHI1[1,2]-WBASE;
        MNMULT:=ABS(PHI2[1,2]/ODNOSE);
        NSMULT:=PHI1[1,2]/ODMAIN;
        K1:=OK1*MNMULT;
        C1:=OC1*MNMULT;
        KT1:=OKT1*MNMULT;
        CT1:=OCT1*MNMULT;
        K2:=OK2*NSMULT;
        C2:=OC2*NSMULT;
        KT2:=OKT2*NSMULT;
        CT2:=OCT2*NSMULT;
        M1:=OM1*MNMULT;
        M2:=OM2*NSMULT;
        MXTRANS(PHI1T,PHI1);
        MXTRANS(PHI2T,PHI2);
        MI[1,1]:=1/M1;
        MI[2,2]:=1/M2;
        CMI[1,1,1]:=MI[1,1];
        CMI[2,2,1]:=MI[2,2];
```

```
MXPROD(XW,PHI1T,PHI1);
MXPROD(YW,PHI2T,PHI2);
MXCOPY(UW,XW);
MXCOPY(VW,YW);
SCPROD(XW,C1);
SCPROD(YW,C2);
MXSUM(A,XW,YW);
SCPROD(UW,K1);
SCPROD(VW,K2);
MXSUM(B,UW,VW);
MXPROD(XW,MJ,WJ);
MXCOPY(YW,XW);
SCPROD(XW,BETA);
MXSUM(SMC5,XW,A);
MXPROD(XW,YW,WJ);
MXSUM(SMK5,XW,B);
MXCOPY(SMC1,PHI1);
SCPROD(SMC1,-C1);
MXCOPY(SMC2,PHI2);
SCPROD(SMC2,-C2);
MXCOPY(SMC3,PHI1T);
SCPROD(SMC3,-C1);
MXCOPY(SMC4,PHI2T);
SCPROD(SMC4,-C2);
MXCOPY(SMK1,PHI1);
SCPROD(SMK1,-K1);
MXCOPY(SMK2,PHI2);
SCPROD(SMK2,-K2);
MXCOPY(SMK3,PHI1T);
SCPROD(SMK3,-K1);
MXCOPY(SMK4,PHI2T);
SCPROD(SMK4,-K2);
FORMMX(C,0.0,I,J);
C[1,1]:=C1+CT1;
C[2,2]:=C2+CT2;
```

```
"FOR" J:=1 "STEP" 1 "UNTIL" NM "DO"
"BEGIN" C[1,J+2]:=SMC1[1,J];
        C[2,J+2]:=SMC2[1,J];
"END";
"FOR" I:=1 "STEP" 1 "UNTIL" NM "DO"
"BEGIN" C[I+2,1]:=SMC3[I,1];
        C[I+2,2]:=SMC4[I,1];
"END";
"FOR" I:=1 "STEP" 1 "UNTIL" NM "DO" "FOR" J:=1 "STEP" 1
"UNTIL" NM "DO" C[I+2,J+2]:=SMC5[I,J];
FORMMX(K,0.0,I,J);
K[1,1]:=KT1+K1;
K[2,2]:=KT2+K2;
"FOR" J:=1 "STEP" 1 "UNTIL" NM "DO"
"BEGIN" K[1,J+2]:=SMK1[1,J];
        K[2,J+2]:=SMK2[1,J];
"END";
"FOR" I:=1 "STEP" 1 "UNTIL" NM "DO"
"BEGIN" K[I+2,1]:=SMK3[I,1];
        K[I+2,2]:=SMK4[I,1];
"END";
"FOR" I:=1 "STEP" 1 "UNTIL" NM "DO" "FOR" J:=1 "STEP" 1
"UNTIL" NM "DO" K[I+2,J+2]:=SMK5[I,J];
MXPROD(STFMX,MI,K);
MXPROD(DMPMX,MI,C);
FORMMX(COEFF,0.0,I,J);
"FOR" I:=1 "STEP" 1 "UNTIL" NM+2 "DO" "FOR" J:=1 "STEP"
1 "UNTIL" NM+2 "DO"
"BEGIN" COEFF[I,J]:=-DMPMX[I,J];
        COEFF[I,J+NM+2]:=-STFMX[I,J];
"END";
"FOR" I:=1 "STEP" 1 "UNTIL" NM+2 "DO"
 COEFF[I+NM+2,I]:=1;
 BALANCE(2*(NM+2),2,COEFF,LOW,HI,D);
```

```
          ELMHES(2*(NM+2),LOW,HI,COEFF,INT);   HQR2(2*(NM+2),LOW,HI,MACHEPS,COEFF,WR,WI,CNT,F,FAIL);
       "PRINT"''L2S2'NDMAIN=',SAMELINE,PHI1[1,2], ''L2S6'K1=',K1,''S5'K2=',K2,
    ''S5'C1=',C1,''S5'C2=',C2,
    ''L2S5'KT1=',KT1,''S4'KT2=',KT2,
    ''S4'CT1=',CT1,''S4'CT2=',CT2.
    ''L2S6'M1=',M1,''S5'M2=',M2;
  NNEGO:=0;
   "FOR" I:=1 "STEP" 1 "UNTIL" 2*(NM+2) "DO"
   "IF" WI[I]<WFMIN "OR" WI[I]>WFMAX "THEN" NNEGO:=NNEGO+1;
   NEIG:=2*(NM+2)-NNEGO;
   "BEGIN" "REAL" "ARRAY" EIGEN[1:NEIG,1:1,1:2],PSDM,PSDN,PSDP[1:NEIG];
          JE:=1;
          "FOR" I:=1 "STEP" 1 "UNTIL" 2*(NM+2) "DO"
          "IF" WI[I]>WFMIN "AND" WI[I]<WFMAX "THEN"
          "BEGIN" EIGEN[JE,1,1]:=-WR[I];
              EIGEN[JE,1,2]:=WI[I];
                  JE:=JE+1;
          "END";
          "PRINT" ''L2S10'NUMBER OF EIGENVALUES WITHIN SPECIFIED RANGE=',SAMELINE,NEIG,
      ''L2S24'EIGENVALUES';
   "FOR" JE:=1 "STEP" 1 "UNTIL" NEIG "DO"
   "PRINT" ALIGNED(4,6),''L2S13'',SAMELINE,EIGEN[JE,1,1],''S4'',EIGEN[JE,1,2];
  PSDMTOT:=0.0;
  PSDNTOT:=0.0;
  PSDPTOT:=0.0;
   "FOR" JE:=1 "STEP" 1 "UNTIL" NEIG "DO"
   "BEGIN" WF:=EIGEN[JE,1,2];
          POSPDY;
          PSDM[JE]:=PSDMOUT;
          PSDN[JE]:=PSDNOUT;
          PSDP[JE]:=PSDPOUT;
          PSDMTOT:=EIGEN[JE,1,1]*PSDM[JE]+PSDMTOT;
          PSDNTOT:=EIGEN[JE,1,1]*PSDN[JE]+PSDNTOT;
          PSDPTOT:=EIGEN[JE,1,1]*PSDP[JE]+PSDPTOT;
  "END";
```

```
RMSM:=SQRT(PSDMTOT);
RMSN:=SQRT(PSDNTOT);
RMSP:=SQRT(PSDPTOT);
"IF" NEIG=2 "THEN"
"BEGIN" SUMBW:=EIGEN[1,1,1]+EIGEN[2,1,1];
        DIFWF:=ABS(0.75*(EIGEN[1,1,2]-EIGEN[2,1,2]));
        "IF" DIFWF<0.2 "OR"
            DIFWF<0.033*EIGEN[2,1,2]"OR"
            DIFWF<0.05*SUMBW "THEN"
            "GOTO" APFAIL;
        "IF" SUMBW>DIFWF "THEN"
        "BEGIN" BWMULT:=SQRT(DIFWF/SUMBW);
                RMSM:=BWMULT*RMSM;
                RMSN:=BWMULT*RMSN;
                RMSP:=BWMULT*RMSP;
            "END";
    "END";
    "PRINT"''L2S5'ACCELERATION APPROXIMATIONS   RMSM=',
            SAMELINE,RMSM,''LS35'RMSN=',RMSN,
            ''LS35'RMSP=',RMSP;
"END";
FUNK:=RMSM+RMSP;
"PRINT" ''L2S35'FUNK=',SAMELINE,RMSM+RMSP;
"END" FUNK;


"PROCEDURE" STEEP2 (LB,XS,UB,DX,XMIN,FMIN,NV,EPS,RELAX,DXMAX,
ETA,PSI,PMAX,PMULT,PDIV,ZETA,FUNK);


FORMMX(MJ,0.0,I,J);
FORMMX(WJ,0.0,I,J);
"FOR" I:=1 "STEP" 1 "UNTIL" NM "DO" "READ" MJ[I,I];
"FOR" I:=1 "STEP" 1 "UNTIL" NM "DO" "READ" WJ[I,I];
```

```
"READ" BETA,OC1,OC2,OK1,OK2,OCT1,OCT2;
READMX(PHI1);
READMX(PHI2);
"READ"O KT1,OKT2,CM1,OM2,MACHEPS,WBASE,OMEGA,V,CA,
NA,CB,NB,WFMIN,WFMAX;
BETA:=2*BETA;
FORMMX(MI,0.0,I,J);
"FOR" I:=1 "STEP" 1 "UNTIL" NM "DO"
MI[I+2,I+2]:=1/MJ[I,I];
FORMMX(UNIT,0.0,I,J);
"FOR" I:=1 "STEP" 1 "UNTIL" NM+2 "DO" UNIT[I,I]:=1;
CMXFORM(CMI,MI[I,J],0.0,I,J);
READMX(PHIP);
COUNT:=0;
"READ" NDMAIN;
XS[1]:=NDMAIN;
ODMAIN:=PHI1[1,2];
ODNOSE:=-PHI2[1,2];
   "FOR" I:=1 "STEP" 1 "UNTIL" NV "DO"
   "BEGIN" LB[I]:=XS[I]/2;
           UB[I]:=XS[I]*2;
           DX[I]:=XS[I]/50;
          DXMAX[I]:=XS[I]/5;
   "END";
   "READ" EPS,PSI,ZETA,ETA,RELAX,PMAX,PMULT,PDIV;
   STEEP2(LB,XS,UB,DX,XMIN,FMIN,NV,EPS,RELAX,DXMAX,ETA,PSI,PMAX,PMULT,PDIV,ZETA,FUNK);
   PHI1[1,2]:=XMIN[1];
   PHI2[1,2]:=PHI1[1,2]-WBASE;
   MNMULT:=ABS(PHI2[1,2]/ODNOSE);
   NSMULT:=PHI1[1,2]/ODMAIN;
```

```
"PRINT"  ''L3'OPTIMUM VALUES ARE:-',
         ''S5'ACCELERATION APPROXIMATION,RMSM+RMSP=',
         SAMELINE,FMIN,''L2S58'NDMAIN=',XMIN[1],''L2S62'K1=',OK1*MNMULT,
         ''S5'C1=',OC1*MNMULT,''LS62'K2=',
         OK2*NSMULT,''S5'C2=',OC2*NSMULT,
         ''L2S61'KT1=',OKT1*MNMULT,''S4'CT1=',
         OCT1*MNMULT,''LS61'KT2=',OKT2*NSMULT,
         ''S4'CT2=',OCT2*NSMULT,''L2S62'M1=',
         OM1*MNMULT,''LS62'M2=',OM2*NSMULT;
"END";
    "GOTO" END;
FAIL:"PRINT" ''L'HQR2 FAILURE';
        "GOTO"END;
APFAIL:"PRINT"''L2S5'ACCELERATION APPROXIMATION HAS FAILED',
             ''L2S5'DIFFERENCE IN RESONANT FREQUENCIES=',
             SAMELINE,DIFWF/0.75,
             ''L2S5'SUM OF BANDWIDTHS=',SUMBW;
END: "END";
```